Fundamental and Engineering Application Studies of Pressure-Assisted Injection Forging of Thick-Walled Tubular Components

(Volume II)

Yanling Ma

Glasgow, October 2004

Fundamental and Engineering Application Studies of Pressure-Assisted Injection Forging of Thick-Walled Tubular Components

Yanling Ma

This thesis is submitted to the Department of

Design, Manufacture and Engineering Management,

University of Strathclyde,

for the degree of Doctor of Philosophy

Glasgow, October 2004

Dedication:

The author wishes to dedicate the thesis to her father, mother, her husband and son, for the love and support. Without their support and sacrifice, the thesis would not have been completed. The thesis is also dedicated to all members of the author's extended family for their continuous encouragement and tolerance throughout the whole period of the author's study in the UK.

Acknowledgements

The work exhibited herein was carried out in the Department of Design, Manufacture and Engineering Management, the University of Strathclyde, through a full-time study. Financial support provided by the EPSRC and the university is gratefully acknowledged.

The author is grateful to her supervisors, Dr. Y. Qin and Prof. R. Balendra, for their, untiring guidance, inspiring encouragement, invaluable suggestions throughout the research and writing of the thesis as well as meticulous checking of the manuscript.

The author also would like to express her sincere thanks to Dr. M. Rosochowska and Dr. A. Rosochowski for their advice and help during the author's study.

Last but none the least, the author's thanks go to all the laboratory staff for their skilful technique and constant support, throughout the fabrication of experimental device and conduction of experiments.

Abstract

Fundamental issues and engineering application aspects of Pressure-Assisted Injection Forging (PAIF) of thick-walled tubular components were studied experimentally and analytically. Achievements from this study met its pre-defined goals and are demonstrated with the following facts:

Pressurising materials were selected and qualified under six different loading conditions, based on which a simplified configuration for confined compression tests was proposed, and particularly, a unique biaxial testing machine was developed and used satisfactorily. The test data were subsequently used to establish constitutive descriptions of the materials and to facilitate the FE modelling to simulate the forming processes.

An upper bound analysis of Pressure-assisted injection forging of thick-walled tubular components with hollow flanges was conducted and formulated solution for the forming process was developed, by which the maximum forming-force for a given component geometry can be predicted with sufficient accuracy.

Failure modes and process range for pressure-assisted injection forging of thick-walled tubular components were studied experimentally and numerically, as a result, eight standard failure forms were categorized and three forming limit diagrams were established, which were validated experimentally and can be used as a guidance for the process design.

By combining above results achieved, an approach for synthesising concurrent design and manufacture of thick-walled tubular components with pressure-assisted injection forging was developed, in which technical details of the process and step by step procedure towards producing sound tubular components were provided. The development represents a significant progress towards engineering and industrial applications of the pressure-assisted injection forging (PAIF) technology.

Using the forming limit diagrams as a design guideline and following the approach for synthesising concurrent design and manufacture, an engineering component – hollow gear shaft was formed successfully.

List of the publications

The following publications were prepared based on, (fully or partially) the work presented in this thesis.

[1] Y. Ma, Y. Qin and R. Balendra, "Experimental and FE investigation of performance of polymers under confined compression conditions by using a simplified configuration", Advances in Manufacturing Technology, XVI, The 18th NCMR, 2002, pp. 203-208.

*** Based on the part of the contents of Chapter 3.

[2] Y. Qin, Y. Ma and R. Balendra, "Performance of pressurising-materials and process design considerations for the forming of thick-walled tubular components", Proc. of the 9th ISPE Conference on Concurrent Engineering (CE2002), July, Granfield, UK, pp. 251-262, 2002.

*** Based on the part of the contents of Chapter 3.

[3] Y. Ma, Y. Qin and R. Balendra, "Clamping design for the biaxial tension test of rubbers", Advances in Manufacturing Technology, XVII, The 1st ICMR and 19th NCMR, 2003, pp. 329-333.

*** Based on the part of the contents of Chapter 4.

[4] Y. Qin, Y. Ma and R. Balendra, "Pressurising materials and process design considerations of the Pressure-assisted Injection Forging of thick-walled tubular components", Journal of Materials Processing Technology, Vol. 150, No. 1-2, pp. 30-39, 2004.

*** Based on the part of the contents of Chapter 3.

[5] Y. Ma, Y. Qin and R. Balendra, "Process ranges of pressure-assisted injection forging of thick-walled tubular components", Advances in Manufacturing Technology, The 2nd ICMR and 20th NCMR, 2004, pp. 25-29.

*** Based on the part of the contents of Chapter 6.

[6] Y. Ma, Y. Qin and R. Balendra, "Concurrent design and manufacture in pressure-assisted injection forging of tubular components", Advances in Manufacturing Technology, The 2nd ICMR and 20th NCMR, 2004, pp. 139-144.

*** Based on the part of the contents of Chapter 3, 4 and 5.

[7] Y. Qin, Y. Ma and R. Balendra, "Mechanics of Pressure-assisted Injection Forging of tubular components", Proc. Instn Mech. Engrs. Vol. 218 Part C: J. Mechanical Engineering Science, 2004, pp. 1-18.

*** Based on the part of the contents of Chapter 3, 4 and 6.

[8] Y. Ma, Y. Qin and R. Balendra, "Upper Bound analysis of Pressure-assisted Injection Forging of Thick-Walled Tubular Components with Hollow Flanges", submitted.

*** Based on the part of the contents of Chapter 5.

Contents of Volume I

Contents of Volume II

Figures of Chapter 2

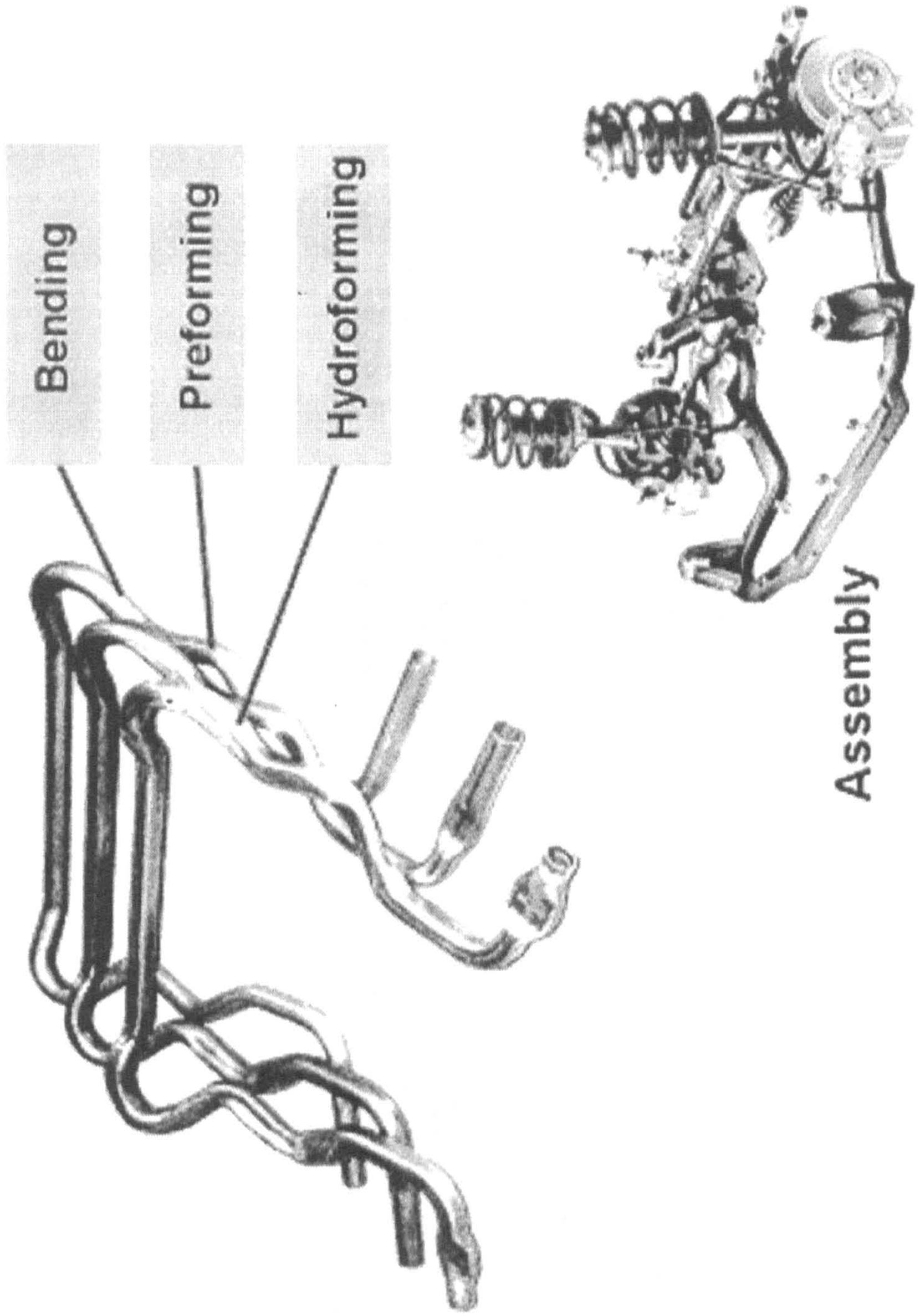

Fig. 2.1 The hydroforming of an engine cradle [12]

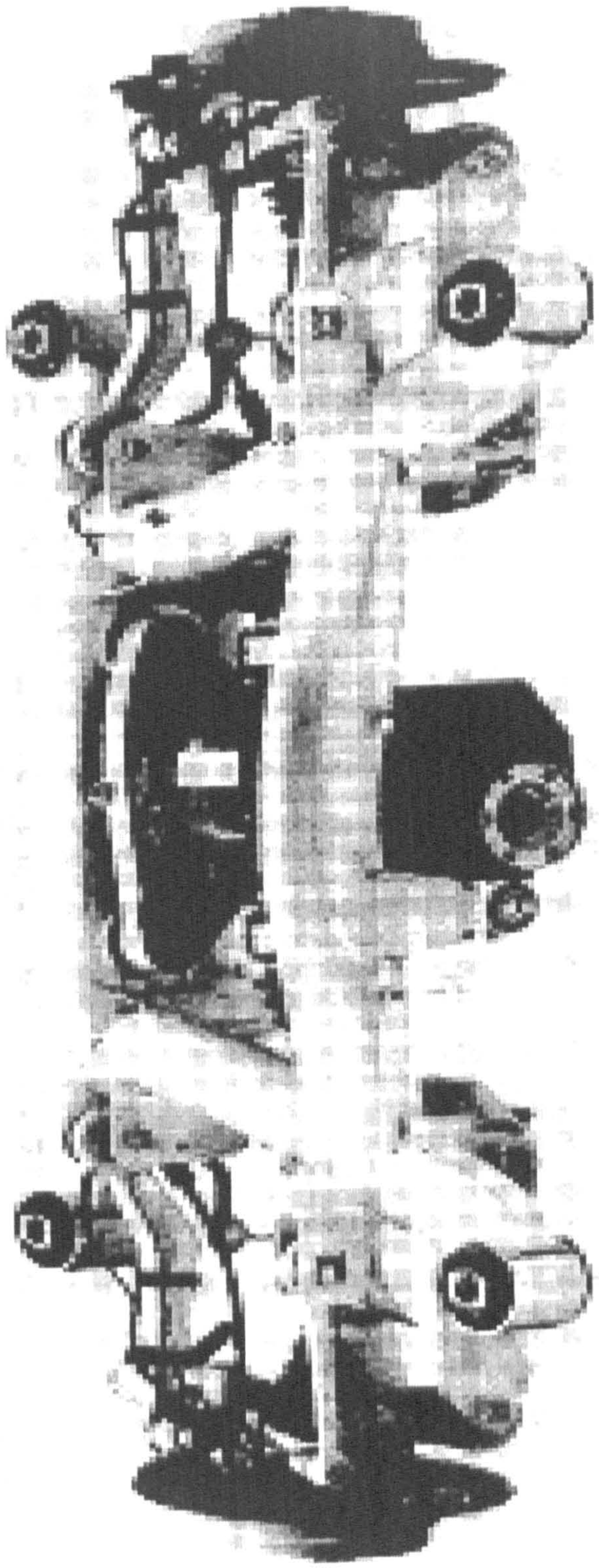

Fig. 2.2 The hydroformed aluminium rear axle used by the BMW [14]

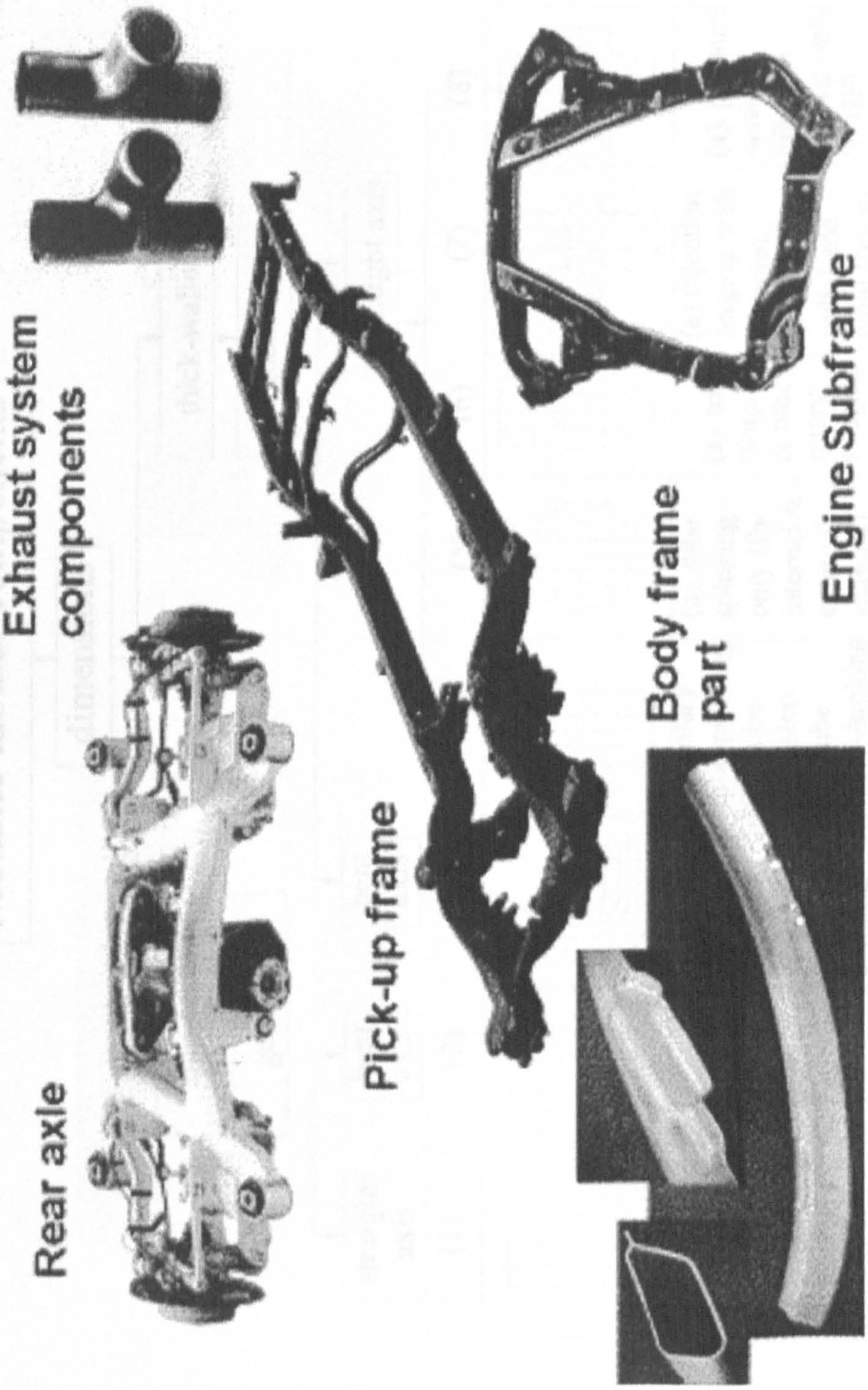

Fig. 2.3 More applications of hydroformed components by automotive industry [12]

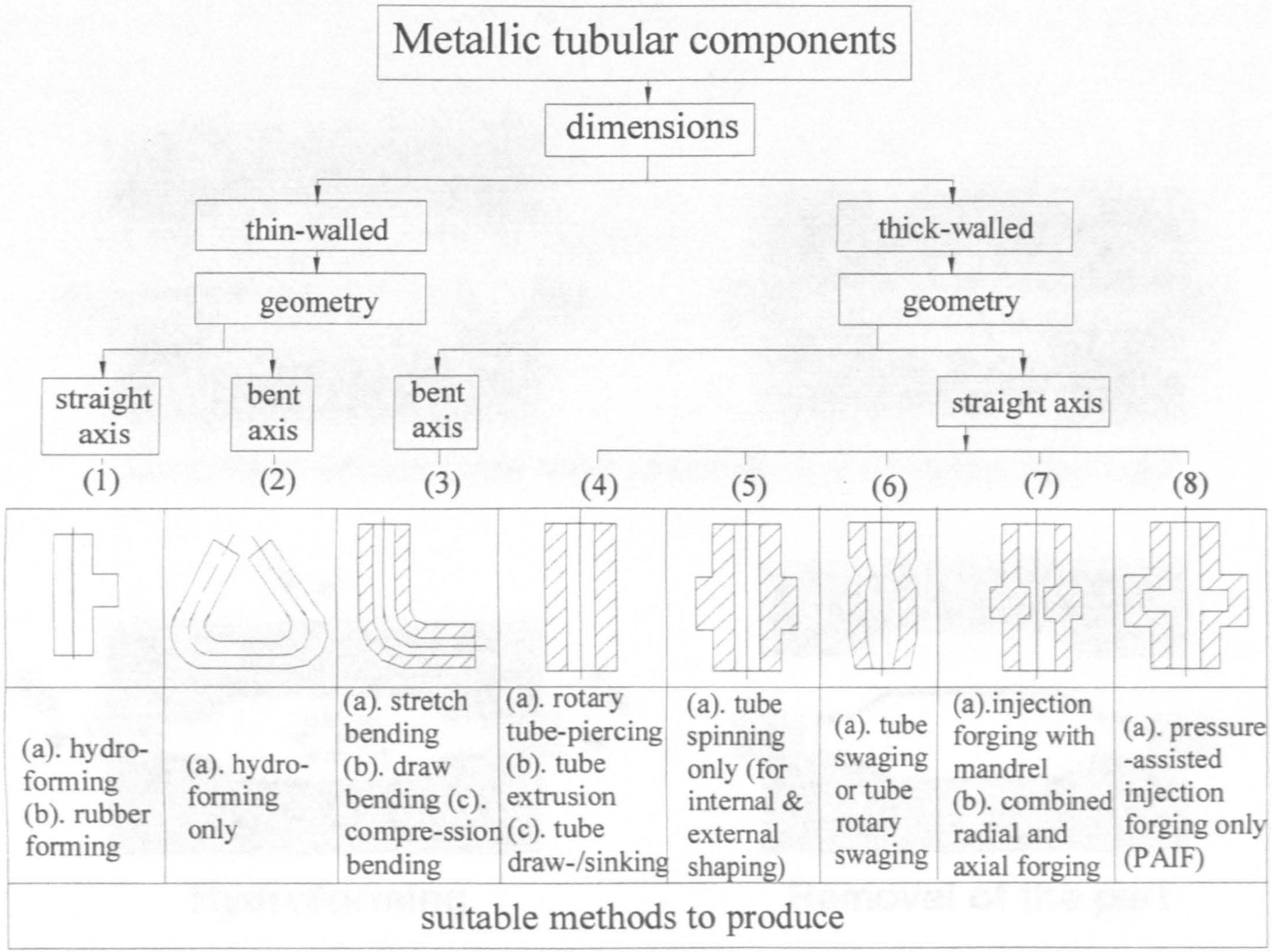

Fig. 2.4 Classification of tubular components

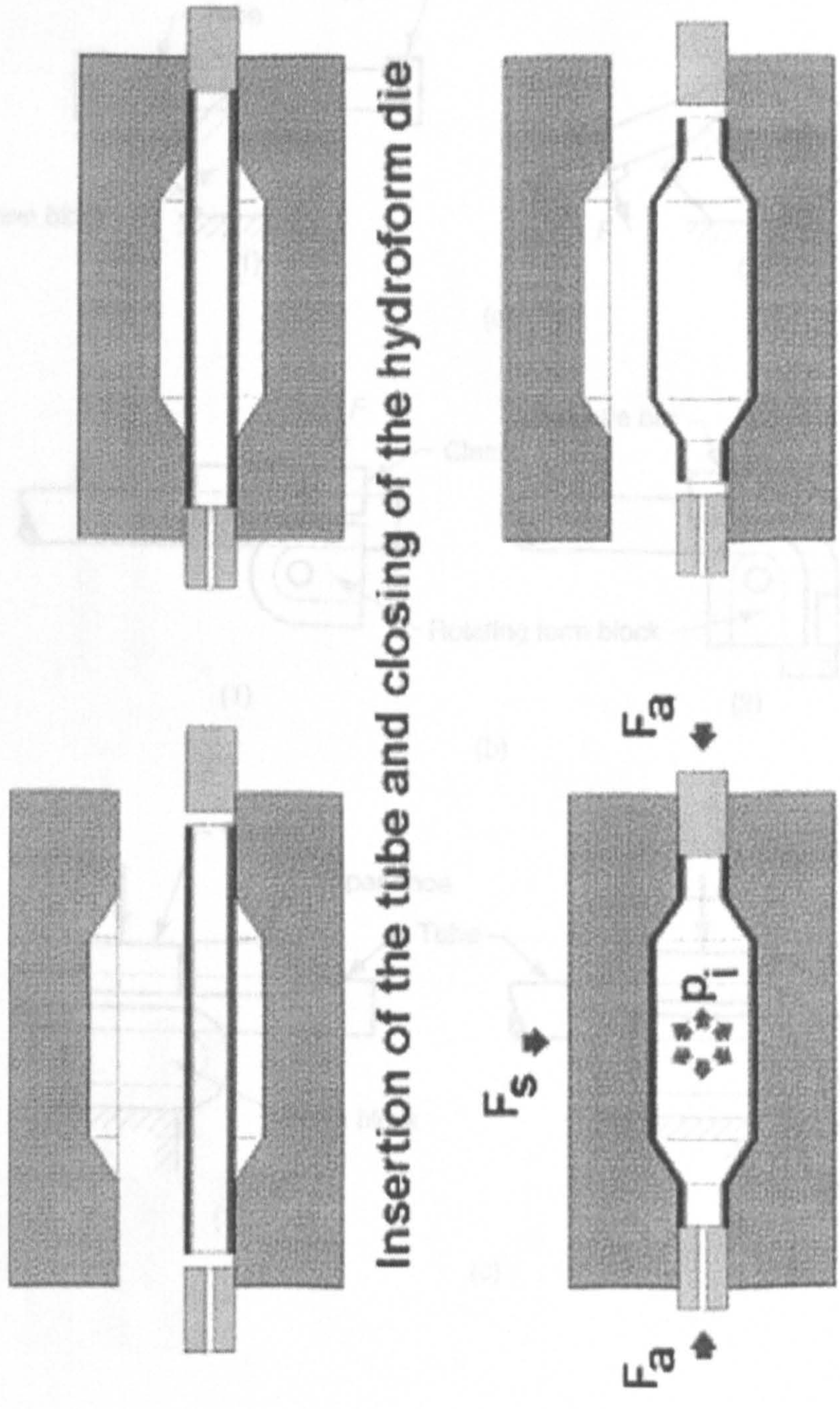

Fig. 2.5 Tube hydroforming process [12]

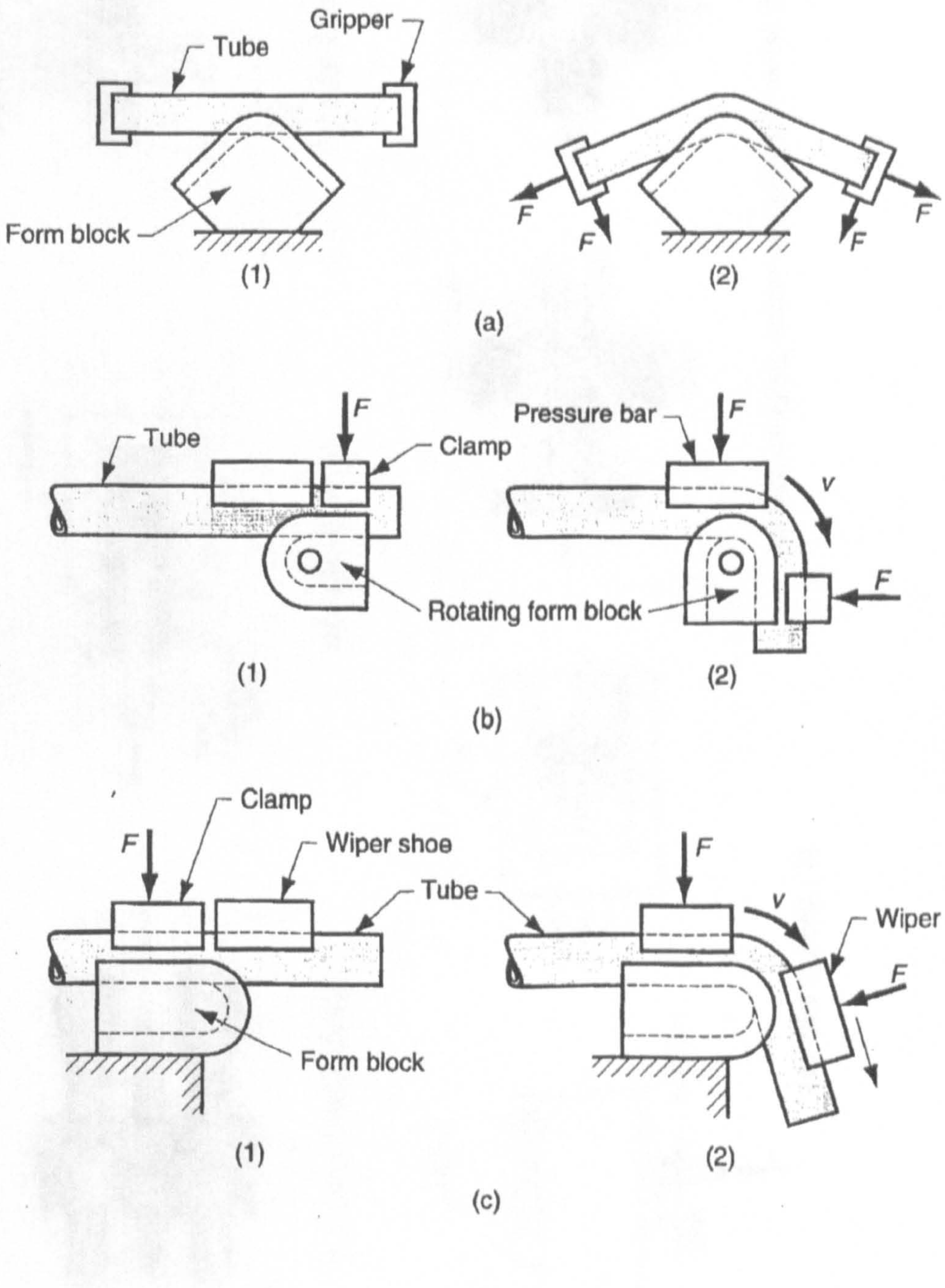

Fig. 2.6 Three tube bending methods: (a) stretch bending; (b) draw bending and (c) compression bending [2]

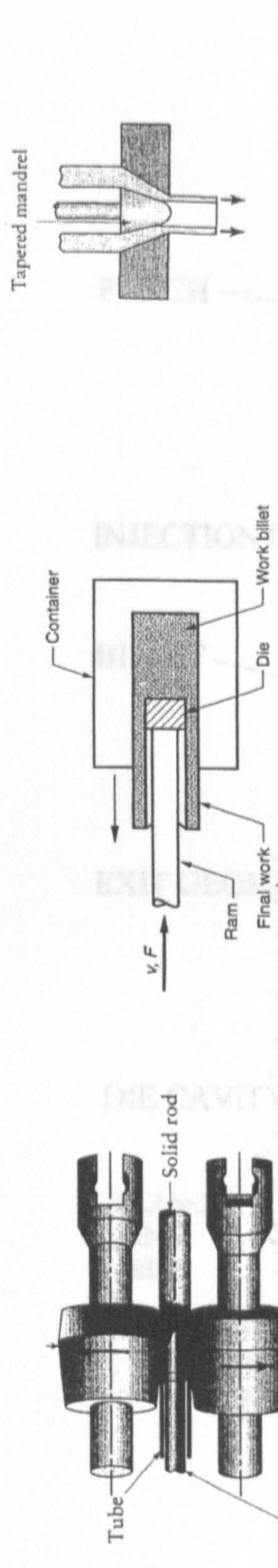

(a) rotary tube piercing

(b) tube extrusion

(c) tube drawing [1]

(d) tube spining [2]

(e) tube swaging, rotary swaging and radial forging [1]

Fig. 2.7 Five conventional tube forming methods

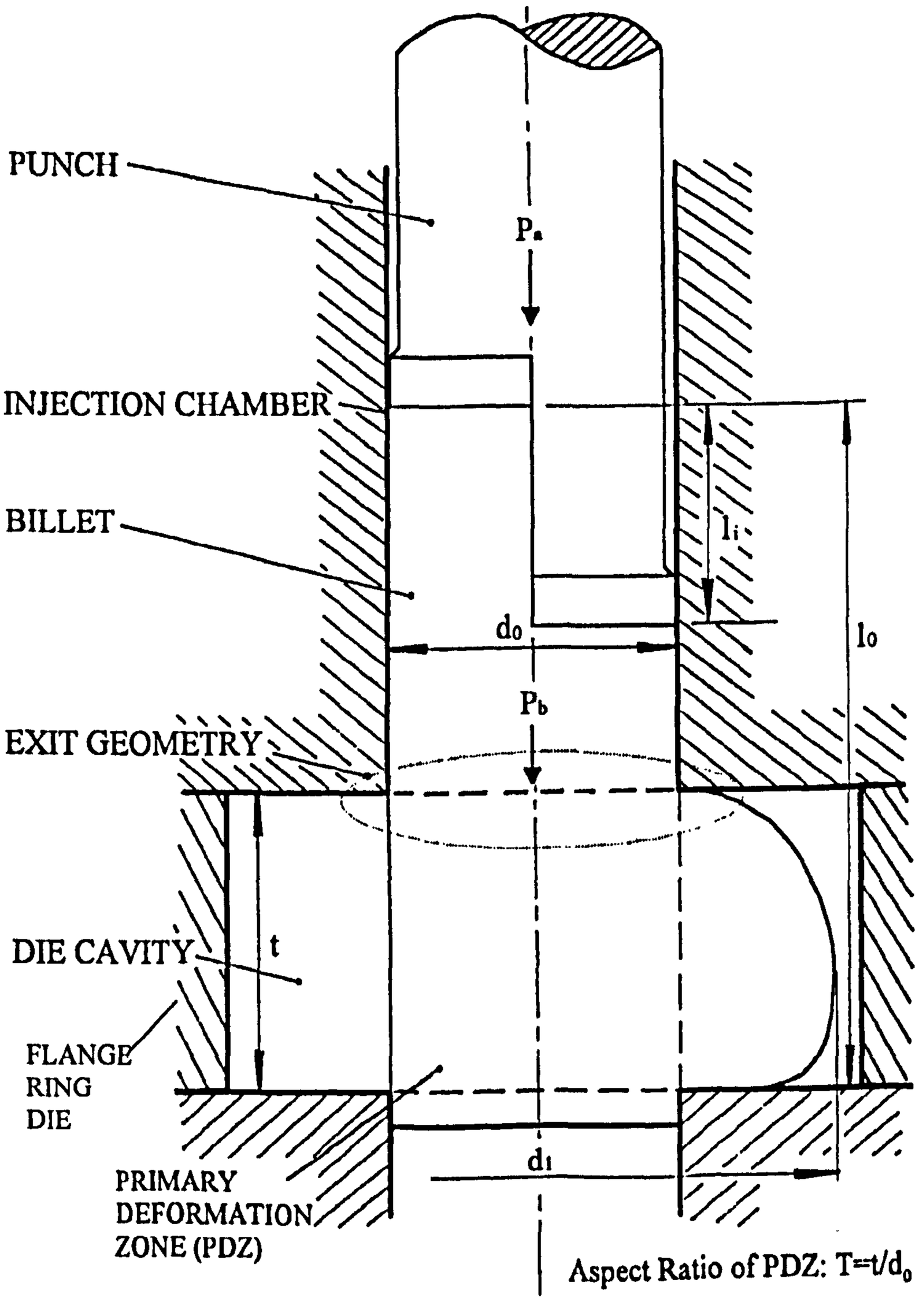

Fig. 2.8 The simplified process model of Injection forging

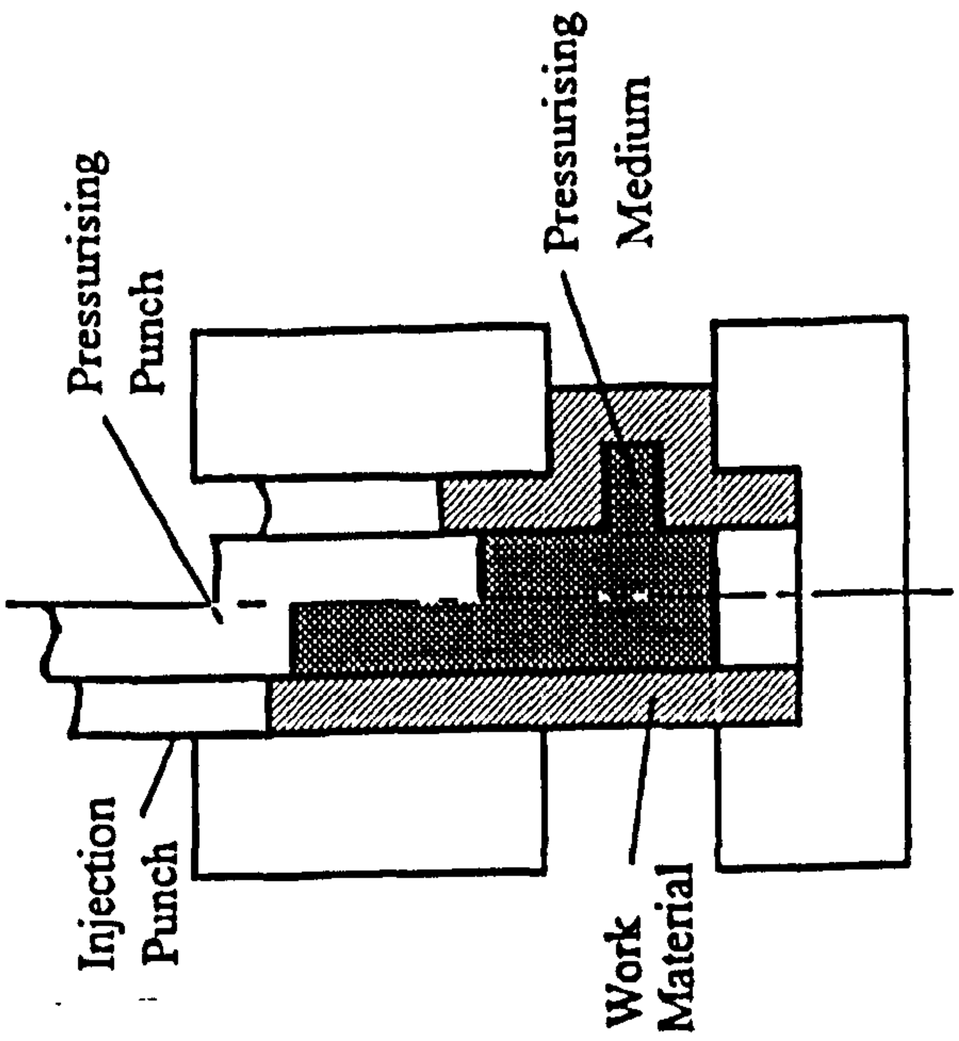

(c) Injection Forging of tubular material with support of pressurising medium

(b) Injection Forging of tubular material with mandrel support

(a) Injection Forging of solid billet

Fig. 2.9 Three typical process configurations of injection forging [64]

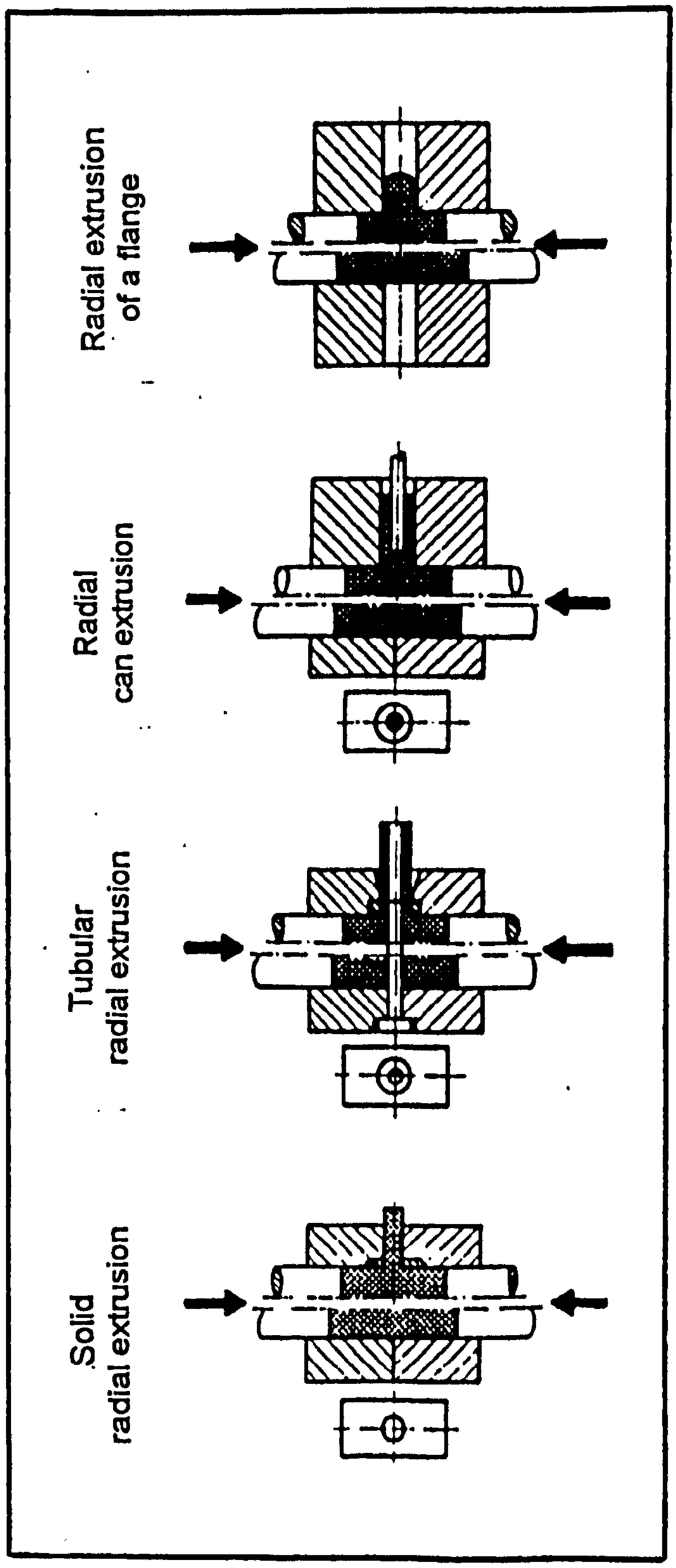

Fig. 2.10 Process classification of radial extrusion using component-forms as criteria [44]

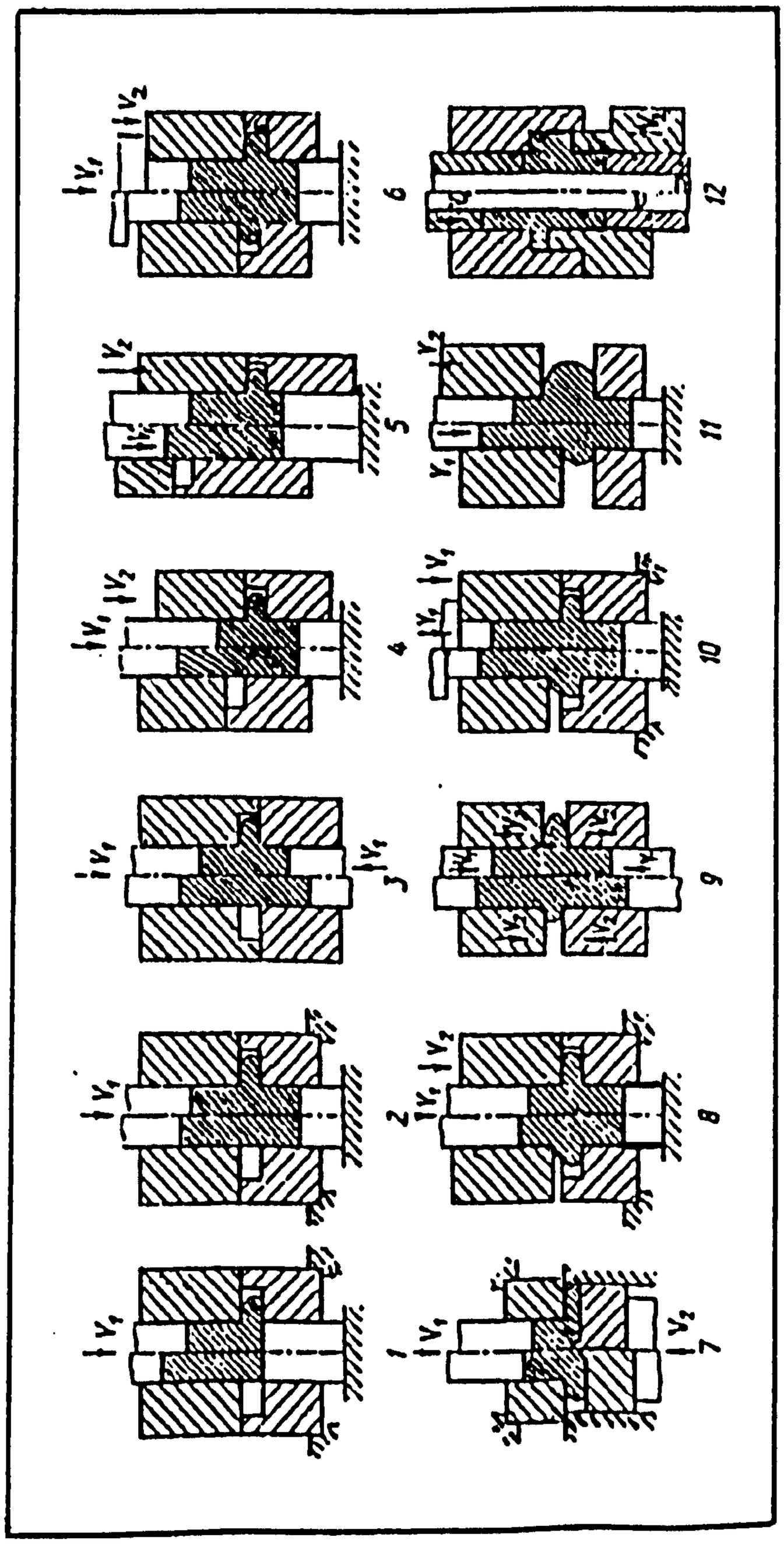

Fig. 2.11 Process classification of injection forging using tool-kinematics as criteria [50]

		TUBULAR SPECIMEN		
		INWARD FLOW	OUTWARD FLOW	FREE FORMING
ONE PUNCH	ONE END CONSTRAINED	1.1 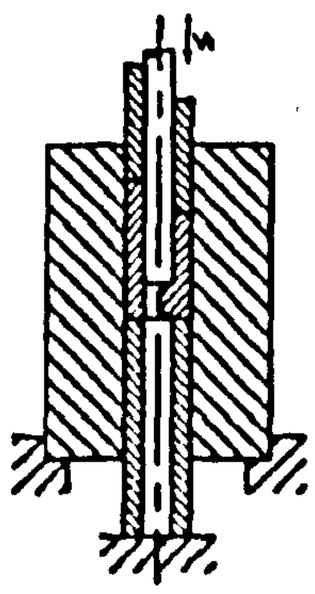	1.2 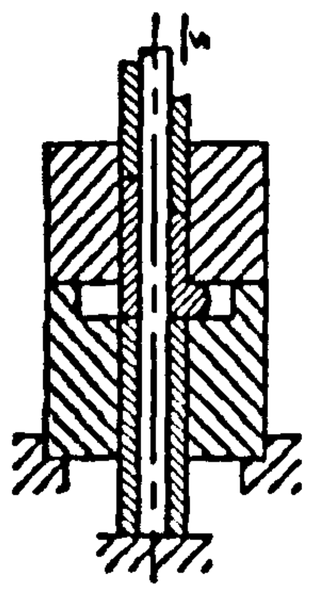	1.3 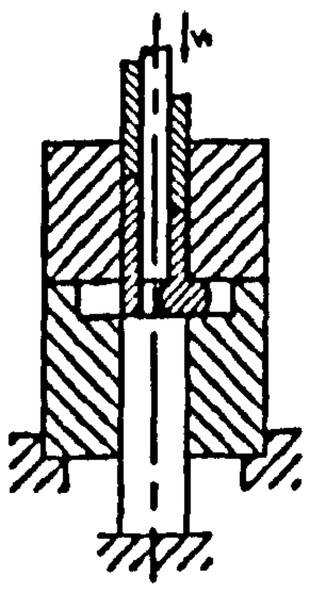
	BOTH ENDS CONSTRAINED	2.1 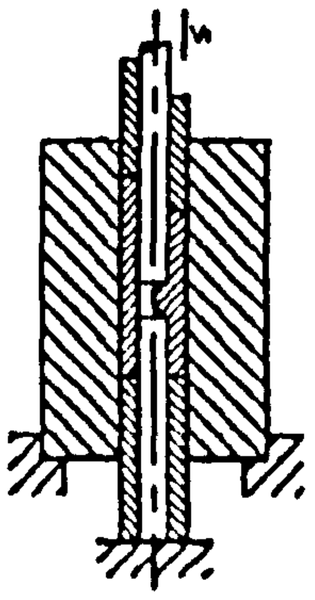	2.2 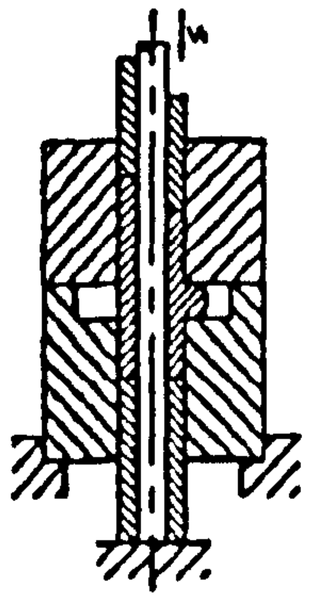	2.3 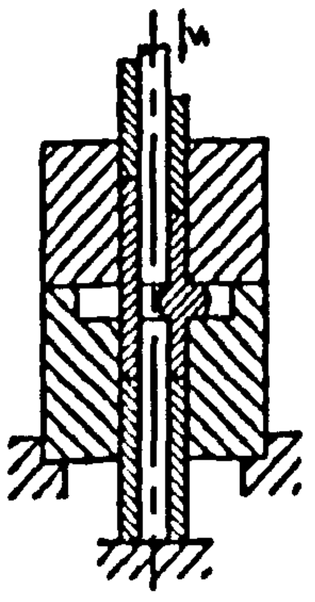
TWO PUNCHES	BOTH ENDS CONSTRAINED	3.1 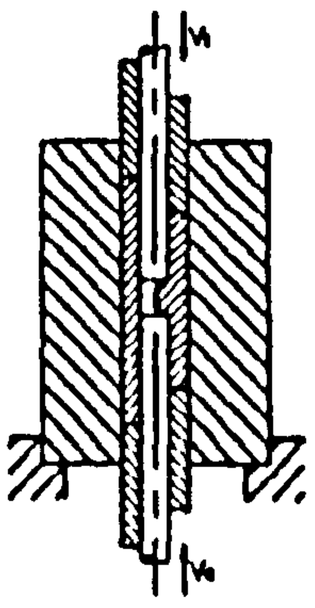	3.2 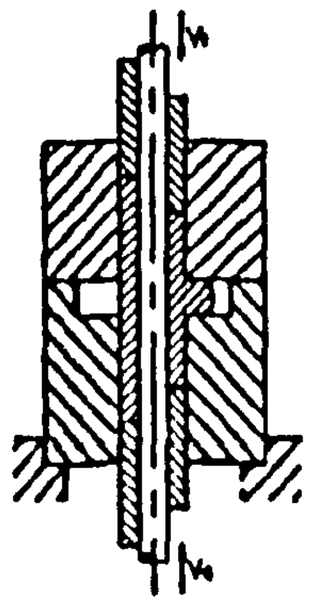	3.3 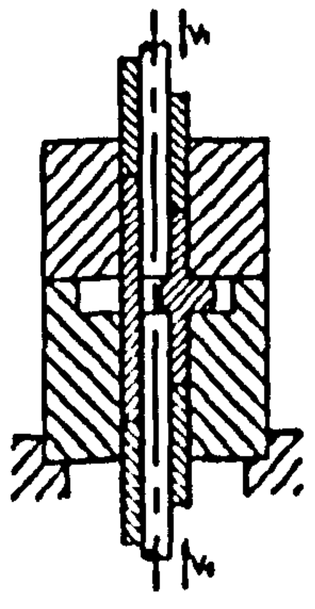

Fig. 2.12 Classification of injection forging of tube with mandrel support [32]

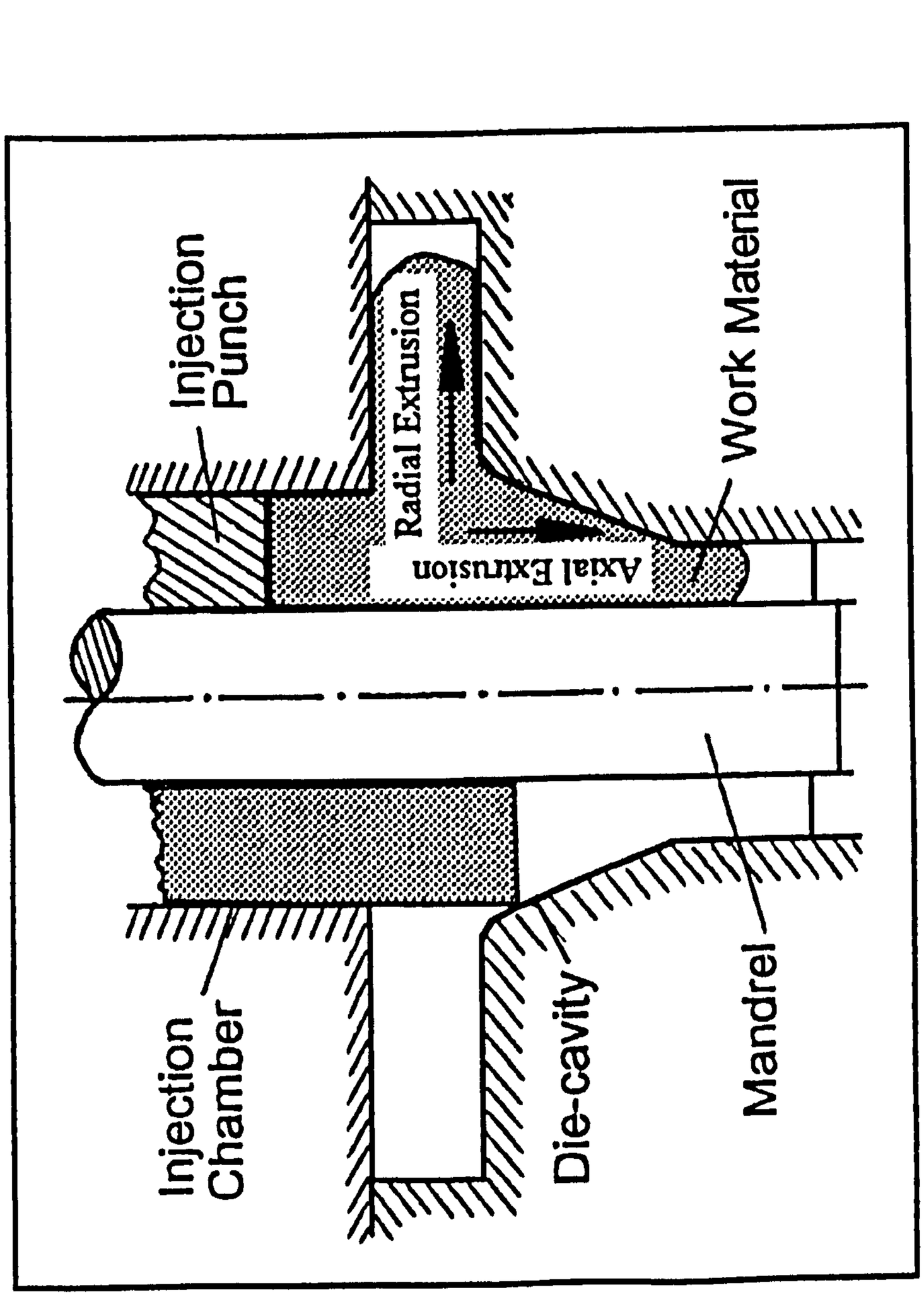

Fig. 2.13 Process configuration of tube forming with simultaneous radial and axial extrusion [47]

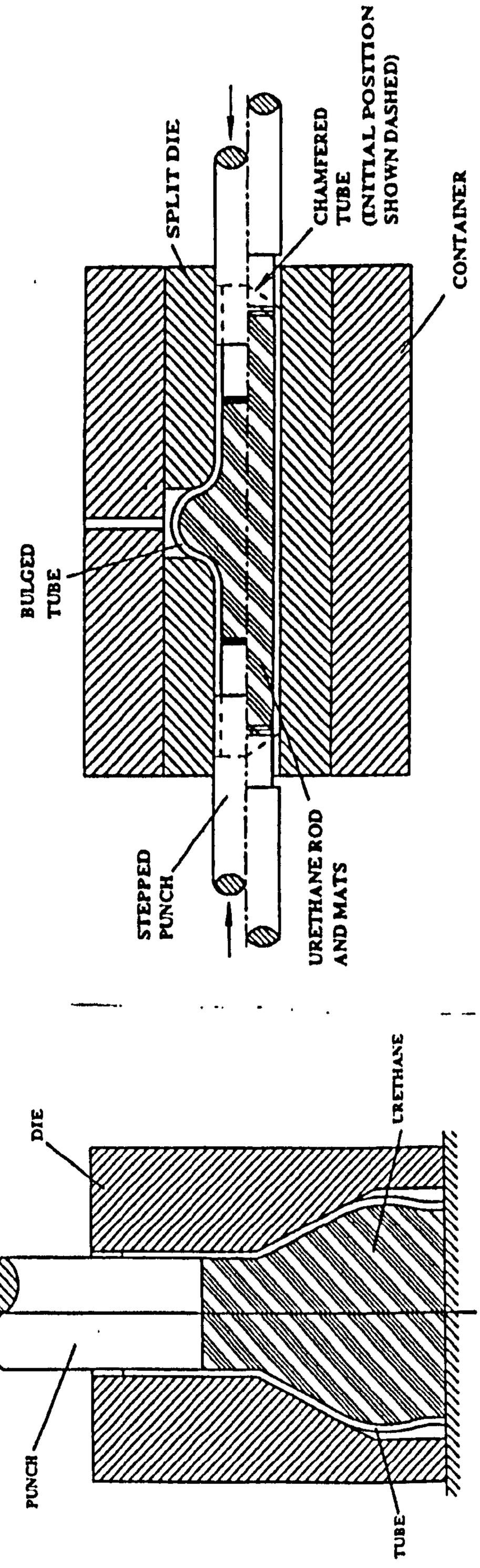

(b) T-joint bulging with urethane plugs

(a) Tube bulging with a urethane rod

Fig. 2.14 Two examples of tube rubber forming [18]

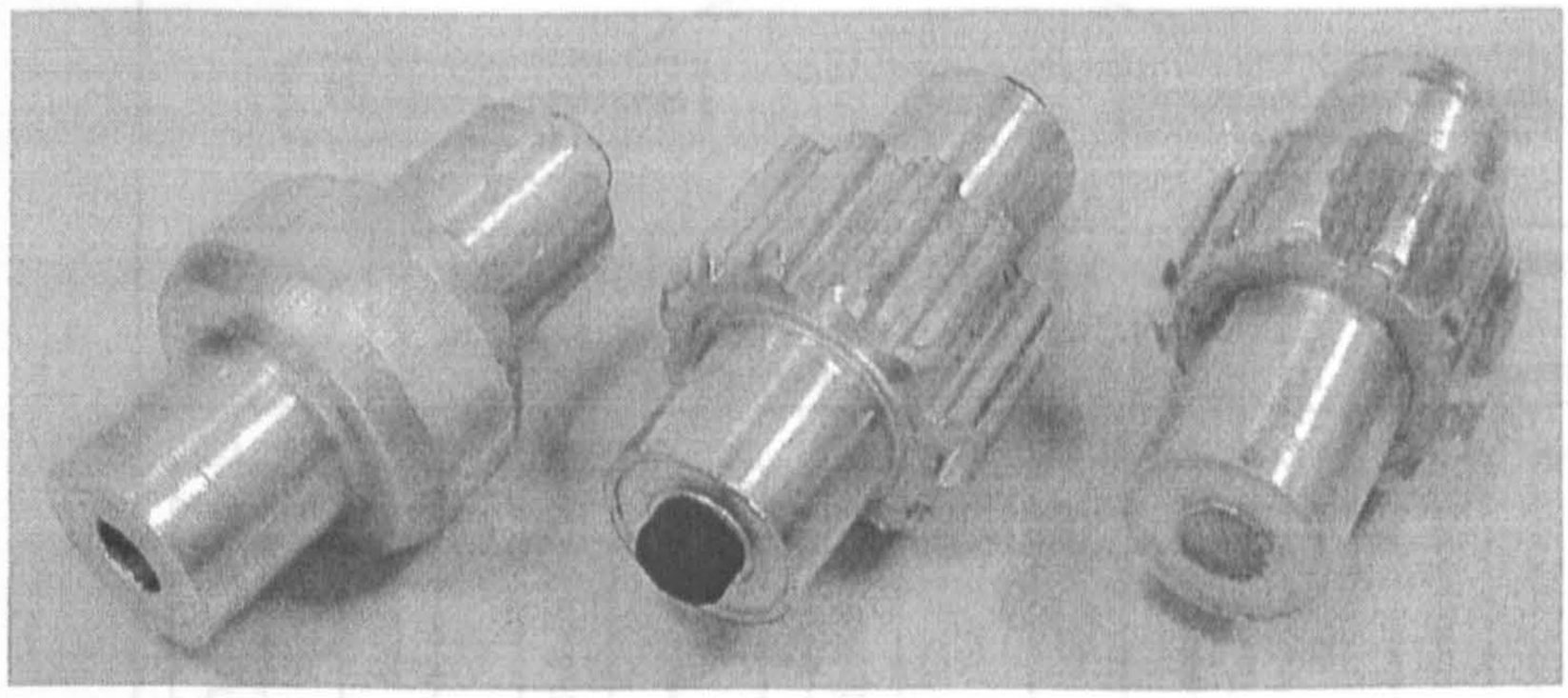

(a) Hollow flange and near-gear-shafts
produced recently

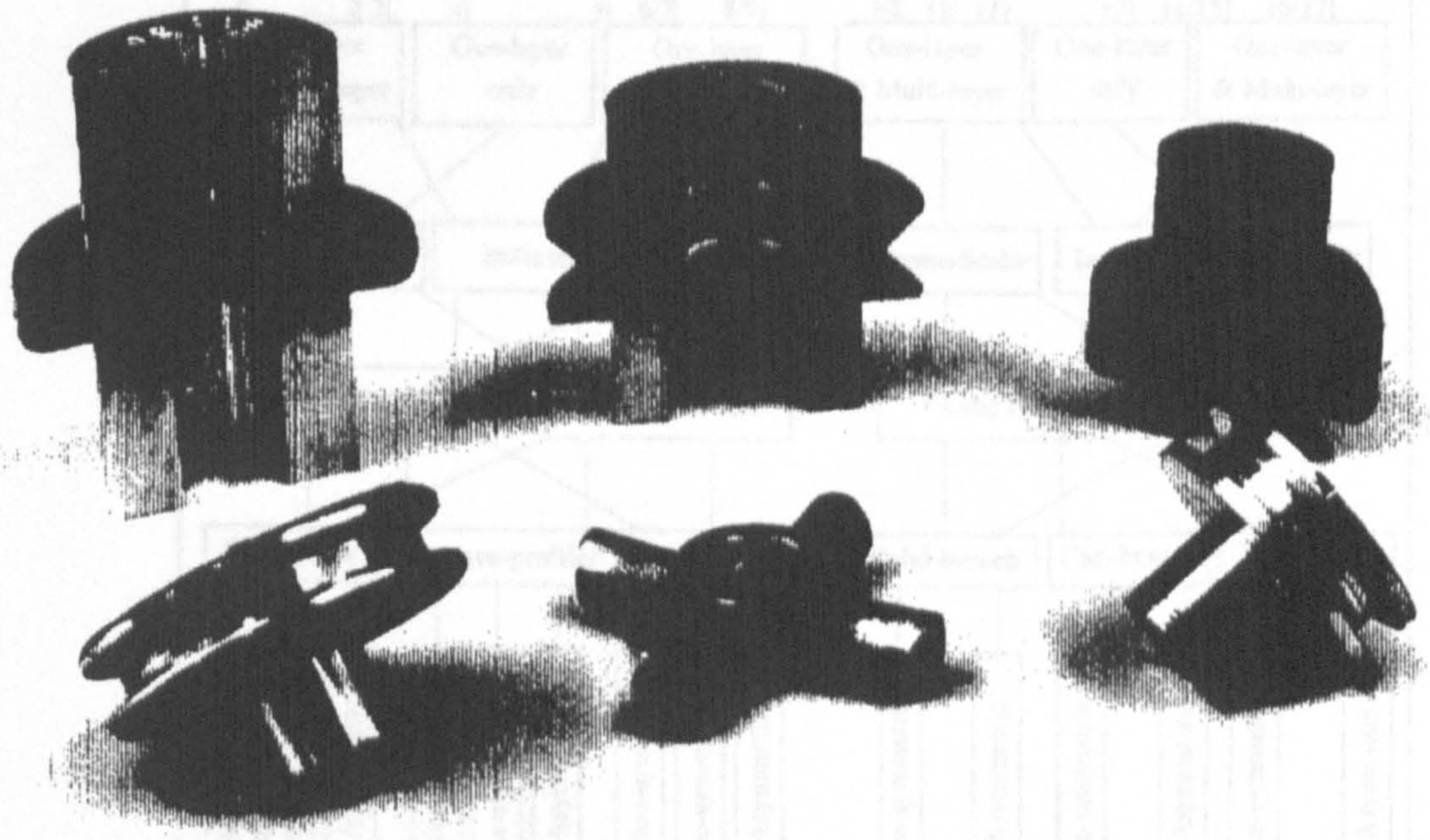

(b) Components produced previously

Fig. 2.15 Components injection-forged at the University of strathclyde

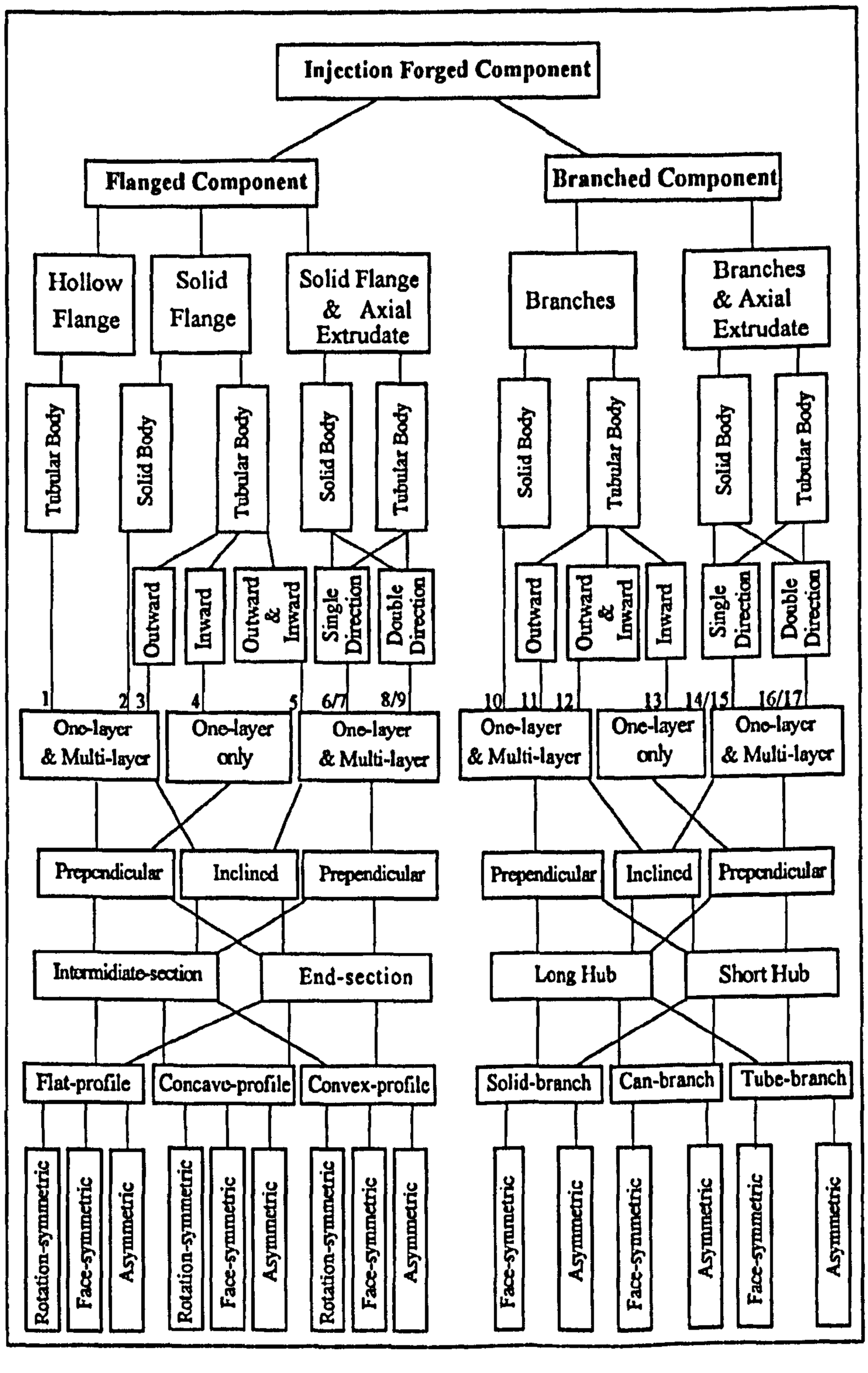

Fig. 2.16 A systematic classification of component-forms formable by injection forging [74]

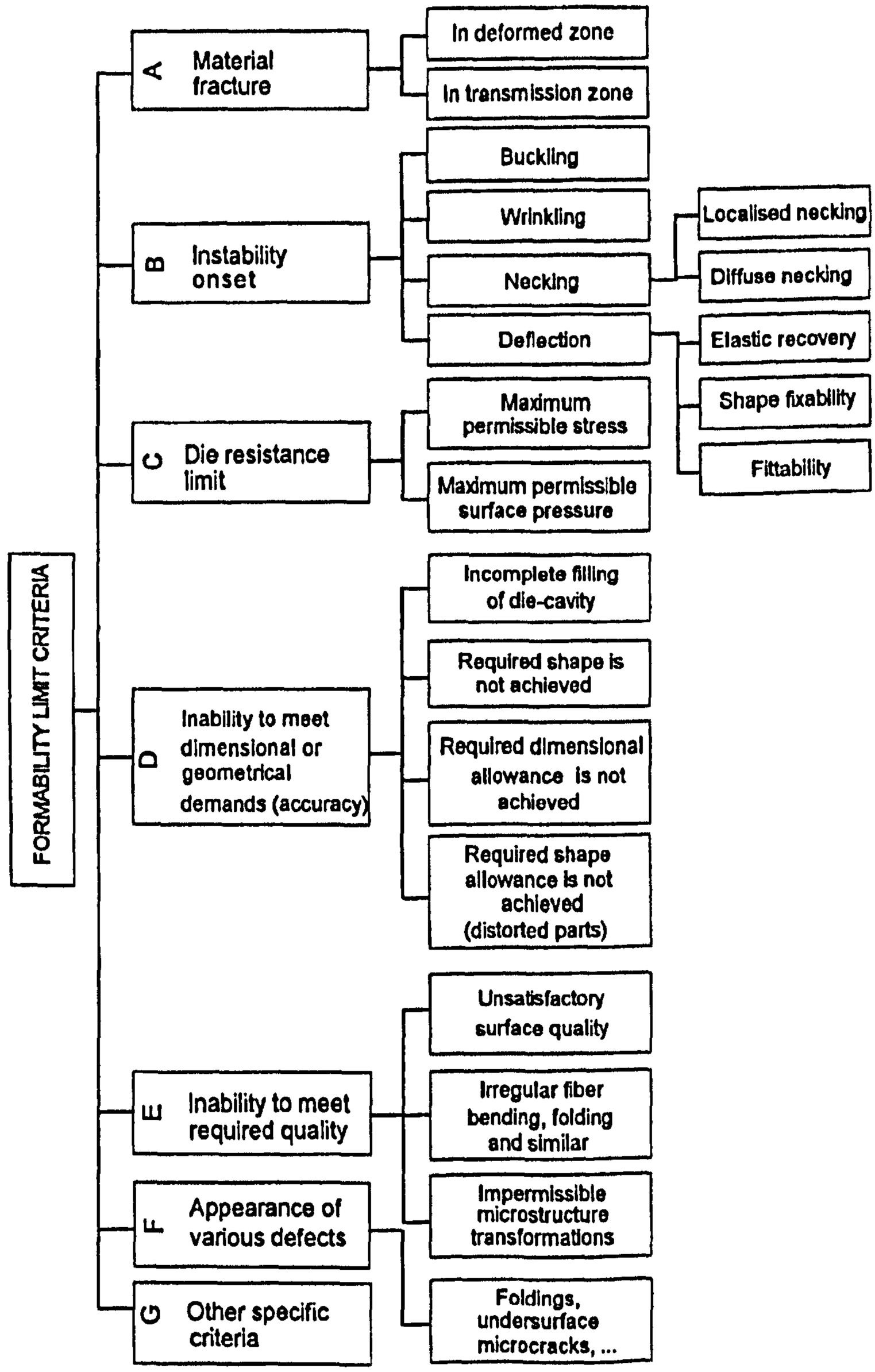

Fig. 2.17 A universal classification of formability limits for metal forming processes [92]

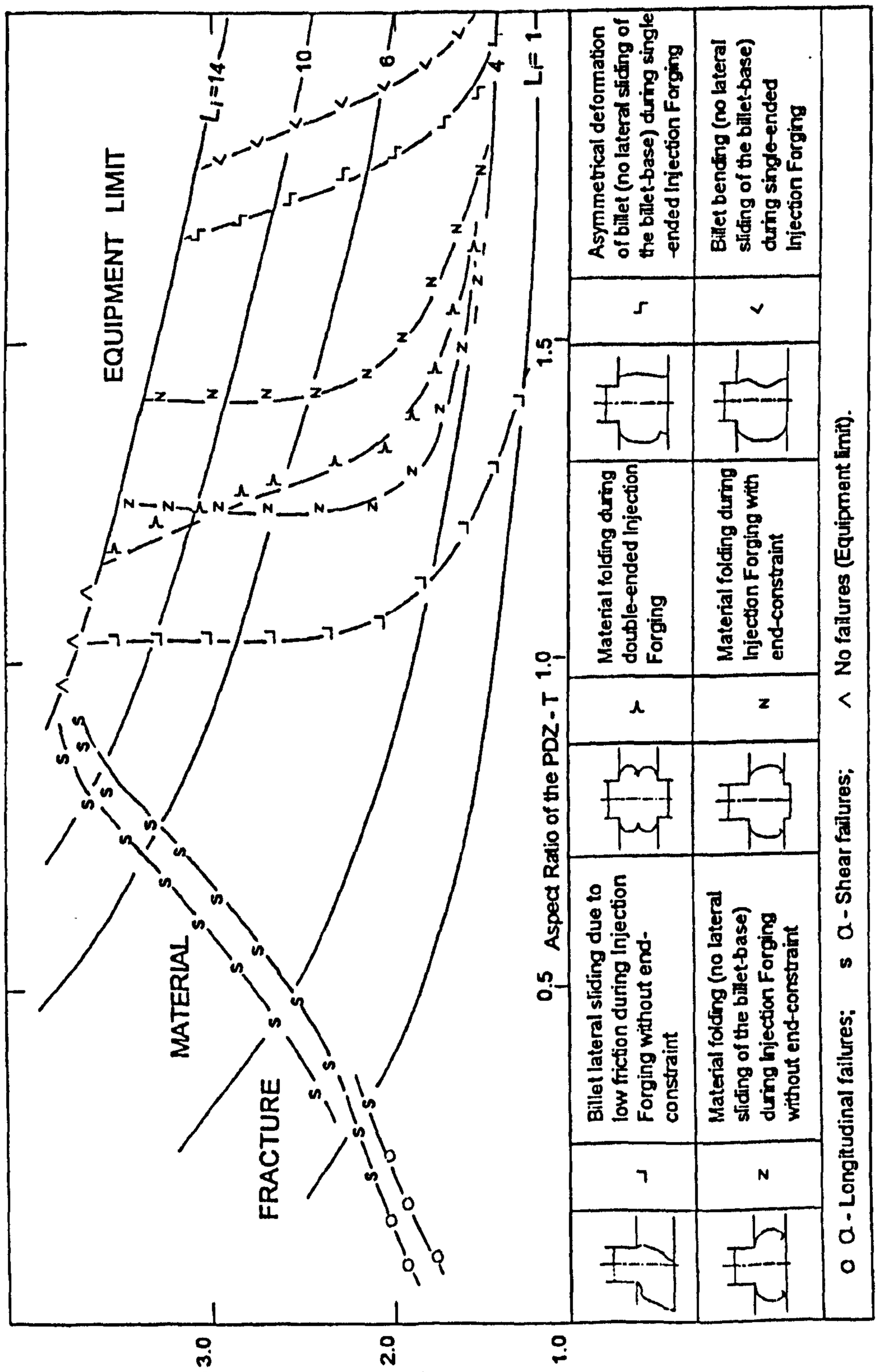

Fig. 2.18 Free forming limit diagram of injection forging of solid billets [64]

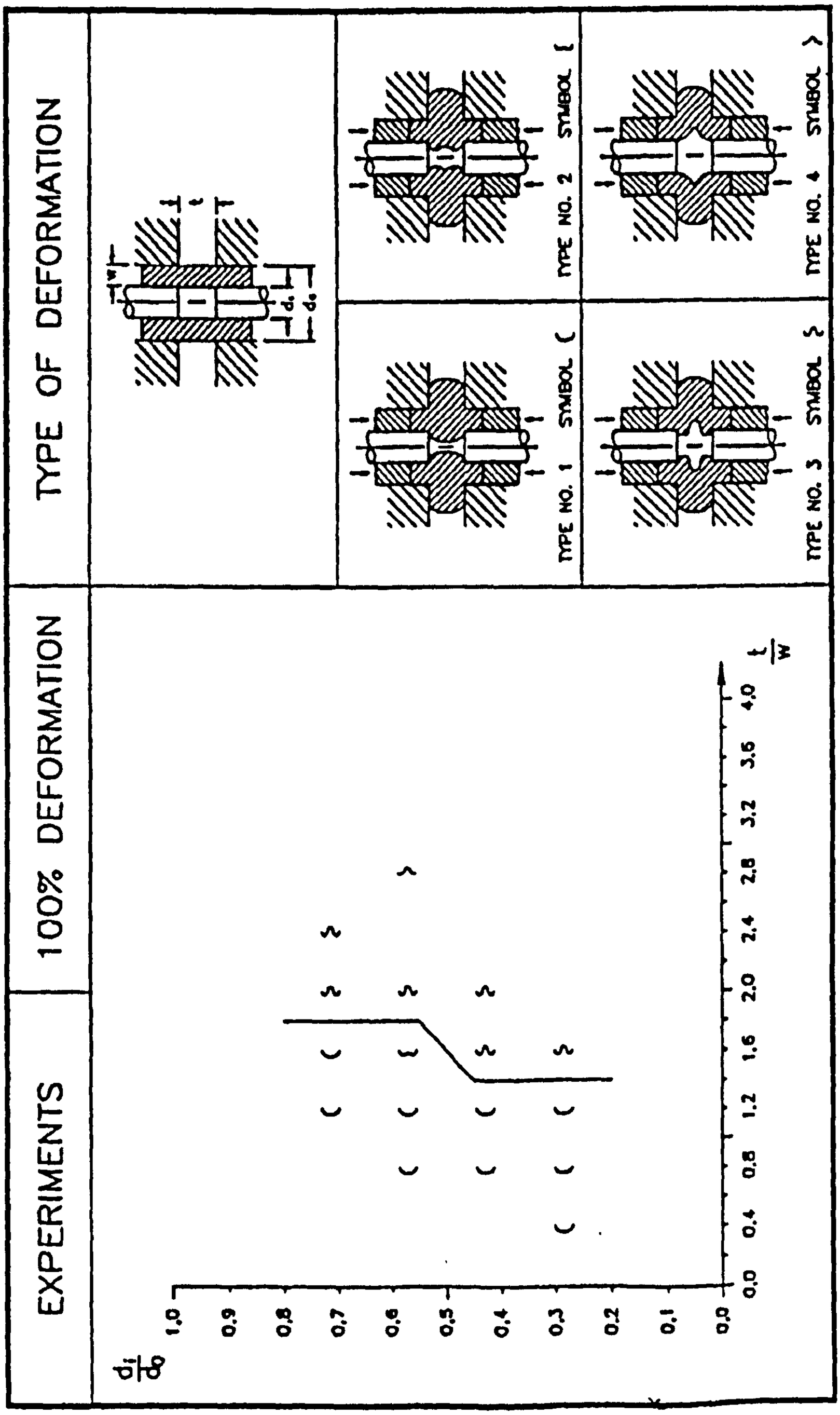

Fig. 2.19 Formability limit diagram of radial extrusion of tubes [32]

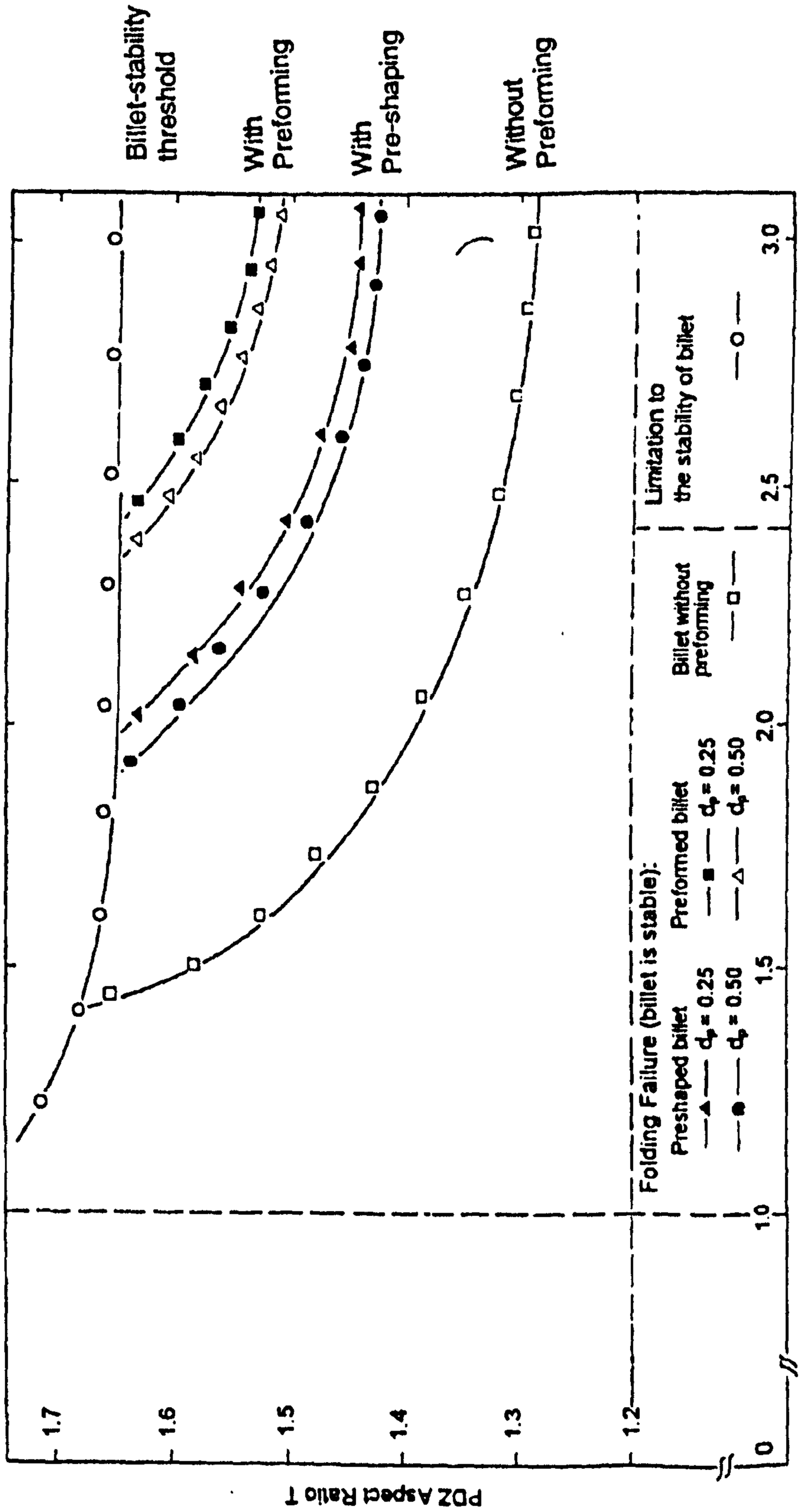

Fig. 2.20 Forming-limit diagram of injection forging using truncated-conical preforms [118]

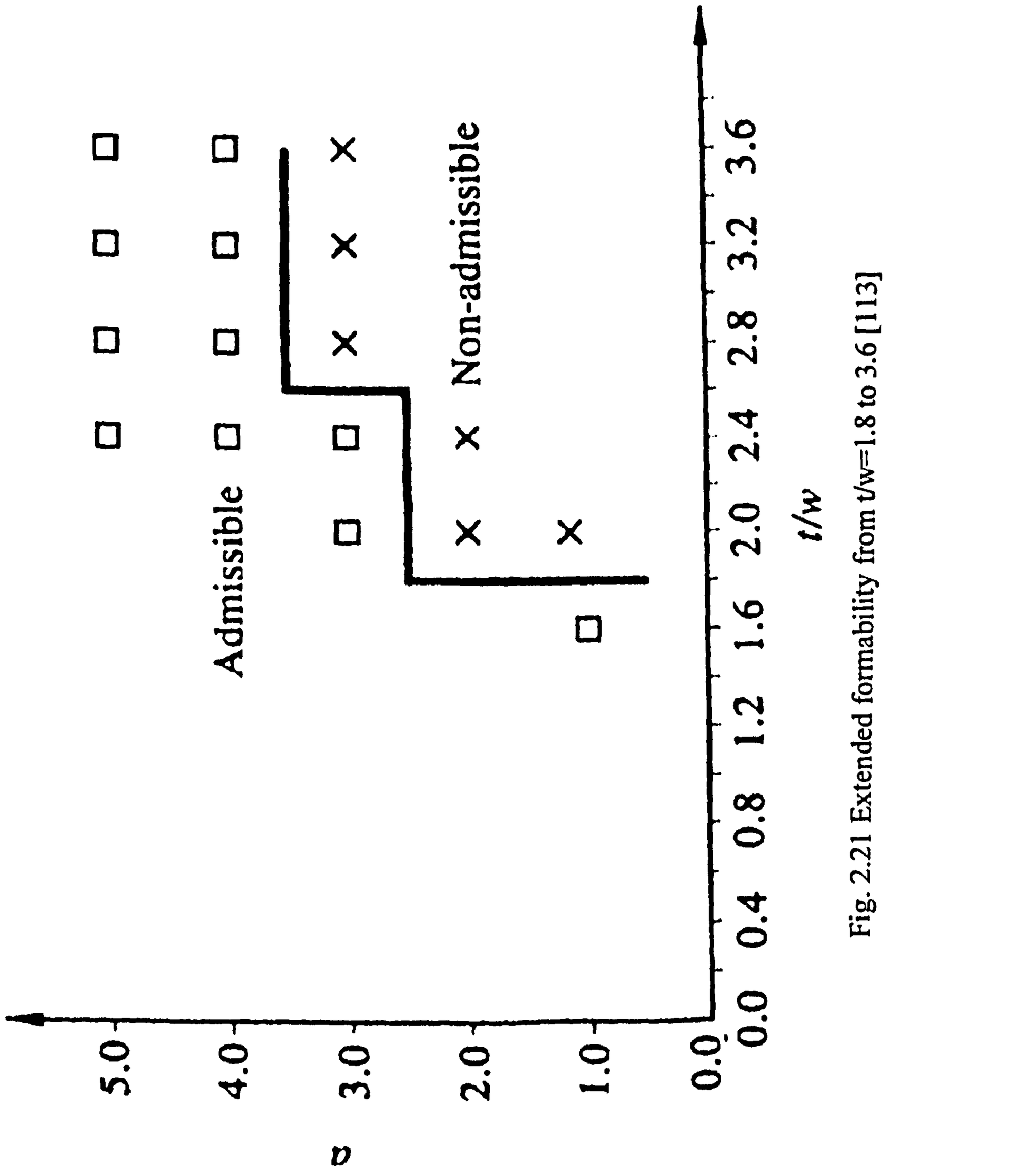

Fig. 2.21 Extended formability from t/w=1.8 to 3.6 [113]

Comparison of flow types			
Flow	FE–analysis	Metal experiments	Wax experiments
Type 1	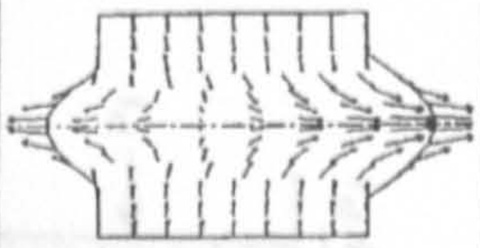	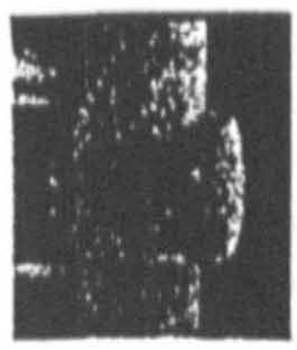	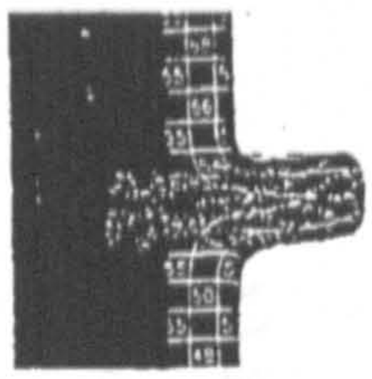
Type 2	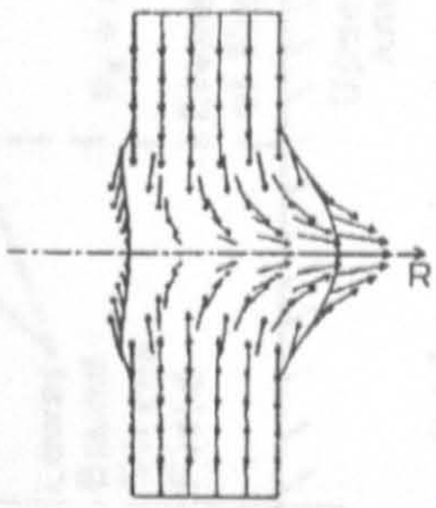	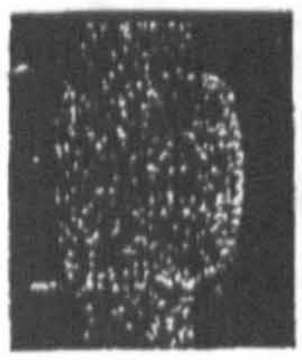	
Type 3	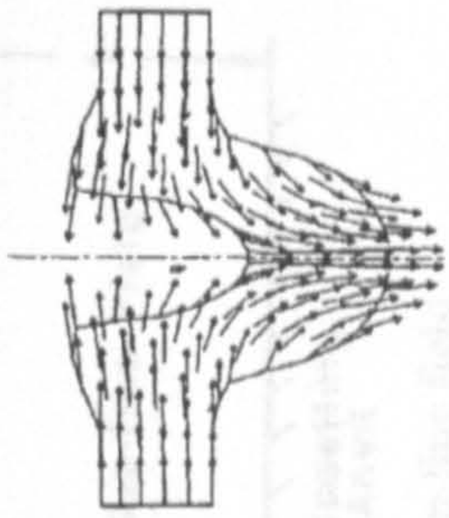		
Type 4		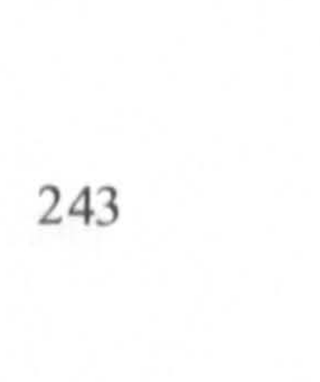	

Fig. 2.22 Comparison of FE simulation, experimental and physical modelling results [32]

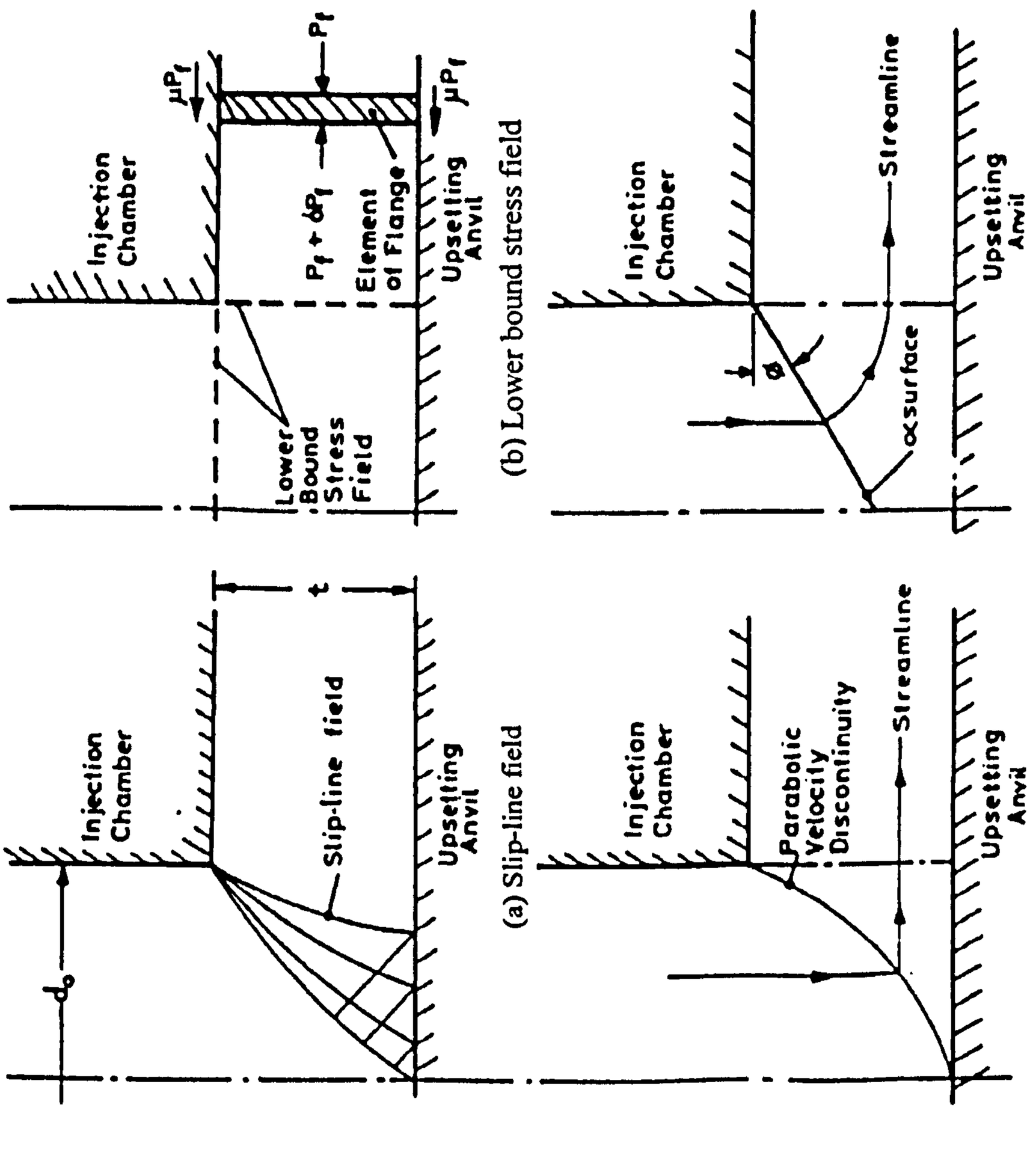

(a) Slip-line field

(b) Lower bound stress field

(c) Parabolic and streamline field

(d) α -surface and streamline field

Fig. 2.23 Velocity discontinuity surfaces for injection forging of solid billet [39, 49]

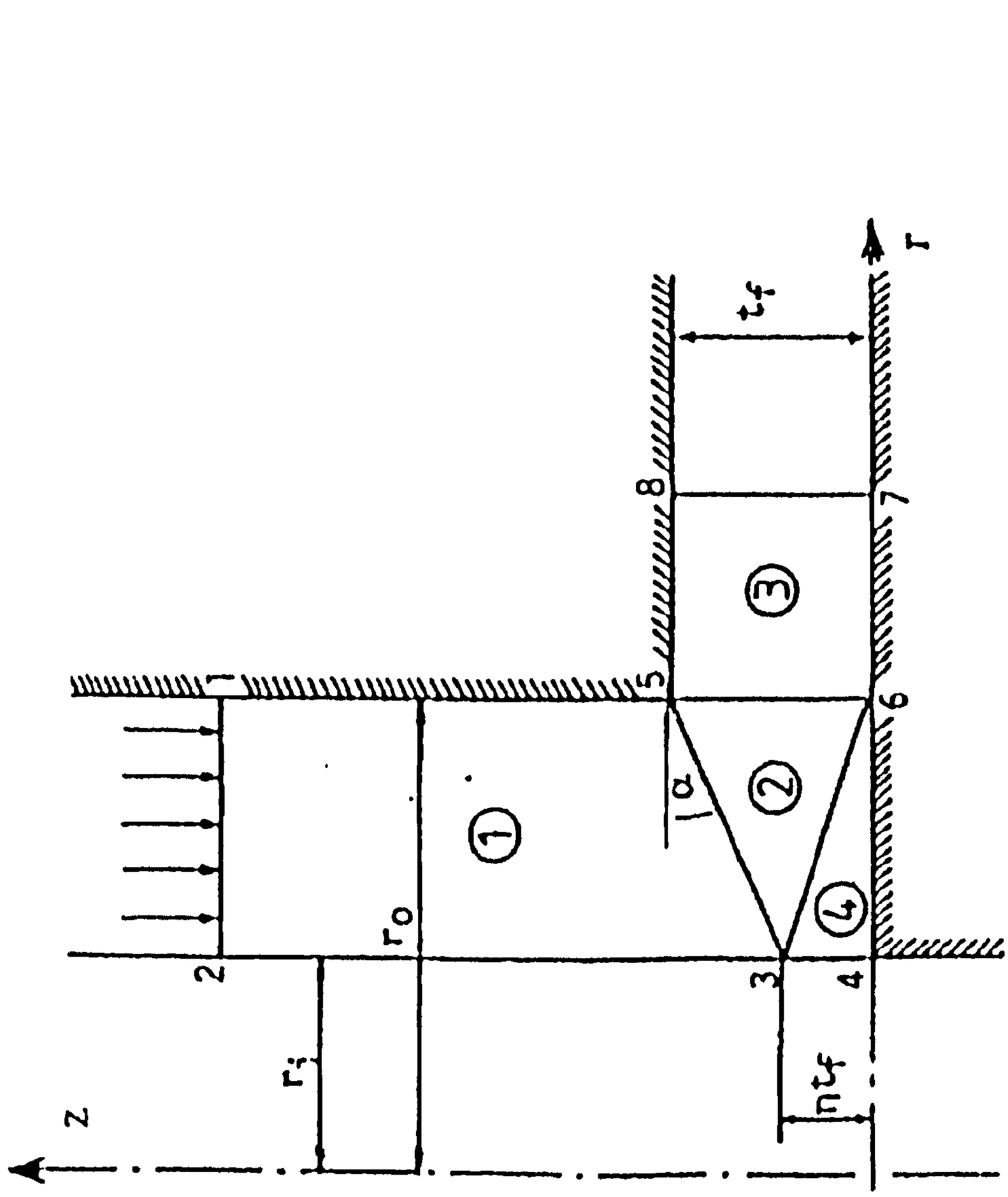

Fig. 2.24 Zones and velocity discontinuities for upper bound analysis of injection forging [111]

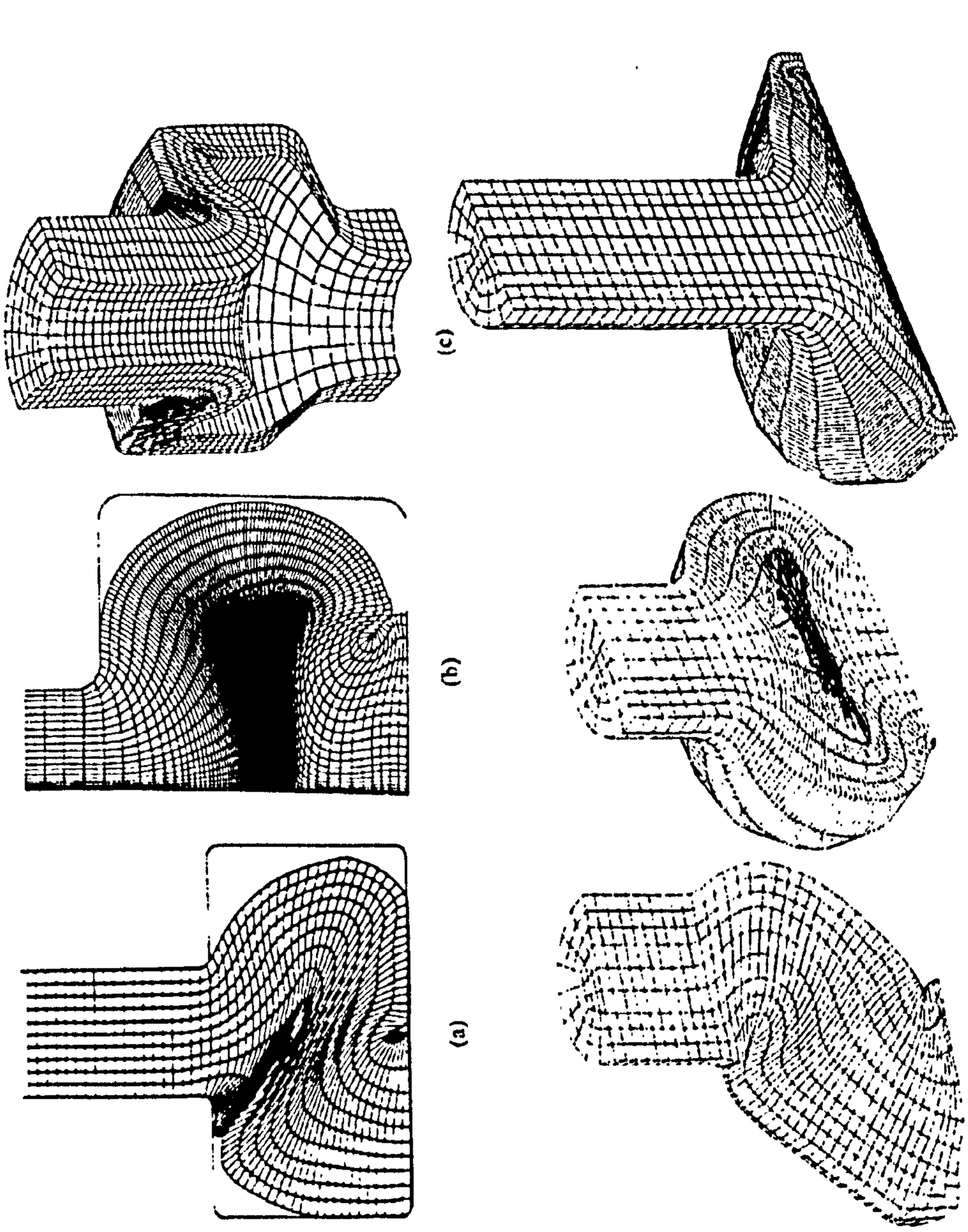

Fig. 2.25 Examples of numerical modelling (FEM) of injection forging [7]

Figures of Chapter 3

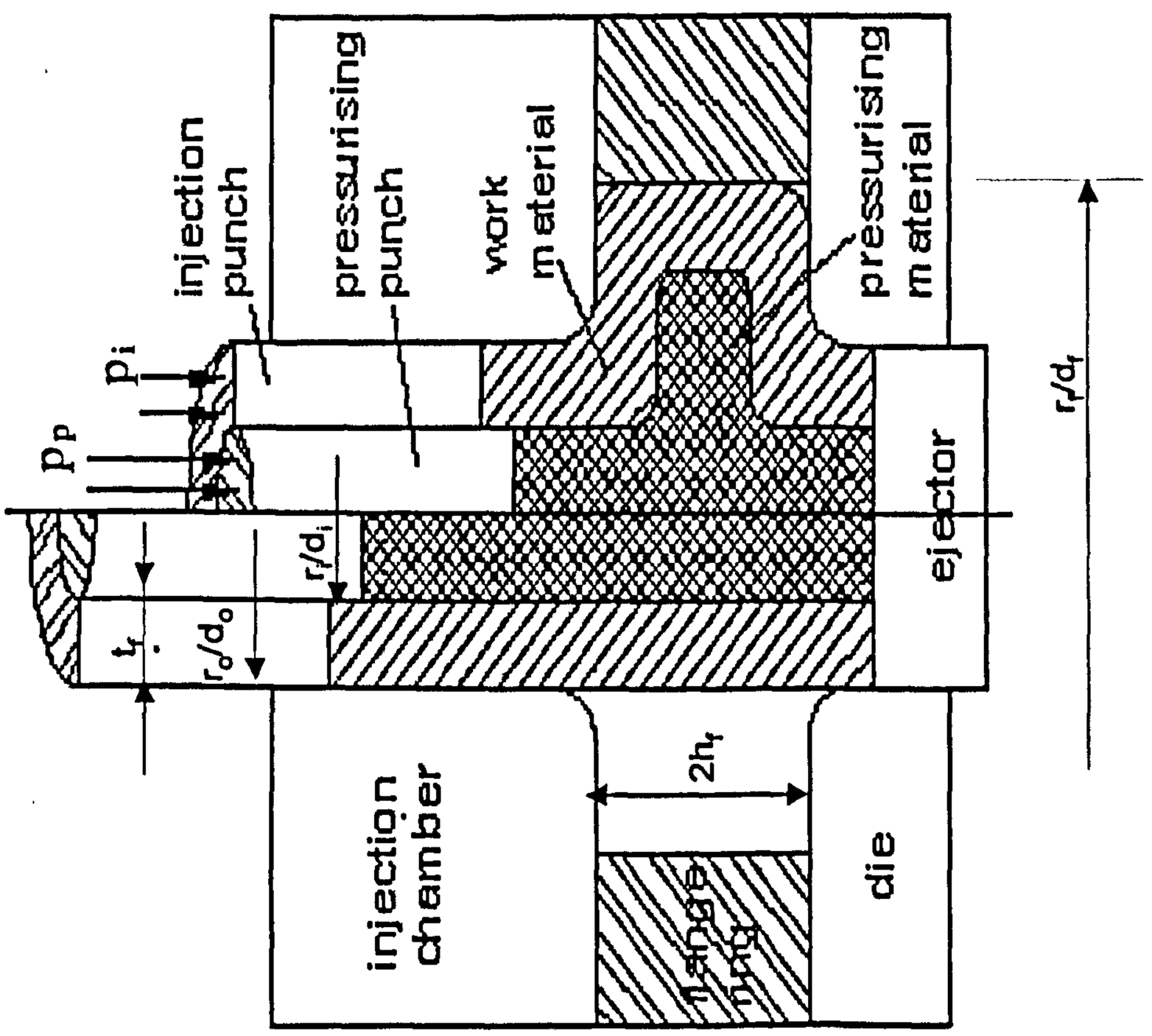

Fig. 3.1 The configuration for the beginning and the final stage of Pressure-assisted injection forging of thick-walled tubes

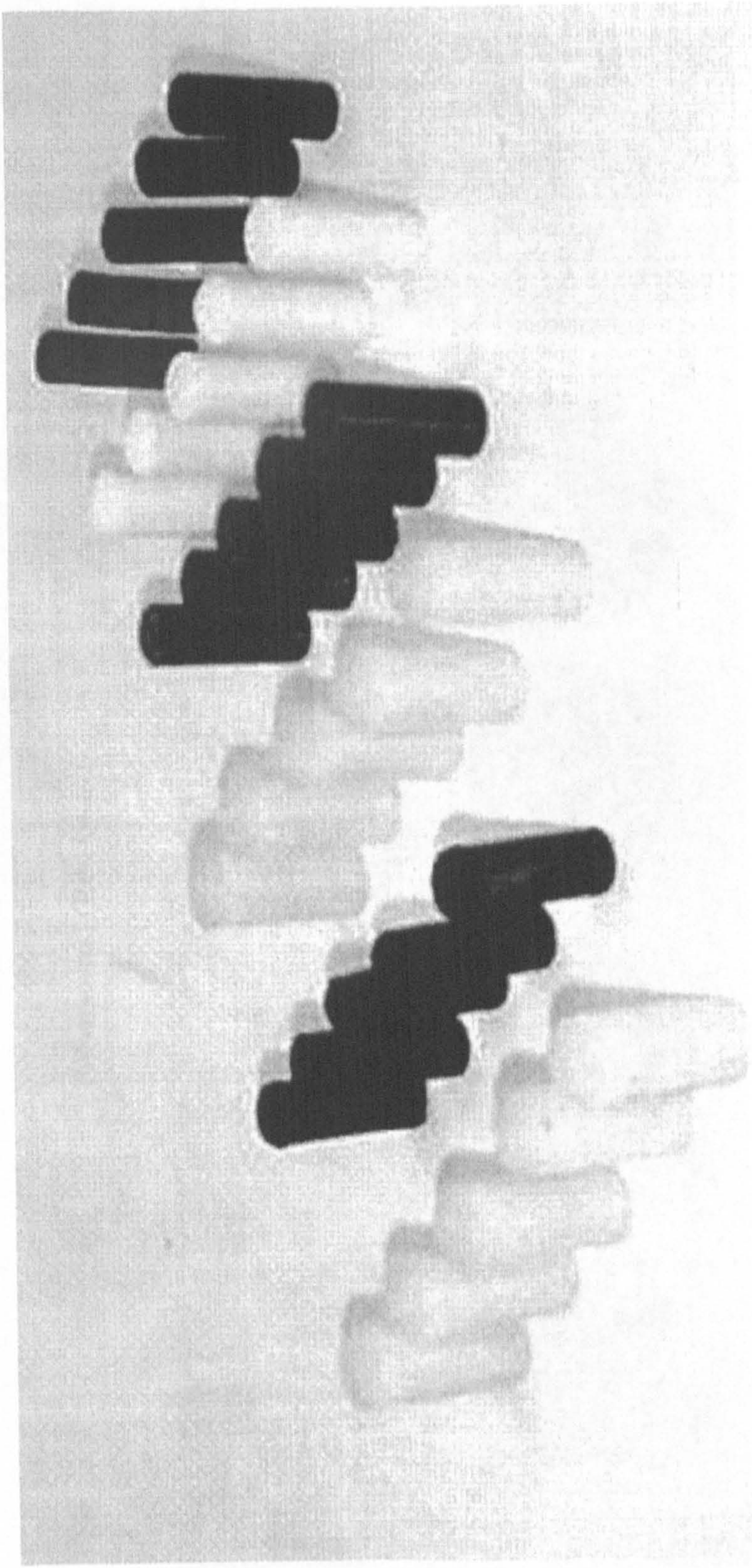

Fig. 3.2 The polymer rod specimens

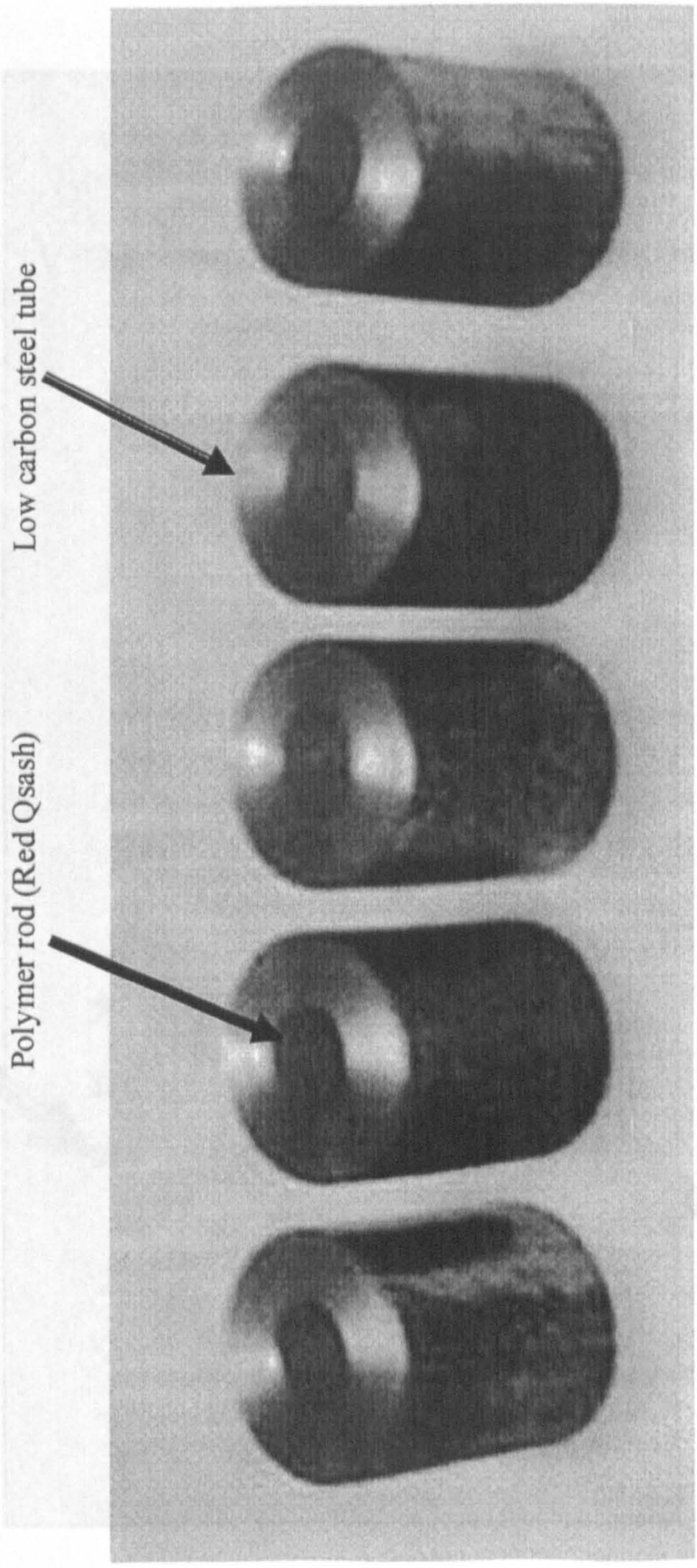

Fig. 3.3 Assembled specimens – compound cylinders

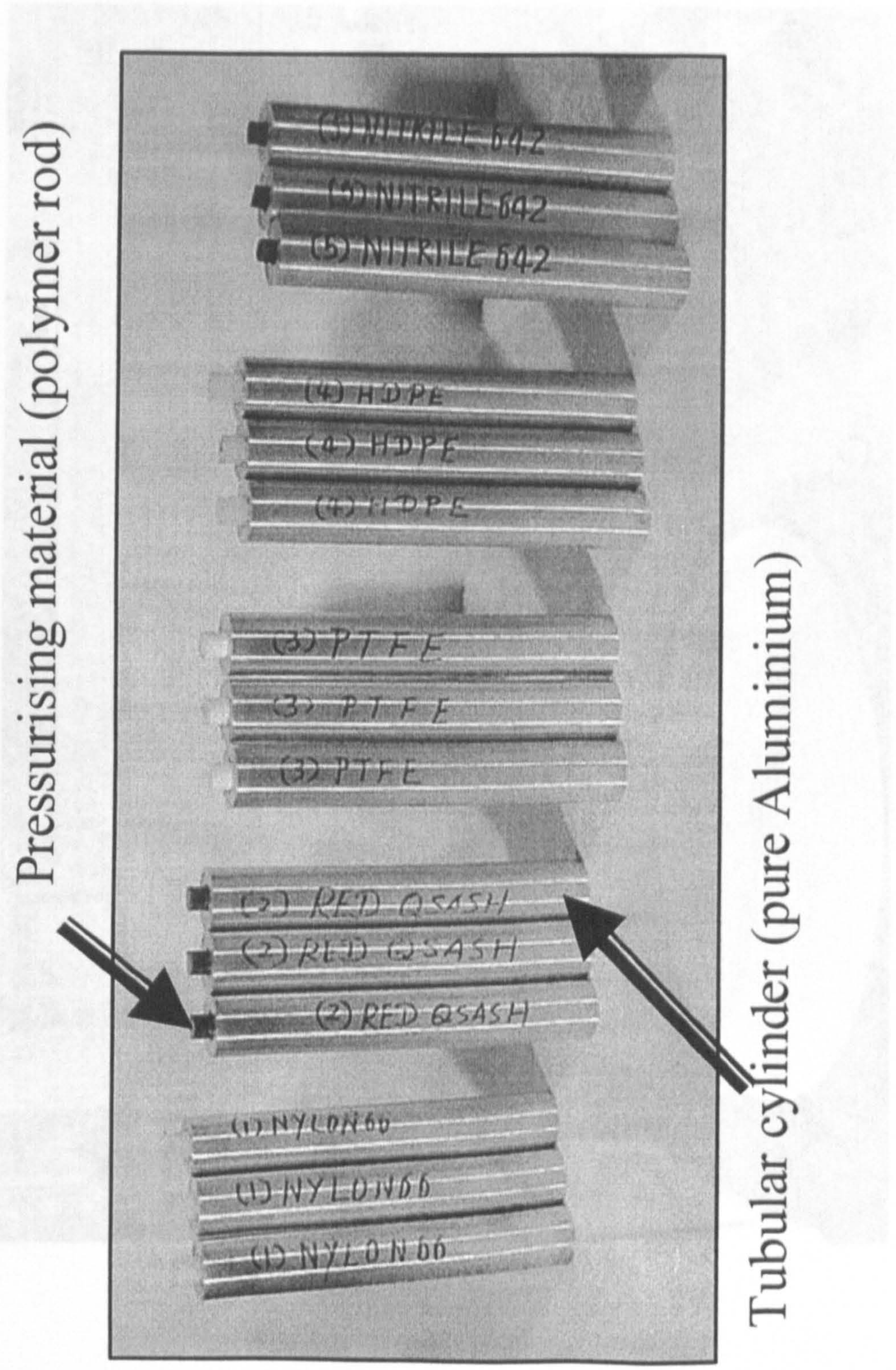

Fig. 3.4 The pecimens used in the forming of hollow flanges

Fig. 3.5 The equipment used by the experiment

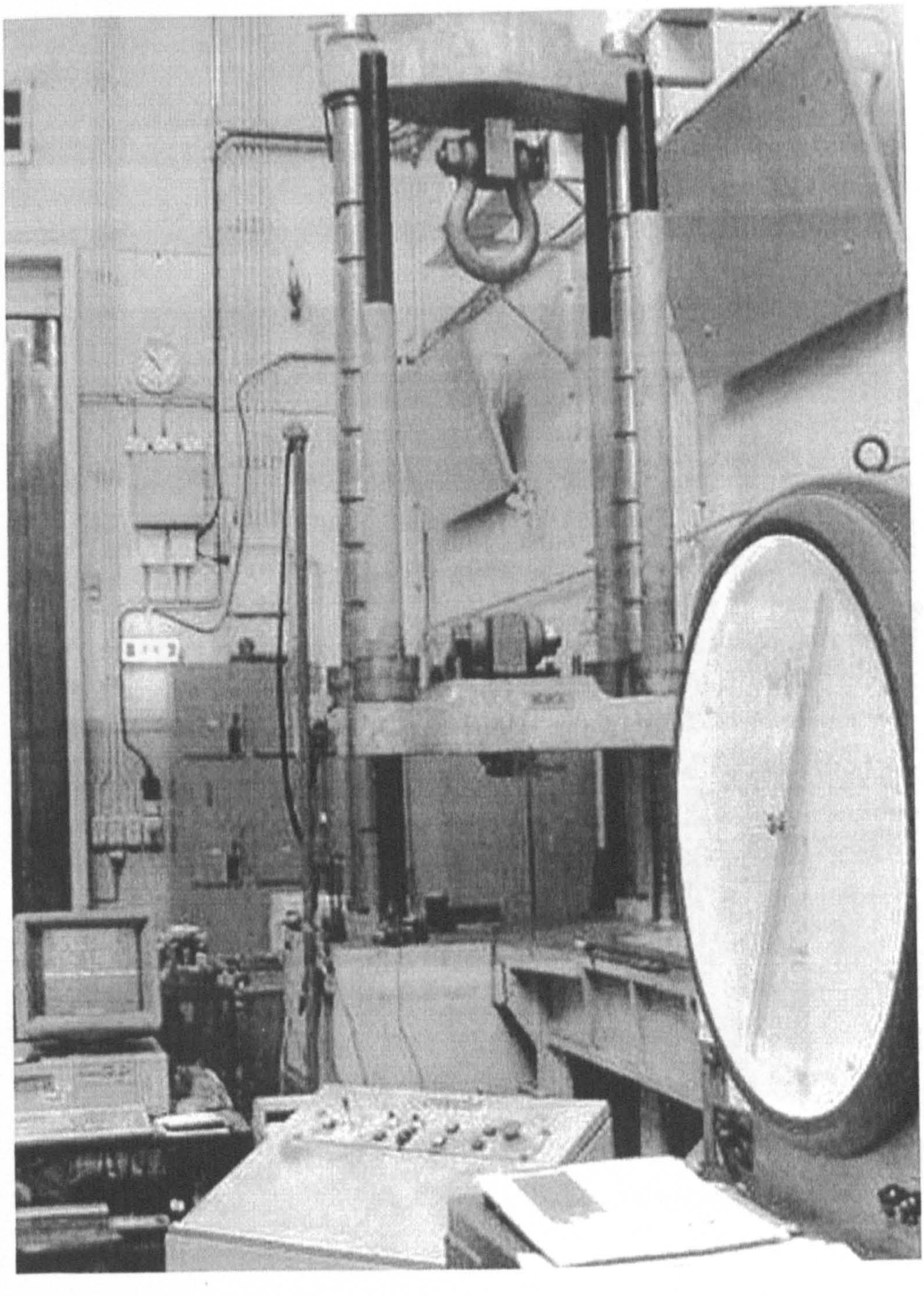

Fig. 3.5 The equipment used by the experiment

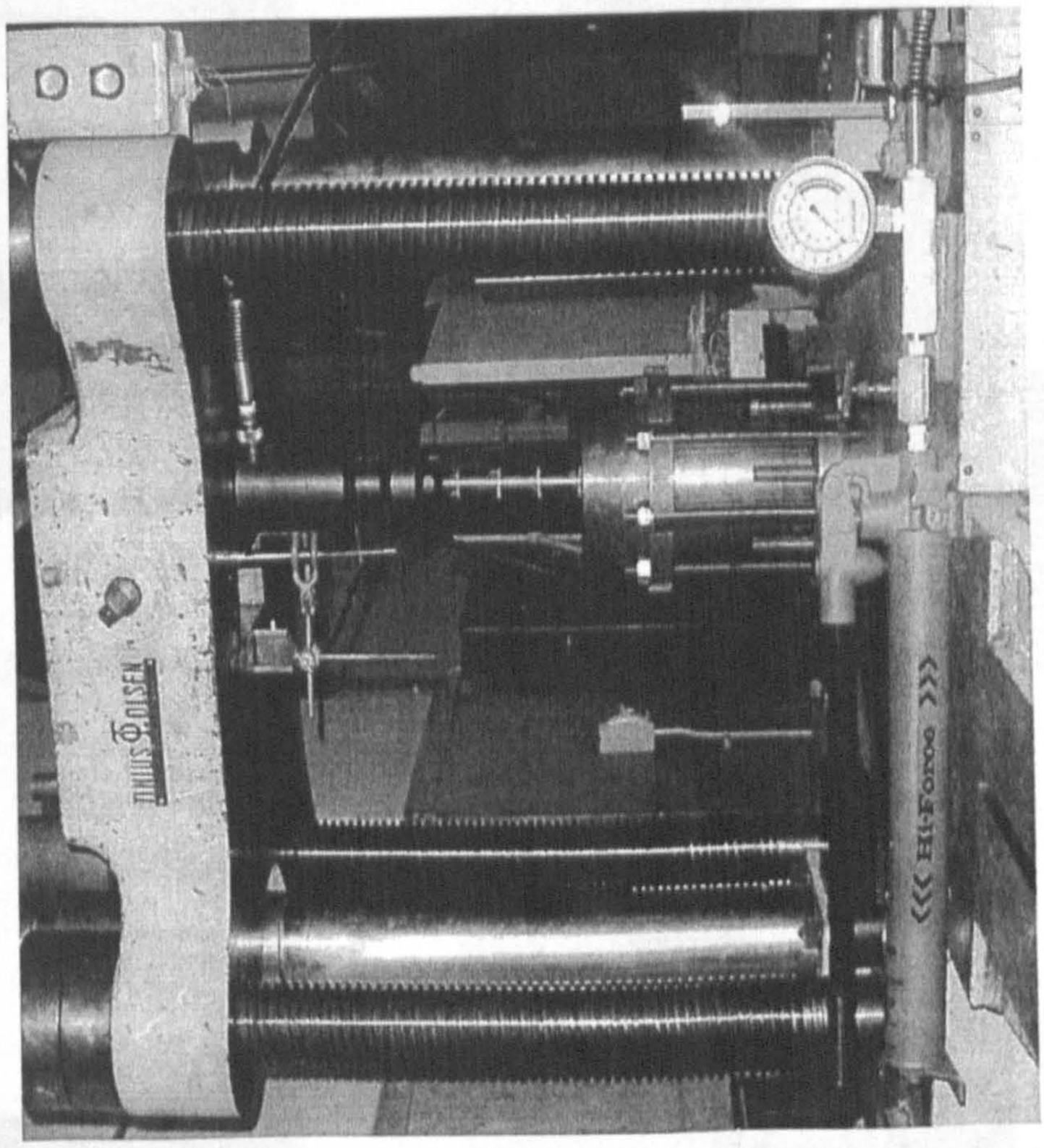

Fig. 3.6 The equipment used for the forming of hollow flanges with PAIF

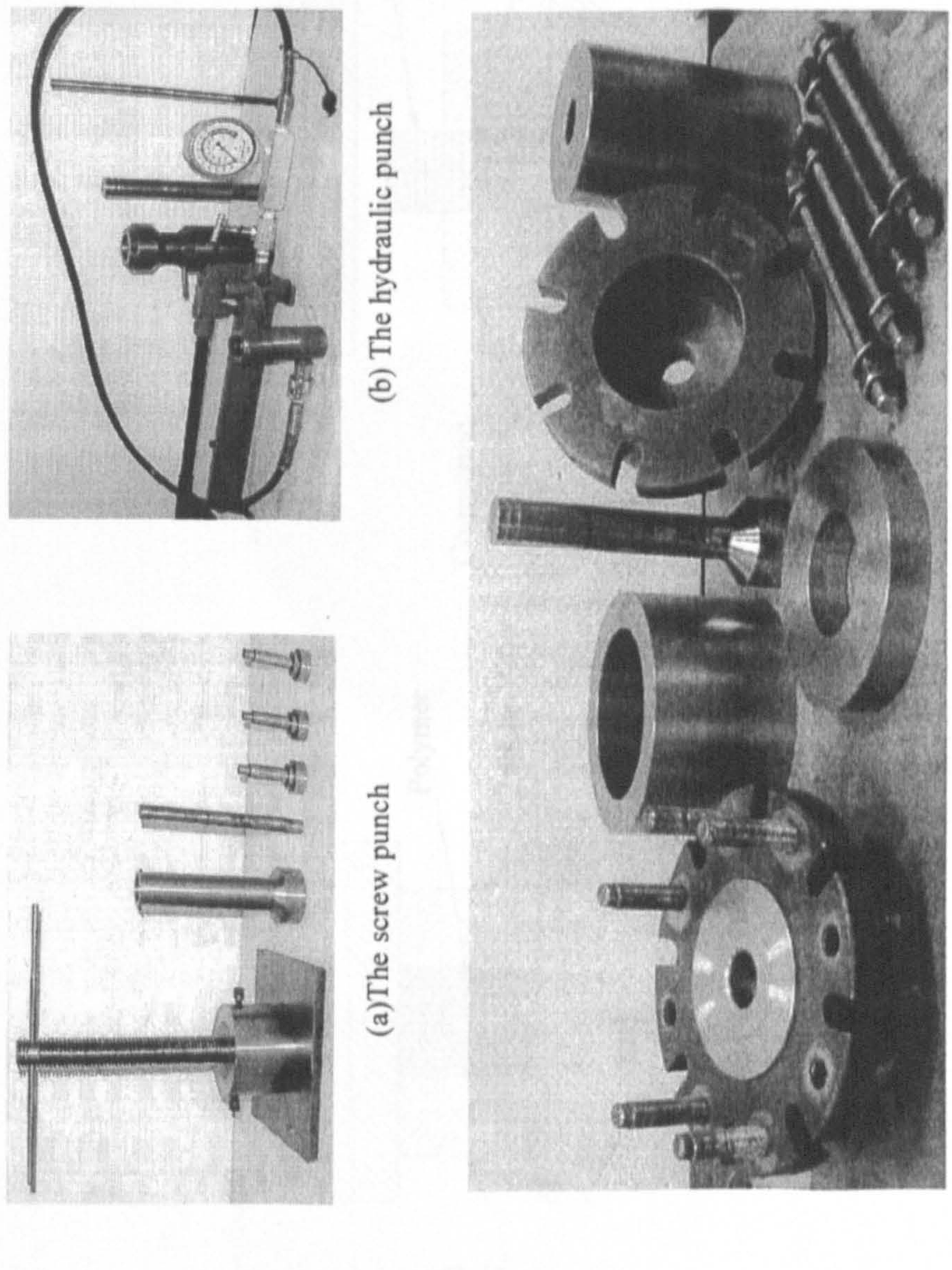

(a)The screw punch

(b) The hydraulic punch

(c) The forming dies

Fig. 3.7 Tools for the forming of hollow flanges

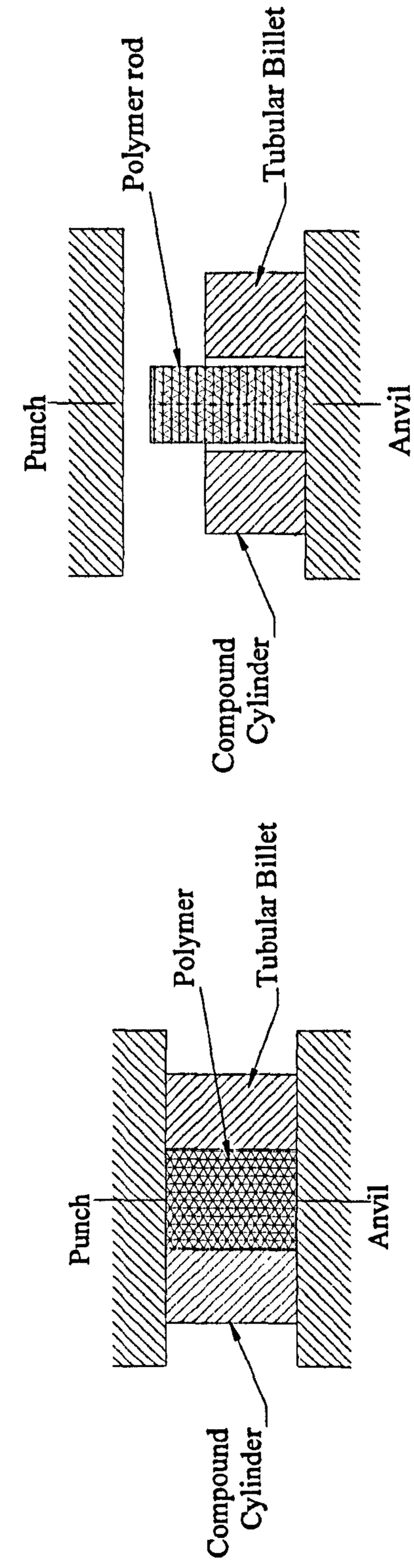

Fig. 3.8 A simplified configuration-compression of compound cylinder for testing of the pressurising materials

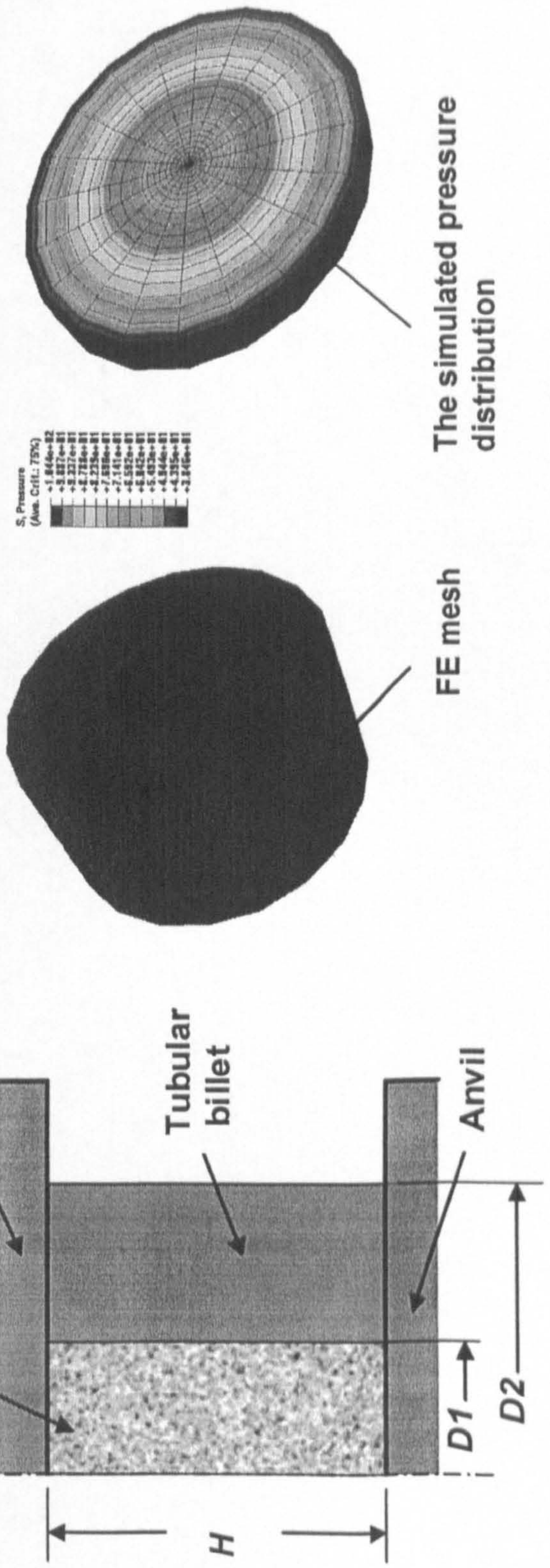

Fig. 3.9 The model of compression of compound cylinder and FE simulation

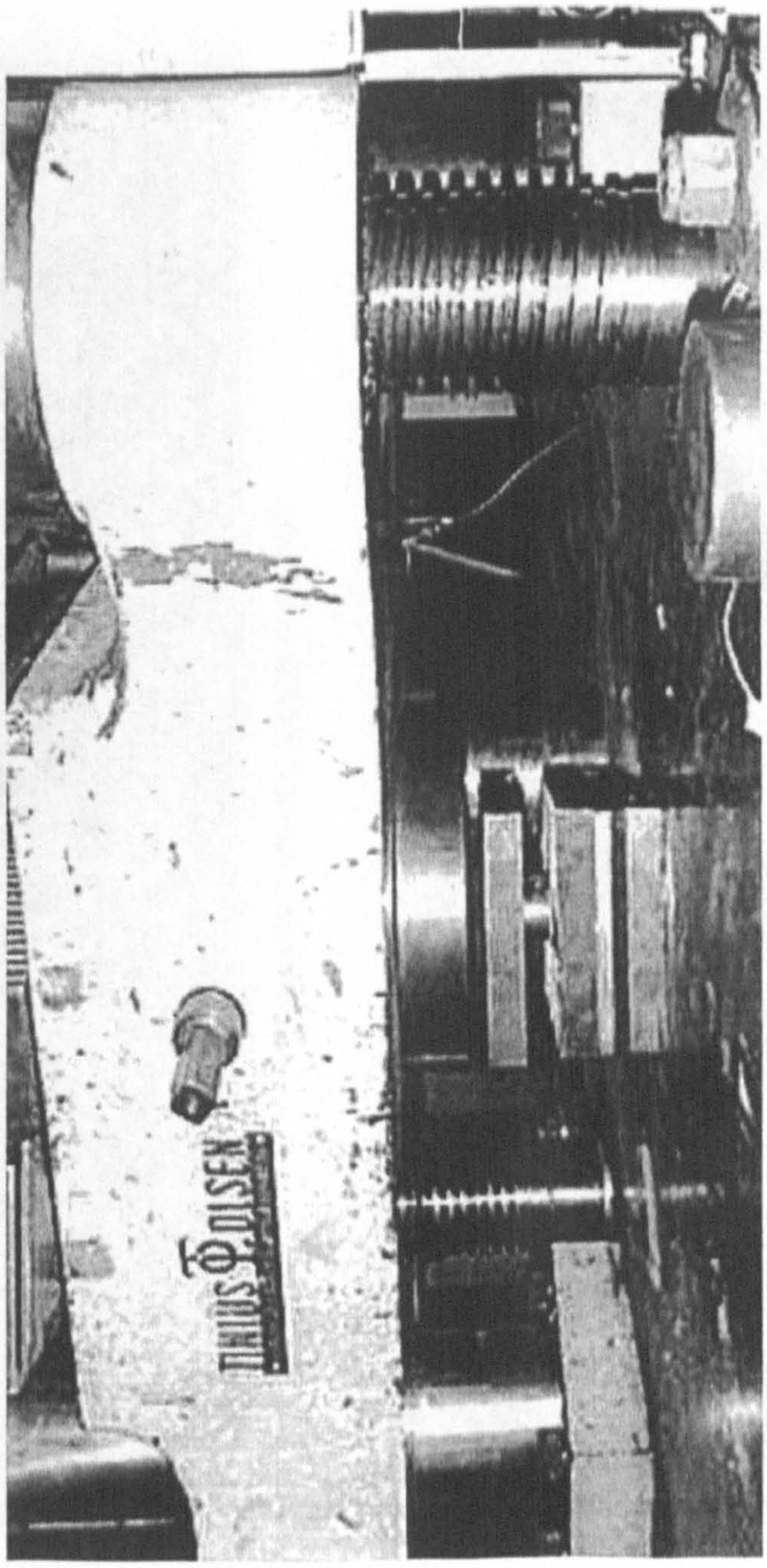

Fig. 3.10 The experimental set-up

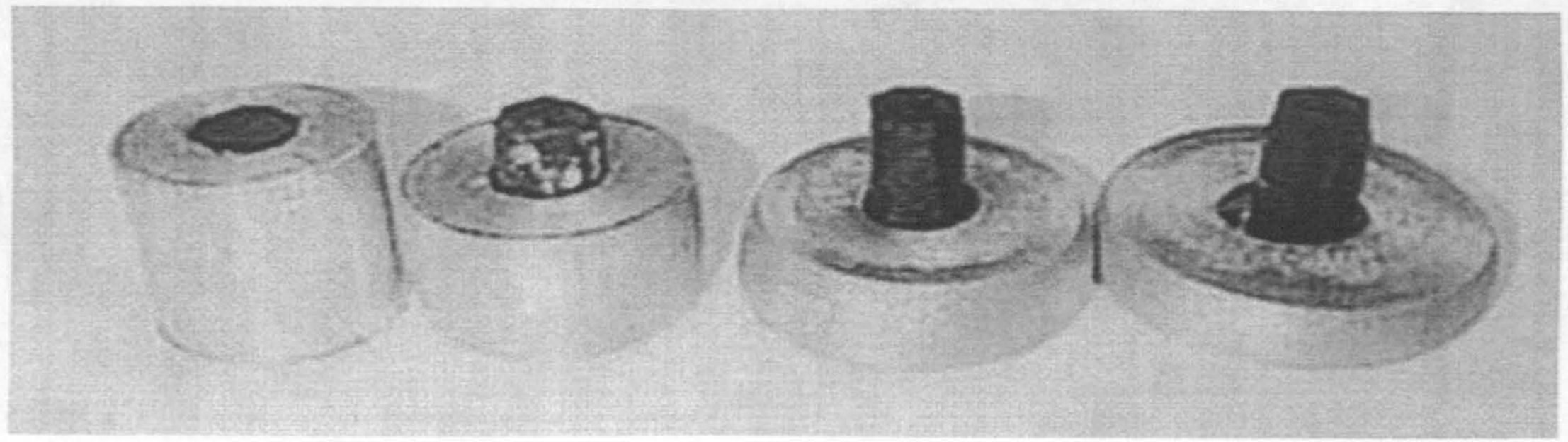

(a) Examples from the specimen group 7

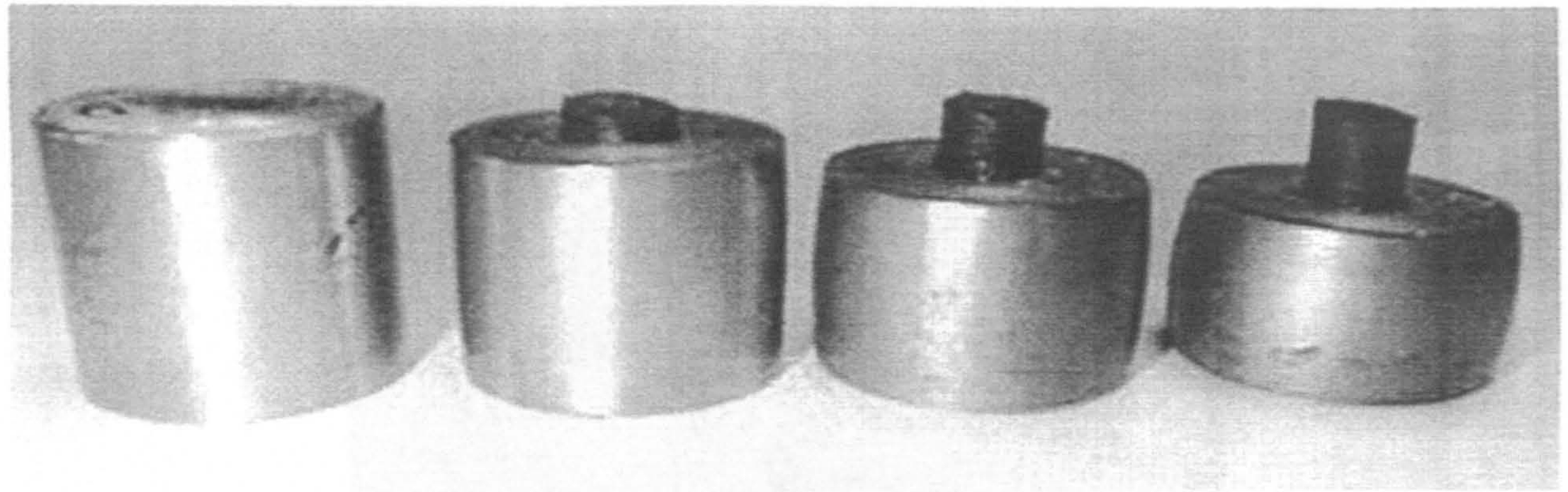

(b) Examples from the specimen group 5

Fig. 3.11 Specimens produced by the compression tests

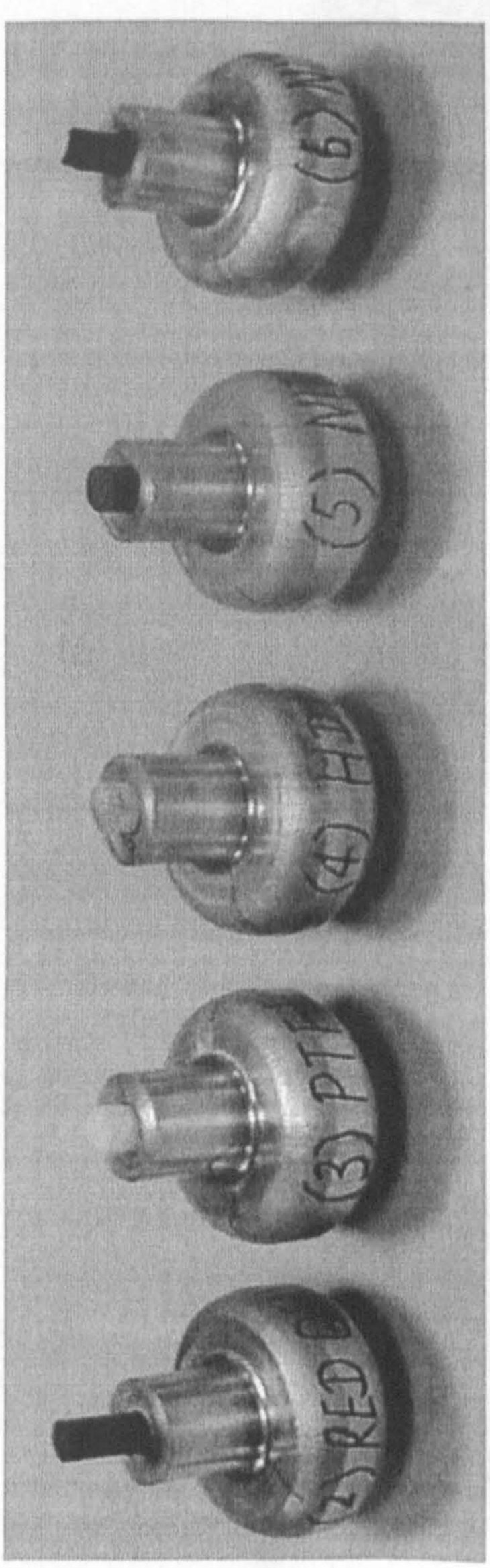

(a) Components with 85 mm diameter

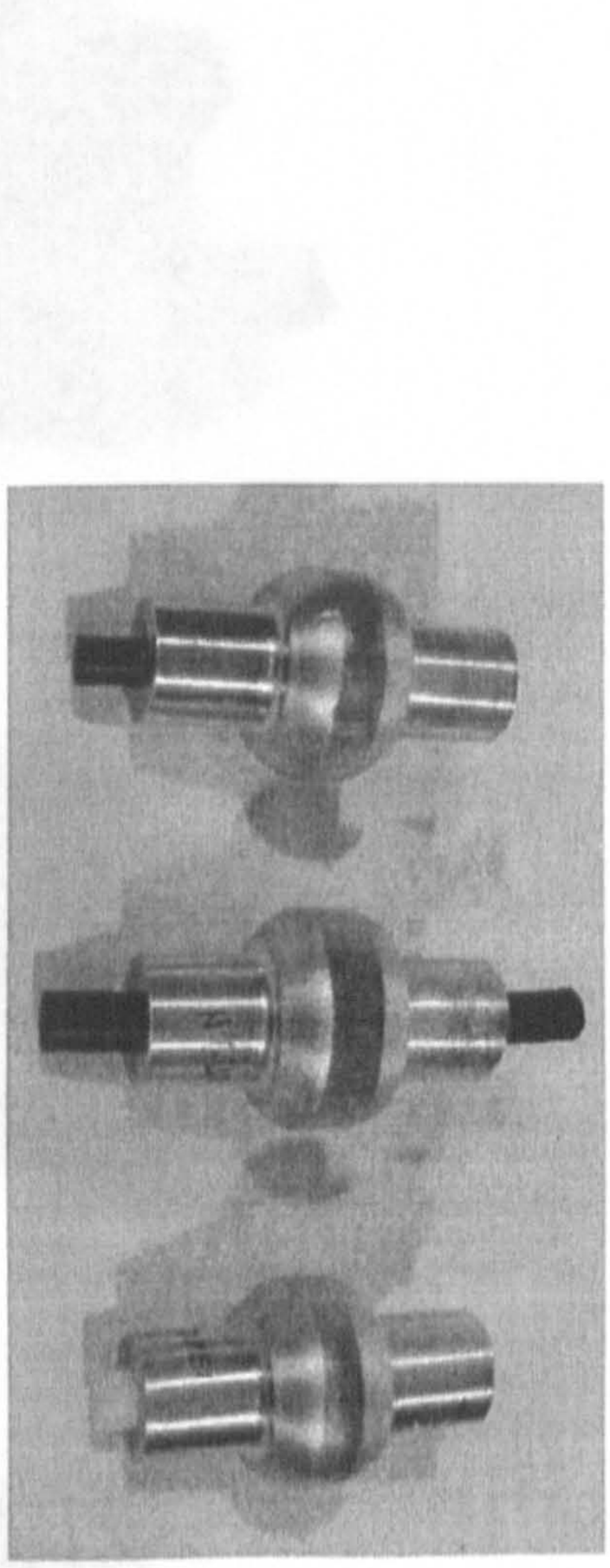

(b) Components with 60 mm diameter

Fig. 3.12 Specimens produced by tube forming experiment

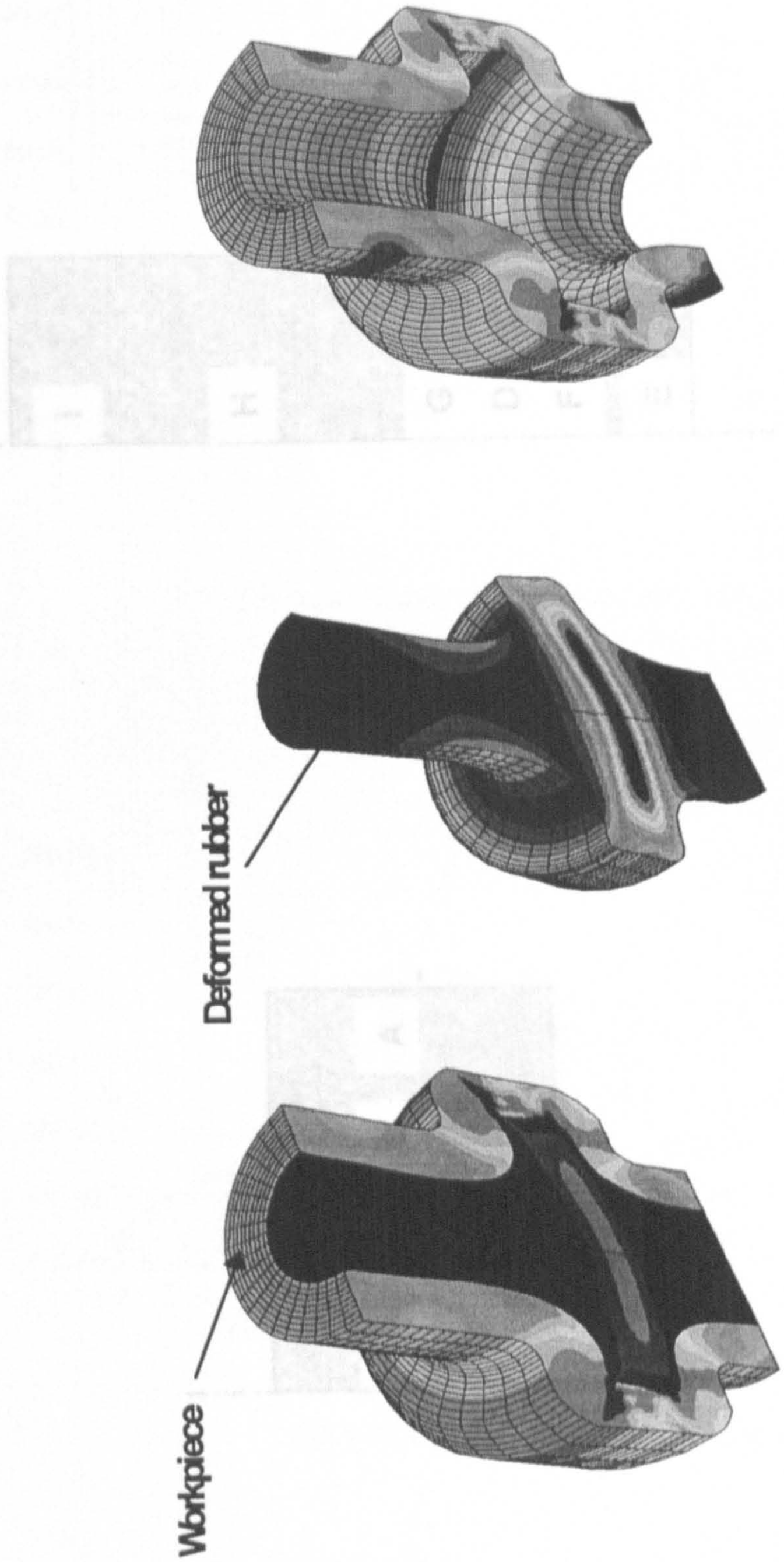

Fig. 3.13 FE simulation of forming of a hollow flange with PAIF

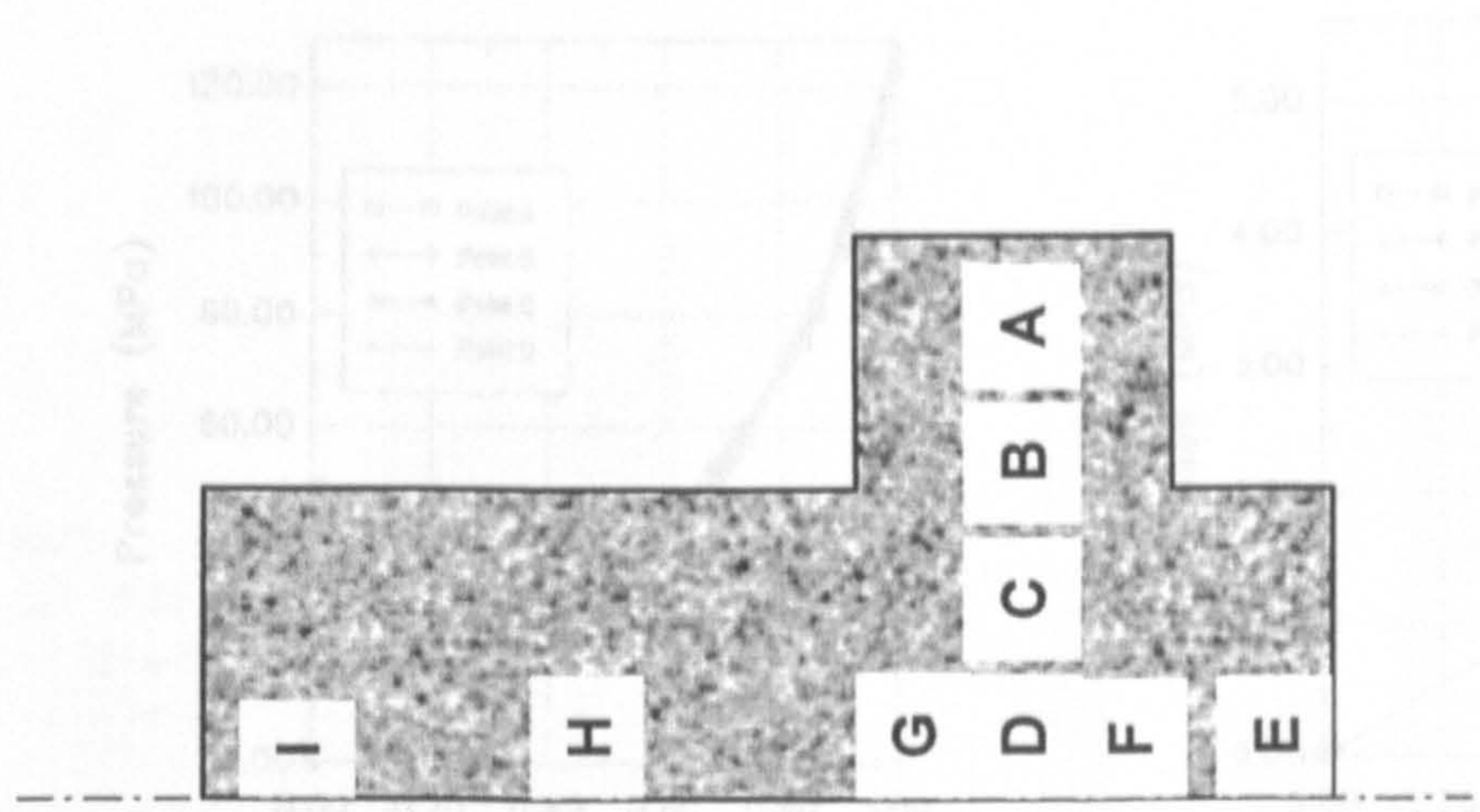

(b) The polymer specimen during the forming of a hollow flange

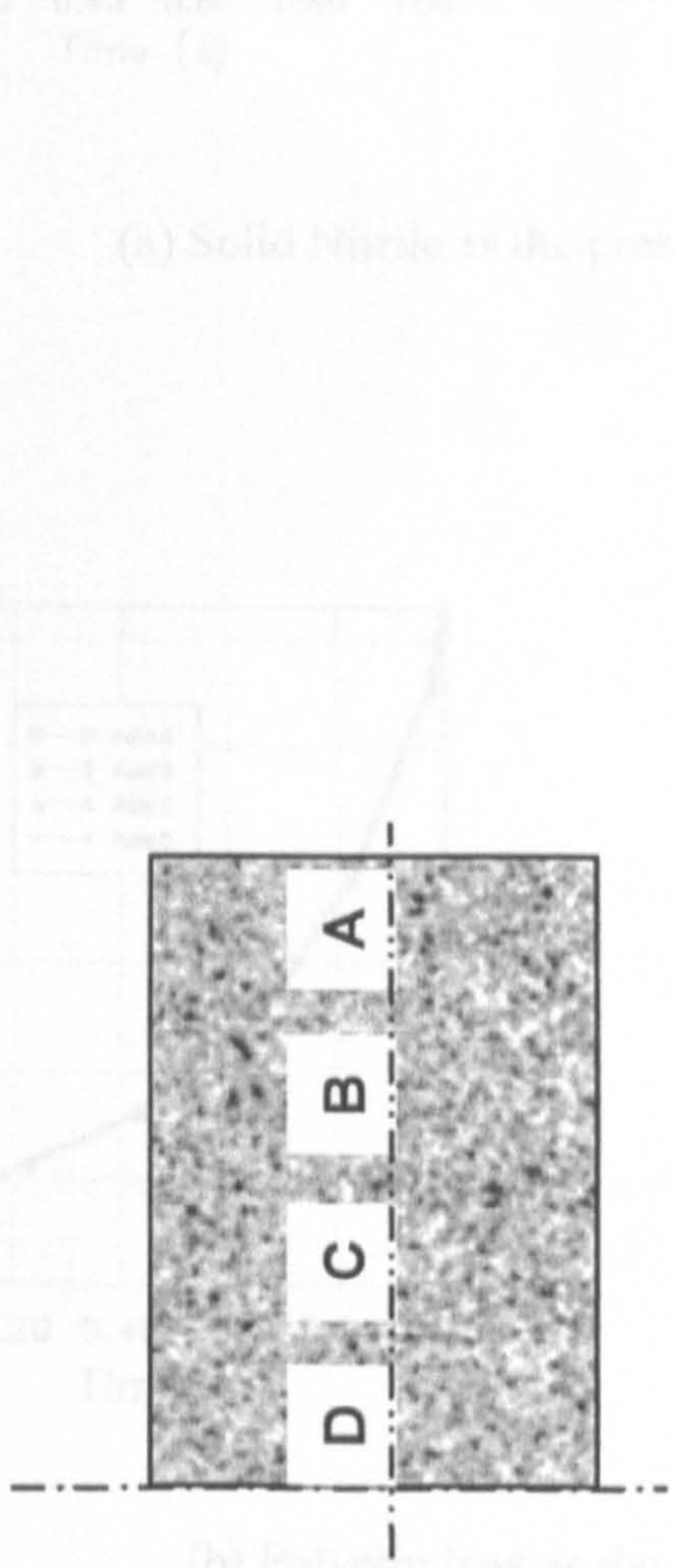

(a) The polymer specimen during the compression test

Fig. 3.14 Definition of locations for FE result output for assessing pressures and Miese stresses in the pressurising materials

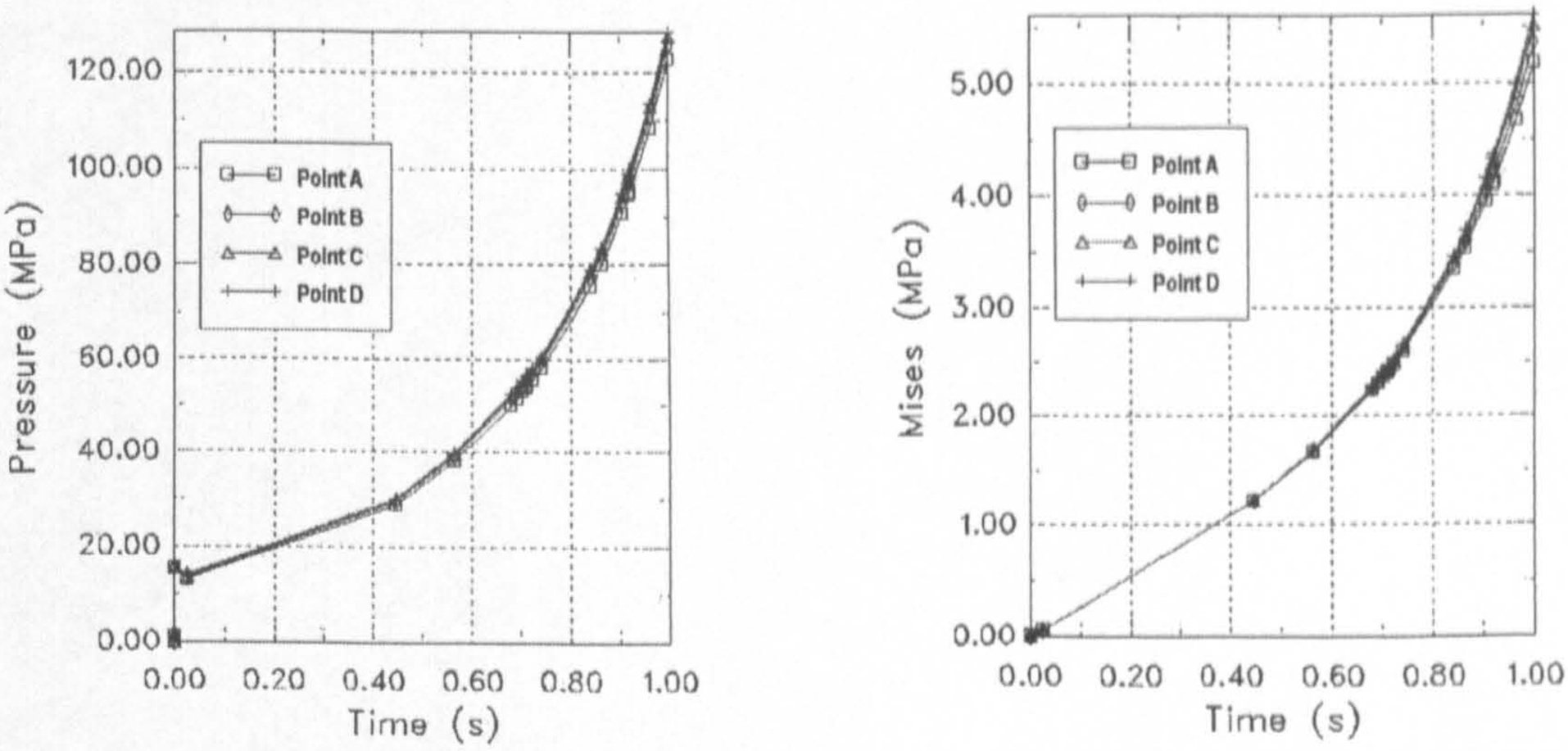

(a) Solid Nitrile as the pressurising material

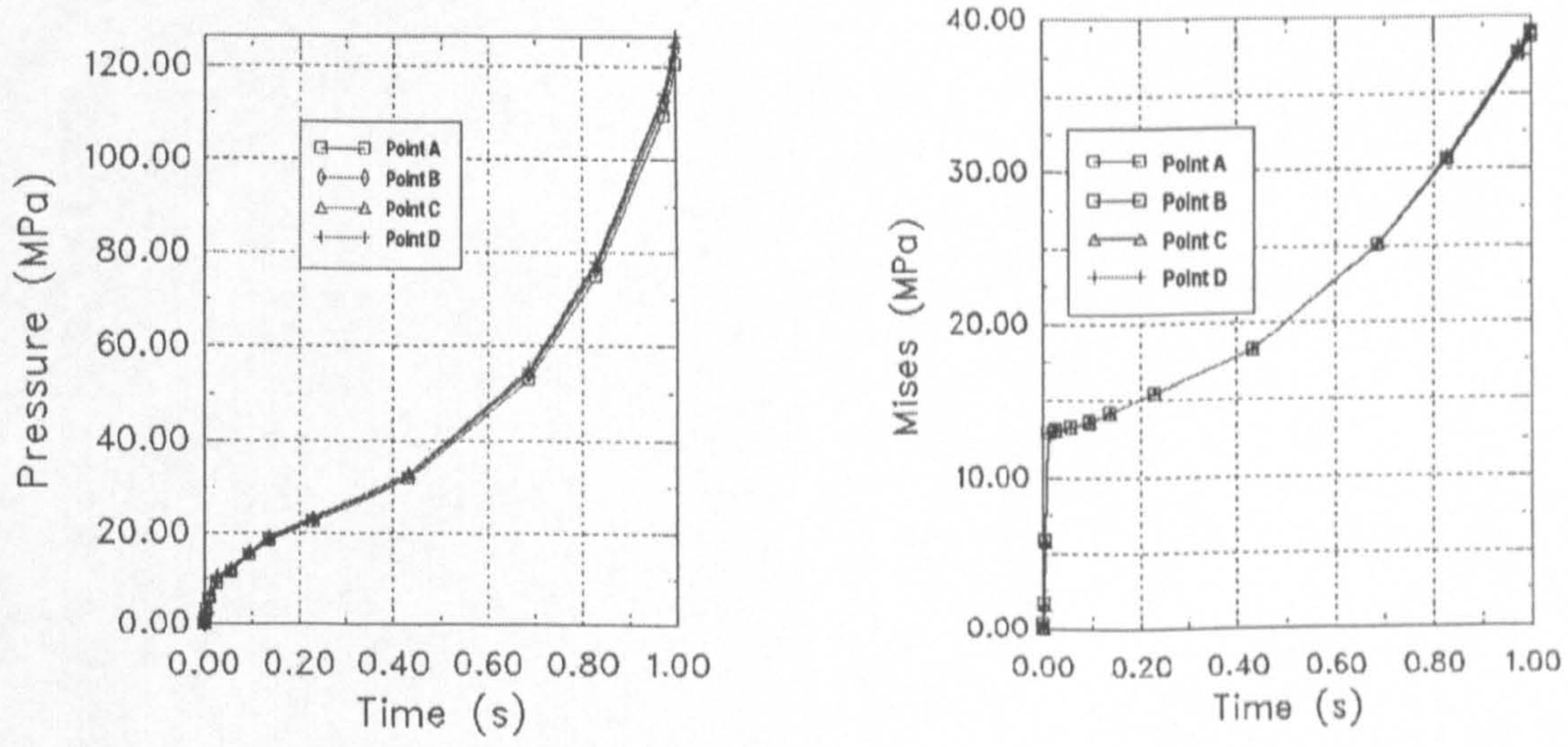

(b) Polyethylene as the pressurising material

Fig. 3.15 Pressure/Miese stress histories at four locations in the pressurising materials of the upsetting of the compound cylinders

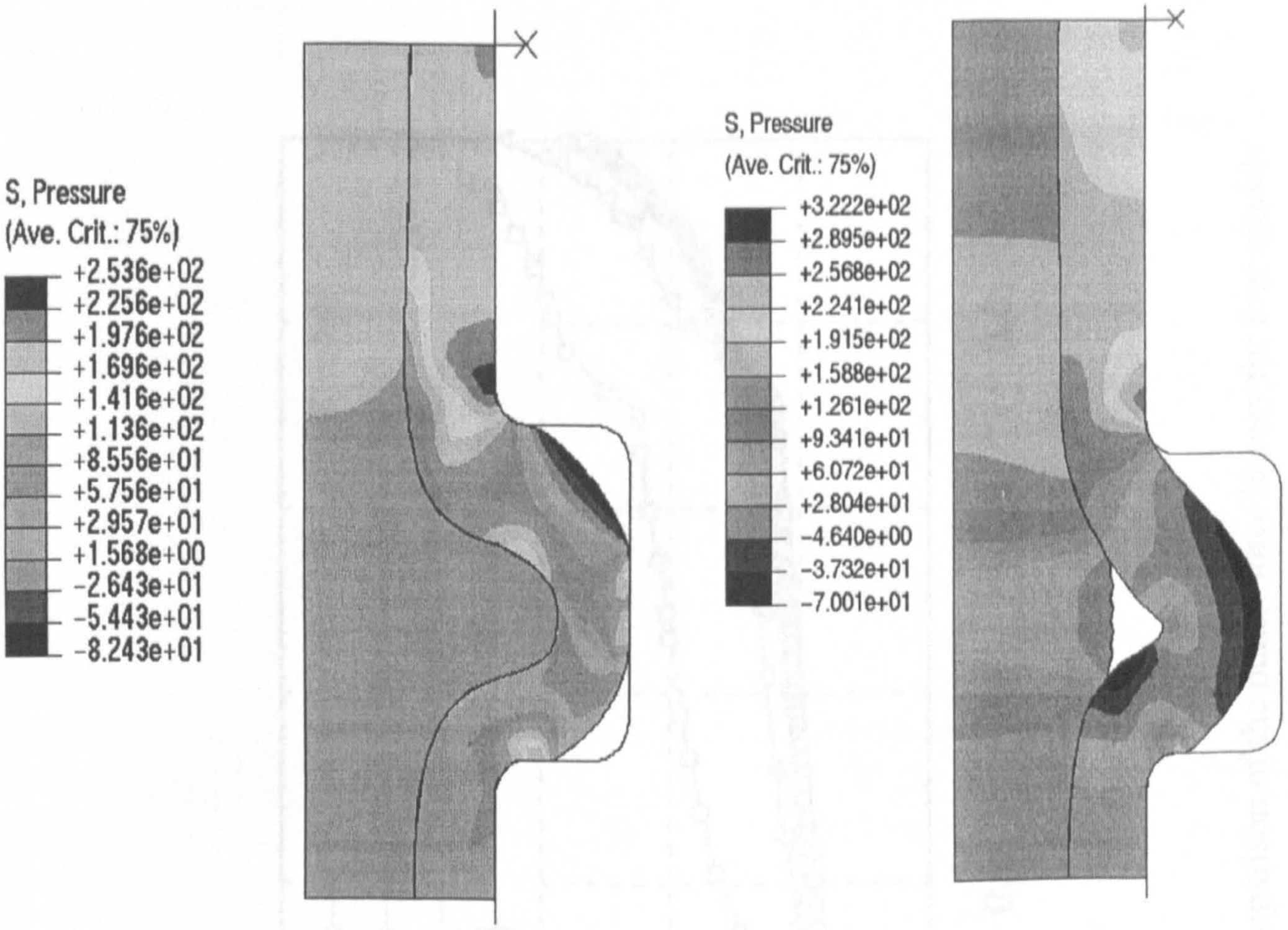

(a) The rubber incompressible during the forming of a hollow flange

(b) The rubber with a small compressibility during the forming of a hollow flange

Fig. 3.16 FE simulation for examining feasibility of the polymers functioning as a pressurising material for PAIF

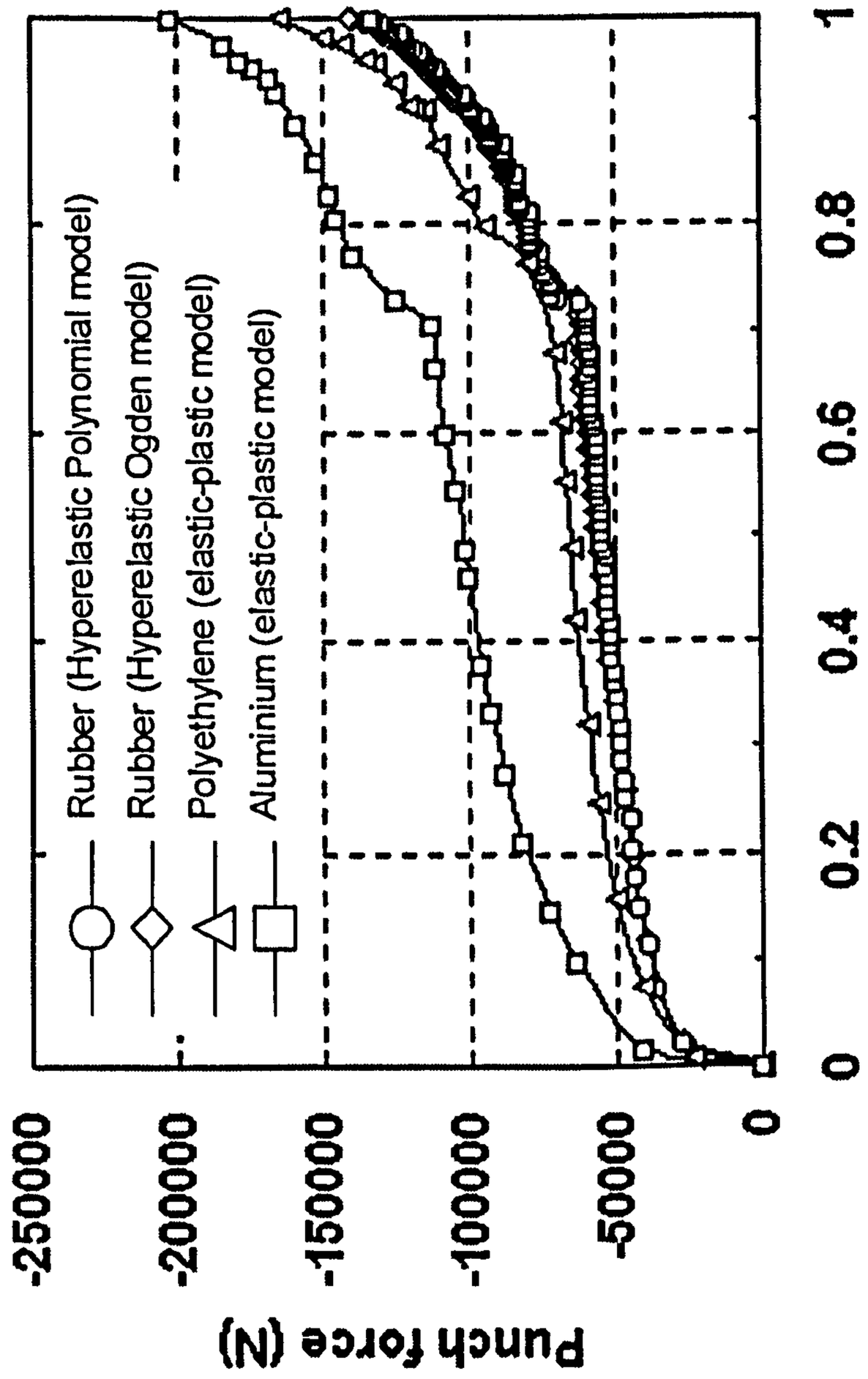

Fig. 3.17 Comparison of the punch-force history for four models

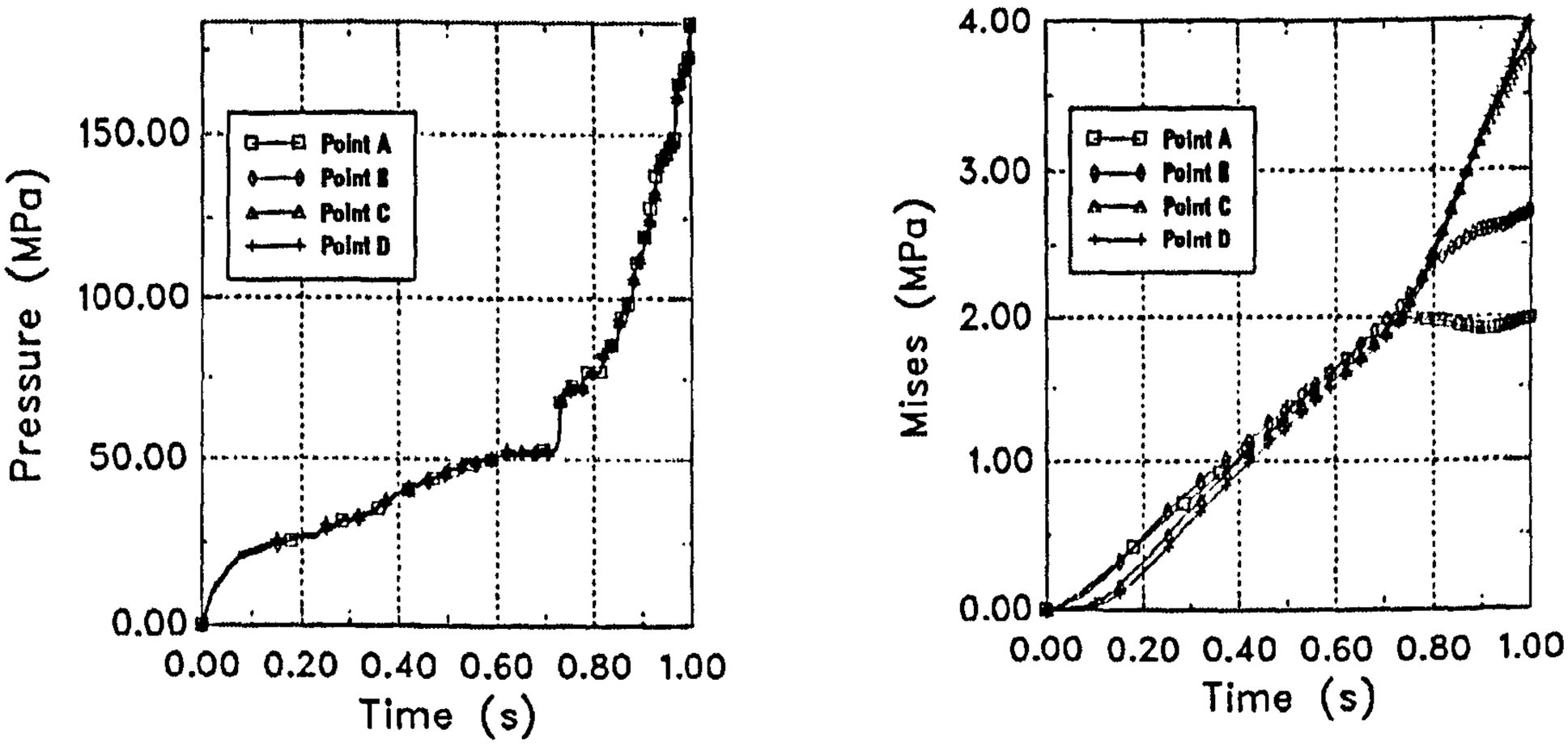

(a) During loading (forming)

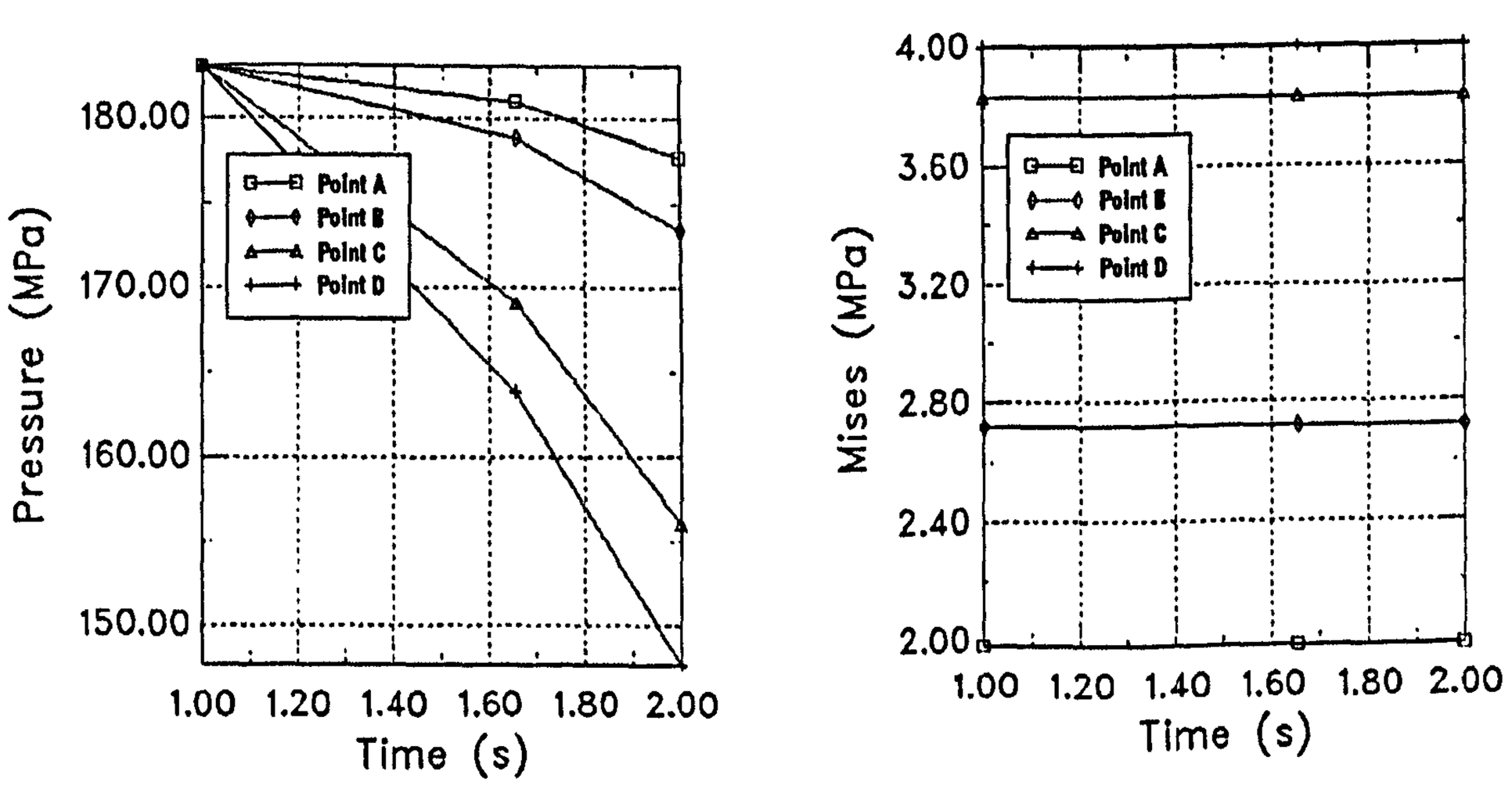

(b) During unloading (punch retract)

Fig. 3.18 Pressure/Miese stress histories at four locations (A-D) in the pressurising materials of the forming of a hollow flange

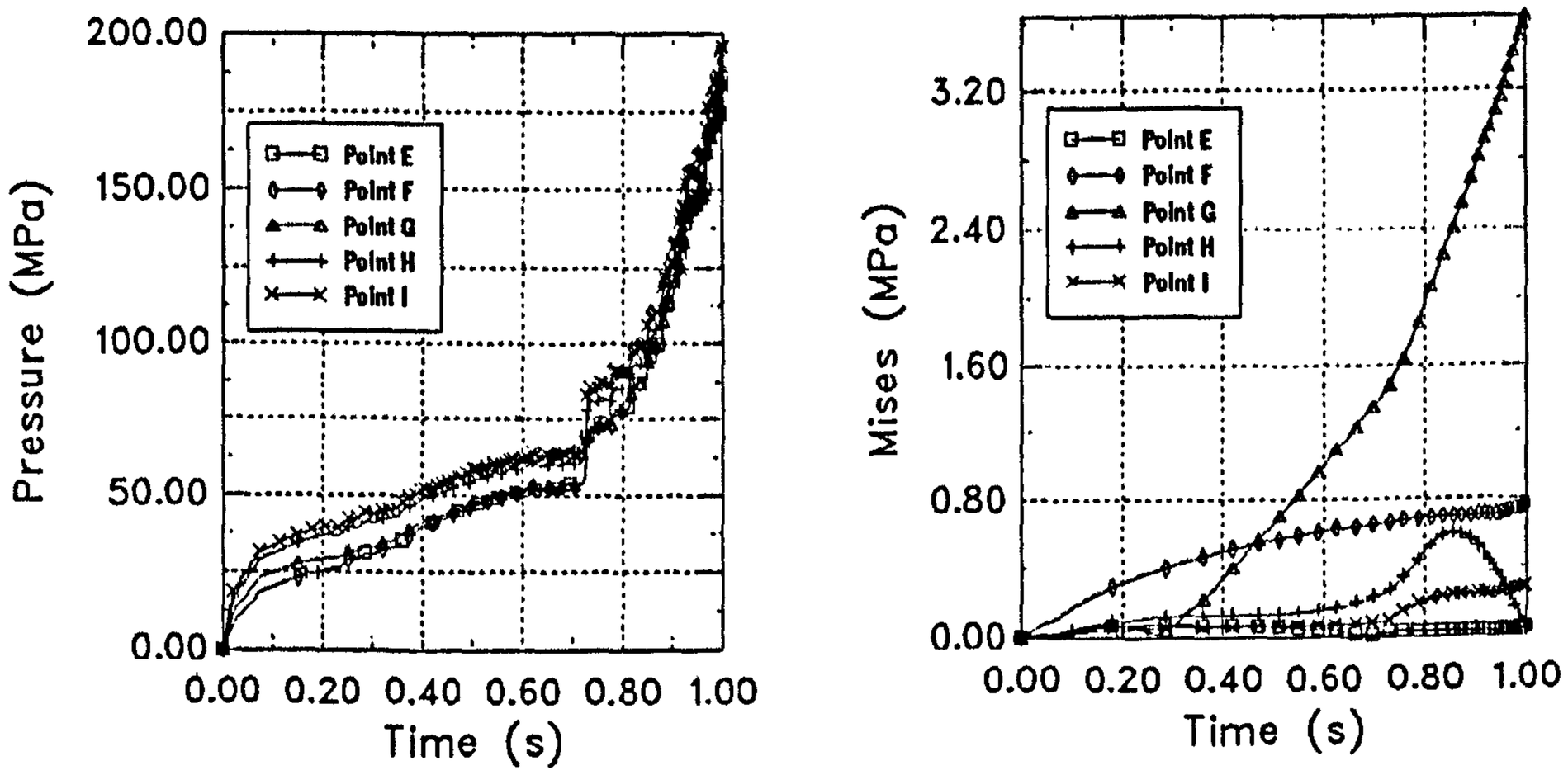

(a) During loading (forming)

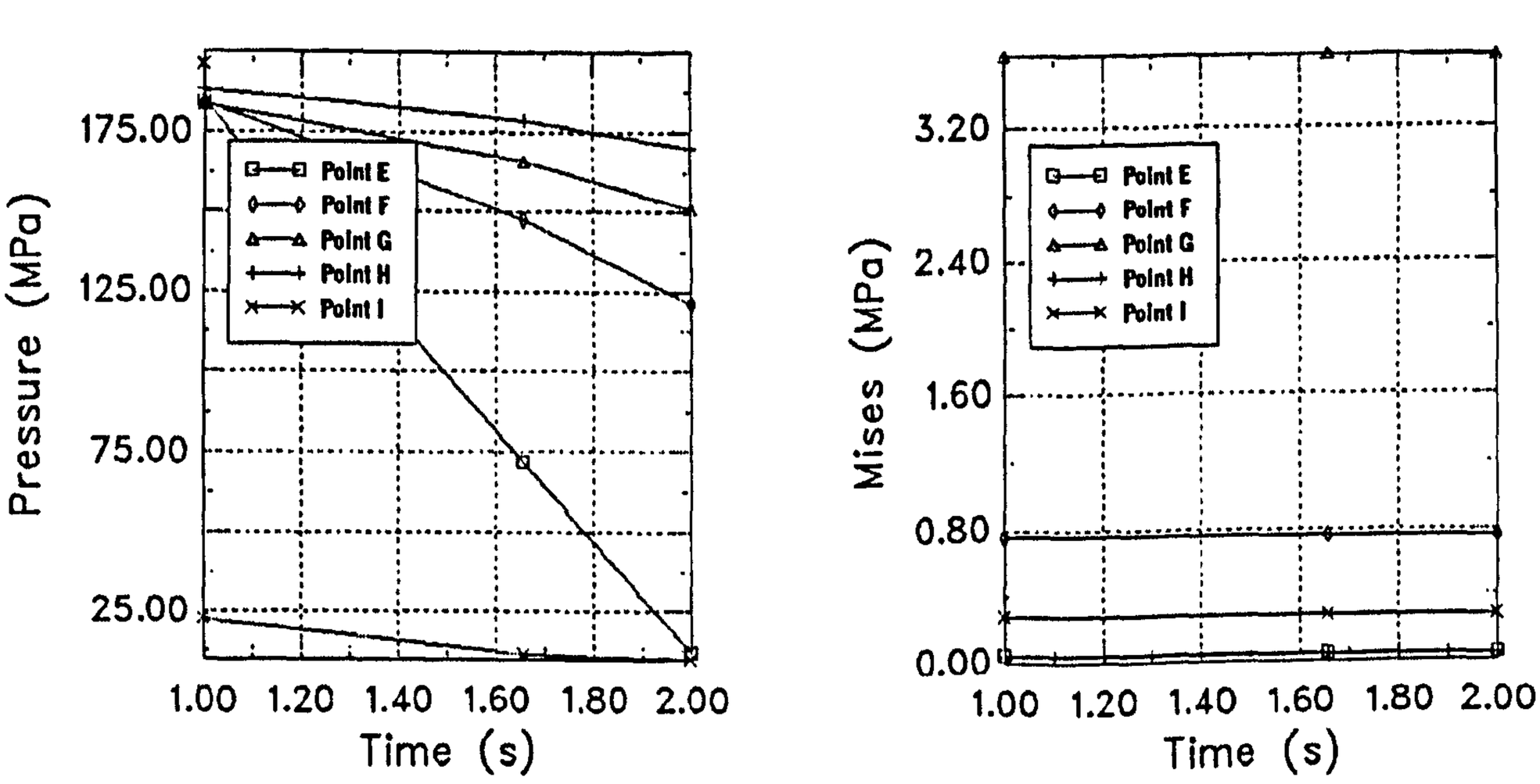

(b) During unloading (punch retract)

Fig. 3.19 Pressure/Miese stress histories at five locations (E-I) in the pressurising materials of the forming of a hollow flange

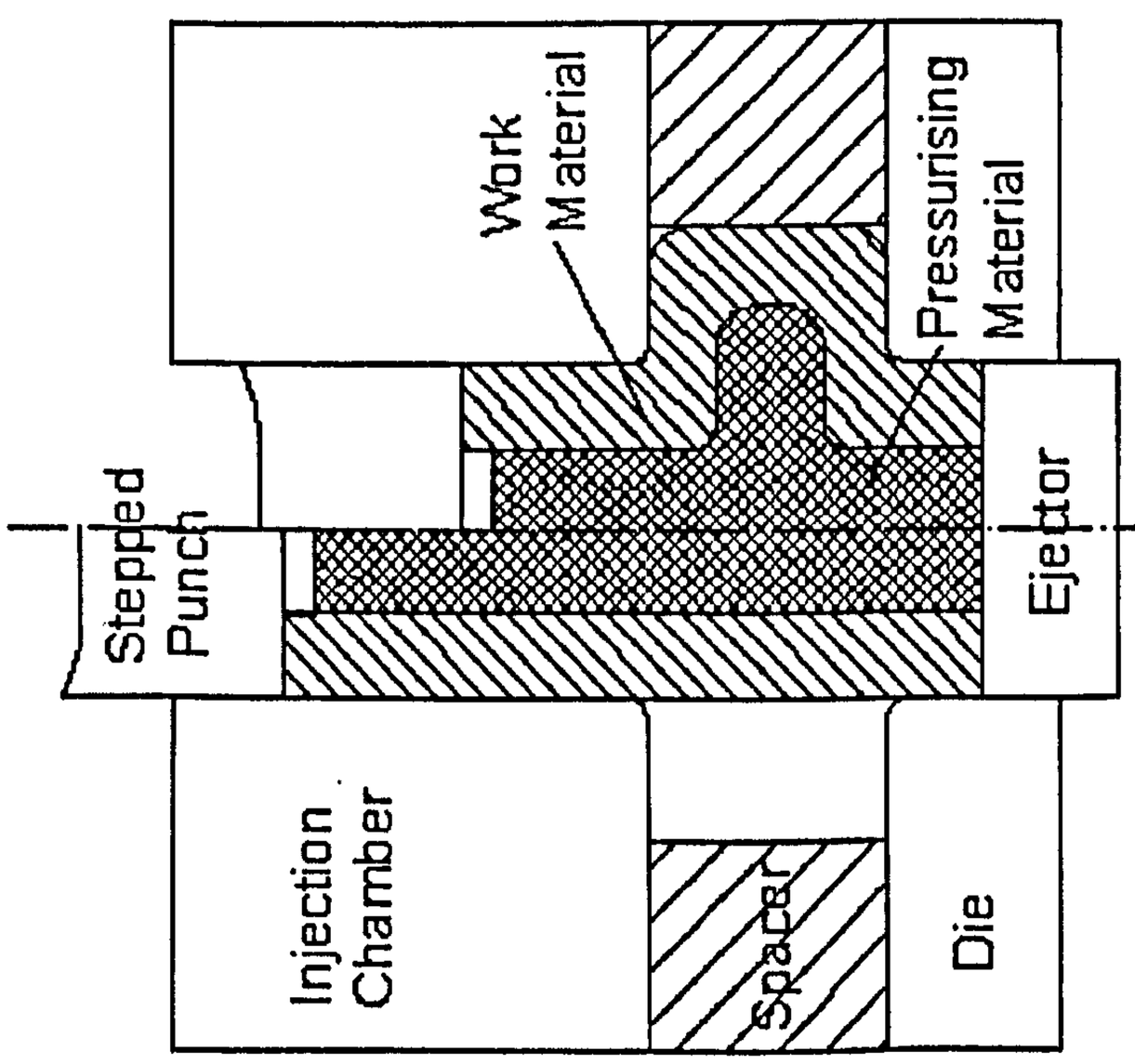

Fig. 3.20 The simplified configuration of Pressure-assisted injection forging of thick-walled tubes

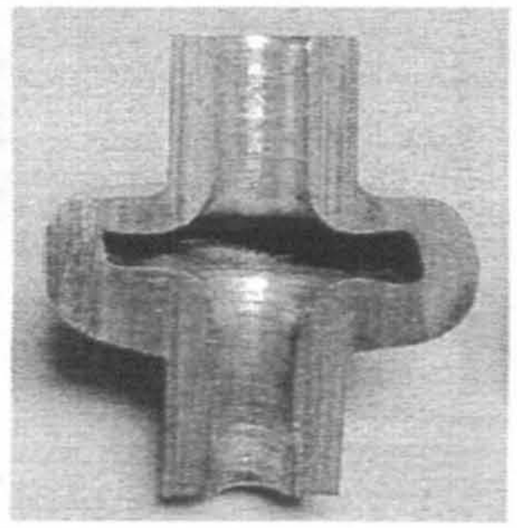

(a)

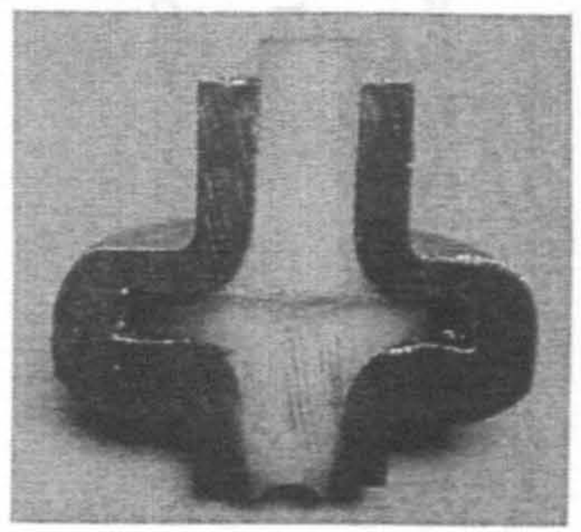

(b)

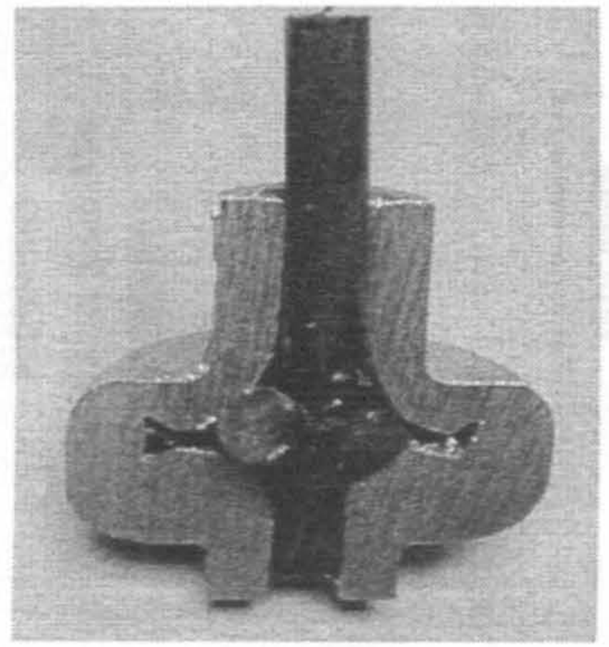

(c)

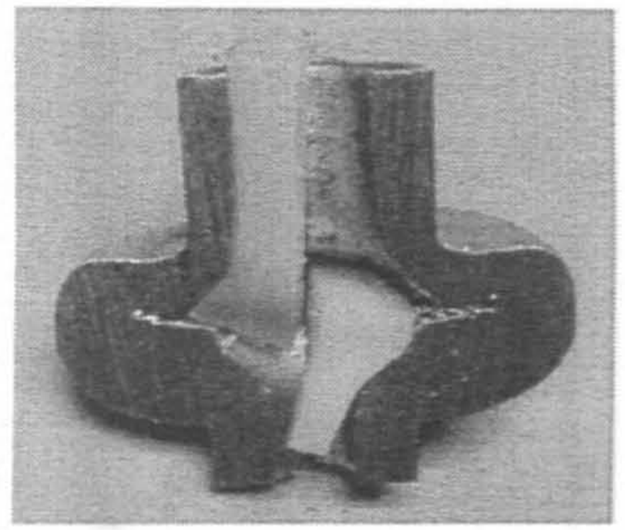

(d)

Components (a) to (d) have a diameter of 85 mm

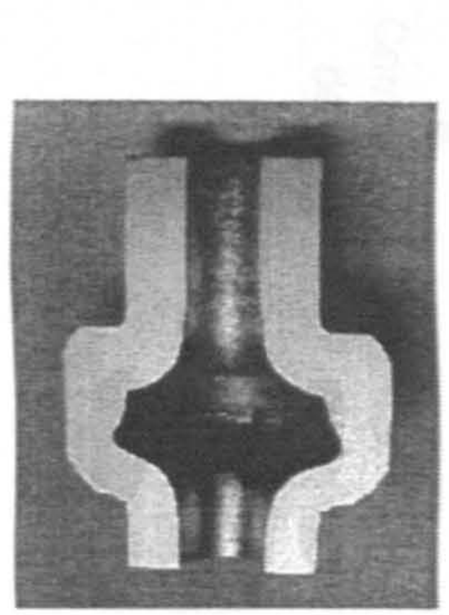

(e)

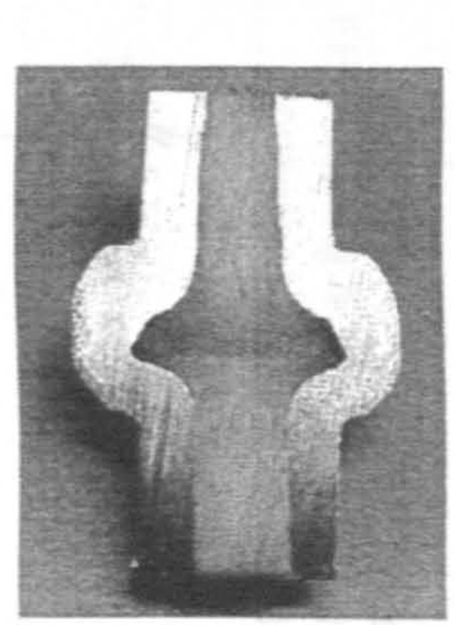

(f)

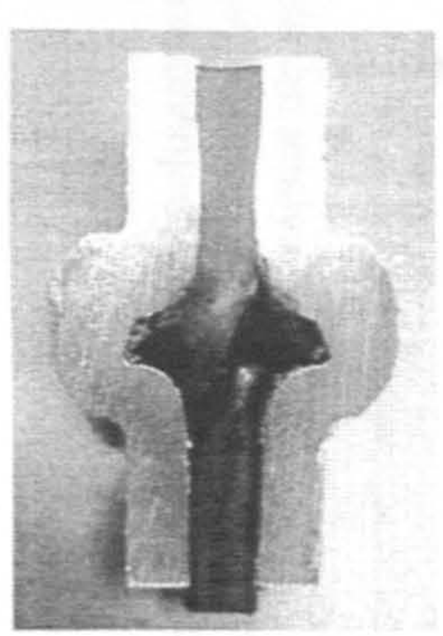

(g)

Components (e) to (g) have a diameter of 60 mm

Components (a) & (e) were formed using Solid Nitrile 642

Components (b) & (f) were formed using HDPE (Polyethylene)

Components (c) & (g) were formed using Red Qsash (Ether Purod)

Components (d) was formed using Natural Nylon 66

Fig. 3.21 Comparison of the influences of different pressurising materials in the forming of hollow flanges with PAIF (sectioned views of formed hollow flanges)

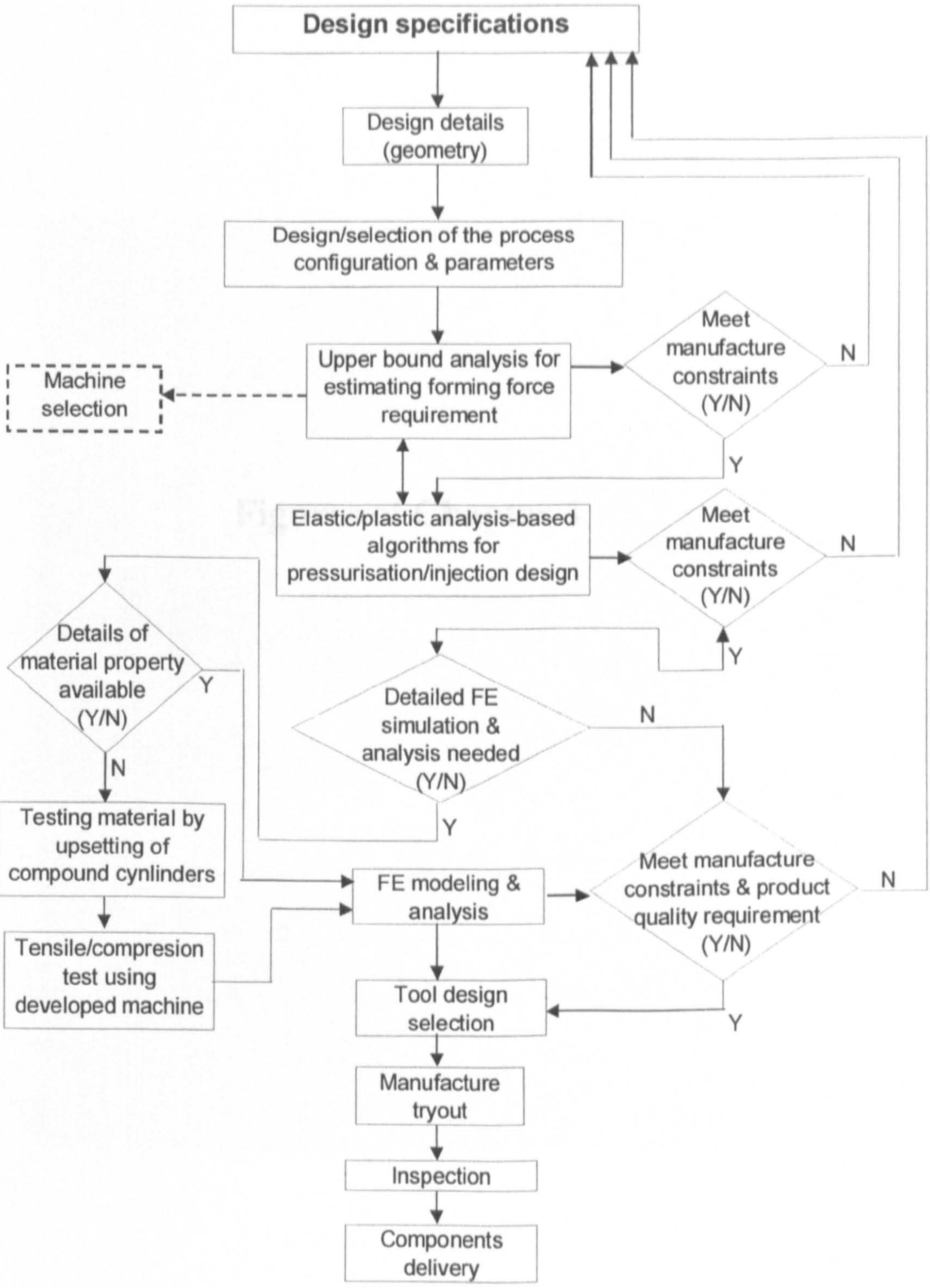

Fig. 3.22 The approach for synthesizing concurrent design and manufacture of hollow flanges with PAIF

Figures of Chapter 4

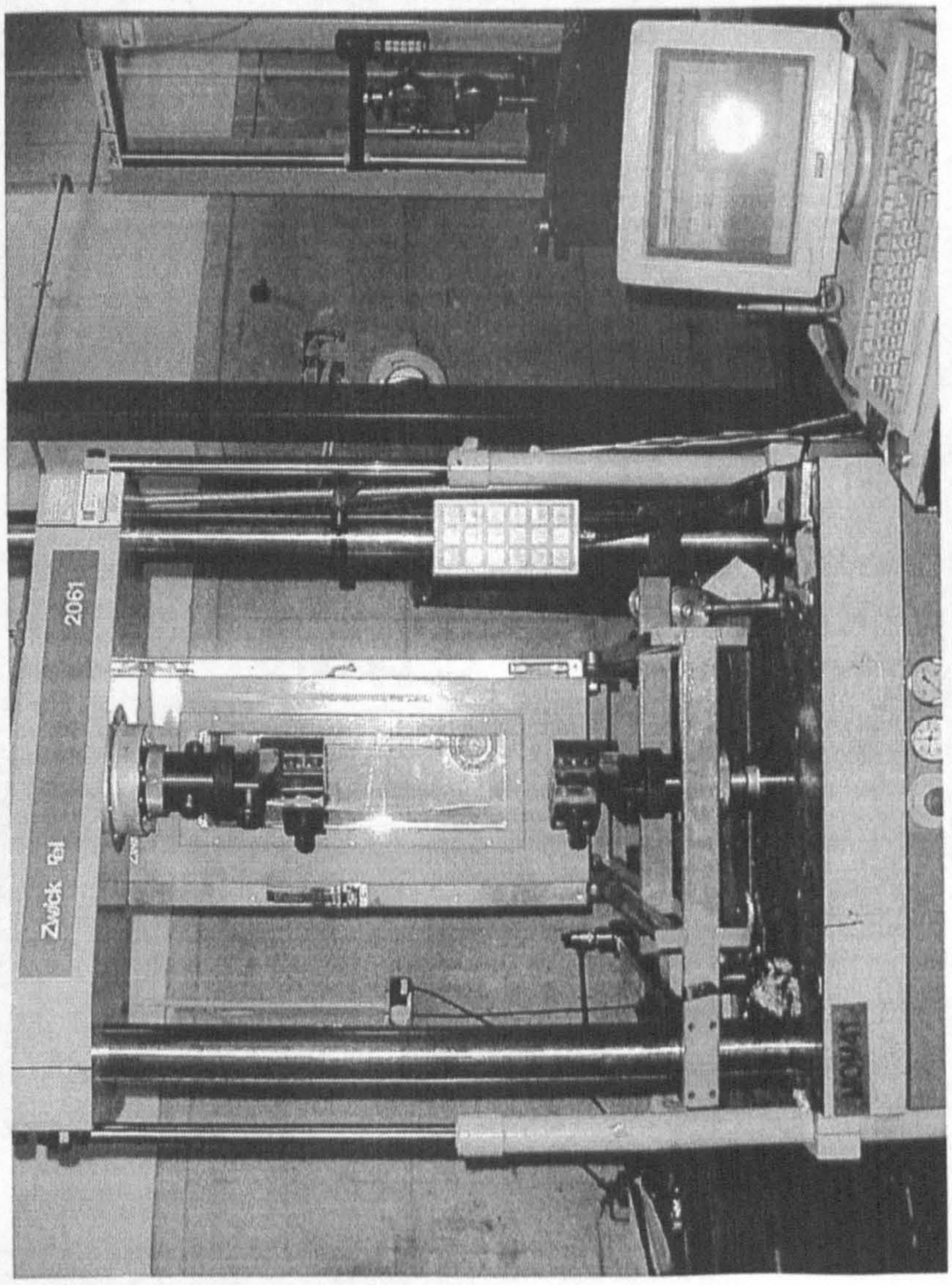

Fig. 4.1 The equipment for uniaxial compression, uniaxial and planar tension tests (stroke<100mm)

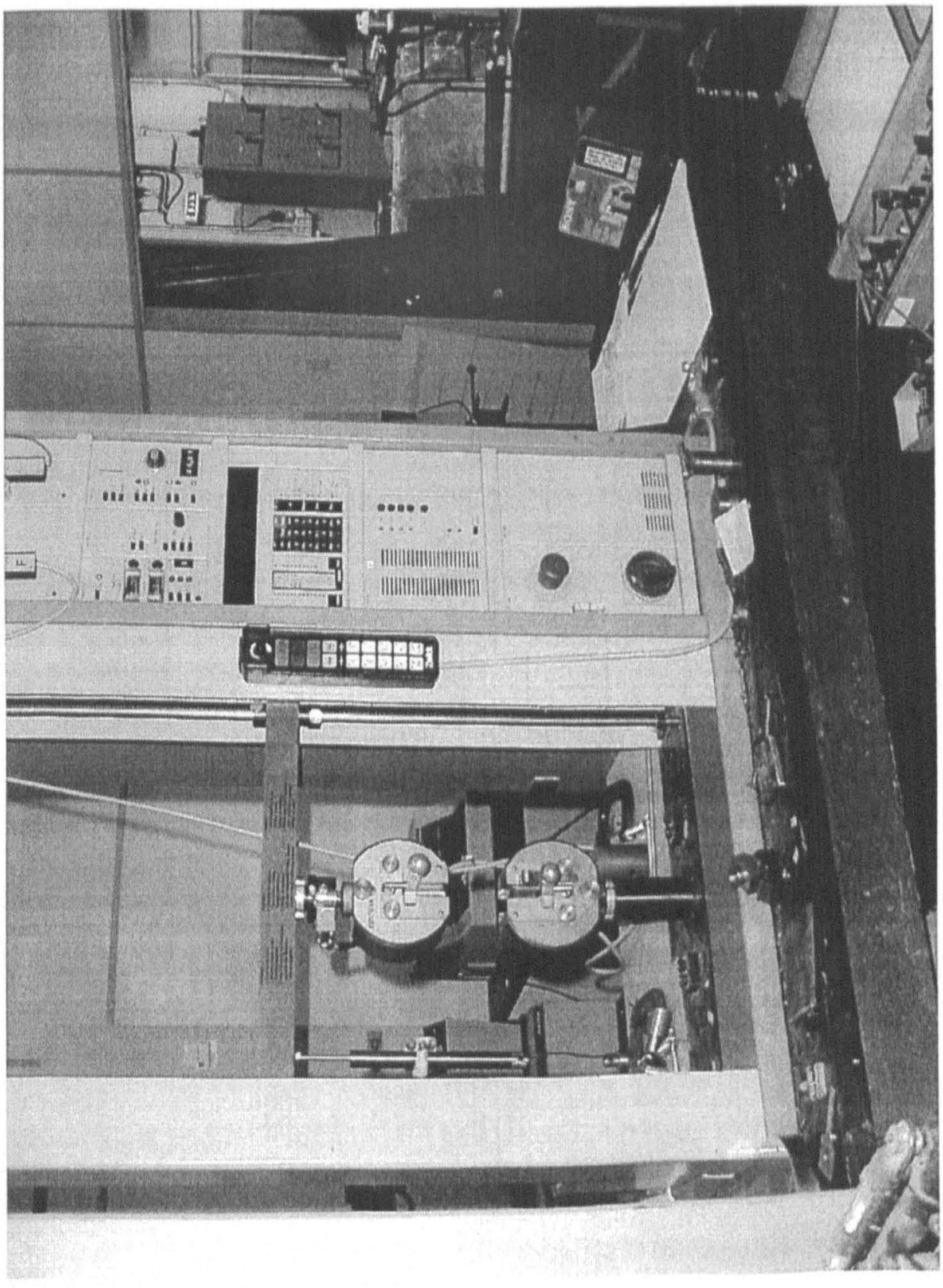

Fig. 4.2 The equipment for uniaxial and planar tension tests (stroke>100mm)

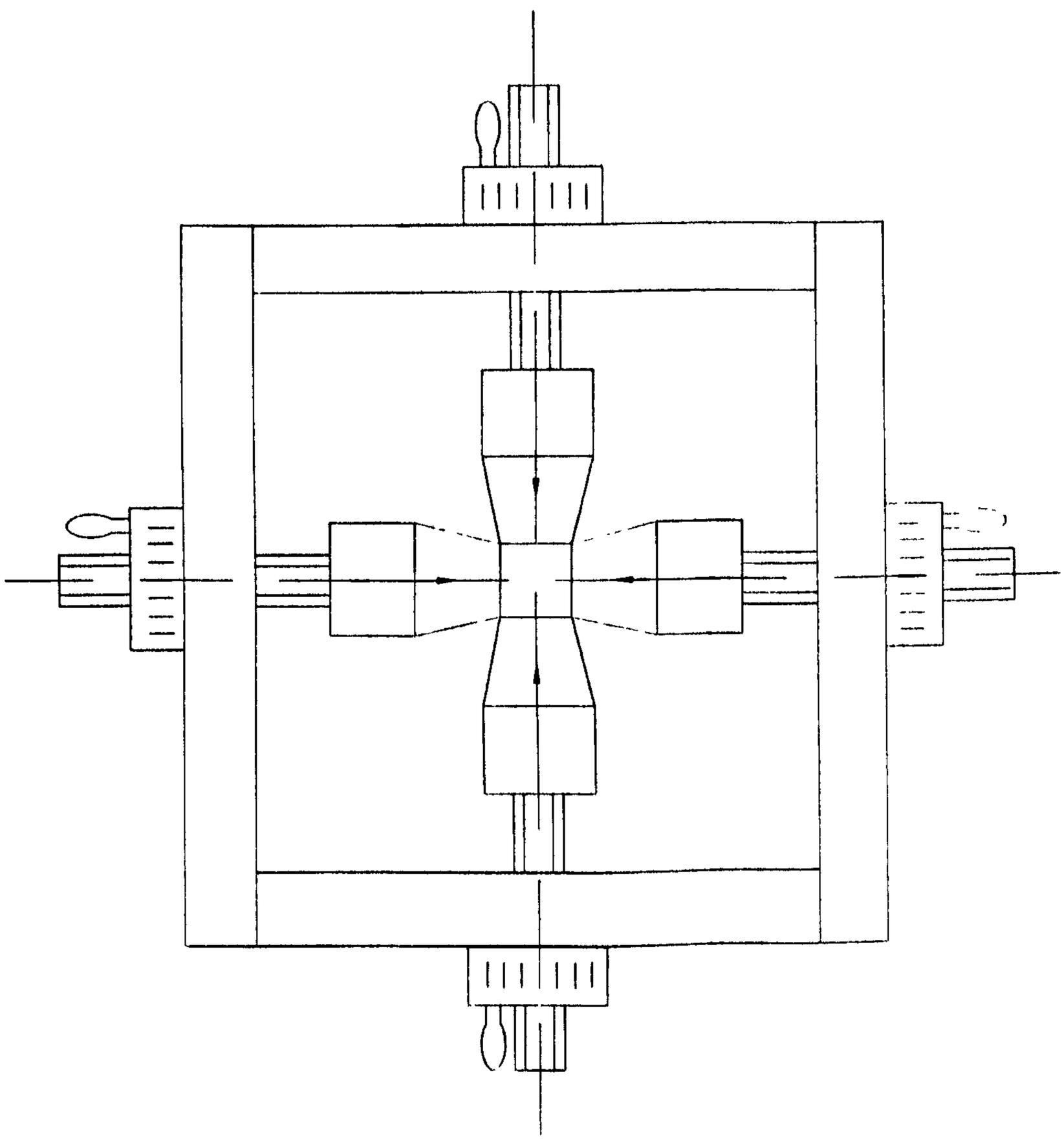

Fig. 4.3 The design concept 1

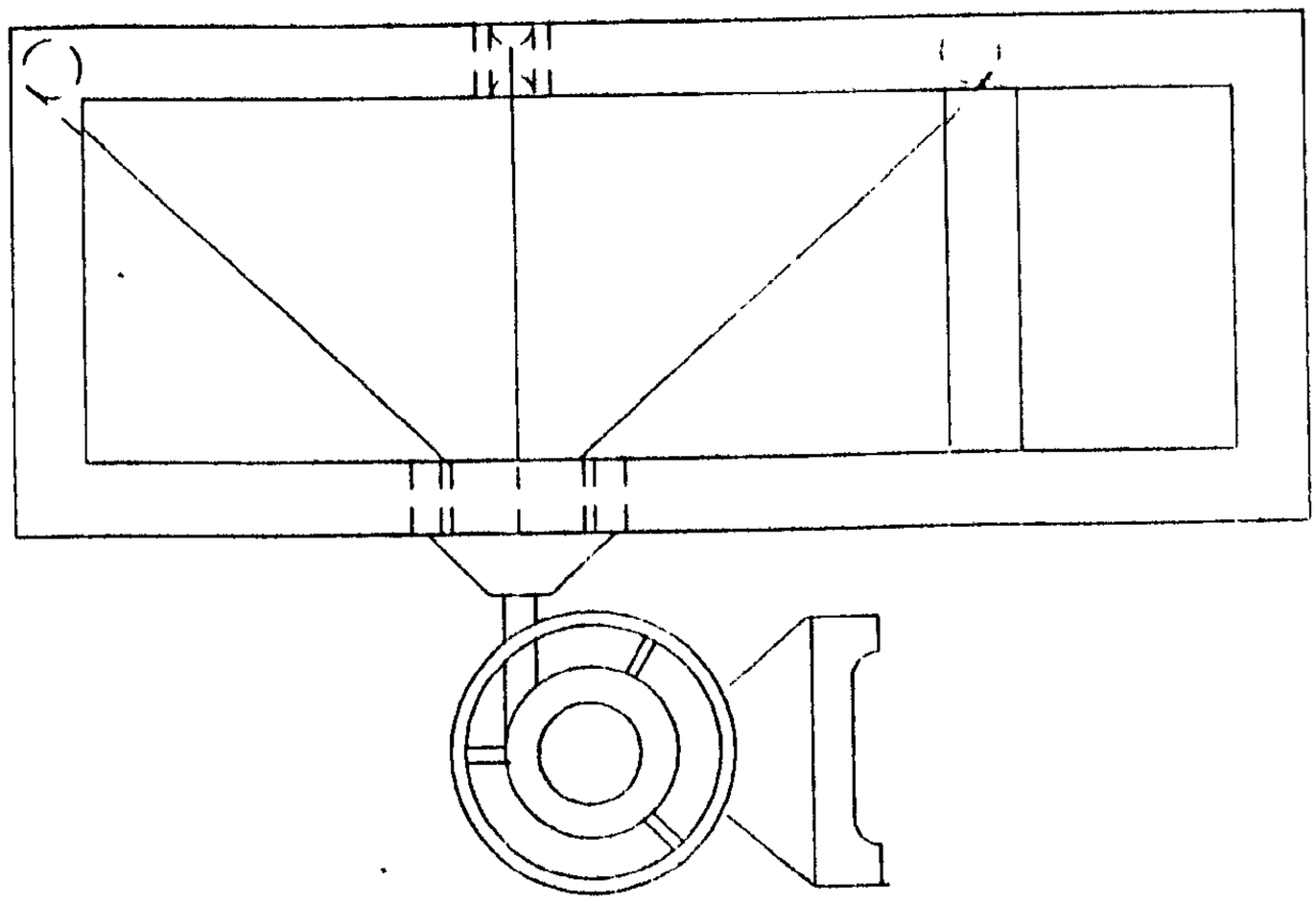

Fig. 4.4 The design concept 2

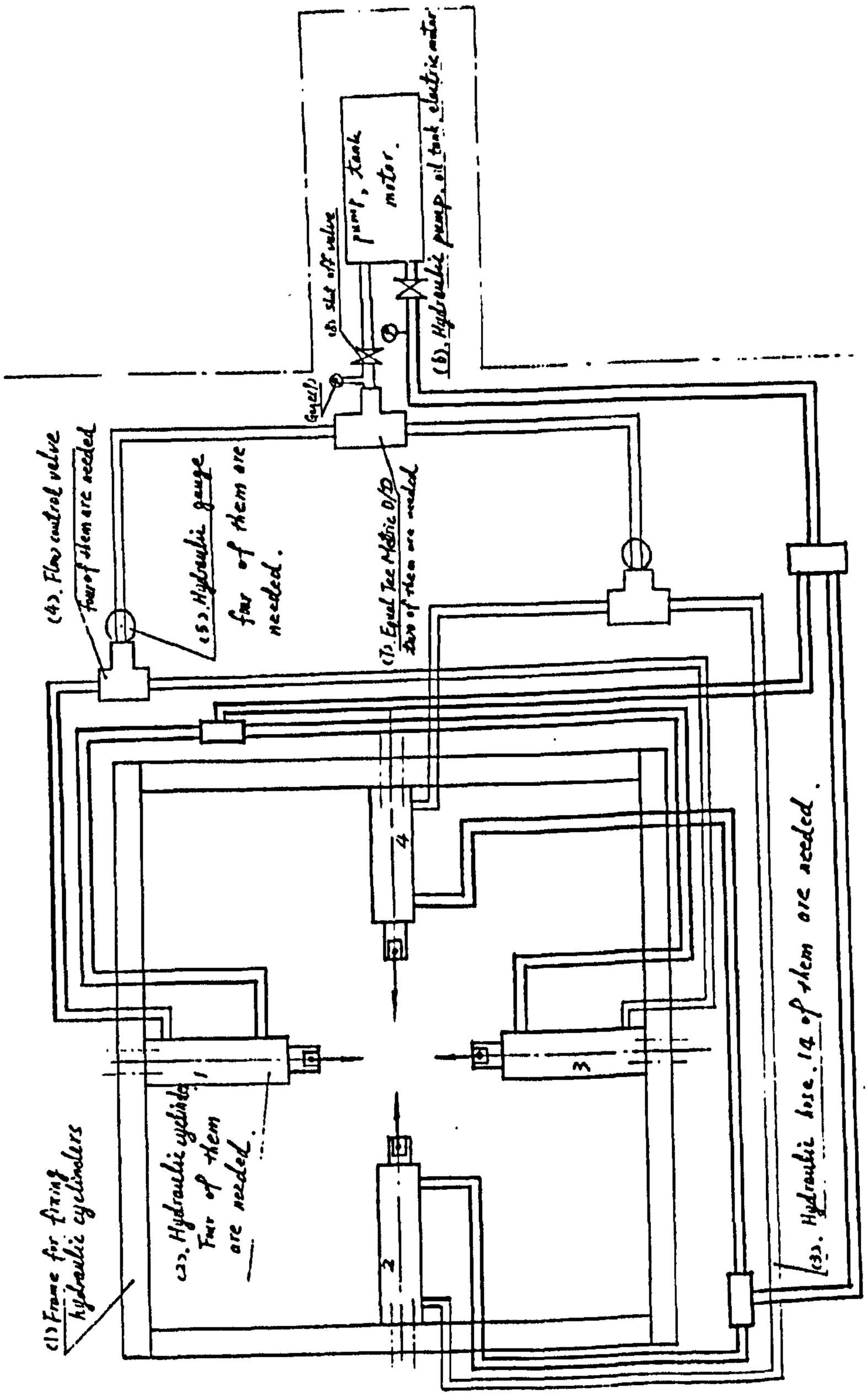

Fig. 4.5 The design concept 3

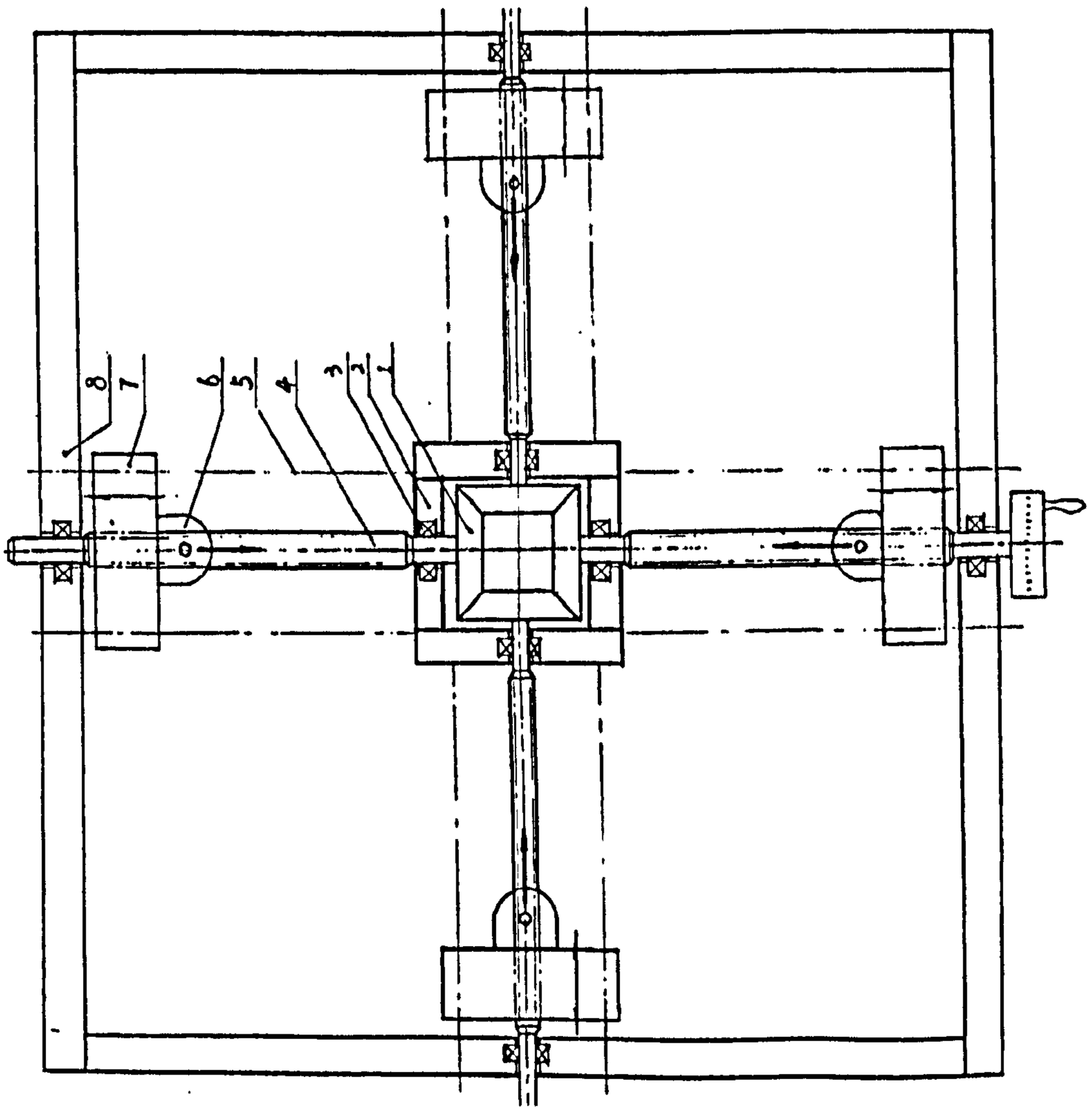

Fig. 4.6 The design concept 4

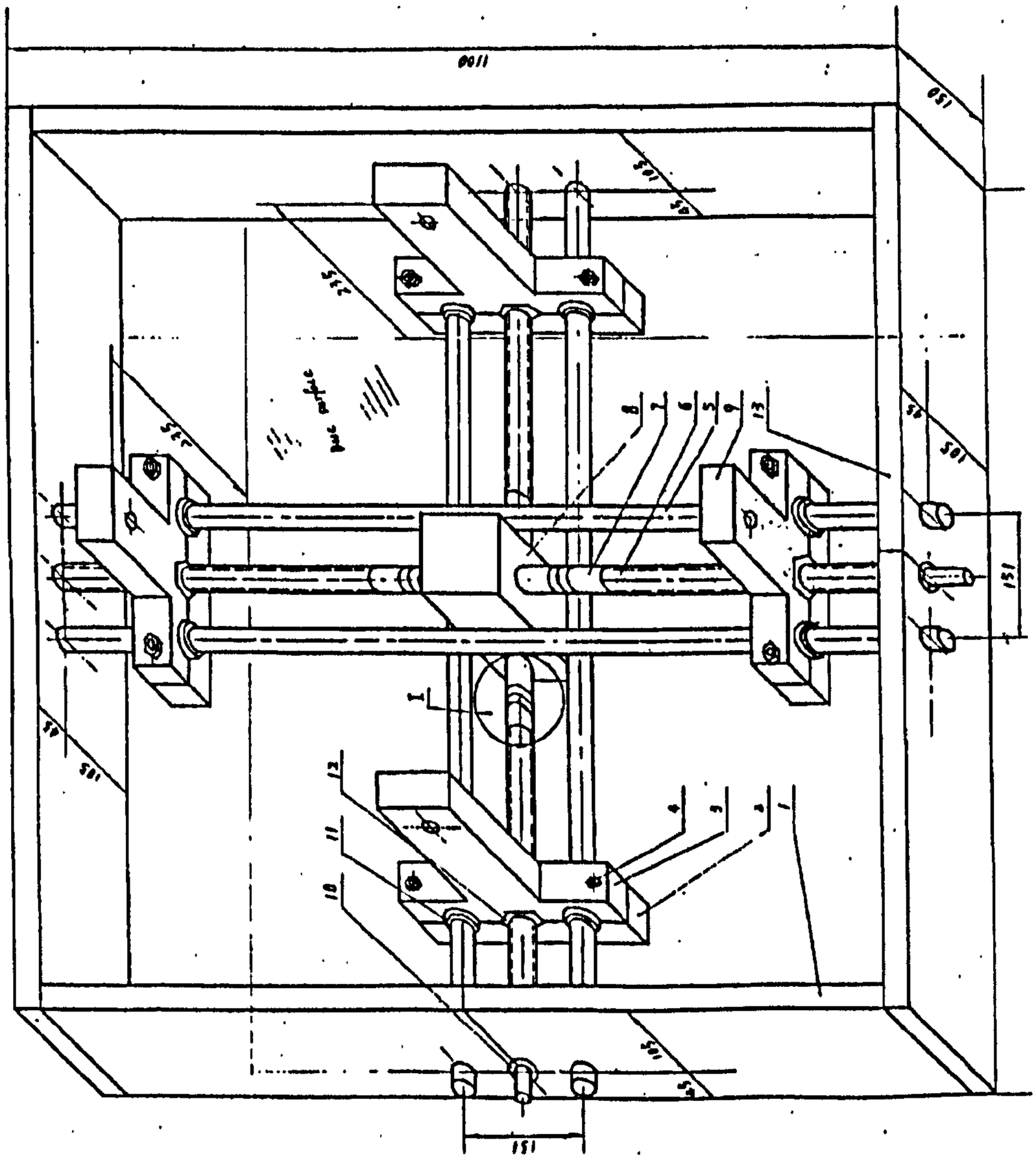

Fig. 4.7 The design concept 5

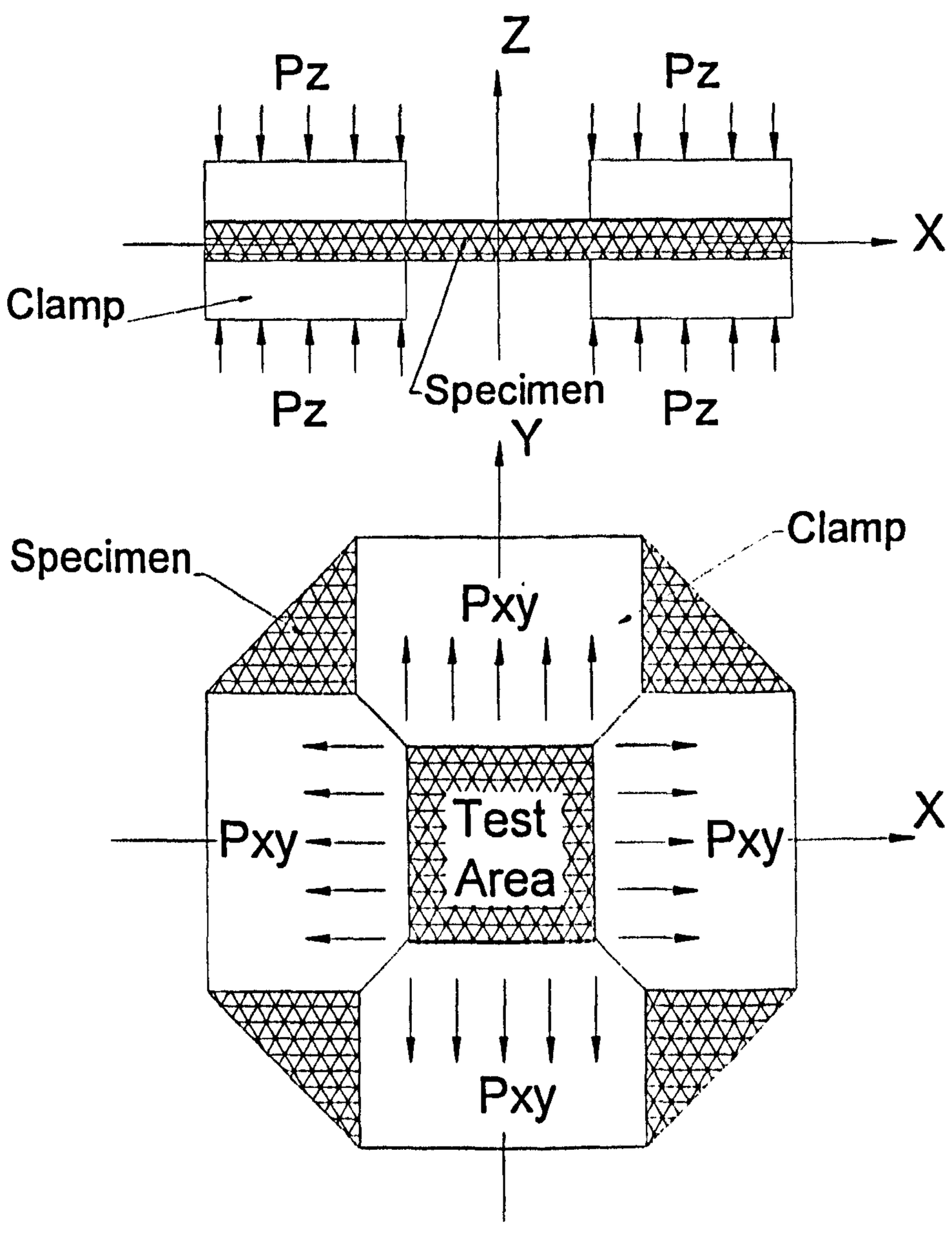

Fig. 4.8 Principle of the clamping design

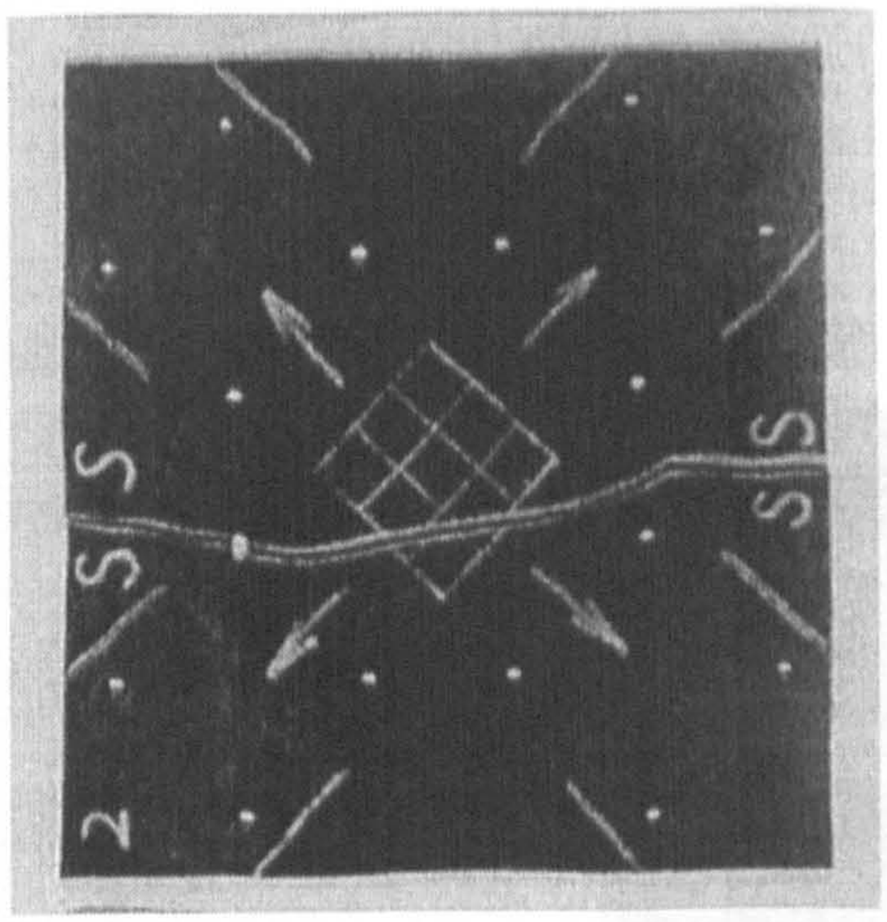

(c)

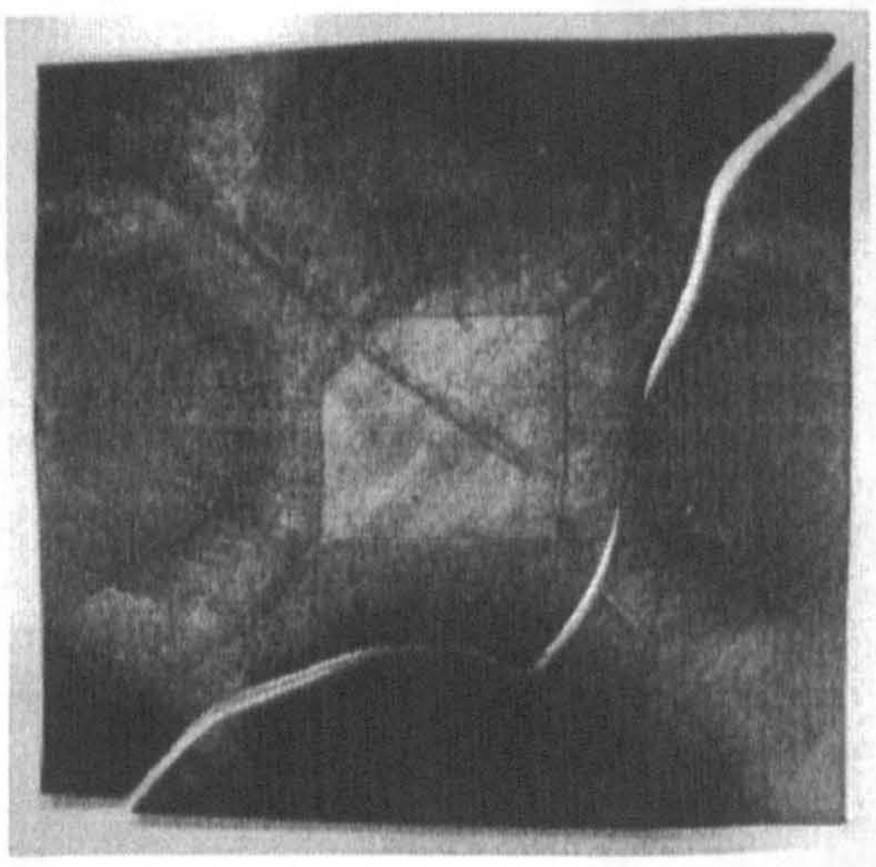

(b)

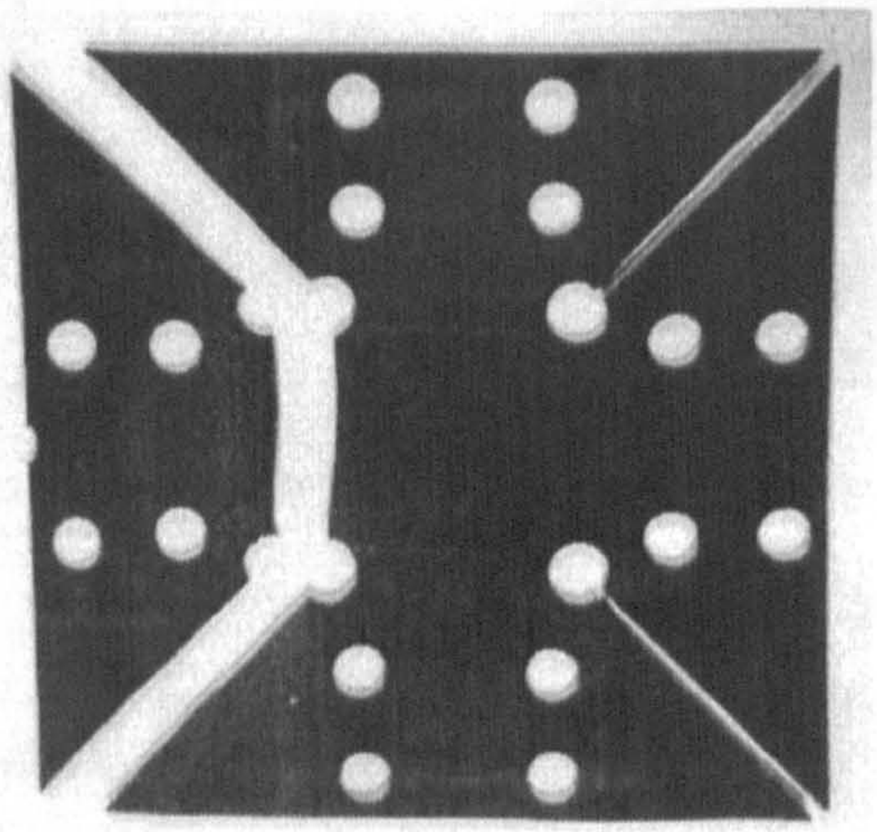

(a)

Fig. 4.9 Failure modes with different clamping concepts

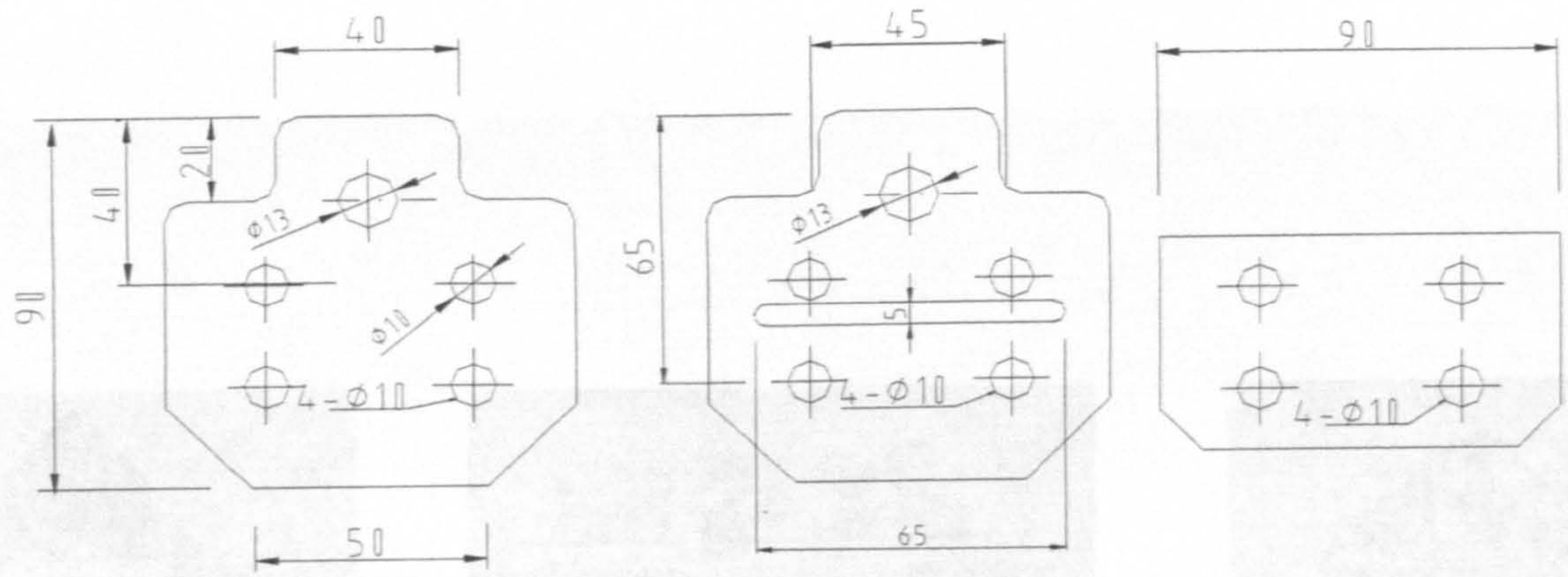

(a) The clamp geometry

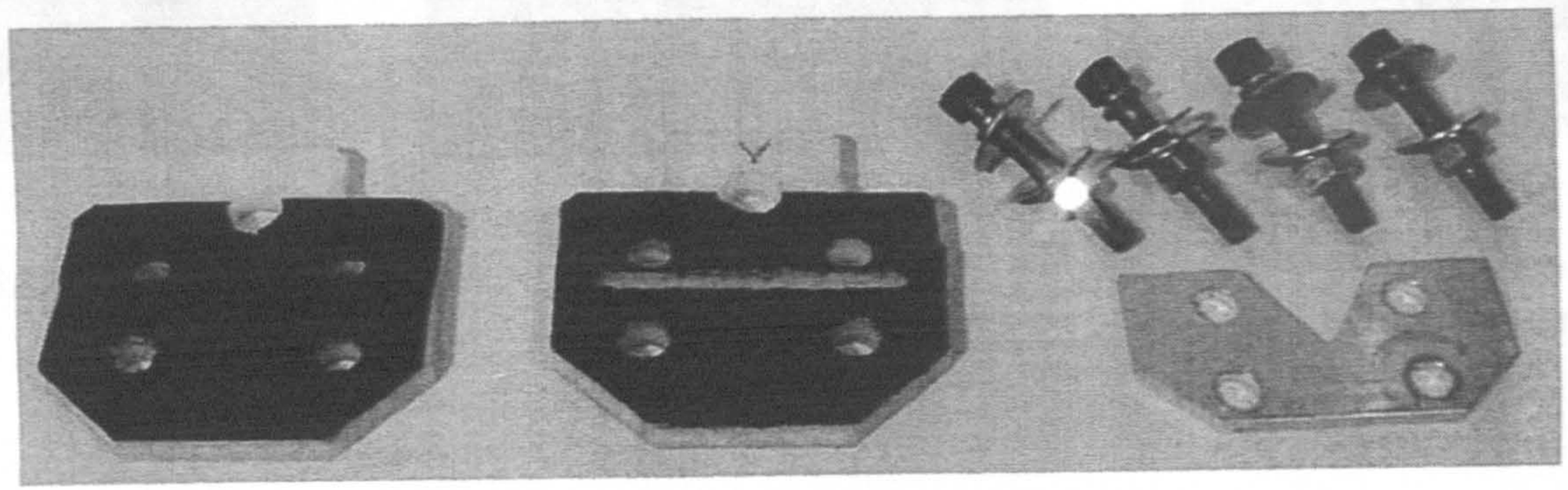

(b) The components of the clamp

Fig. 4.10 The clamp designed

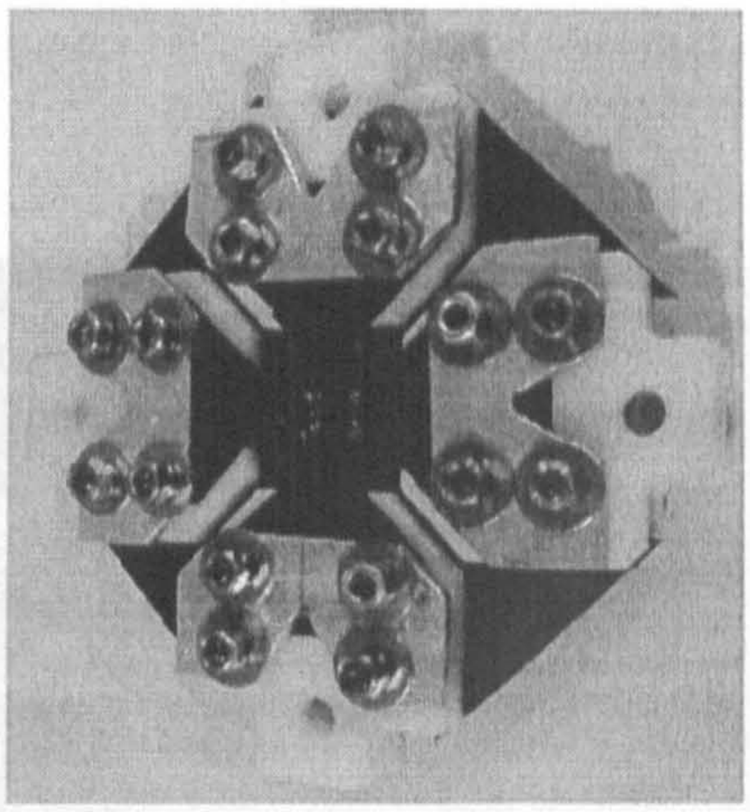

(b) Bottom view after assembled

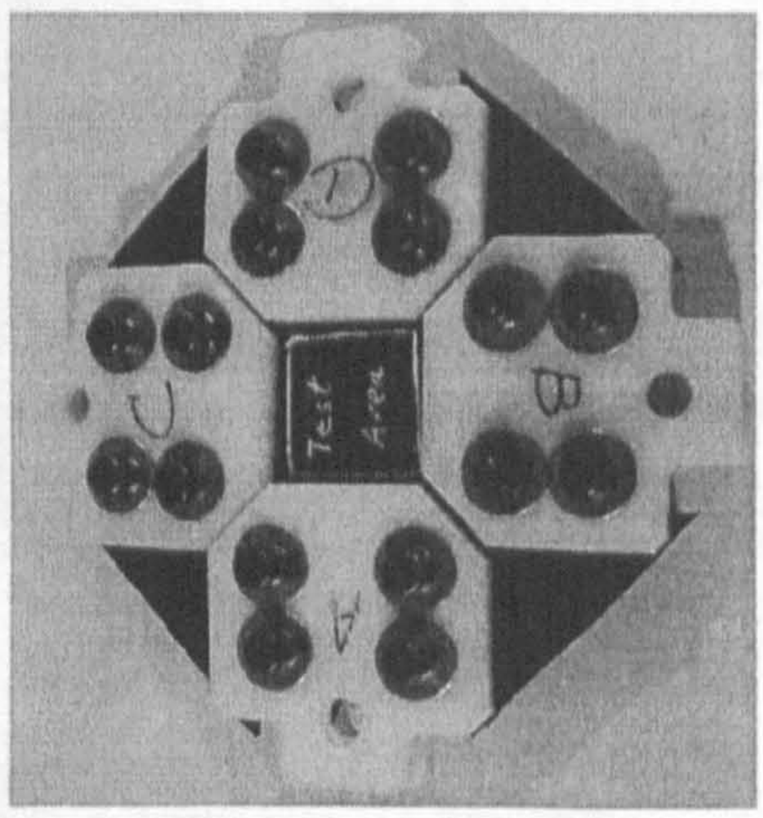

(a) Top view after assembled

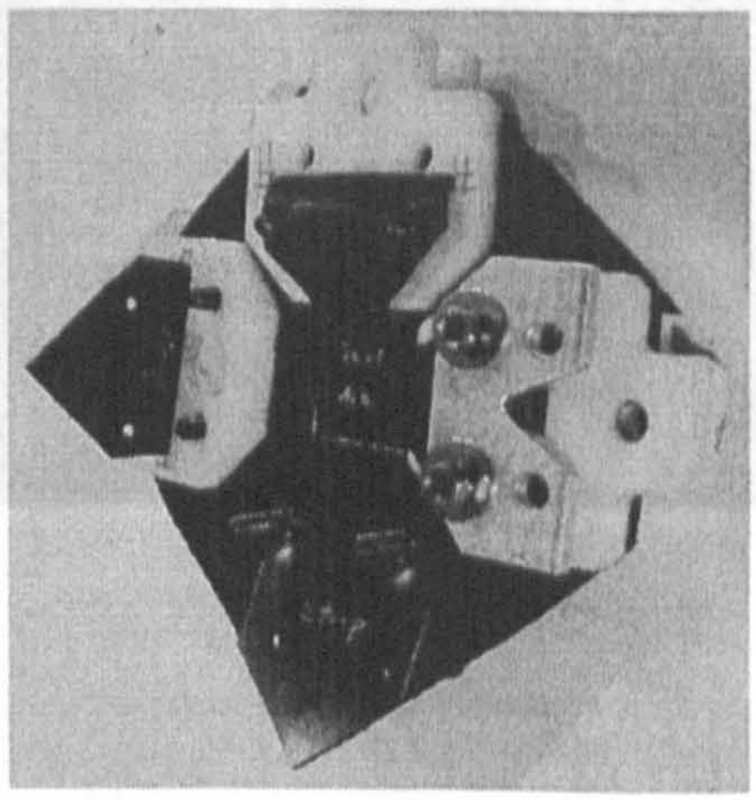

(a) Assembly procedure

Fig. 4.11 The specimen and clamp in assembling

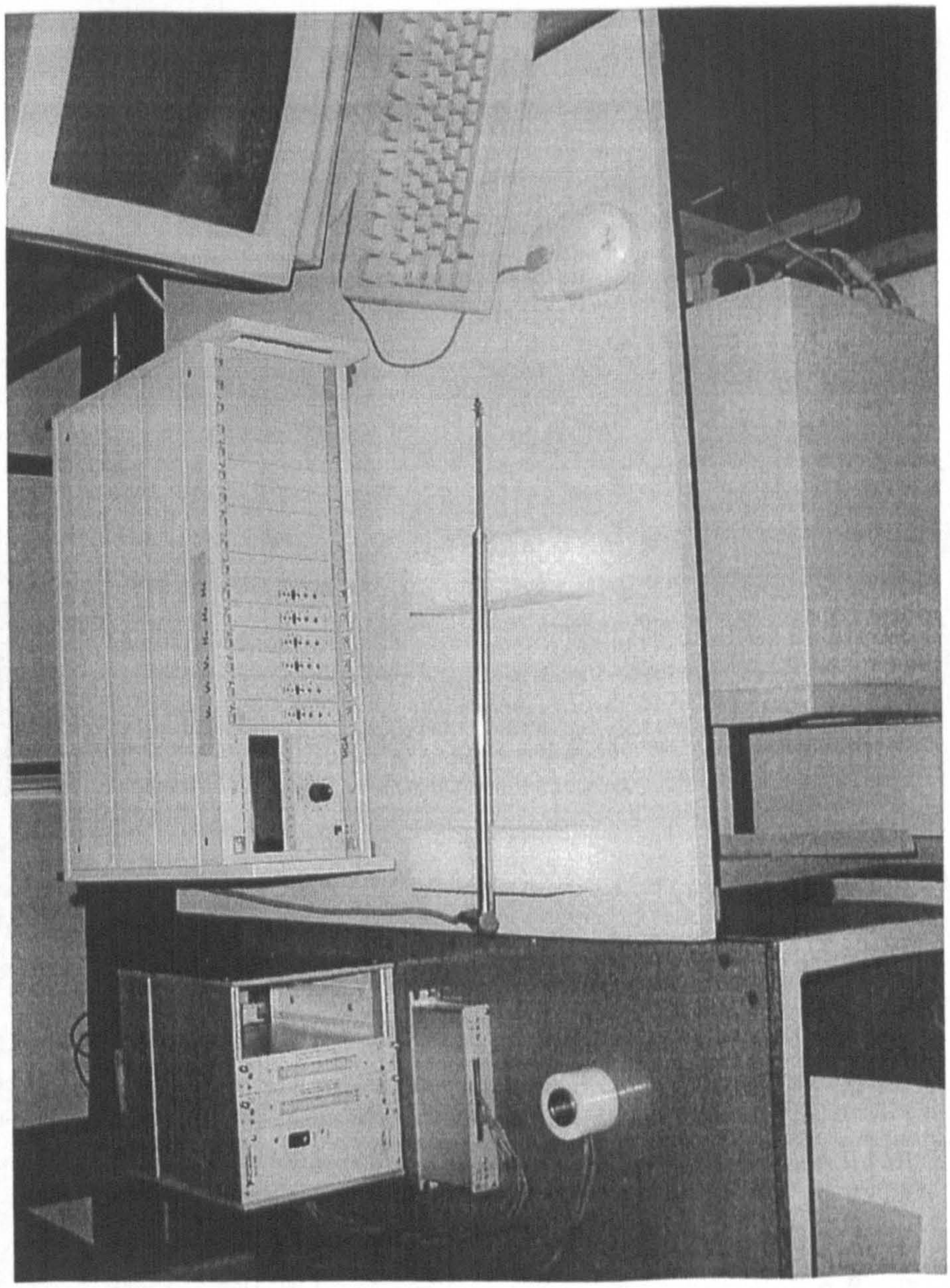

Fig. 4.12 Components of the data acquisition system

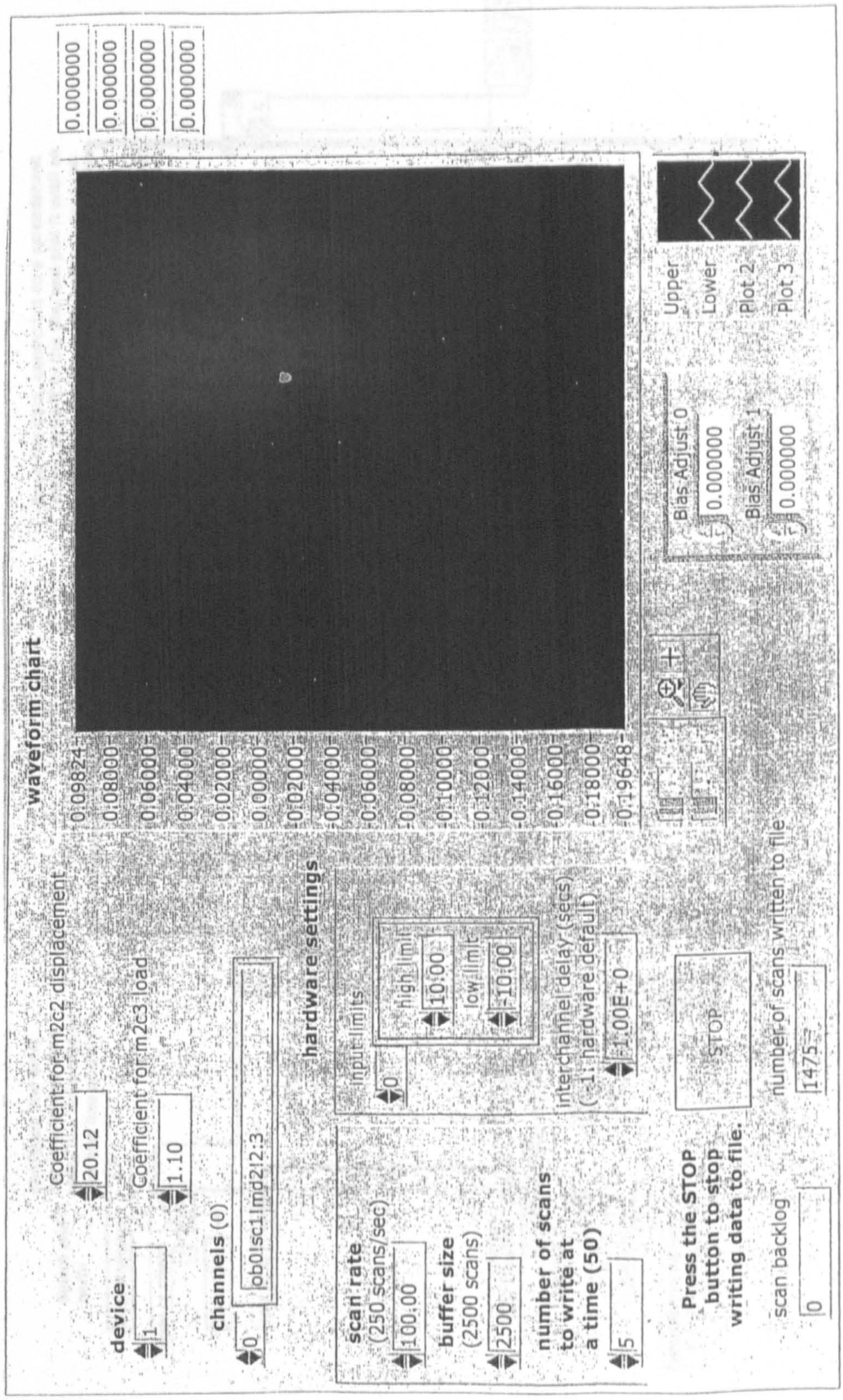

Fig. 4.13 The front panel of the program

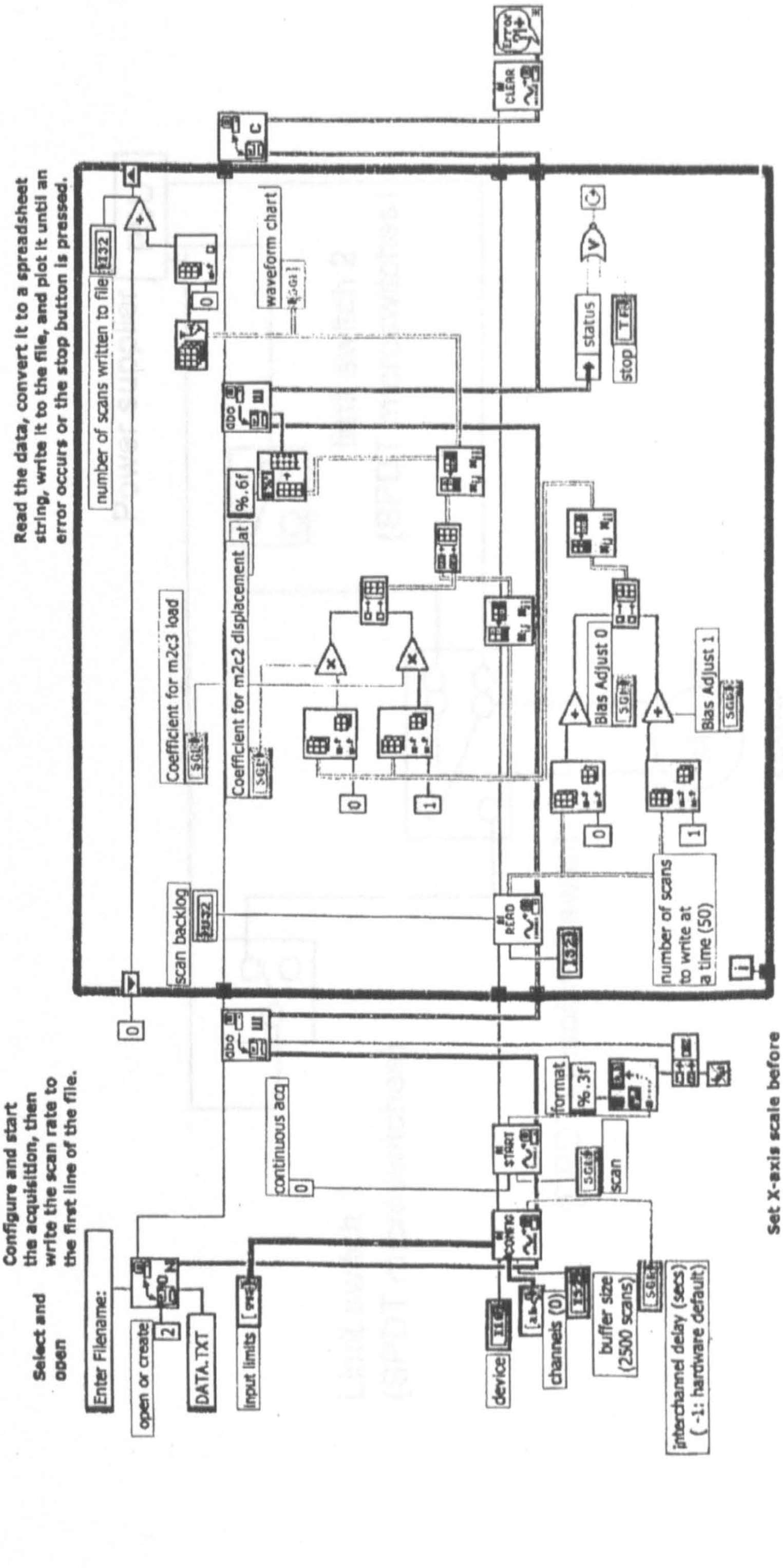

Fig. 4.14 The diagram of the program

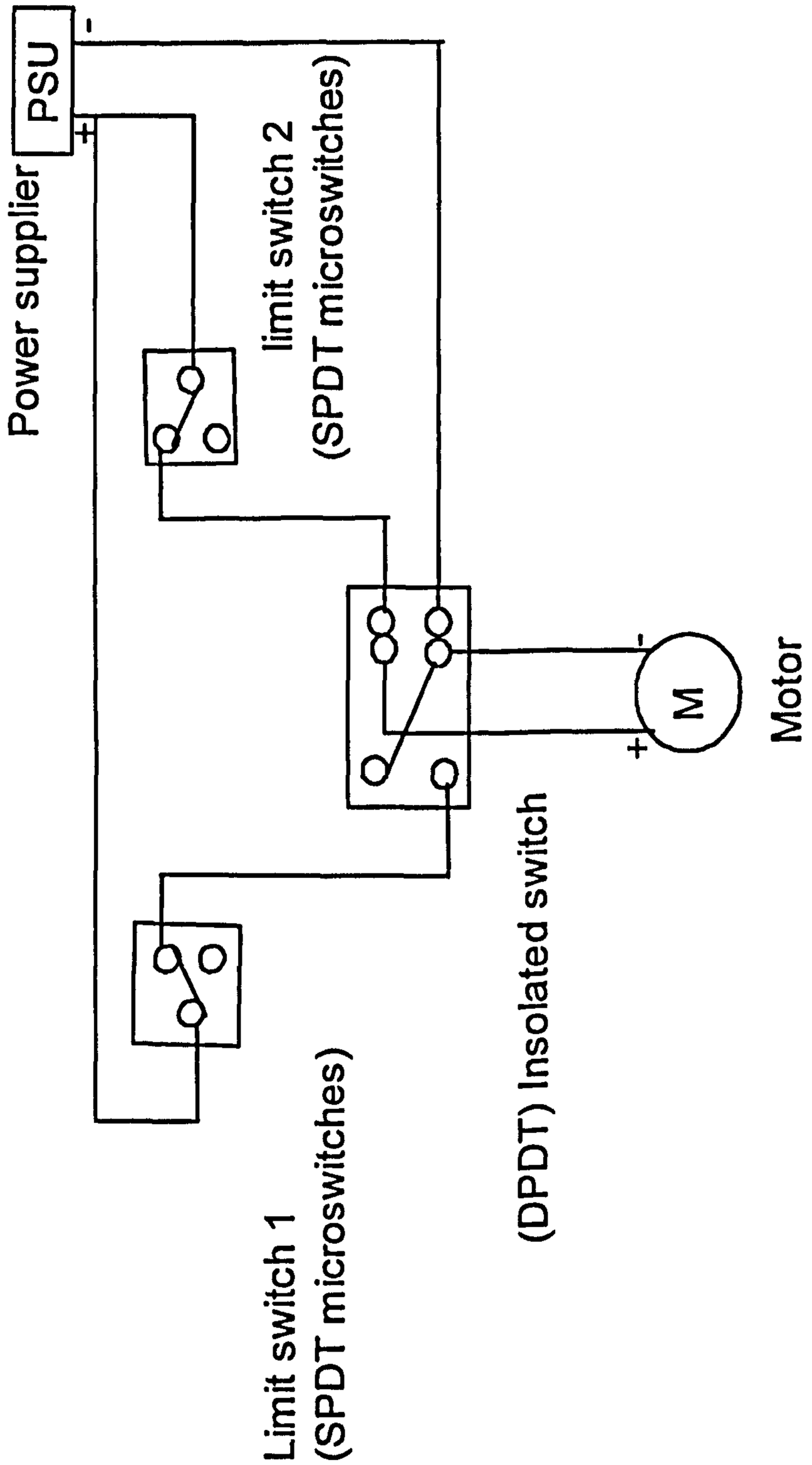

Fig. 4.15 The electrical control circuit

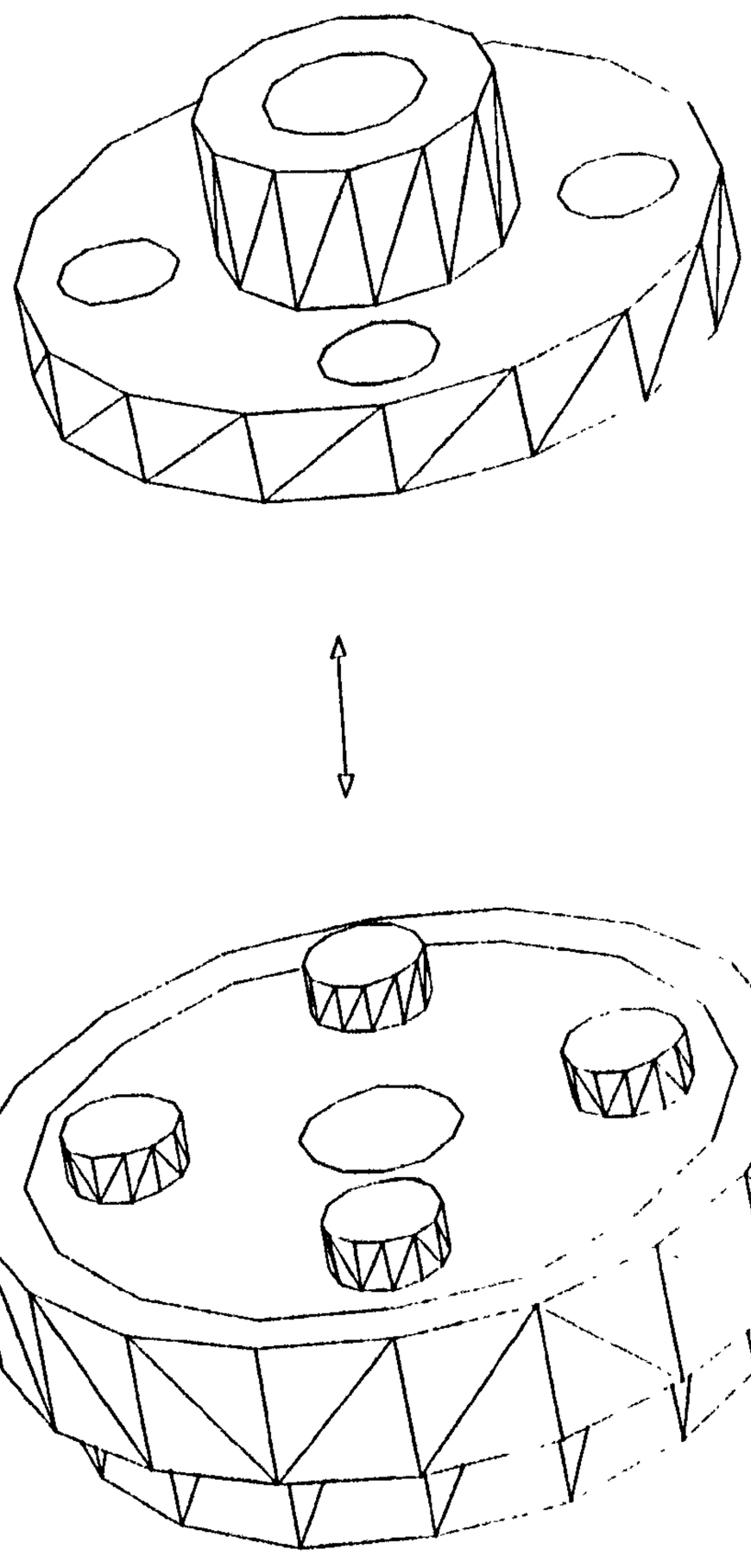

Fig. 4.16 The sliding clutch

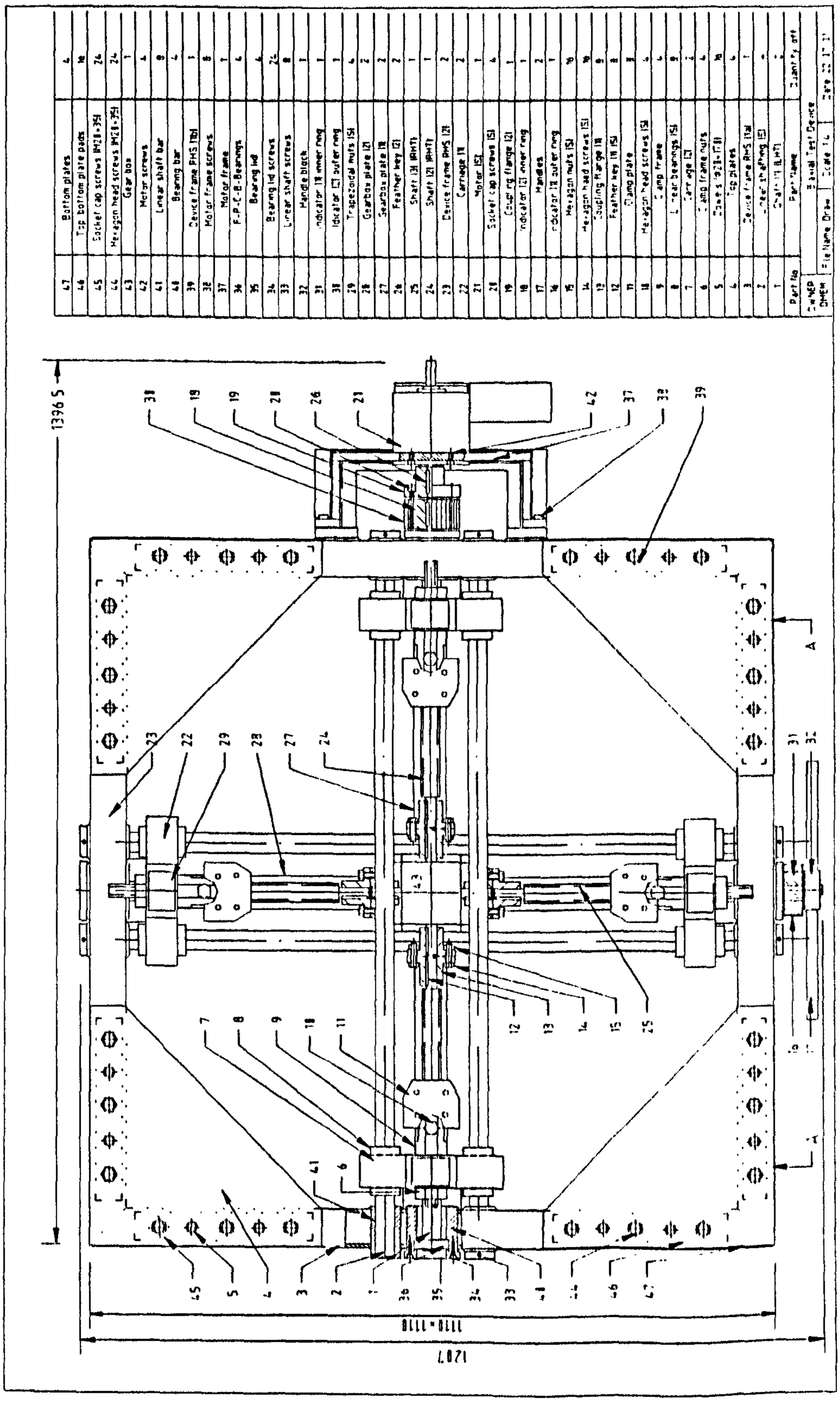

Fig. 4.17 The machine assembled in drawings

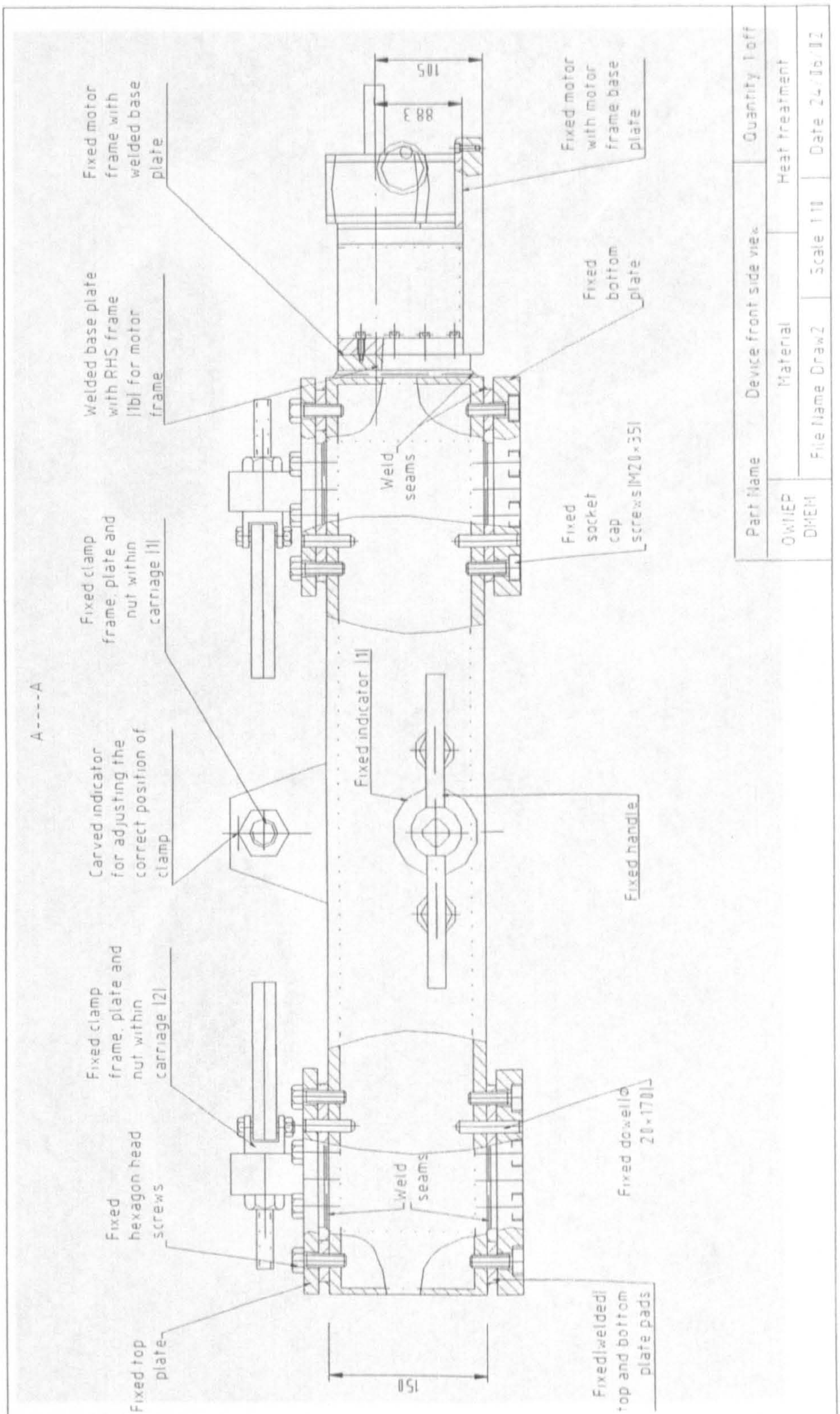

Fig. 4.18 The assembled front view of the machine in drawings

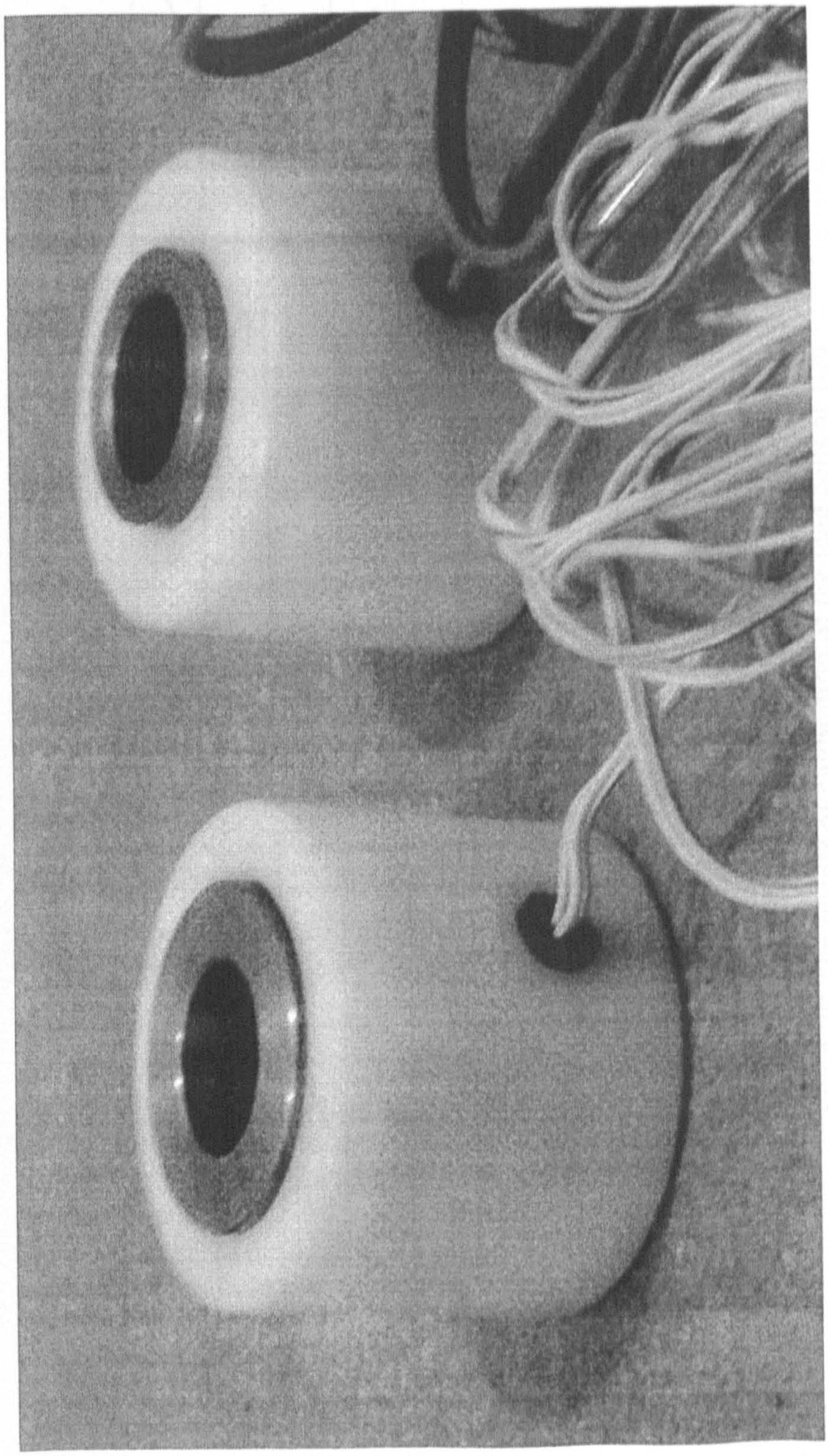

Fig. 4.19 The load cells designed for the tests

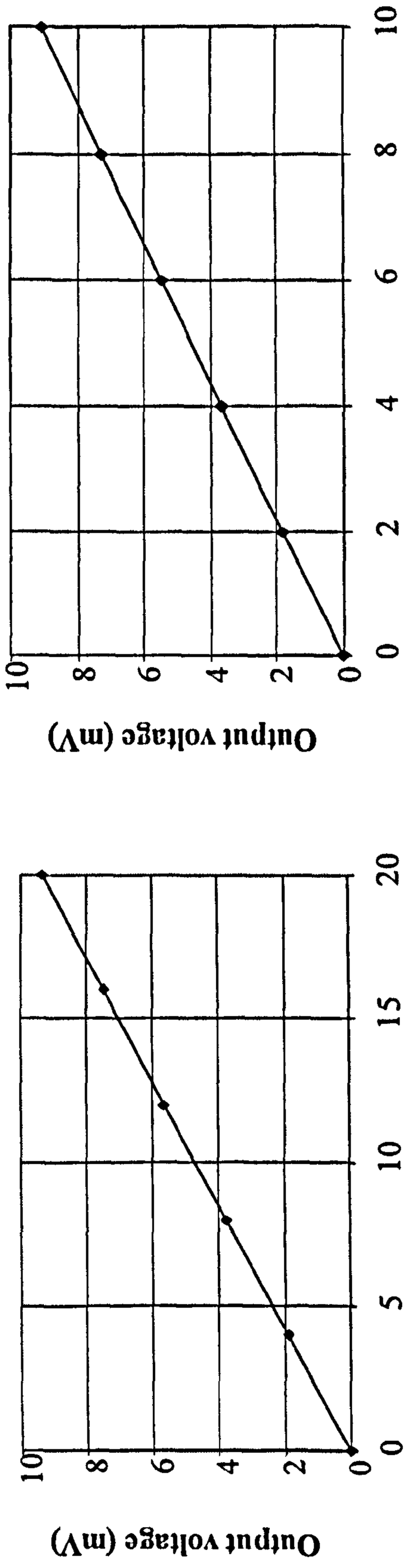

(a) The load cell with 2 ton capacity

(b) The load cell with 1 ton capacity

Fig. 4.20 The results of calibration of the load cells at 10V

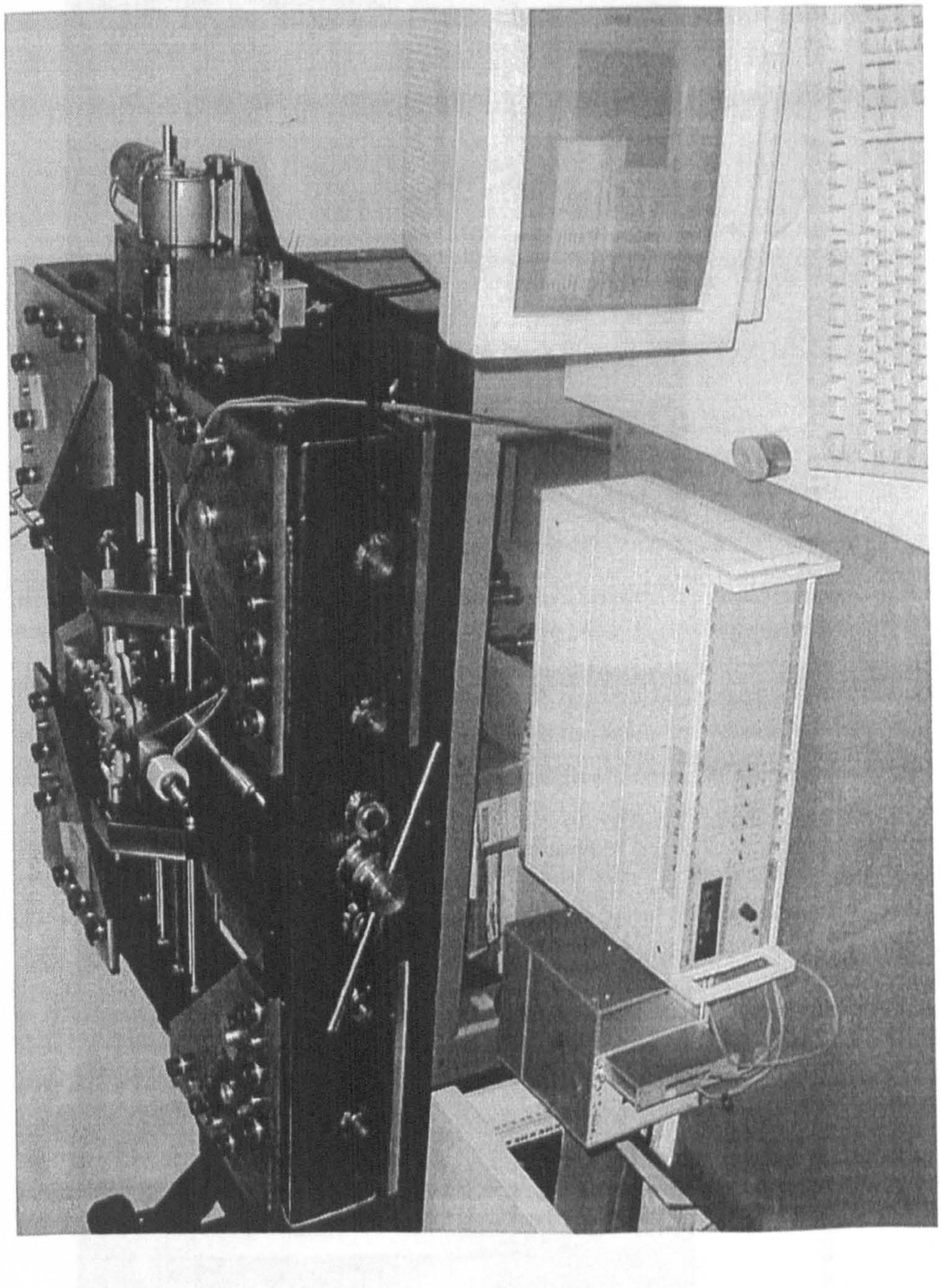

Fig. 4.21 The unique biaxial testing machine

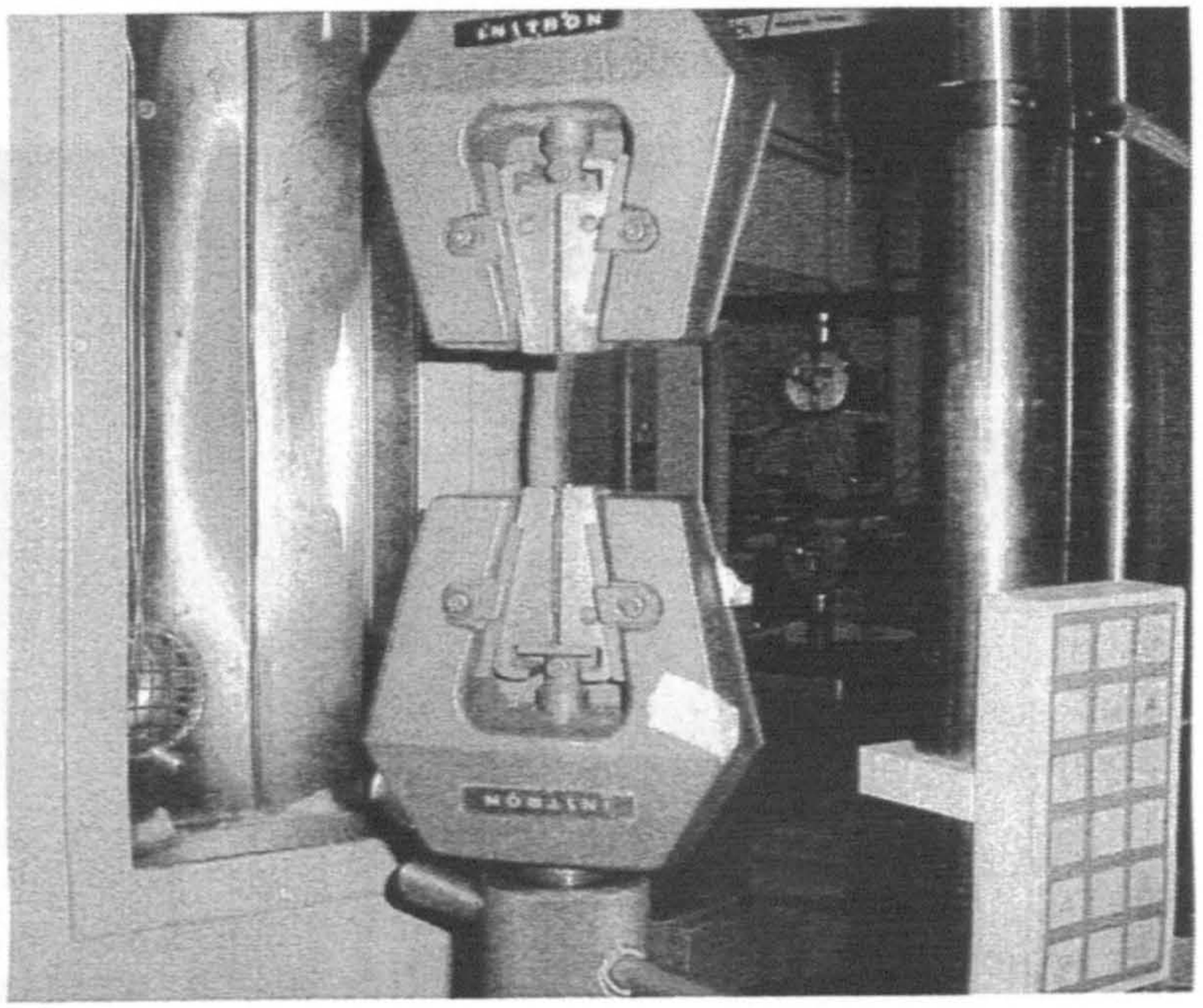

(a) The experimental set-up with hydraulic press

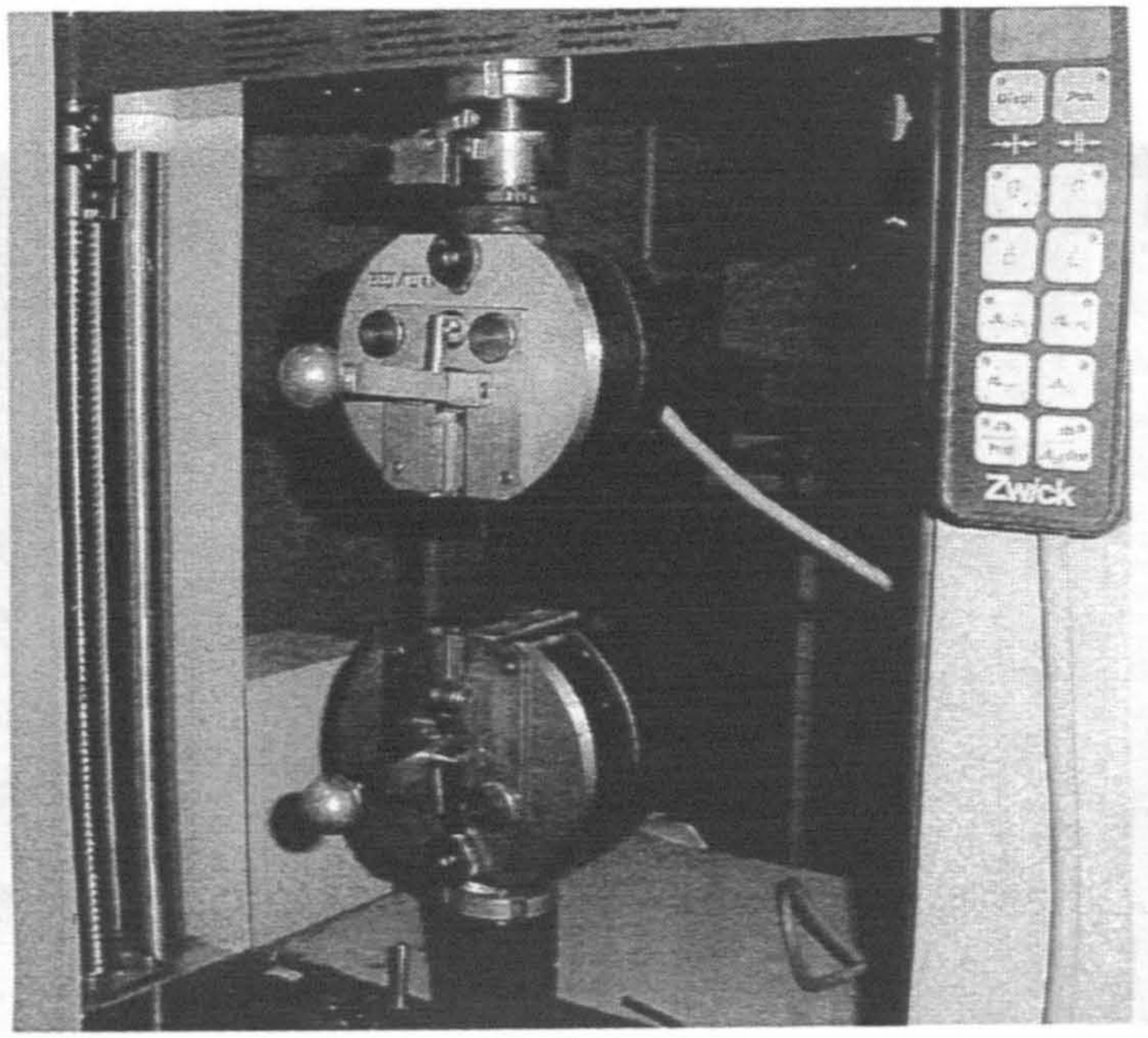

(b) The experimental set-up with mechanic press

Fig. 4.22 The uniaxial tension test-set-ups

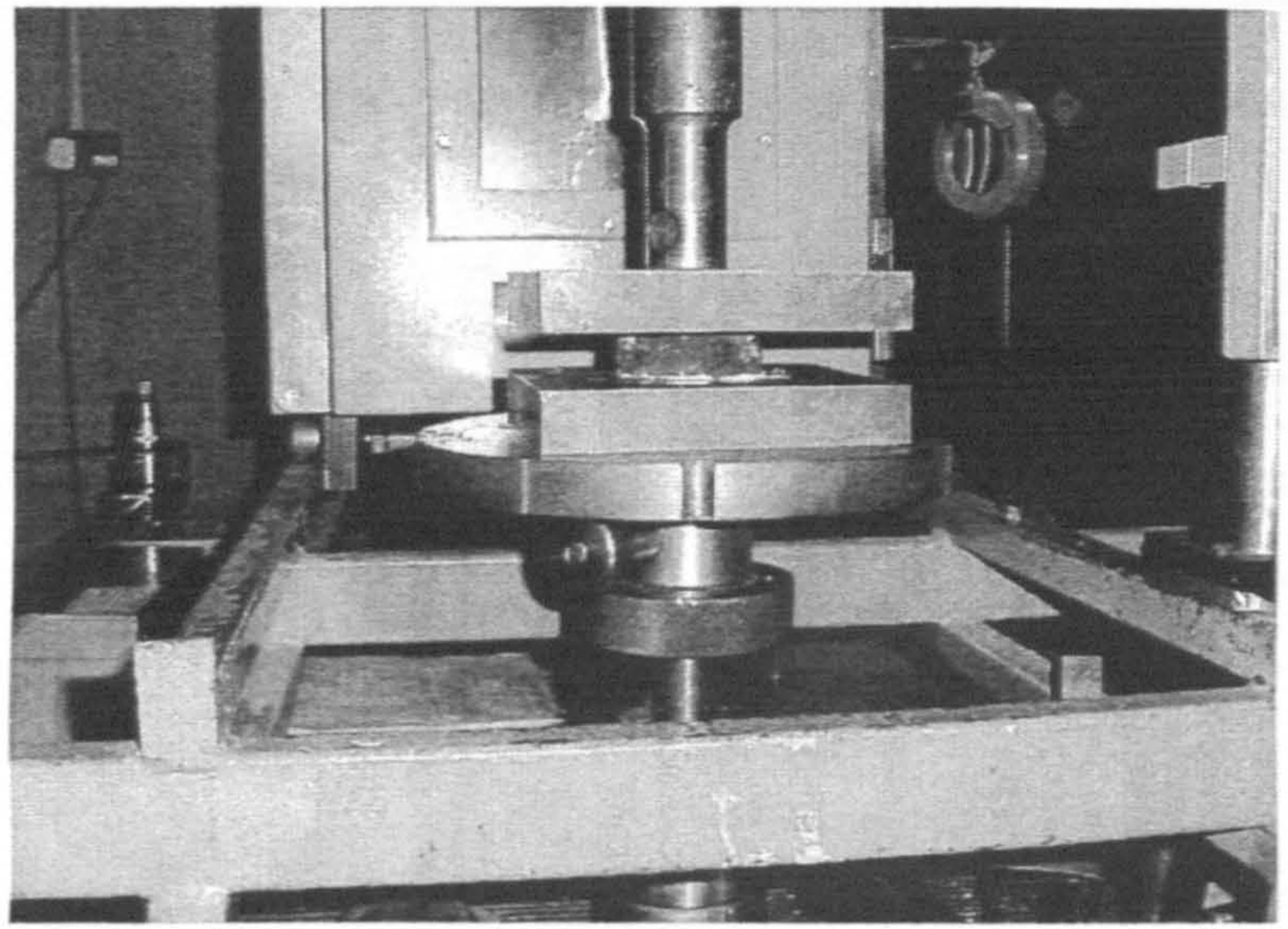

(a) The specimen with lubricant

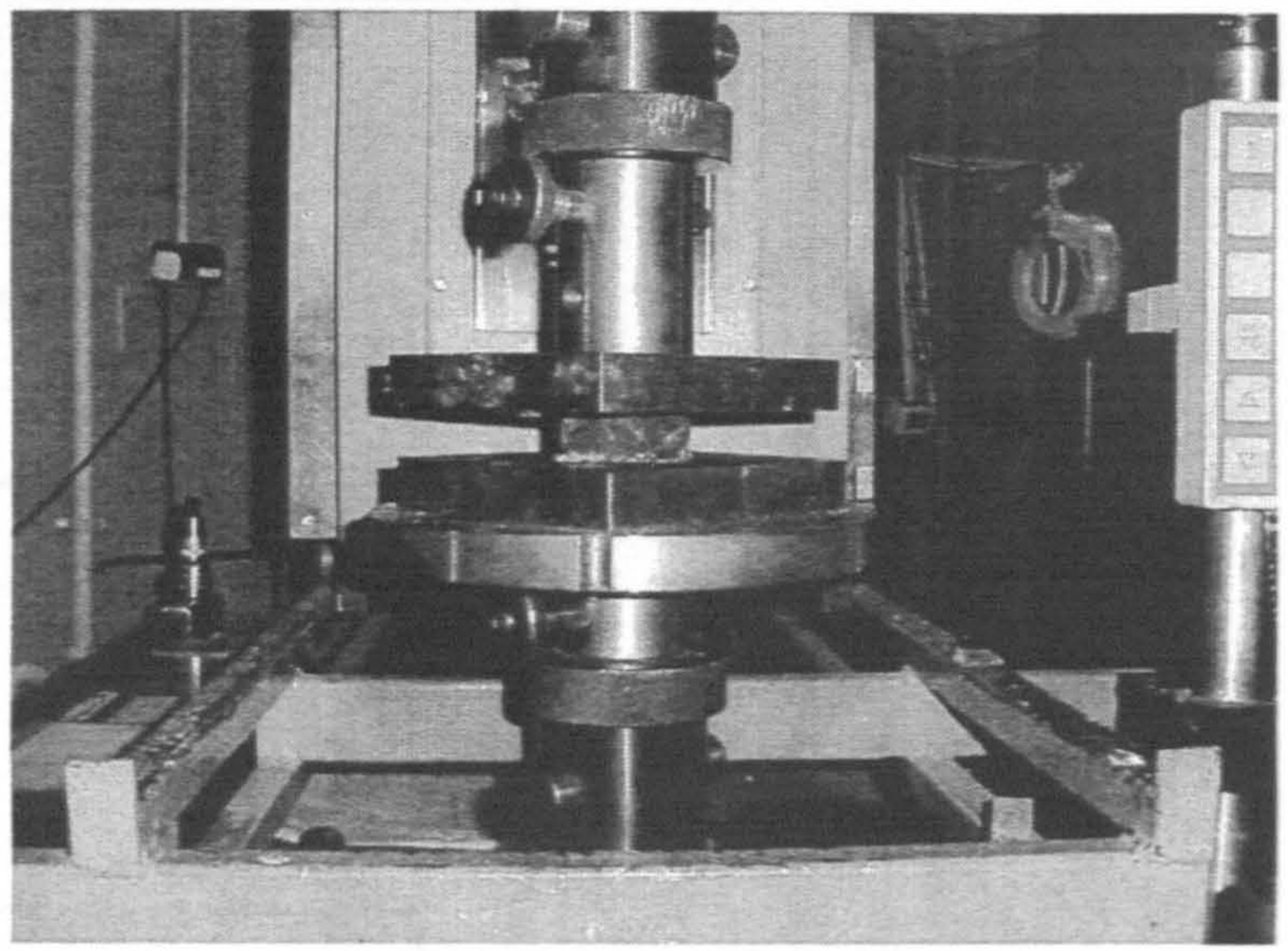

(b) The specimen without lubricant

Fig. 4.23 The uniaxial compression test-set-ups

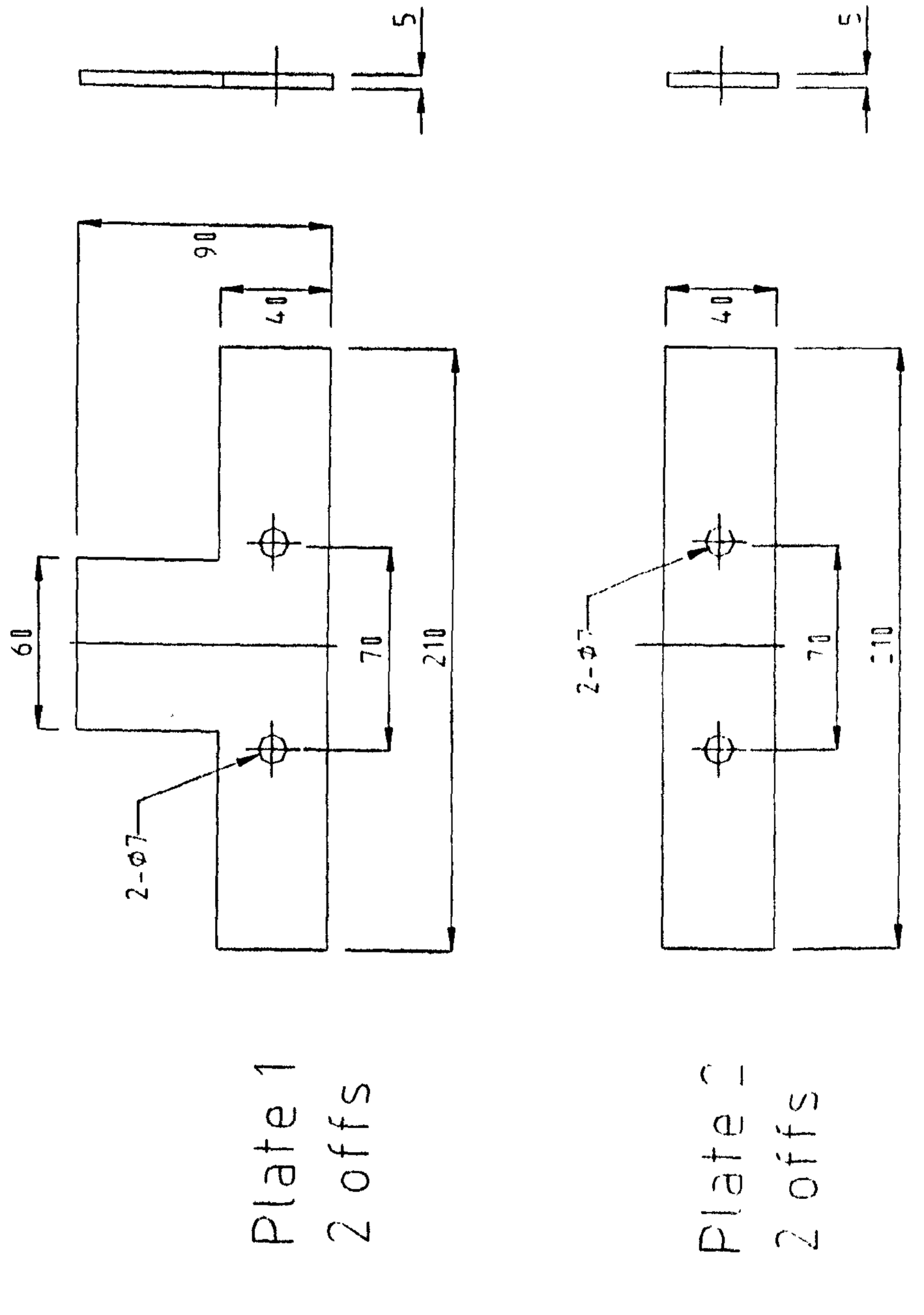

Fig. 4.24 The clamping design for planar tension test

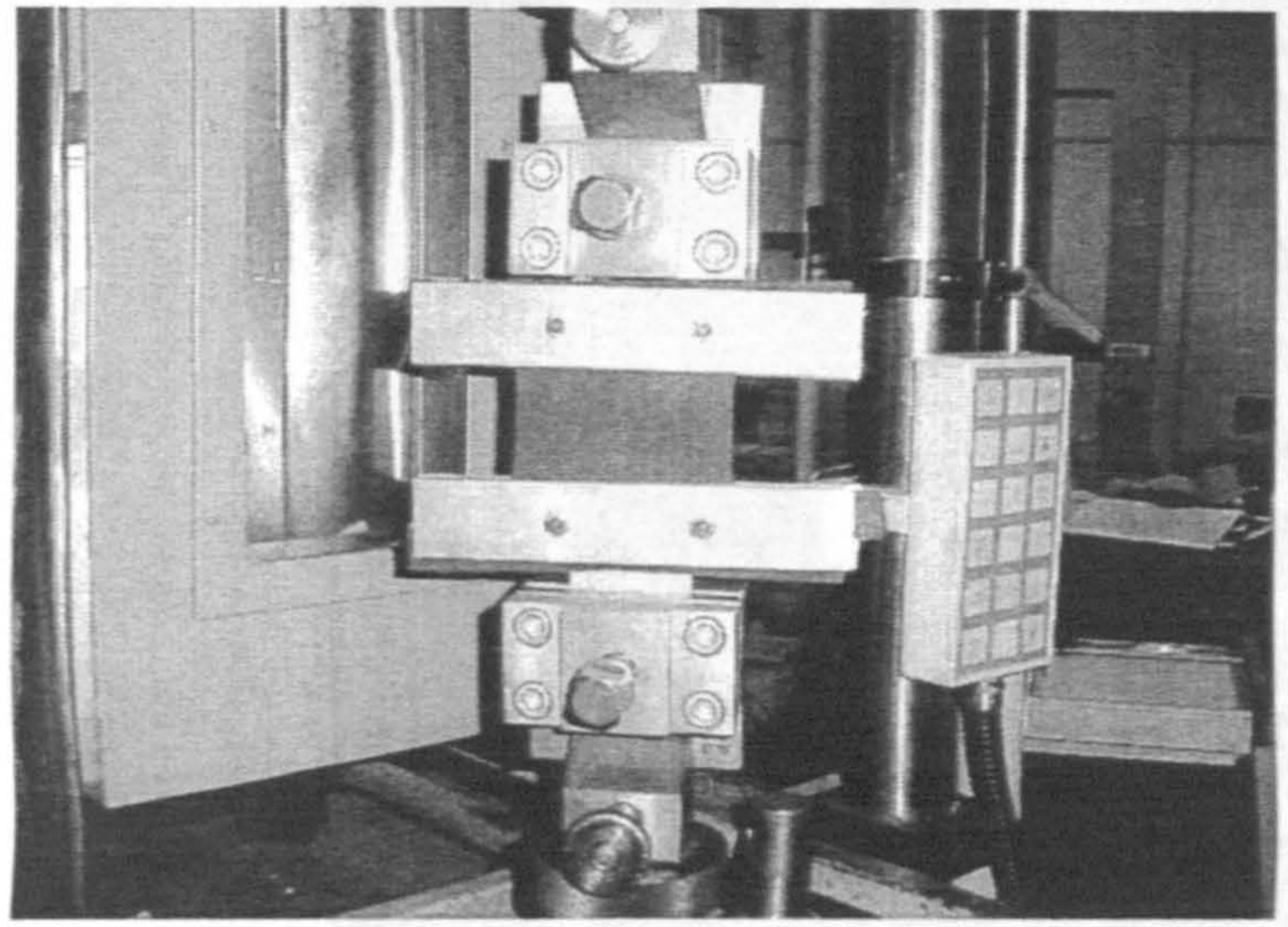

(a) The experimental set-up with hydraulic press

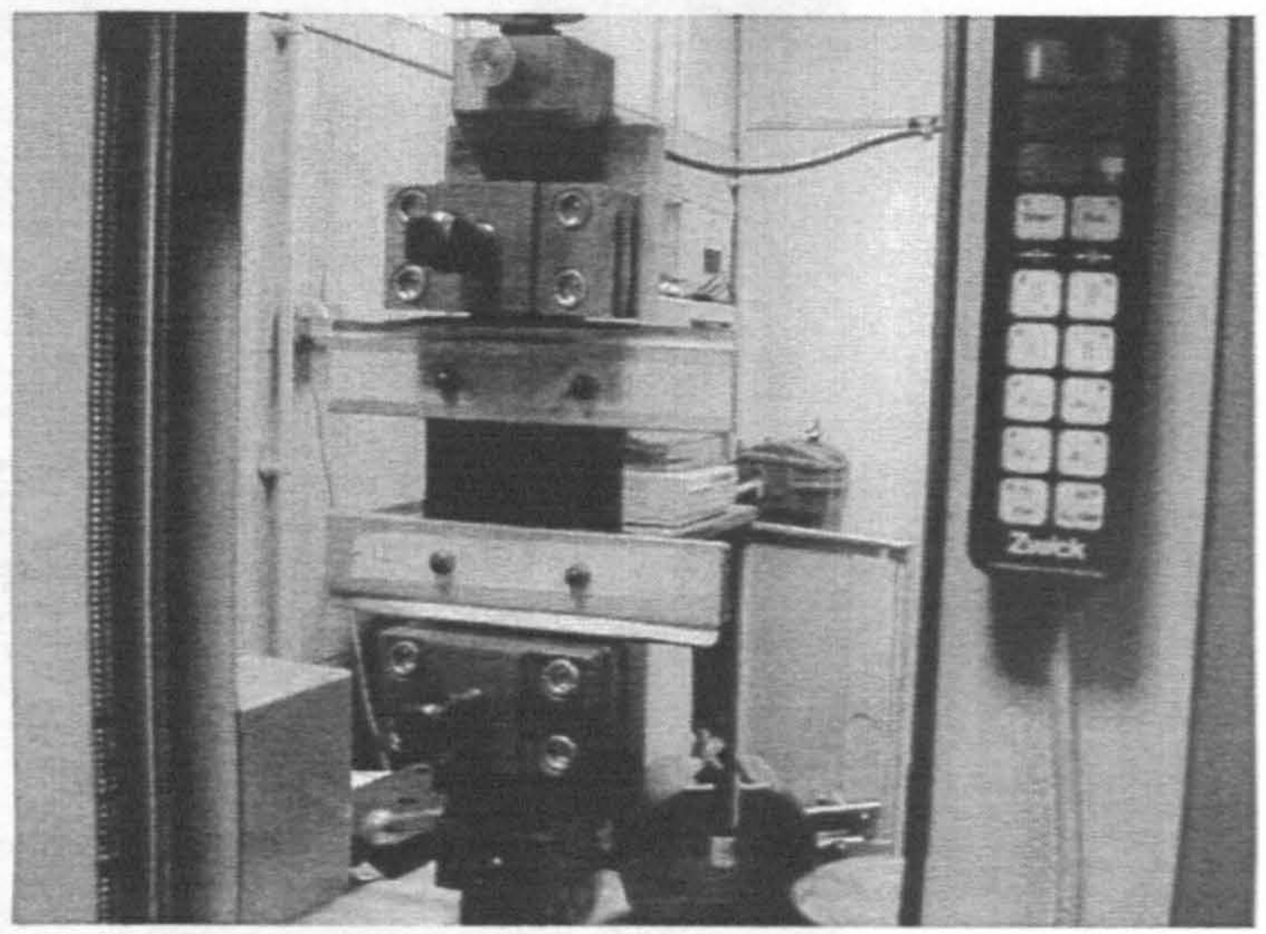

(b) The experimental set-up with mechanical press

Fig. 4.25 The planar tension test-set-ups

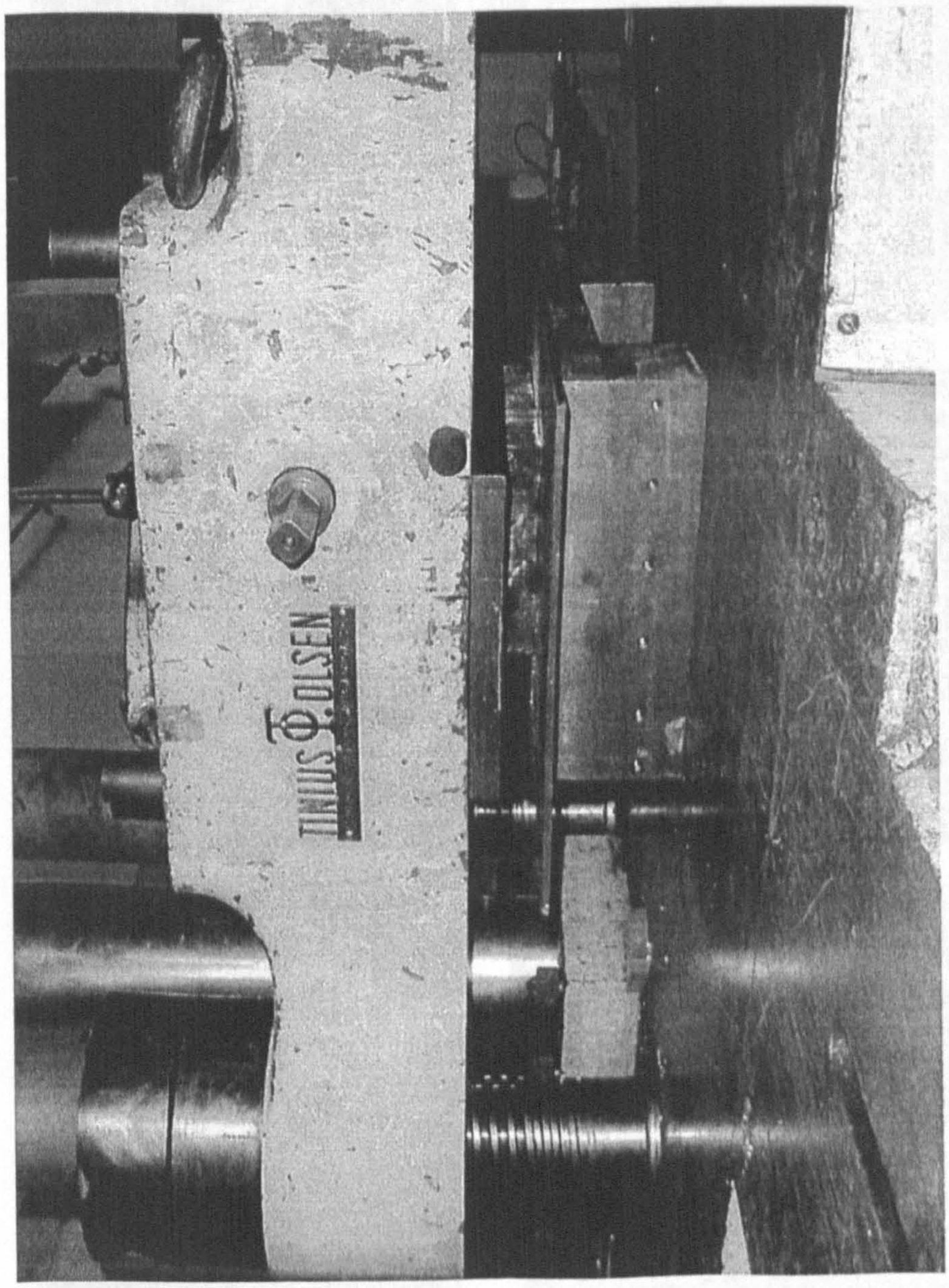

Fig. 4.26 The planar compression test-set-up

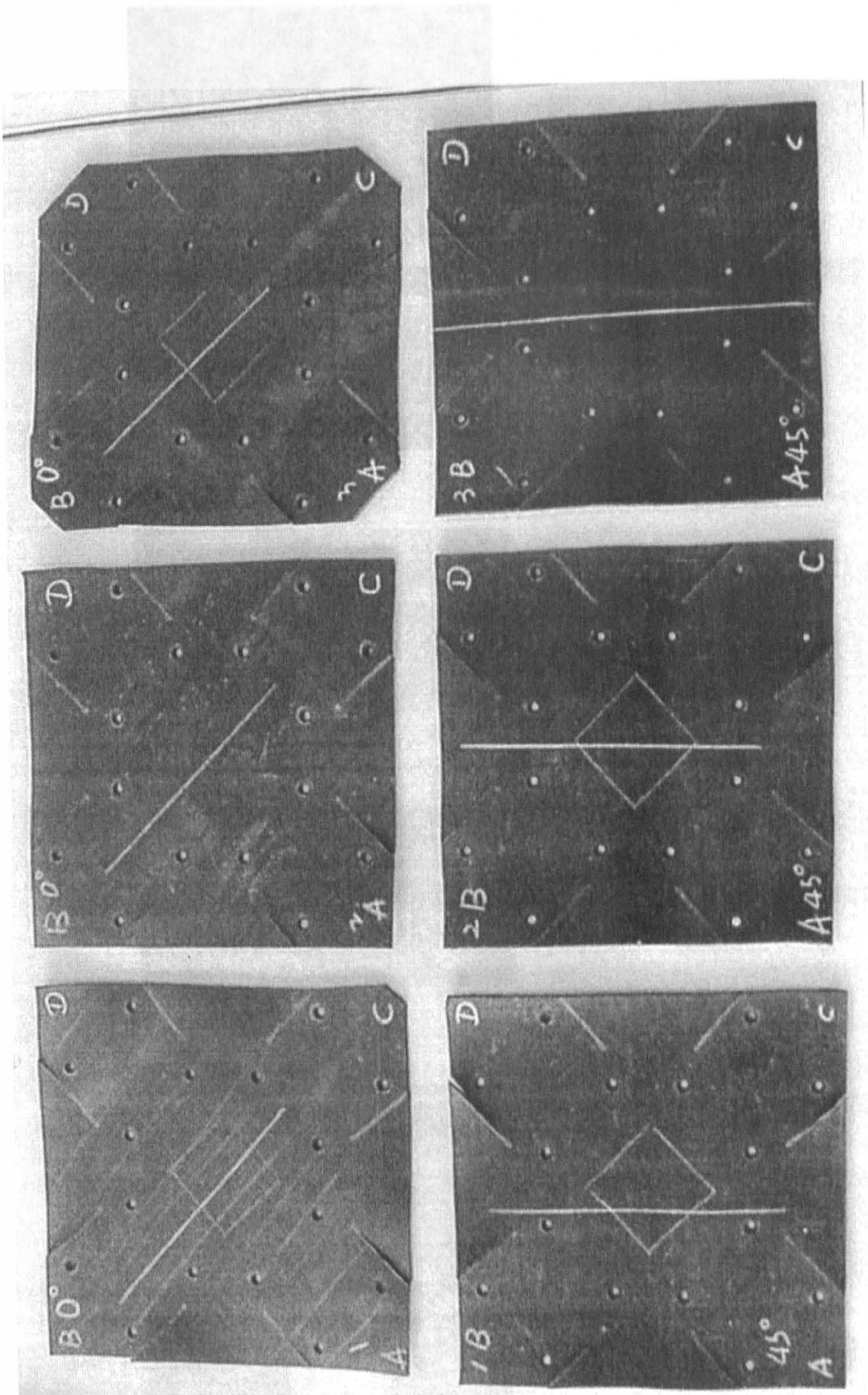

Fig. 4.27 The specimens prepared for biaxial tension test

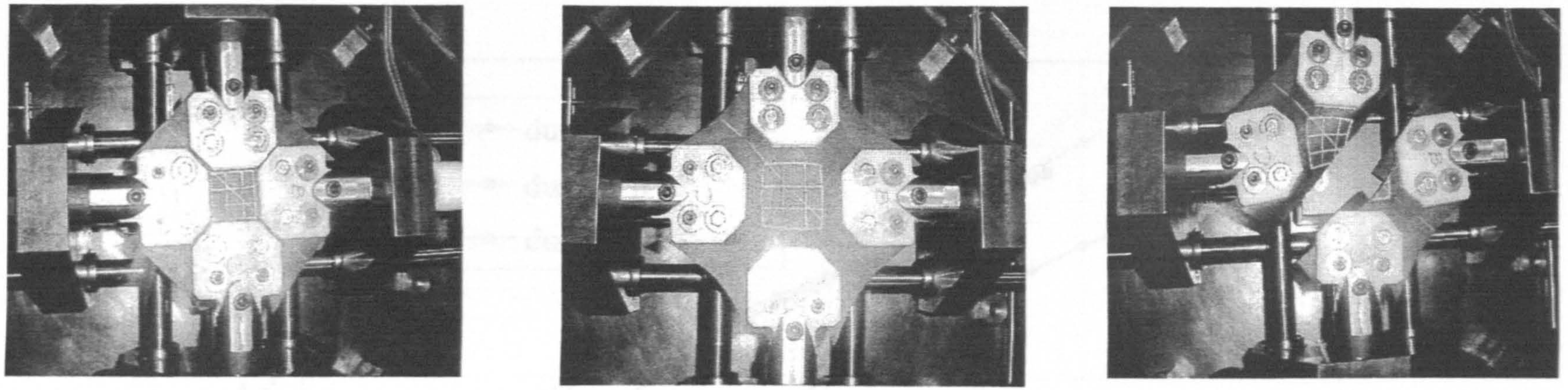

(a) Pre-test (b) During -test (c) Post-test

Fig. 4.28 The biaxial tension test set-ups

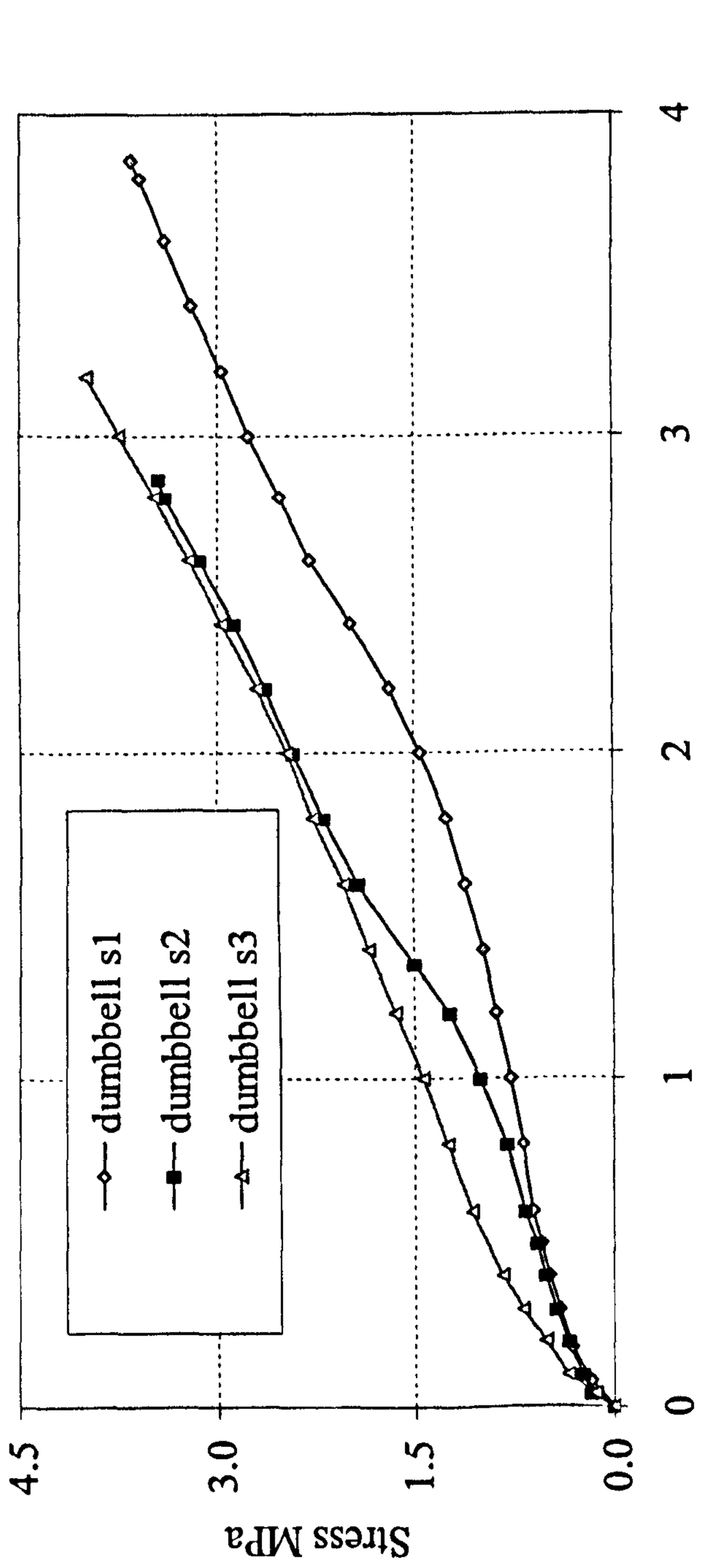

Fig. 4.2.9 Stress strain curves of Nitrile641 with dumbbell shaped specimens under uniaxial tension

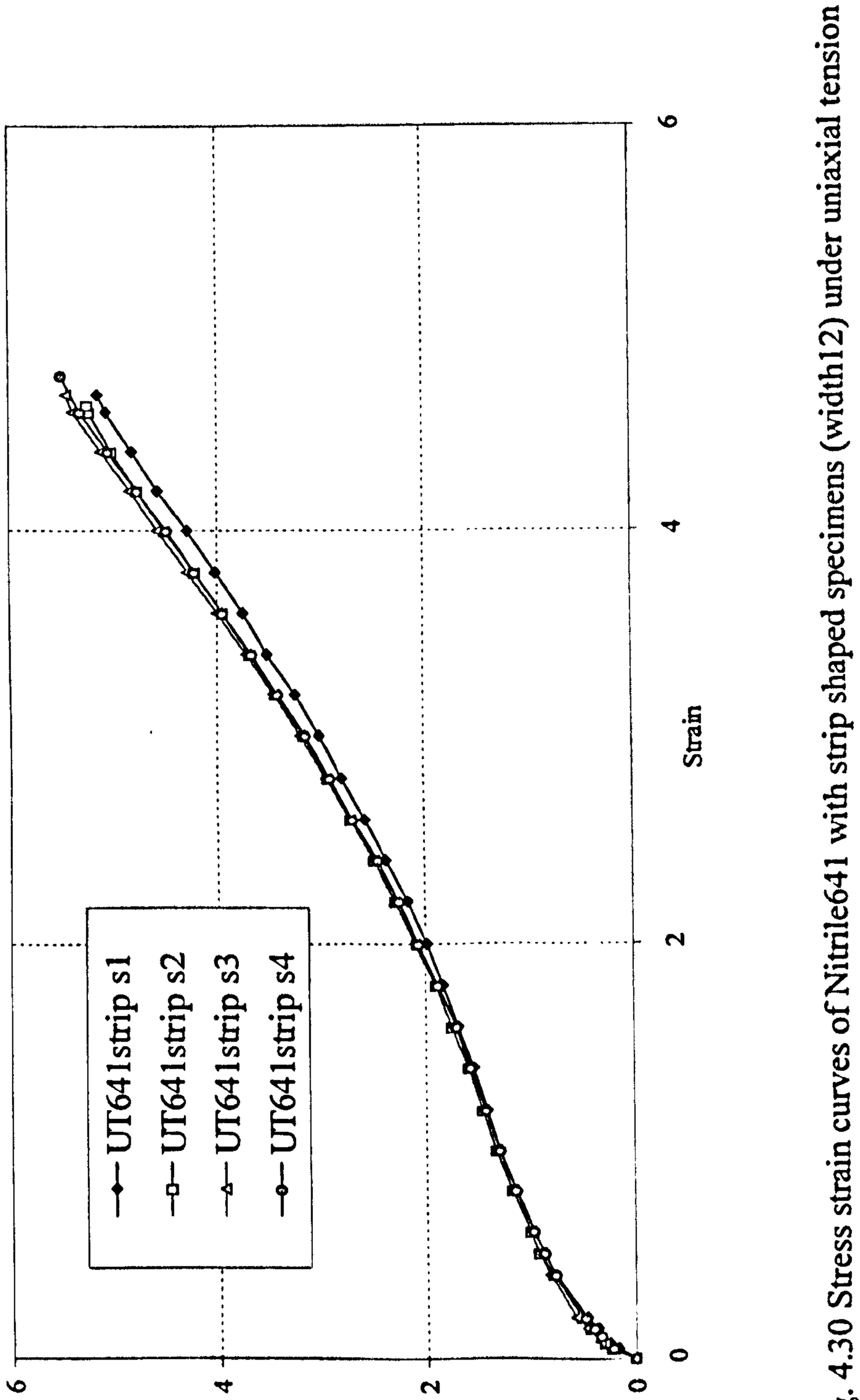

Fig. 4.30 Stress strain curves of Nitrile641 with strip shaped specimens (width12) under uniaxial tension

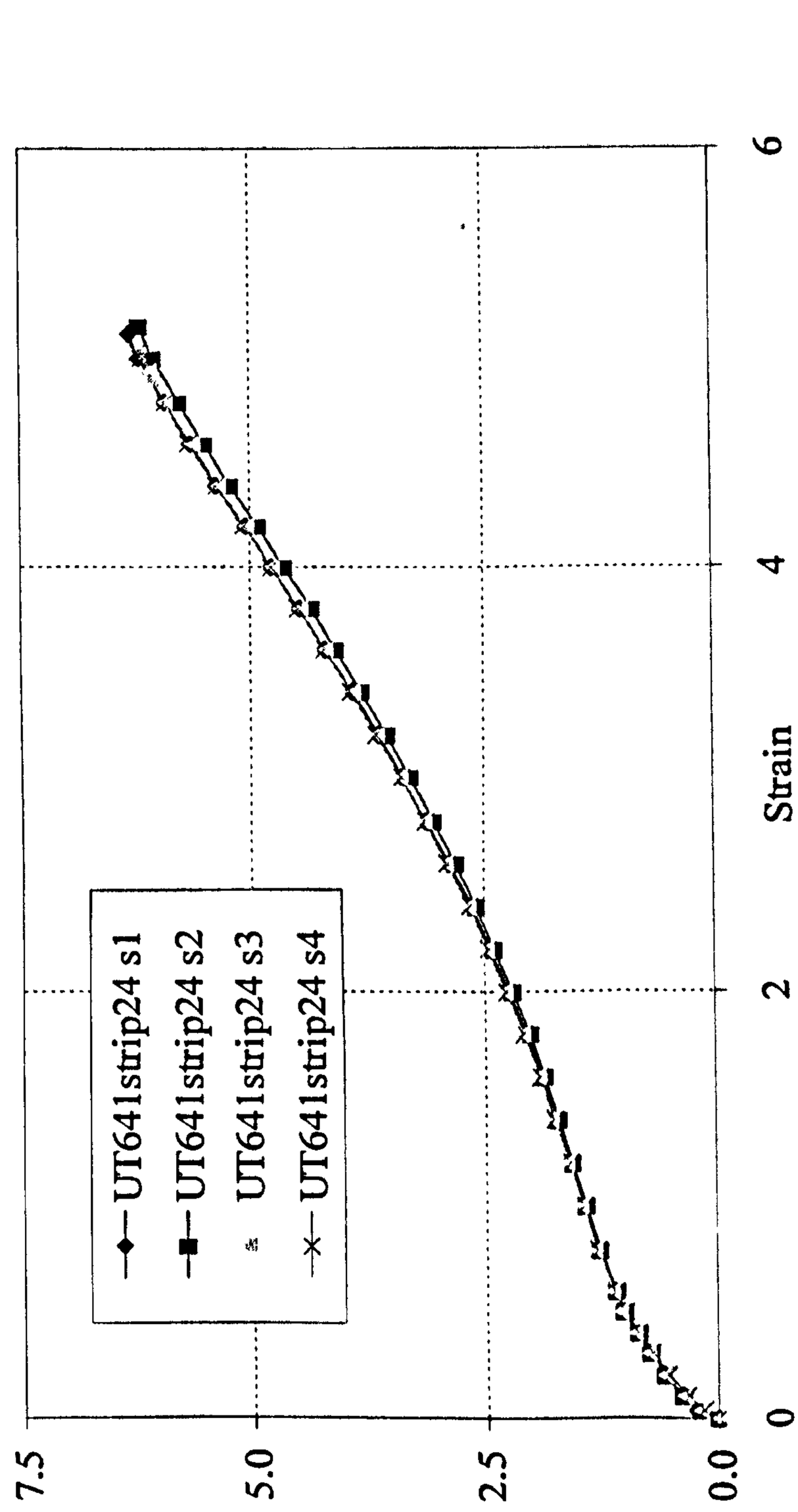

Fig. 4.31 Stress strain curves of Nitrile641 with strip shaped specimens (width24) under uniaxial tension

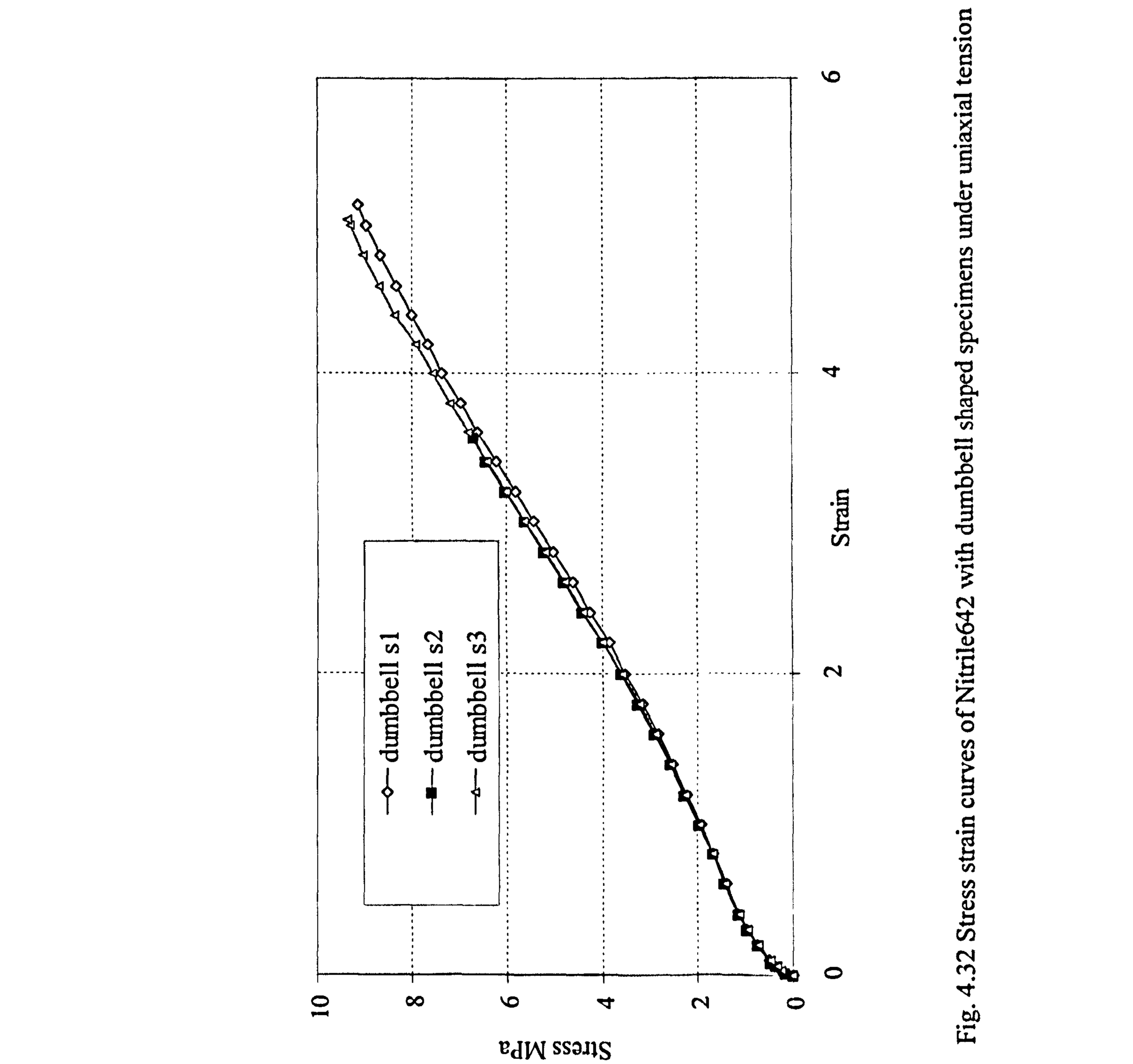

Fig. 4.32 Stress strain curves of Nitrile642 with dumbbell shaped specimens under uniaxial tension

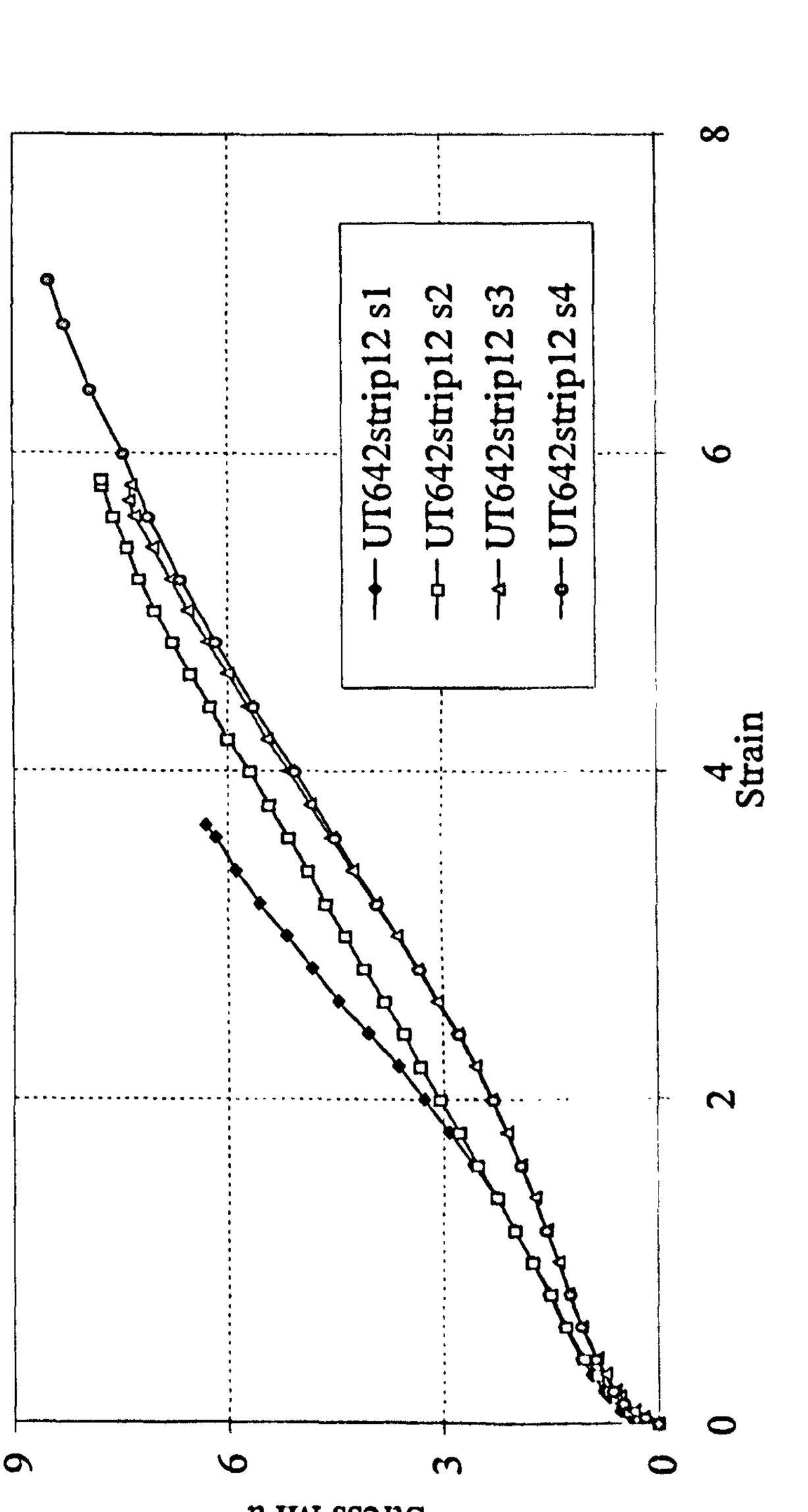

Fig. 4.33 Stress strain curves of Nitrile642 with strip shaped specimens (width12) under uniaxial tension

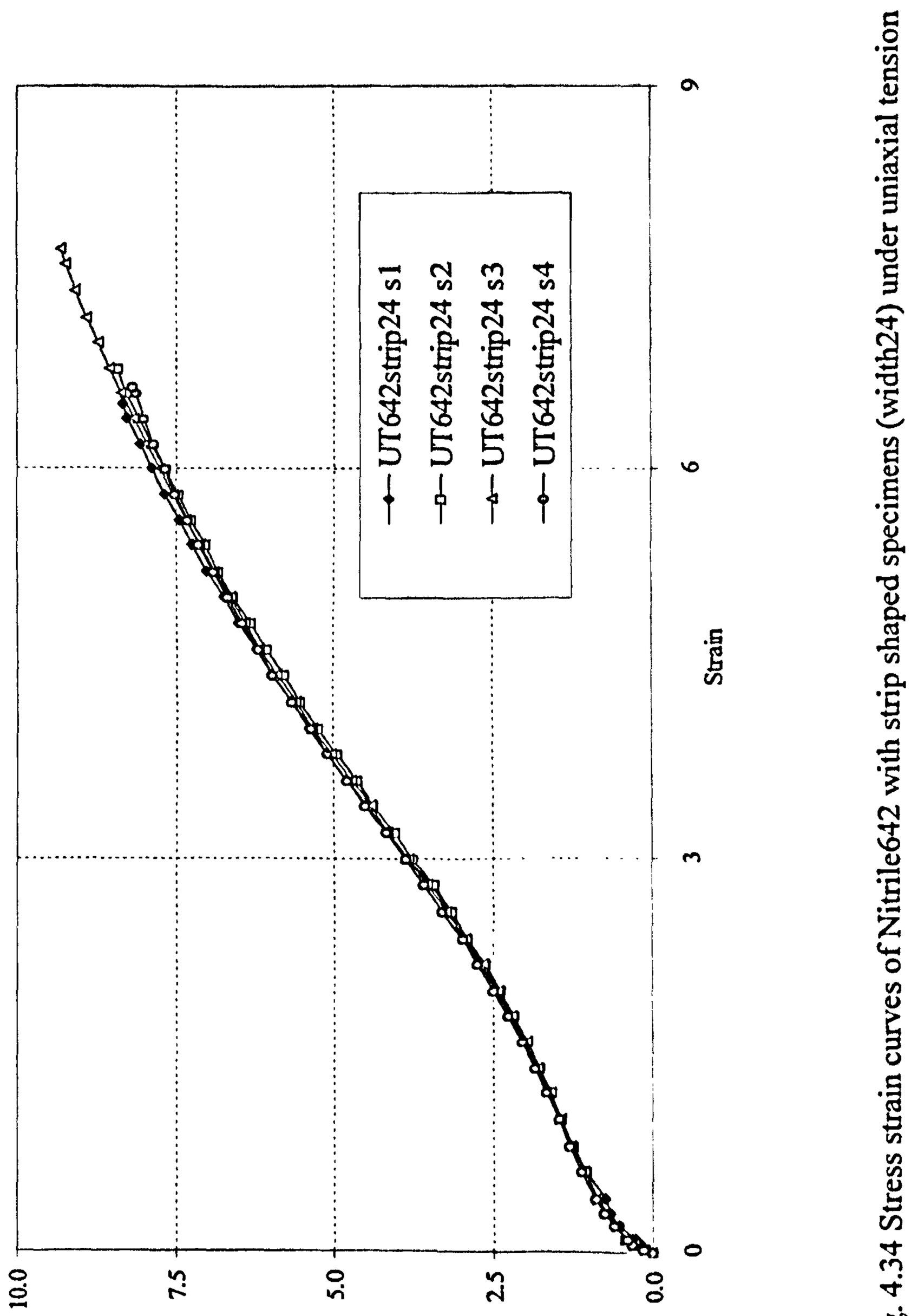

Fig. 4.34 Stress strain curves of Nitrile642 with strip shaped specimens (width24) under uniaxial tension

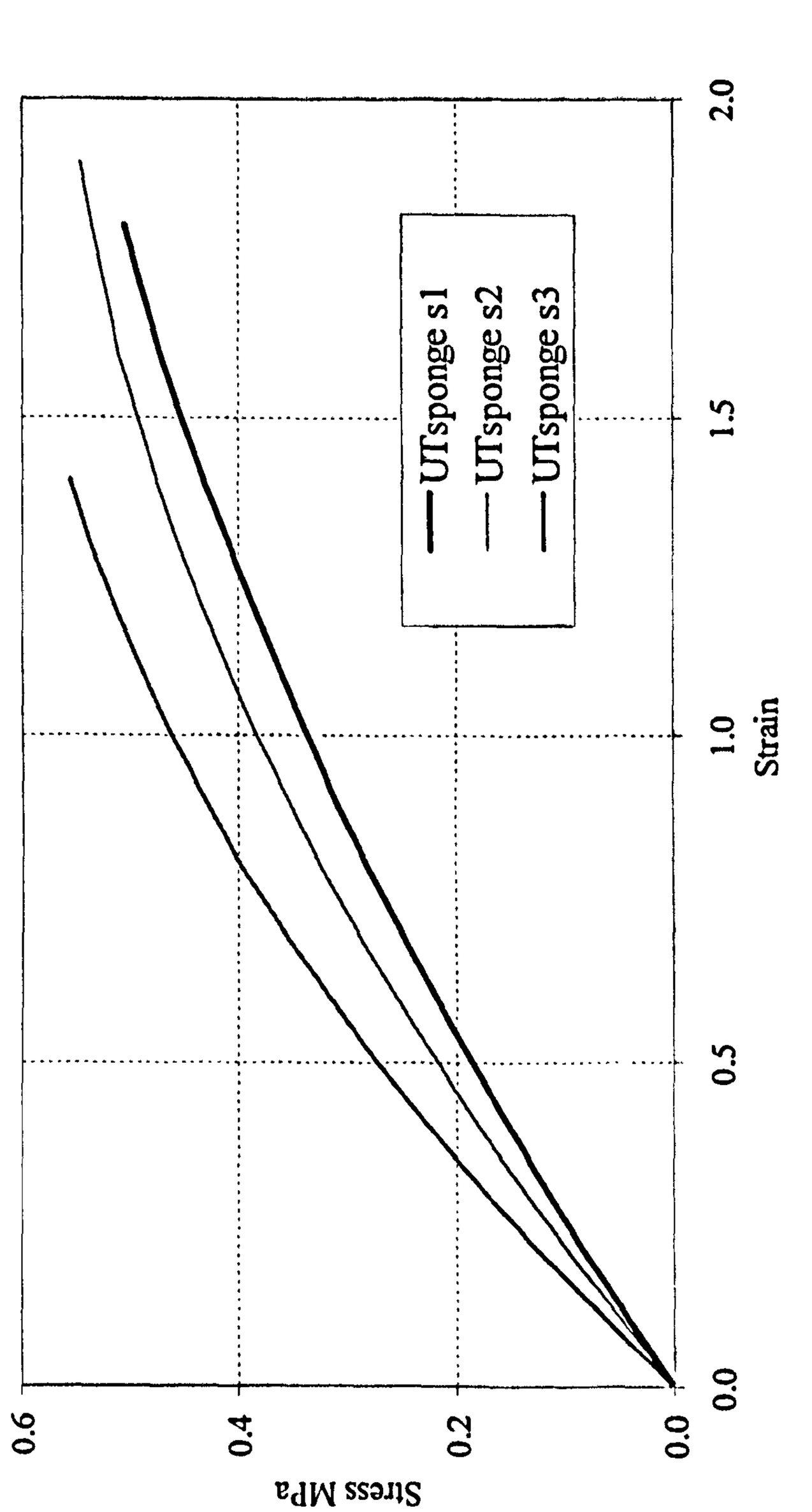

Fig. 4.35 Stress strain curves of Neo Sponge with dumbbell shaped specimens under uniaxial tension

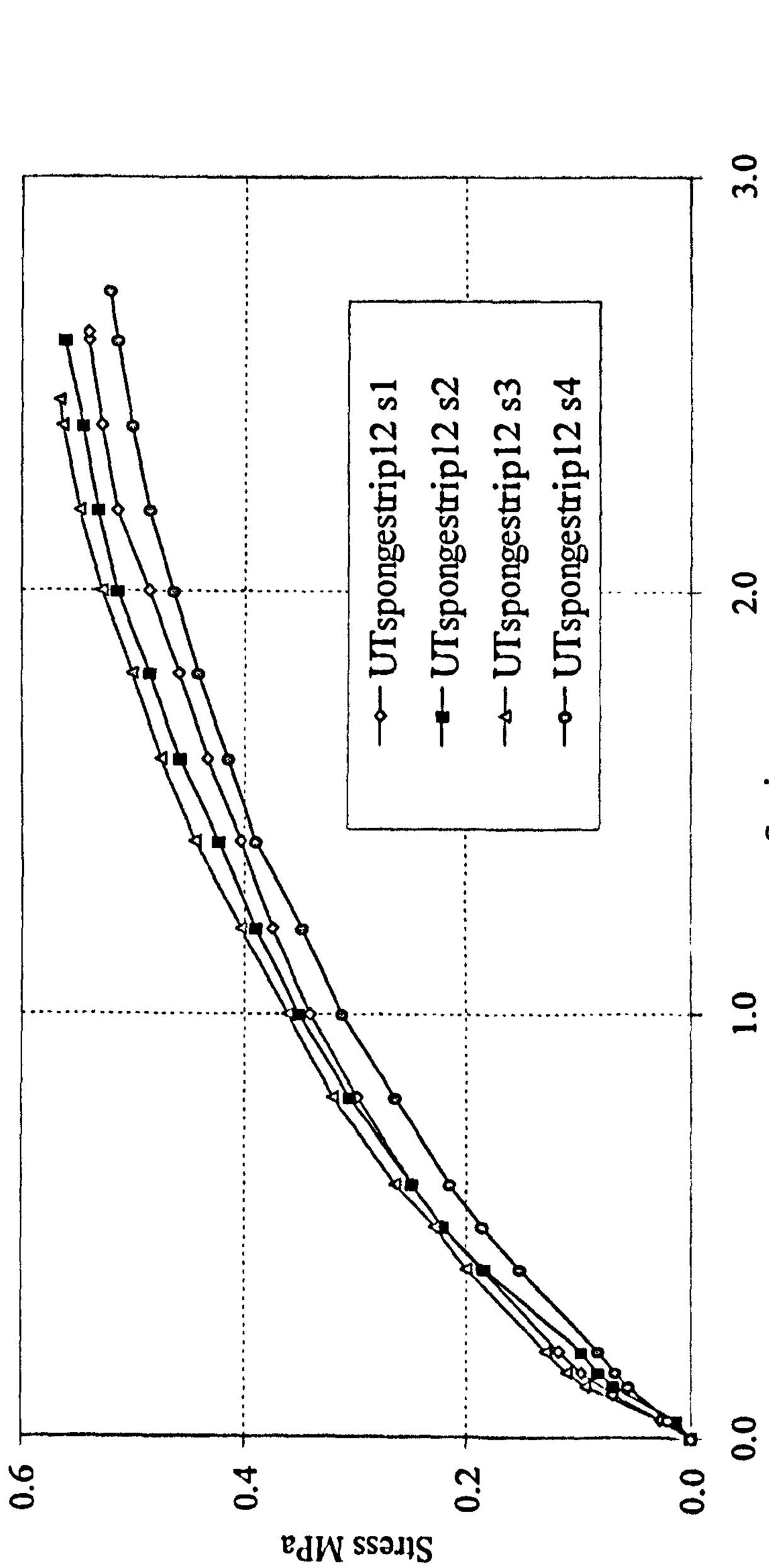

Fig. 4.36 Stress Strain Curves of Neo Sponge with strip shaped specimens (width12) under uniaxial tension

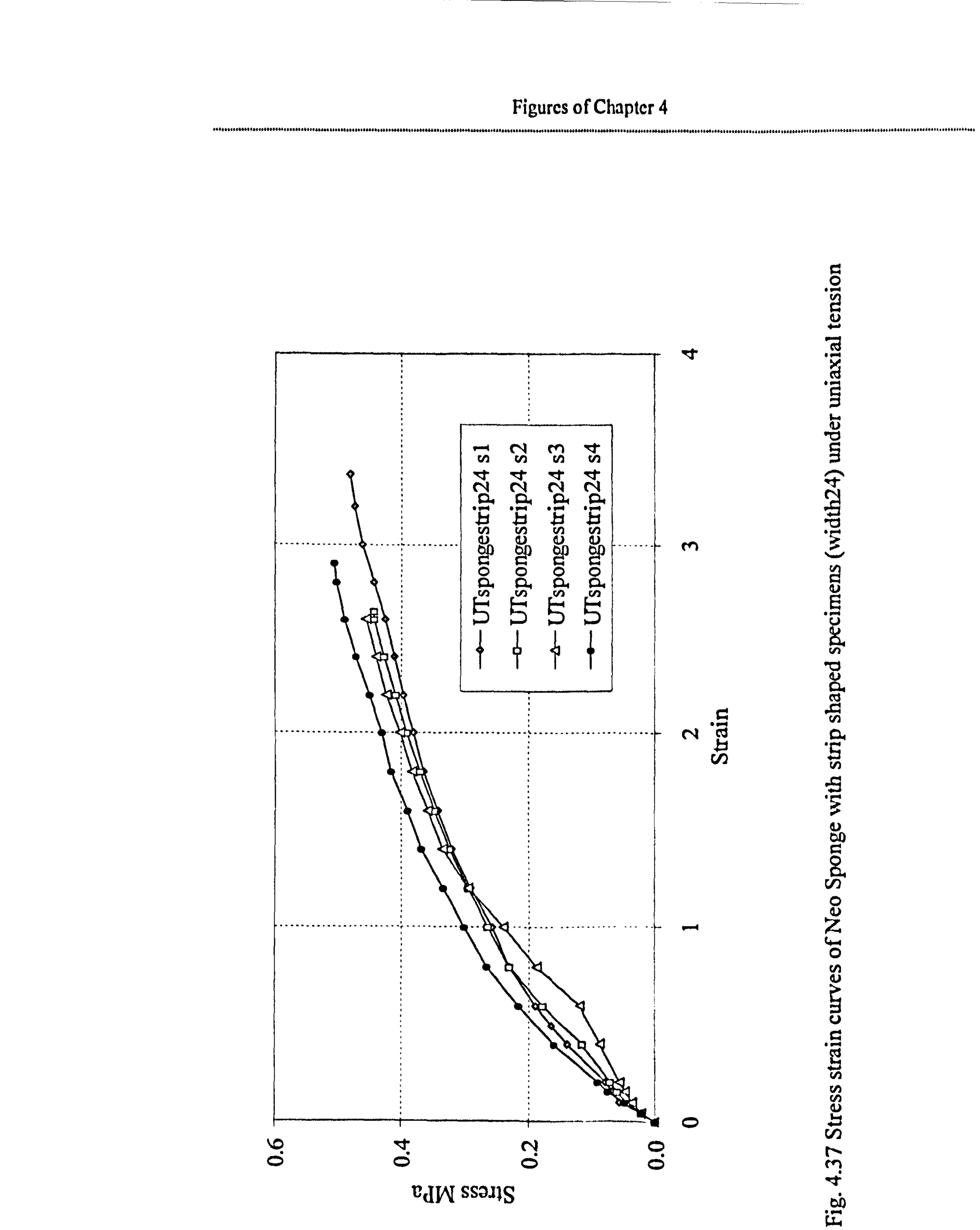

Fig. 4.37 Stress strain curves of Neo Sponge with strip shaped specimens (width24) under uniaxial tension

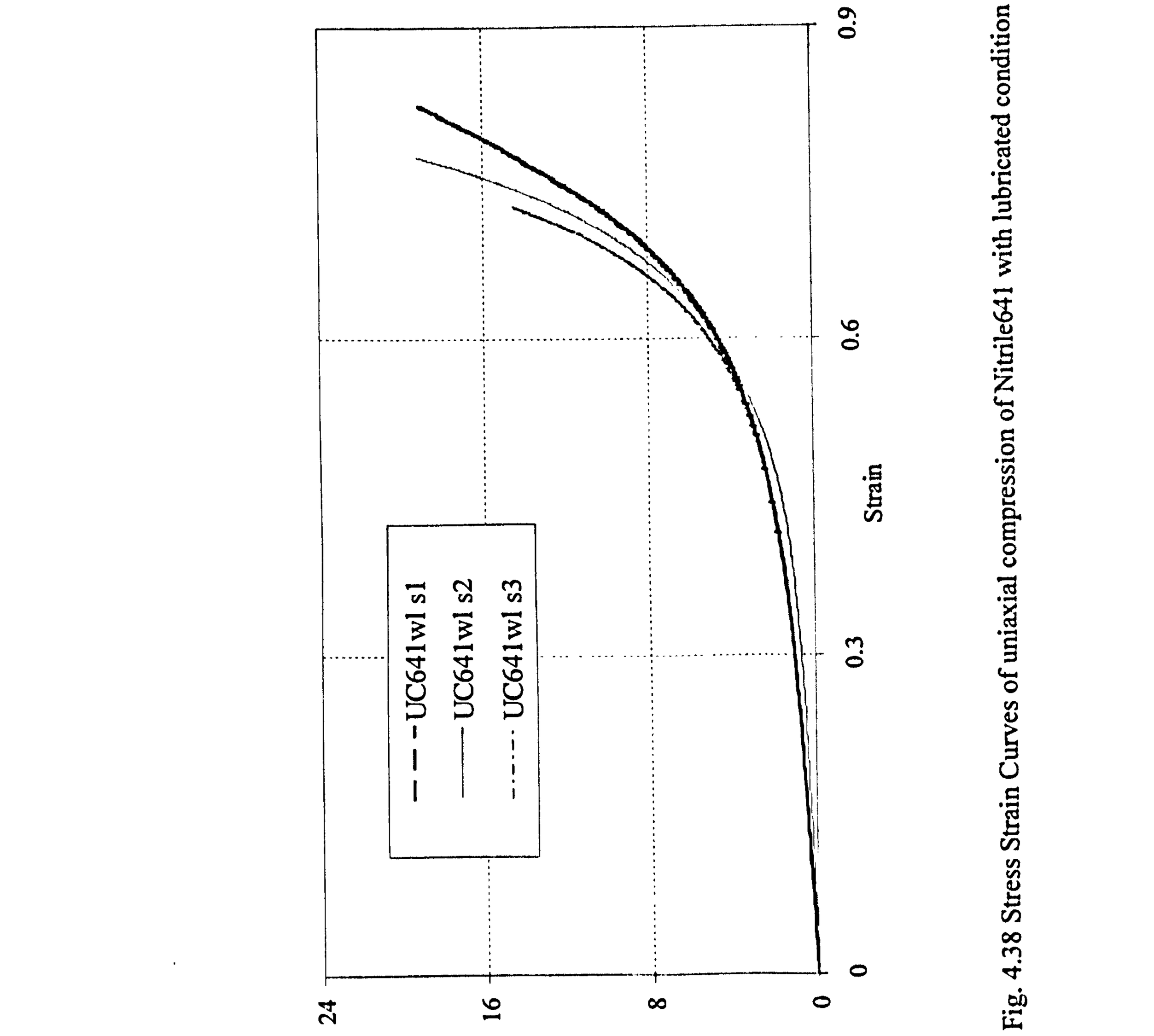

Fig. 4.38 Stress Strain Curves of uniaxial compression of Nitrile641 with lubricated condition

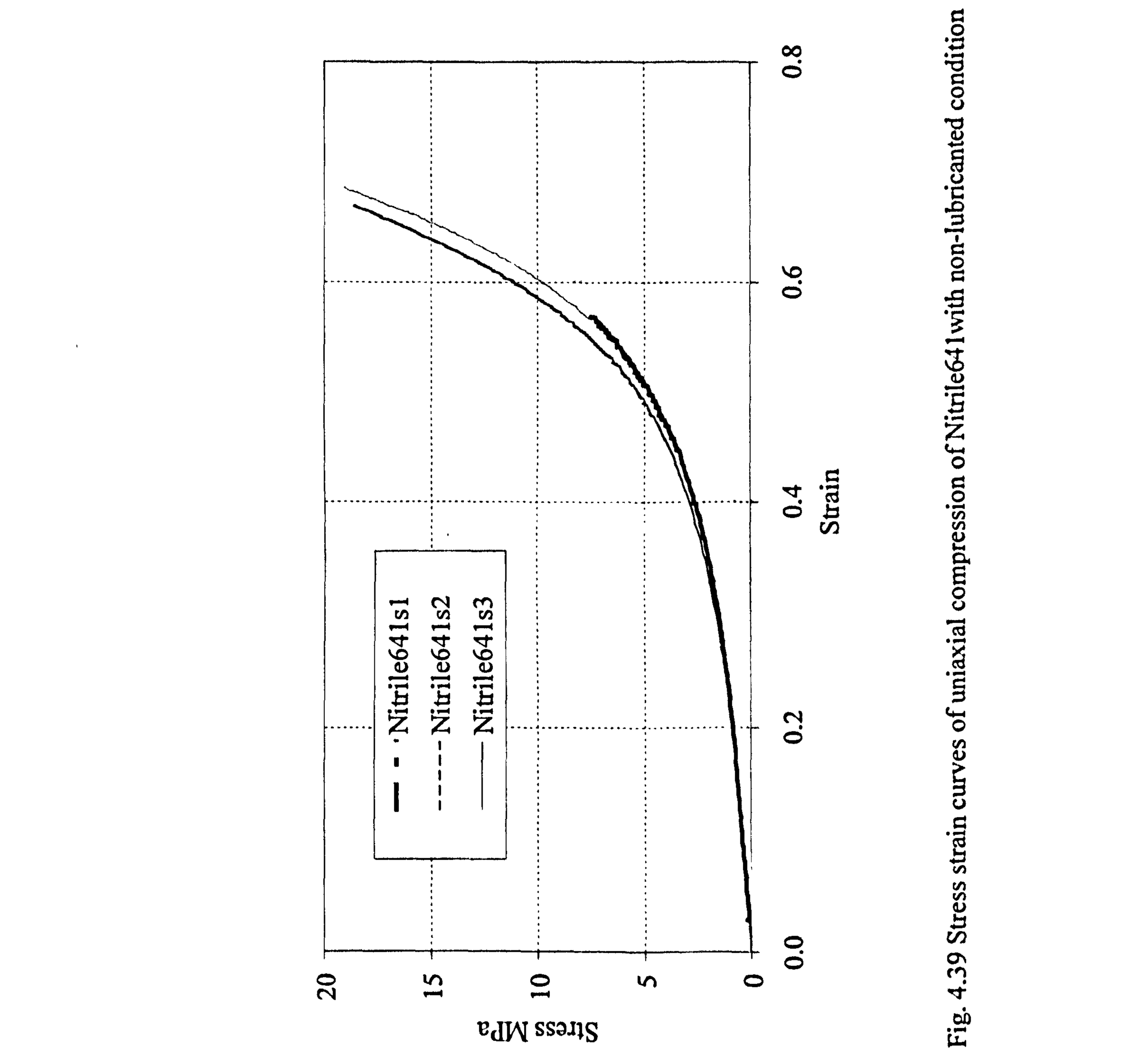

Fig. 4.39 Stress strain curves of uniaxial compression of Nitrile641with non-lubricanted conditi

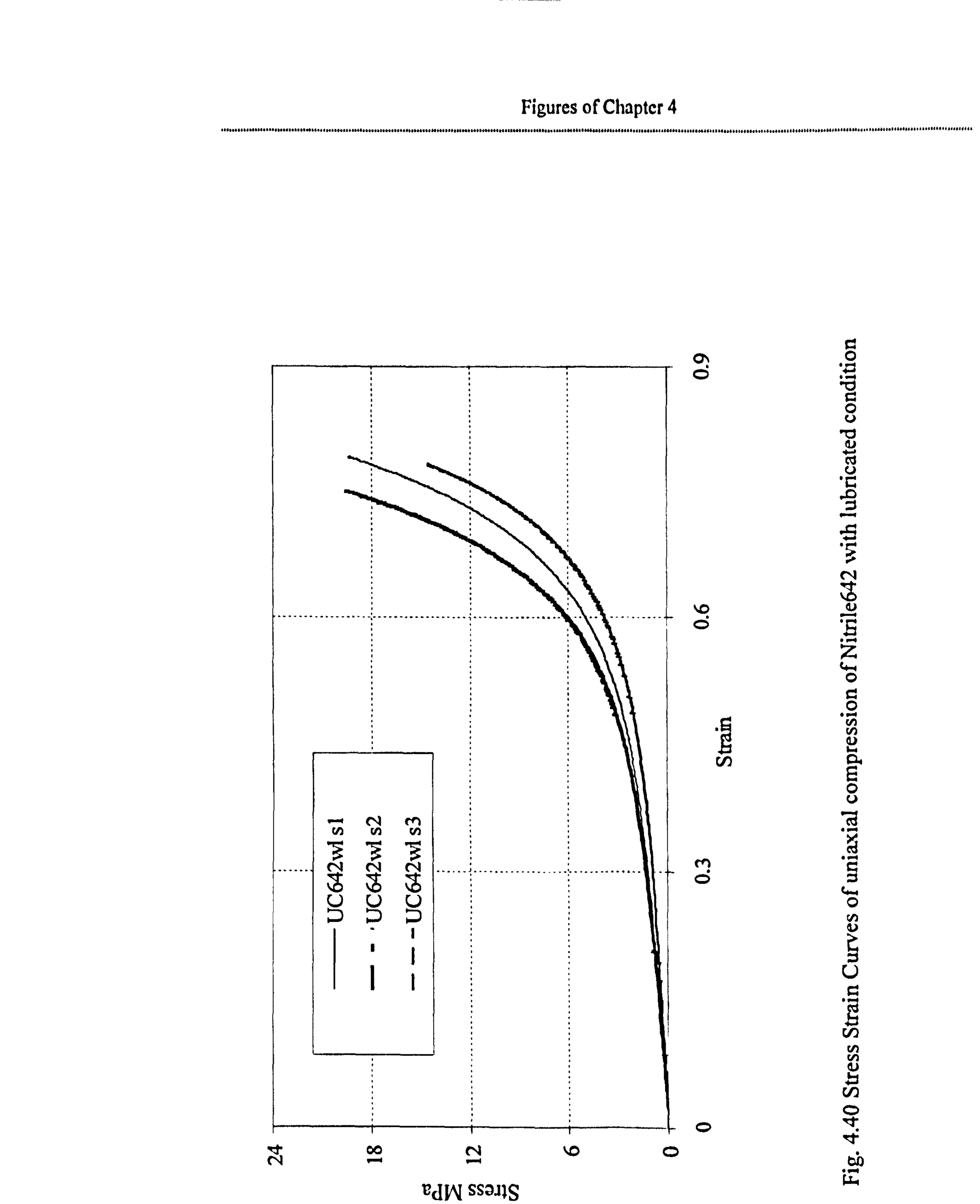

Fig. 4.40 Stress Strain Curves of uniaxial compression of Nitrile642 with lubricated conditio

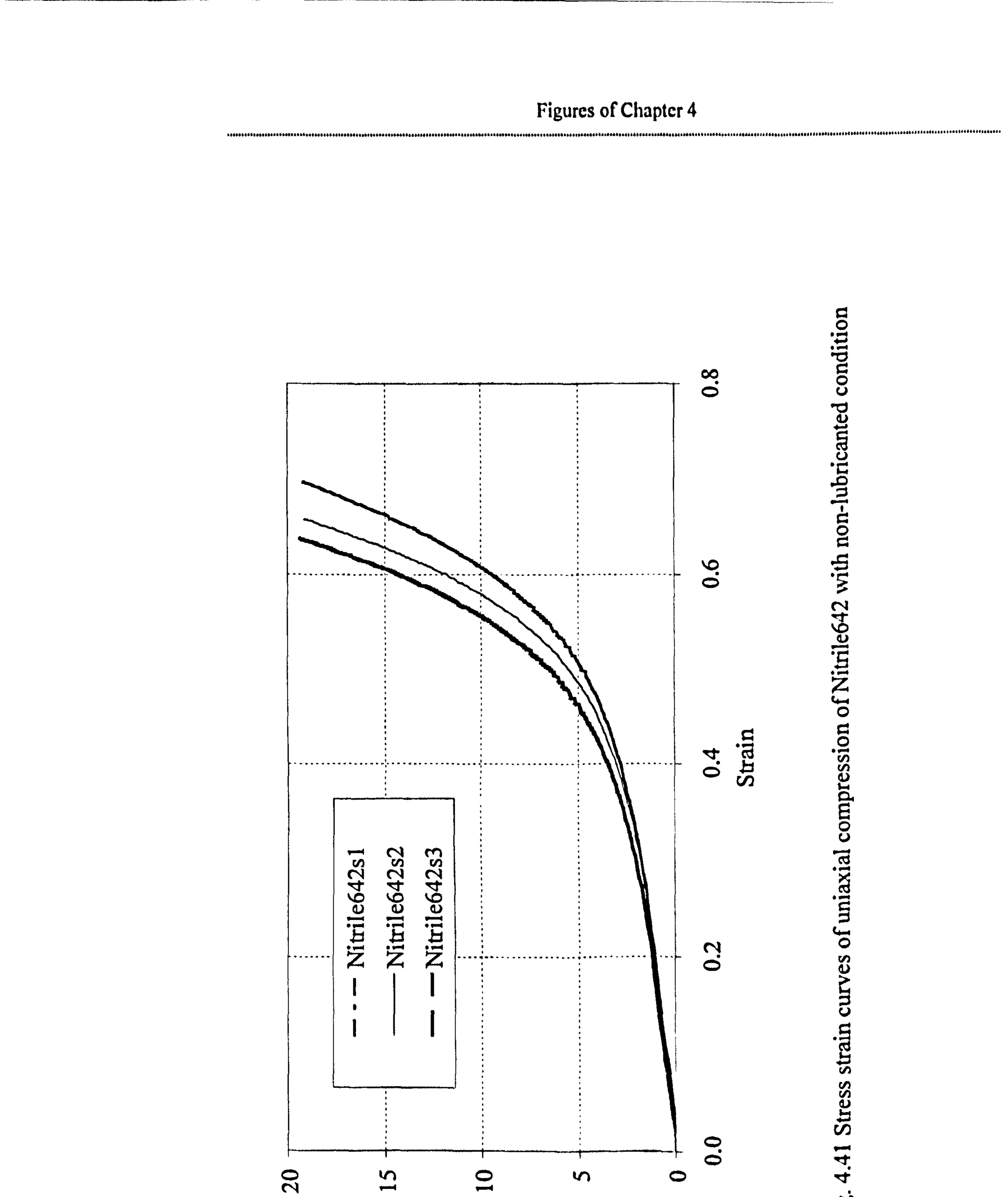

Fig. 4.41 Stress strain curves of uniaxial compression of Nitrile642 with non-lubricanted condition

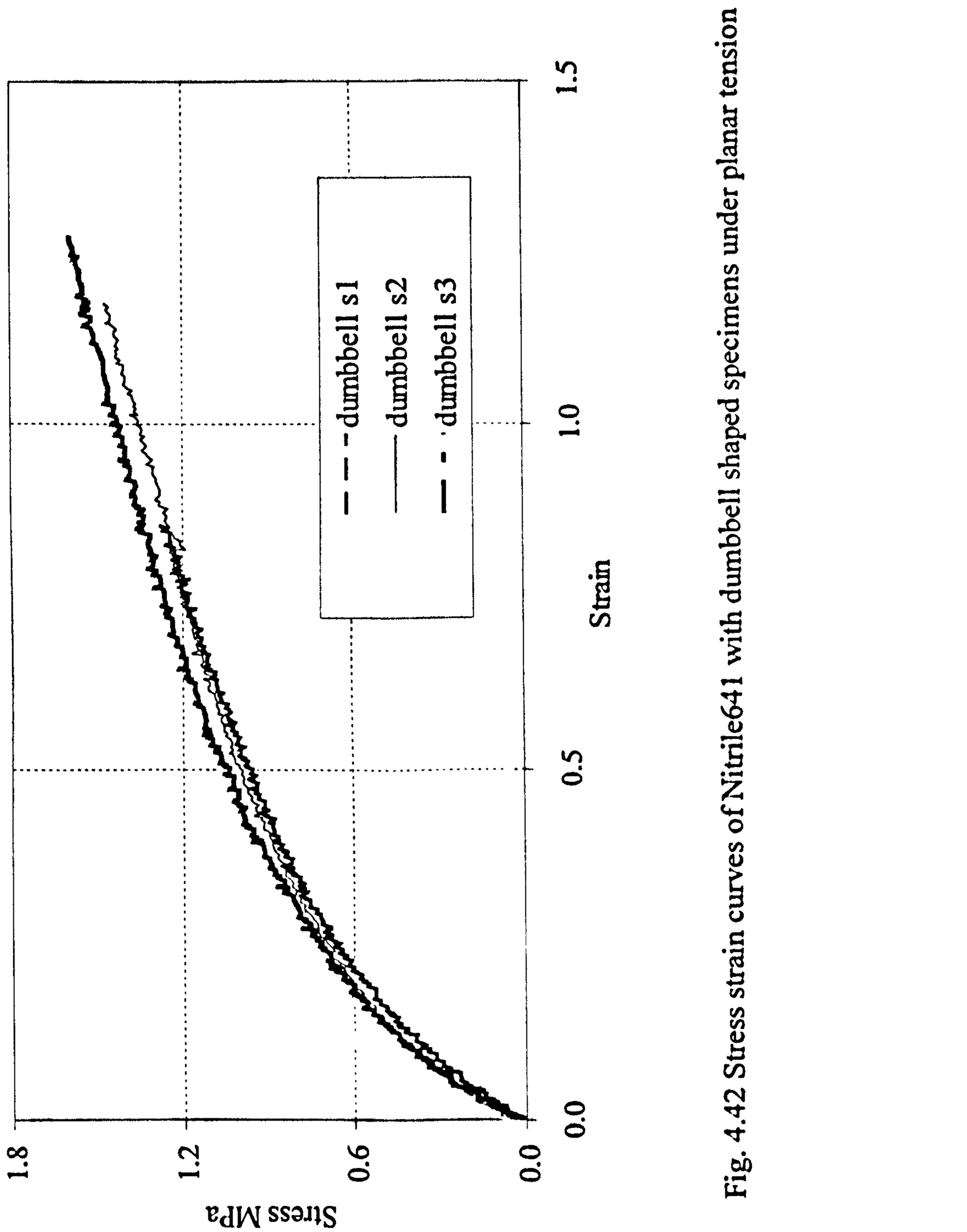

Fig. 4.42 Stress strain curves of Nitrile641 with dumbbell shaped specimens under planar te

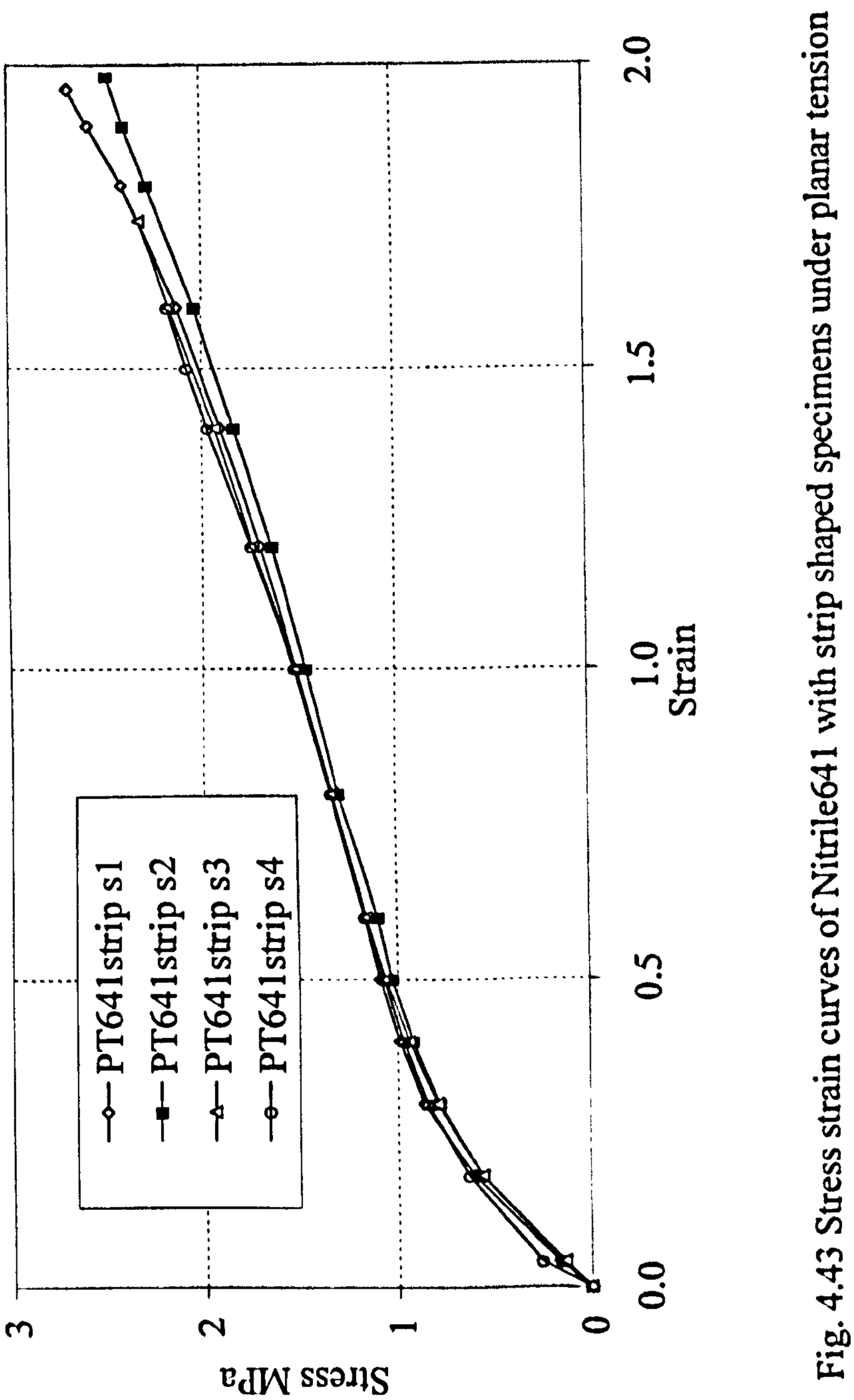

Fig. 4.43 Stress strain curves of Nitrile641 with strip shaped specimens under planar tension

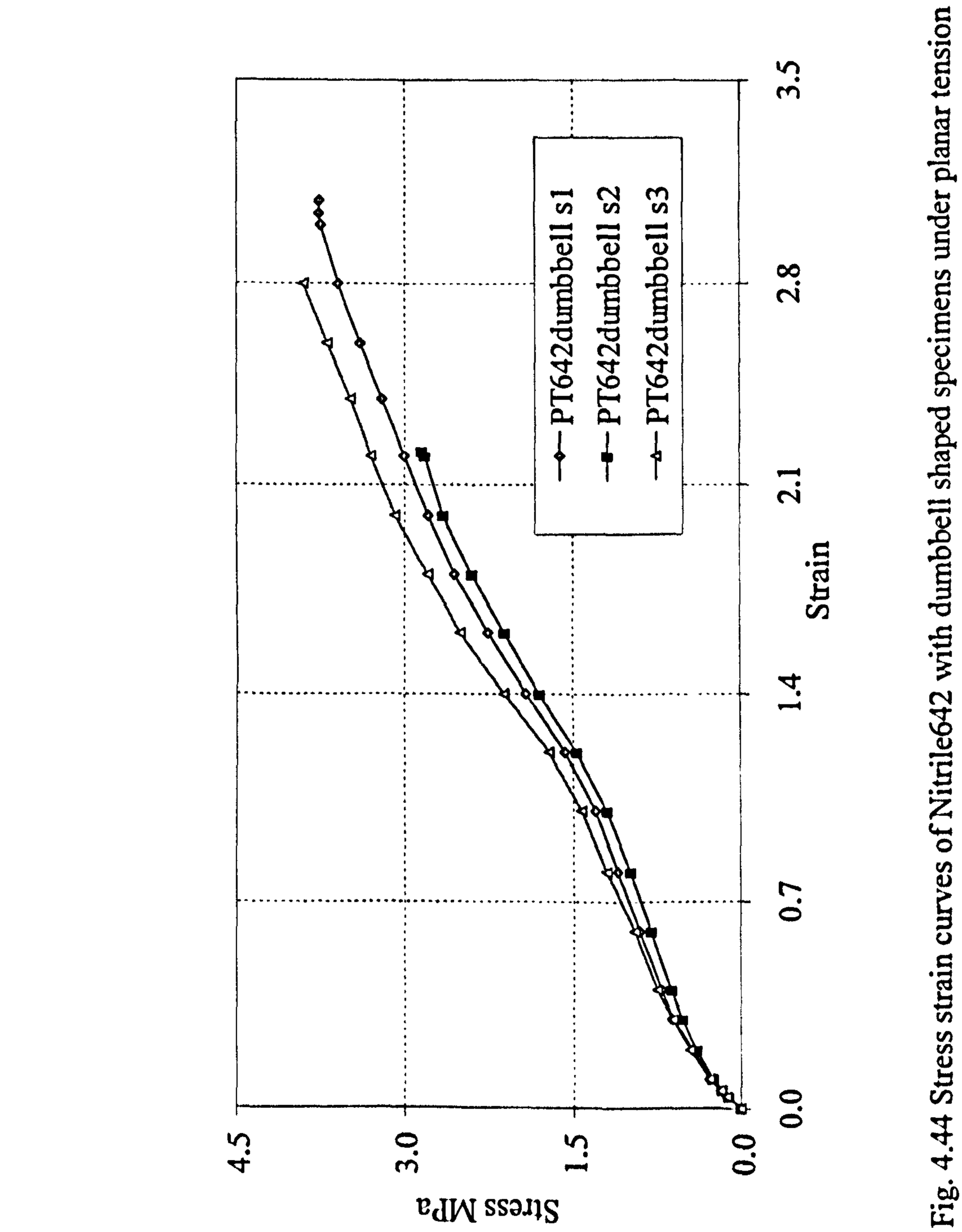

Fig. 4.44 Stress strain curves of Nitrile642 with dumbbell shaped specimens under planar te

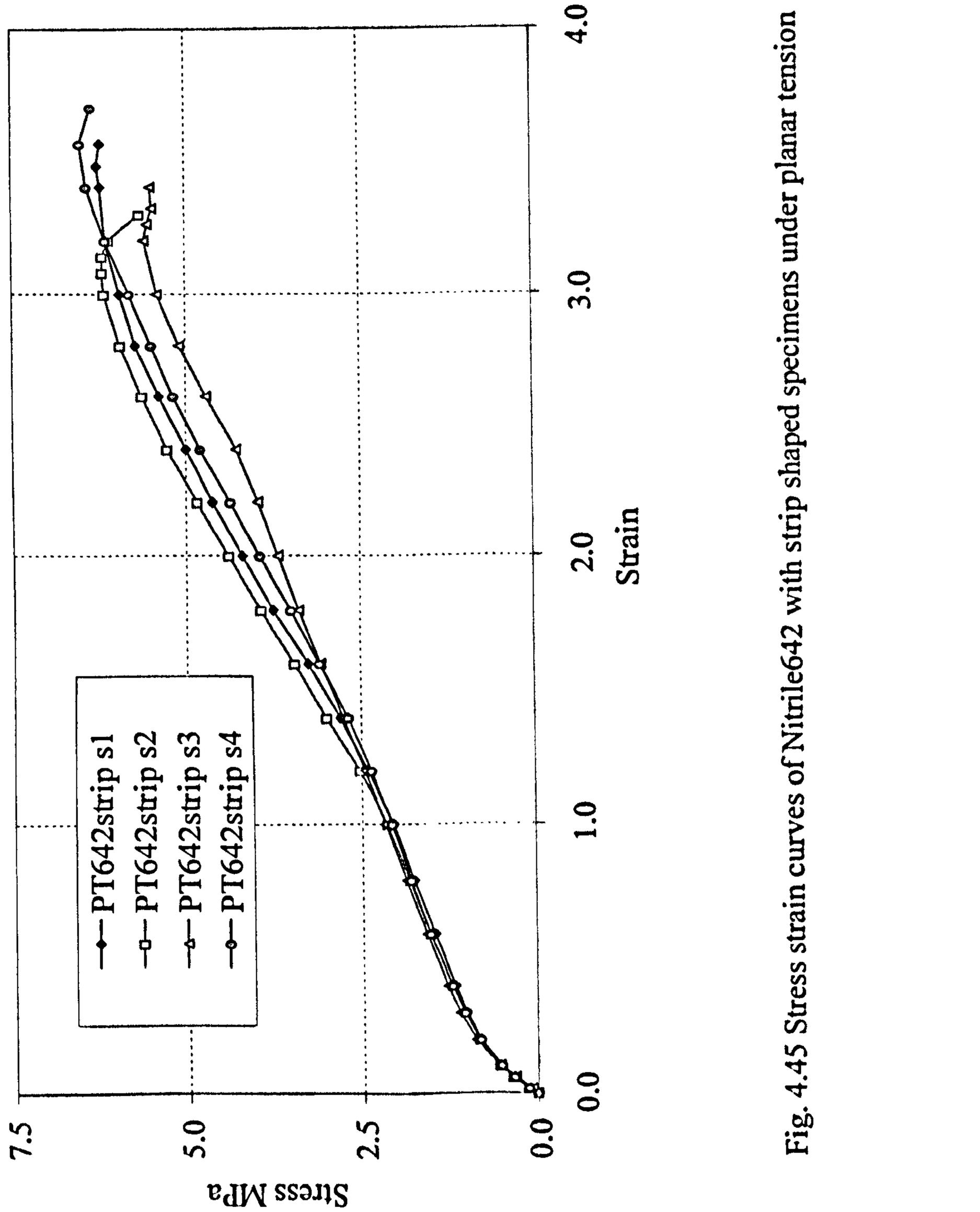

Fig. 4.45 Stress strain curves of Nitrile642 with strip shaped specimens under planar tension

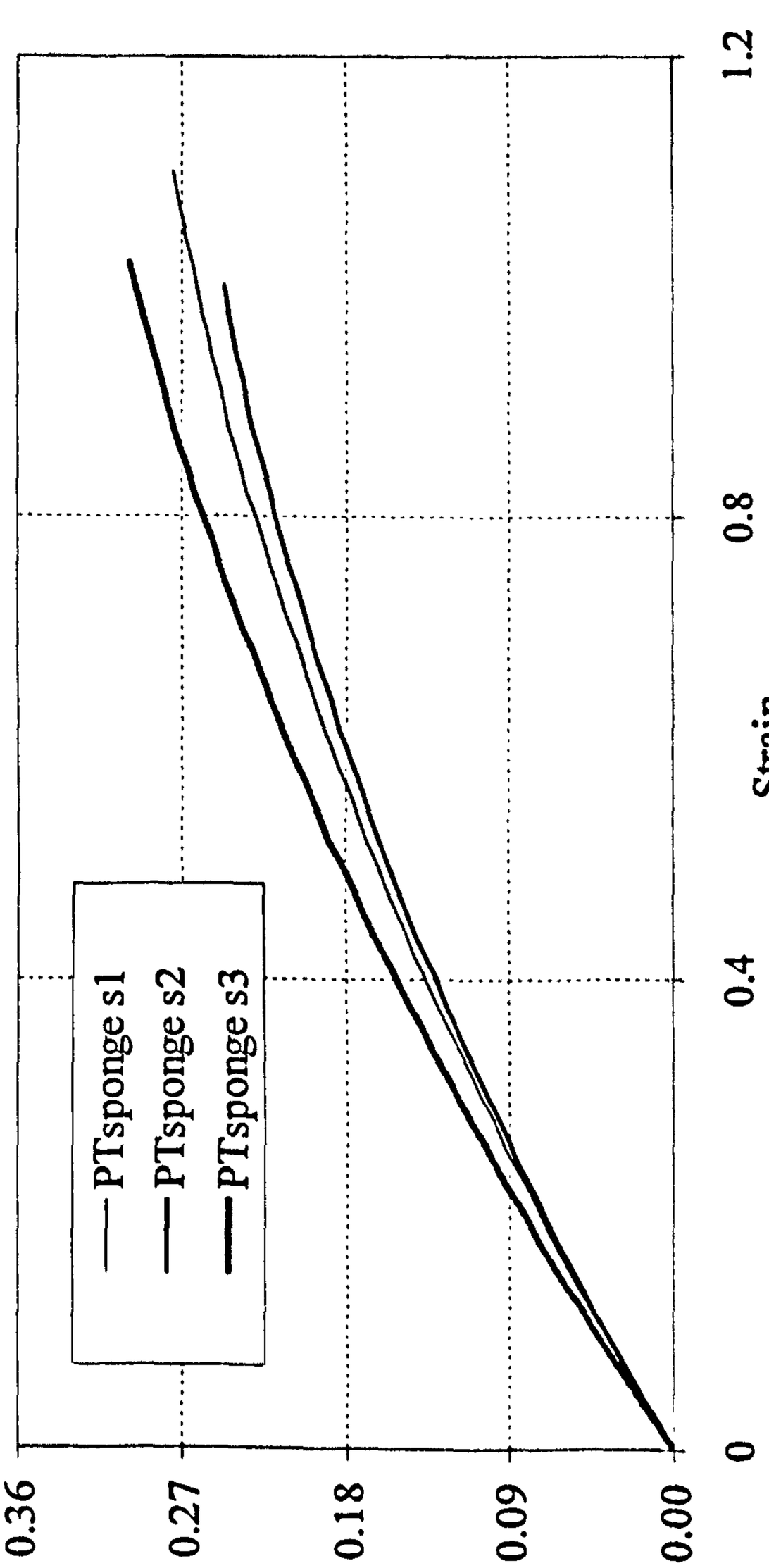

Fig. 4.46 Stress strain curves of Neo Sponge with dumbbell shaped speicmens under planar tensio

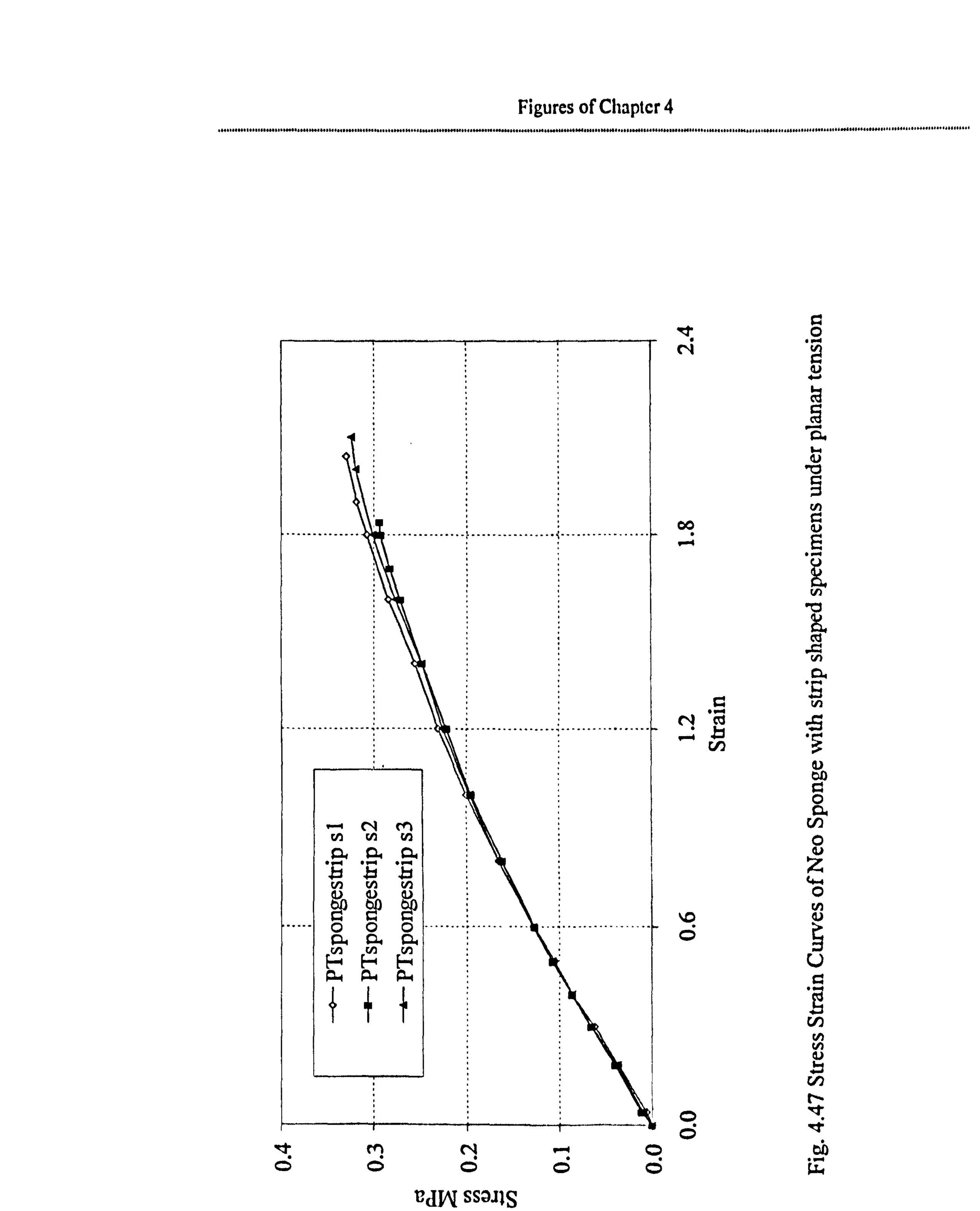

Fig. 4.47 Stress Strain Curves of Neo Sponge with strip shaped specimens under planar tensi

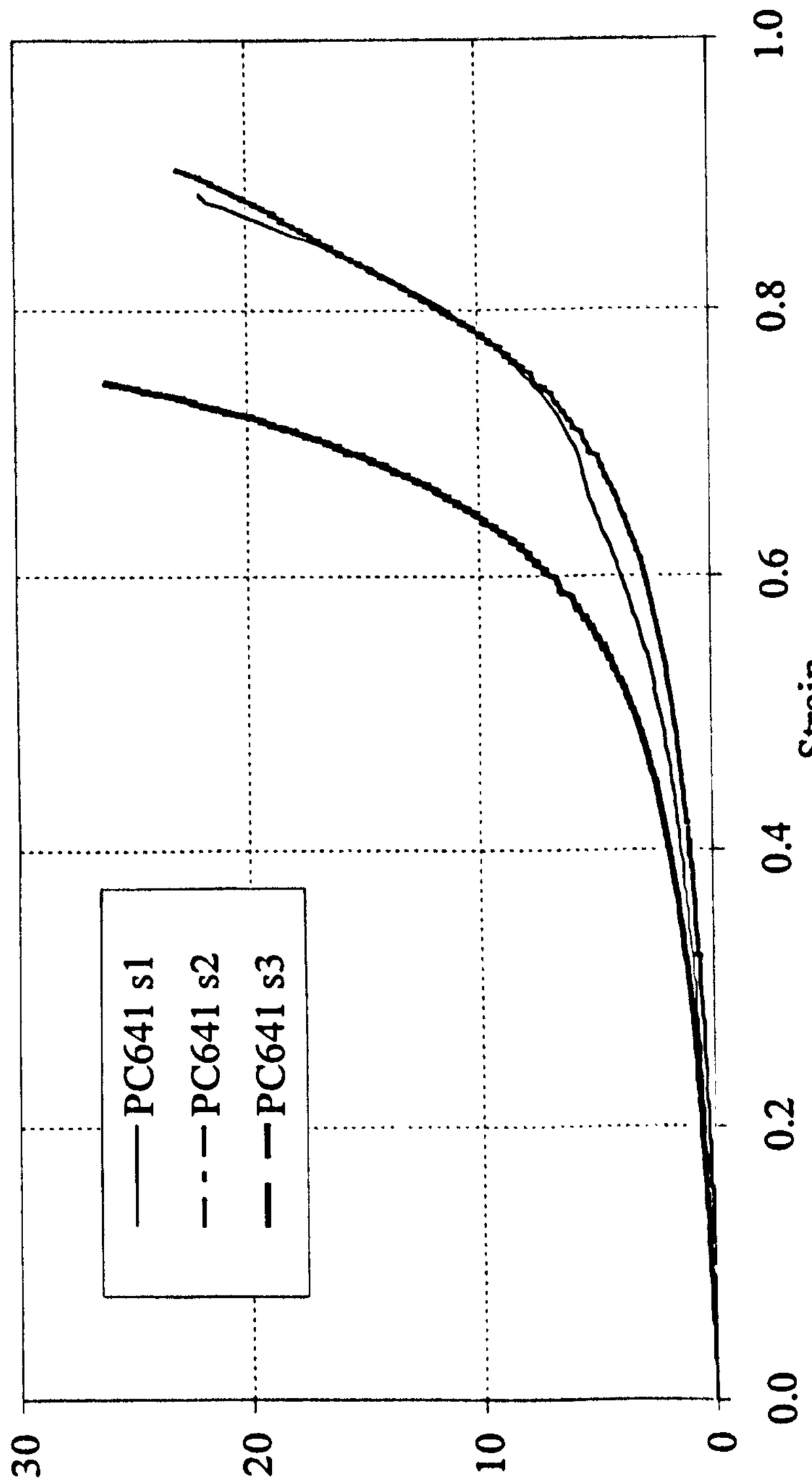

Fig. 4.48 stress strain curves of planar compression of Nitrile641

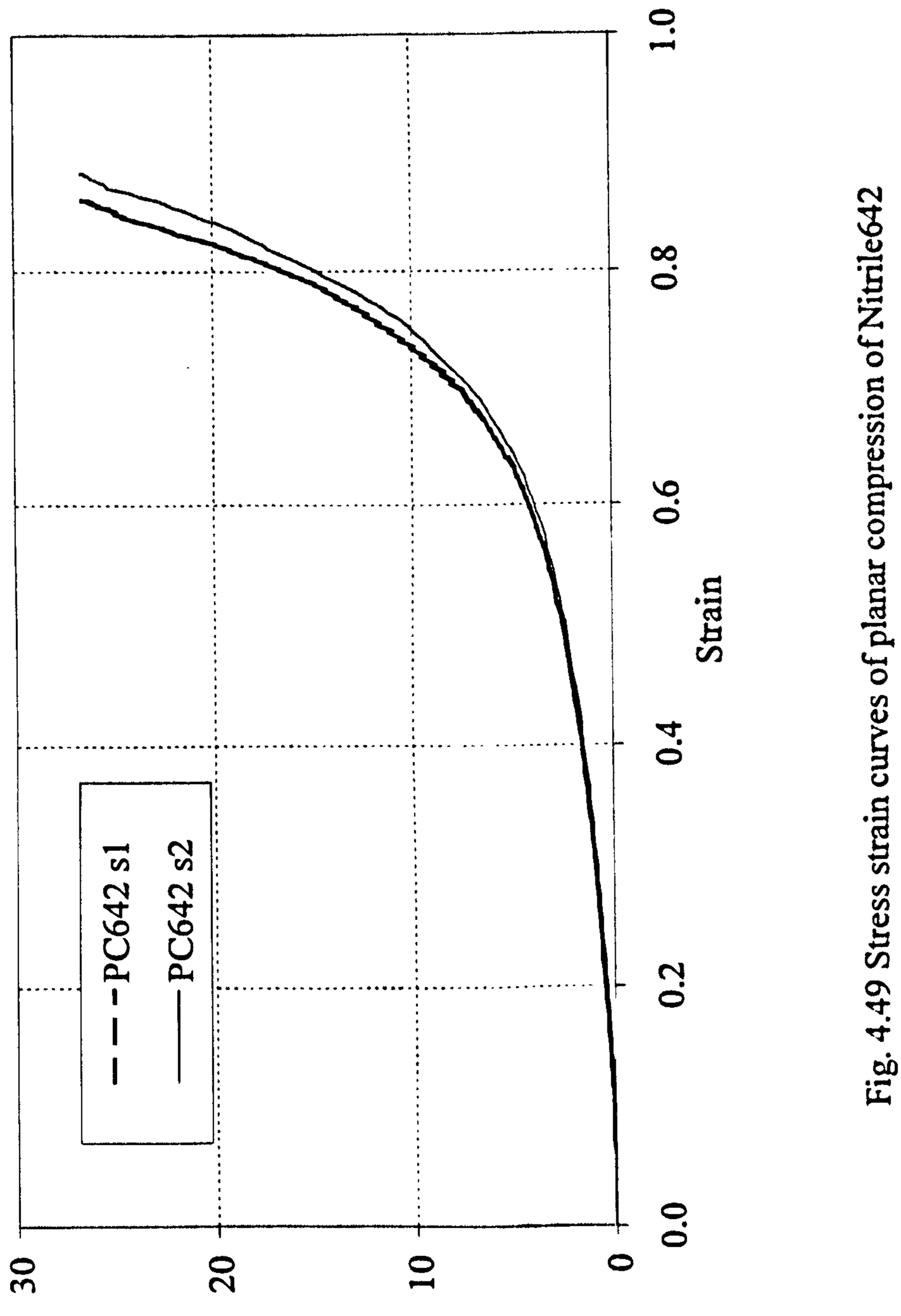

Fig. 4.49 Stress strain curves of planar compression of Nitrile642

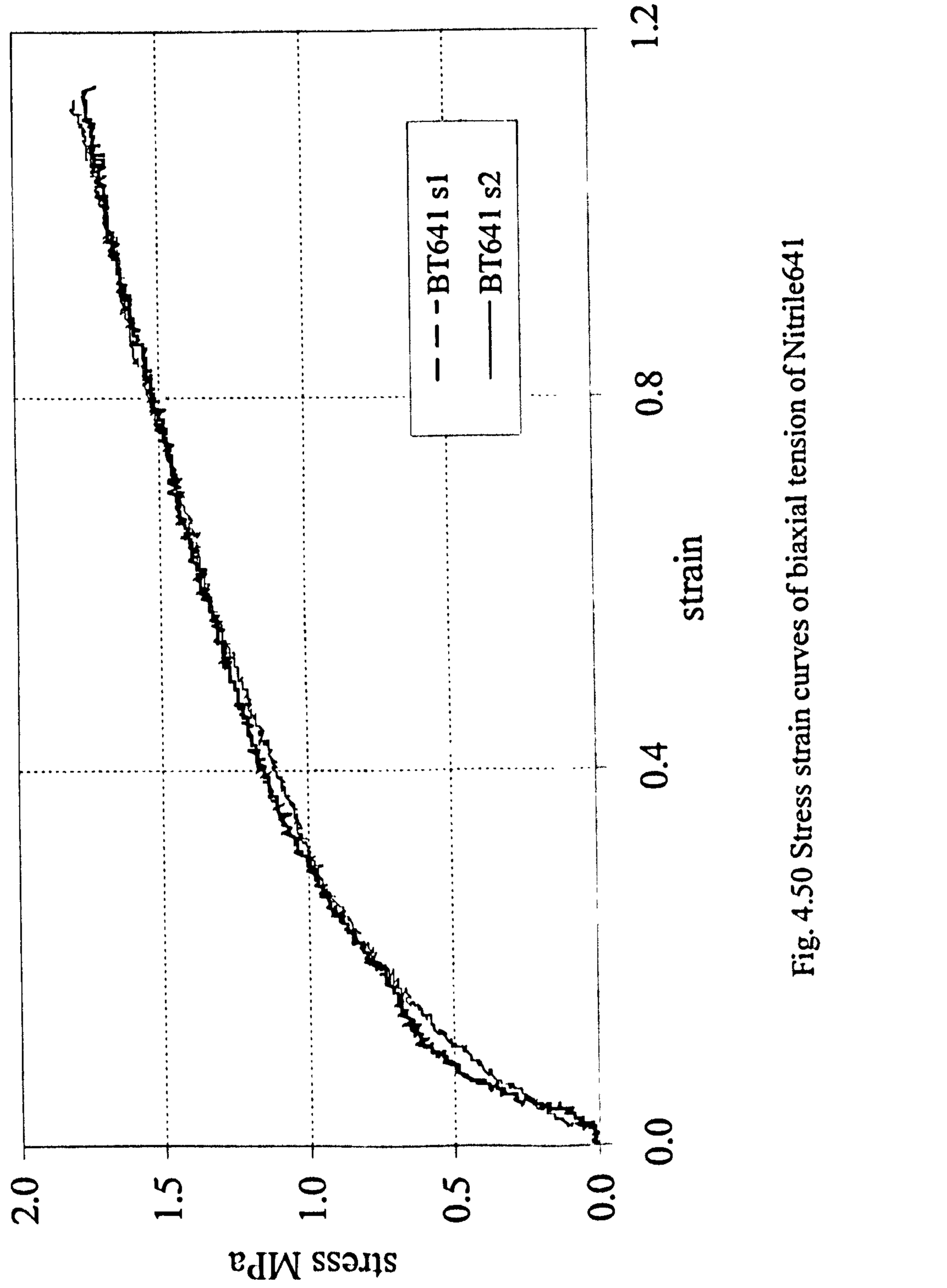

Fig. 4.50 Stress strain curves of biaxial tension of Nitrile641

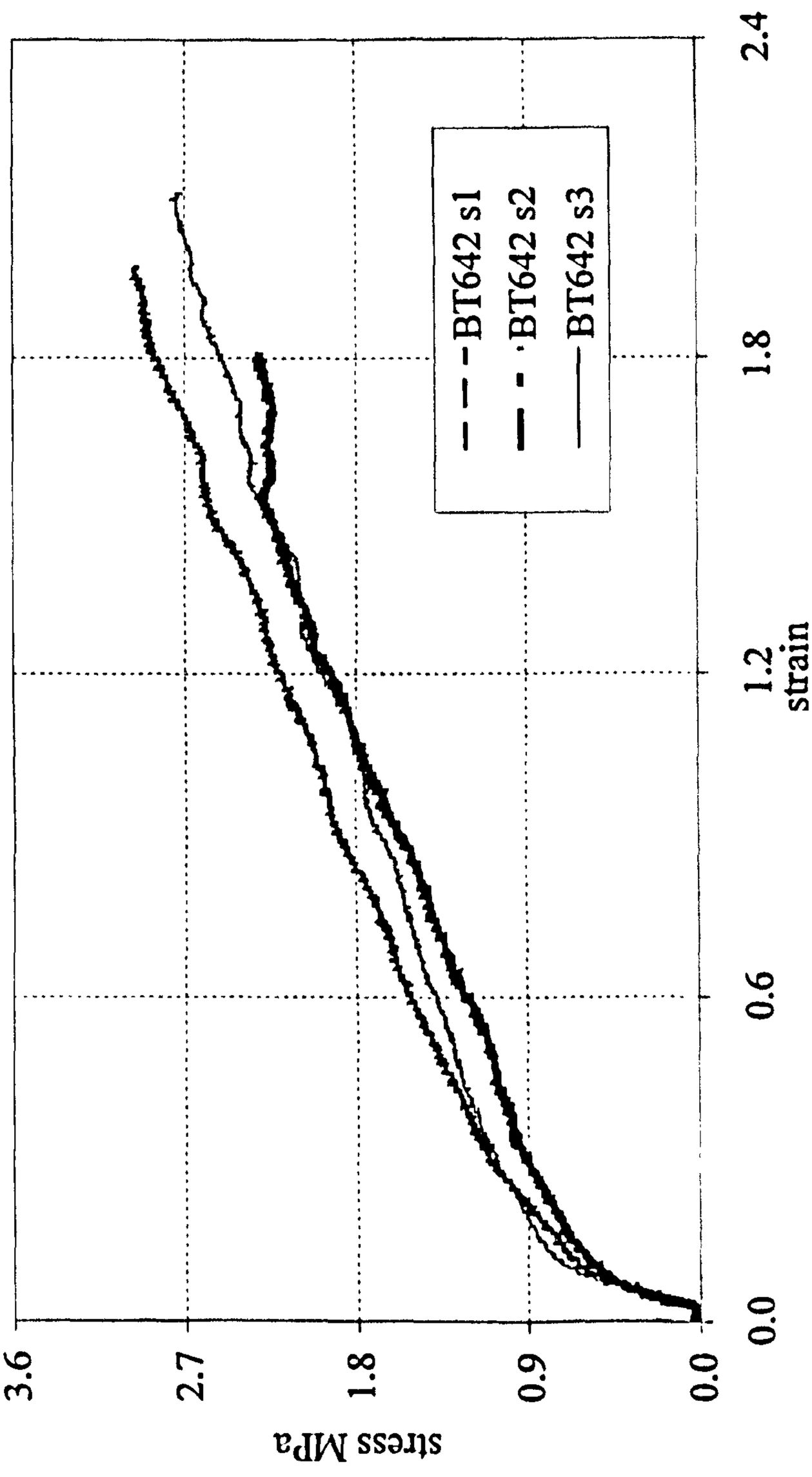

Fig. 4.51 Stress strain curves of biaxial tension of Nitrile642

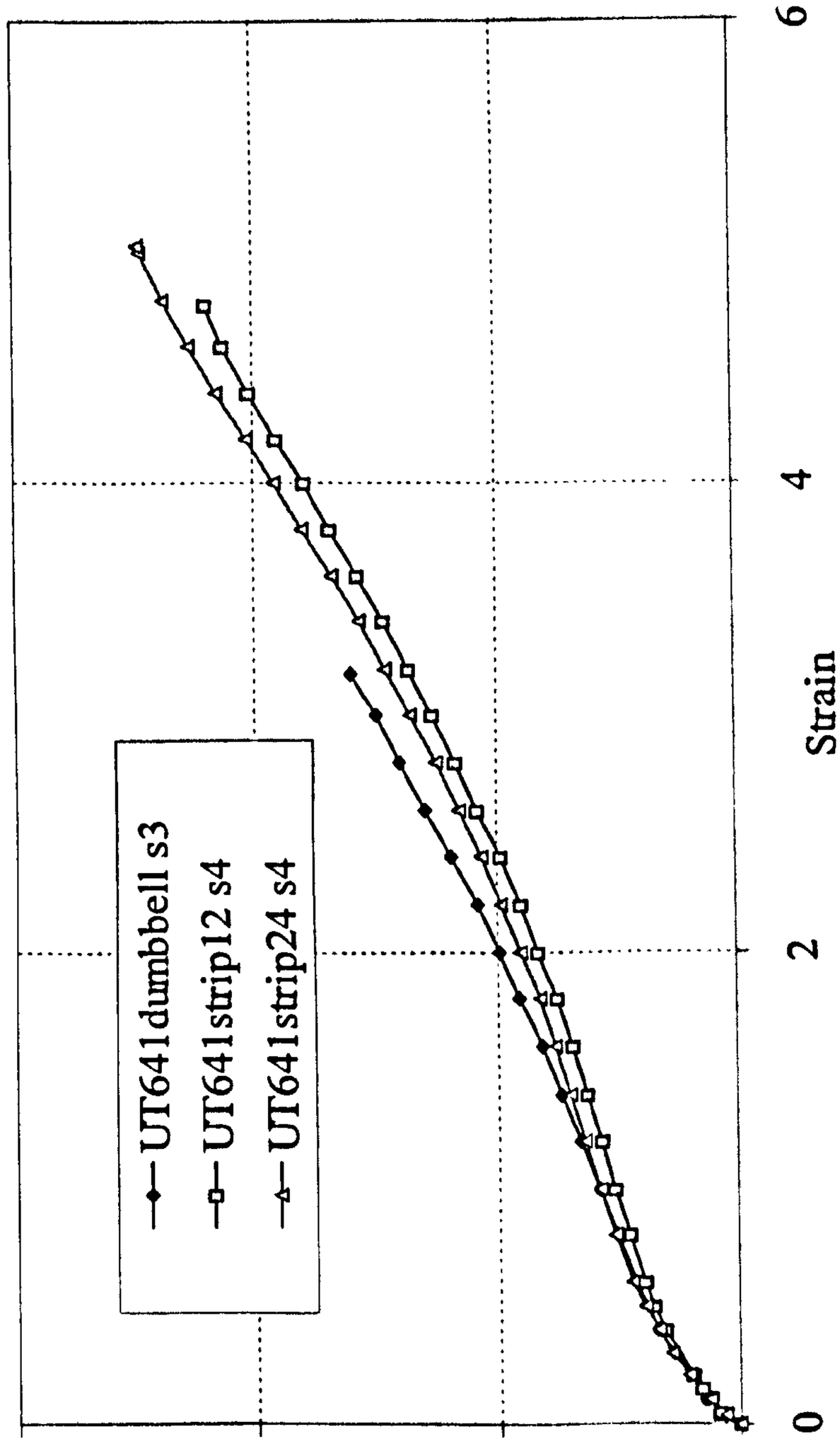

Fig. 4.52 Comparison of uniaxial tension of Nitnile641 with different specimen

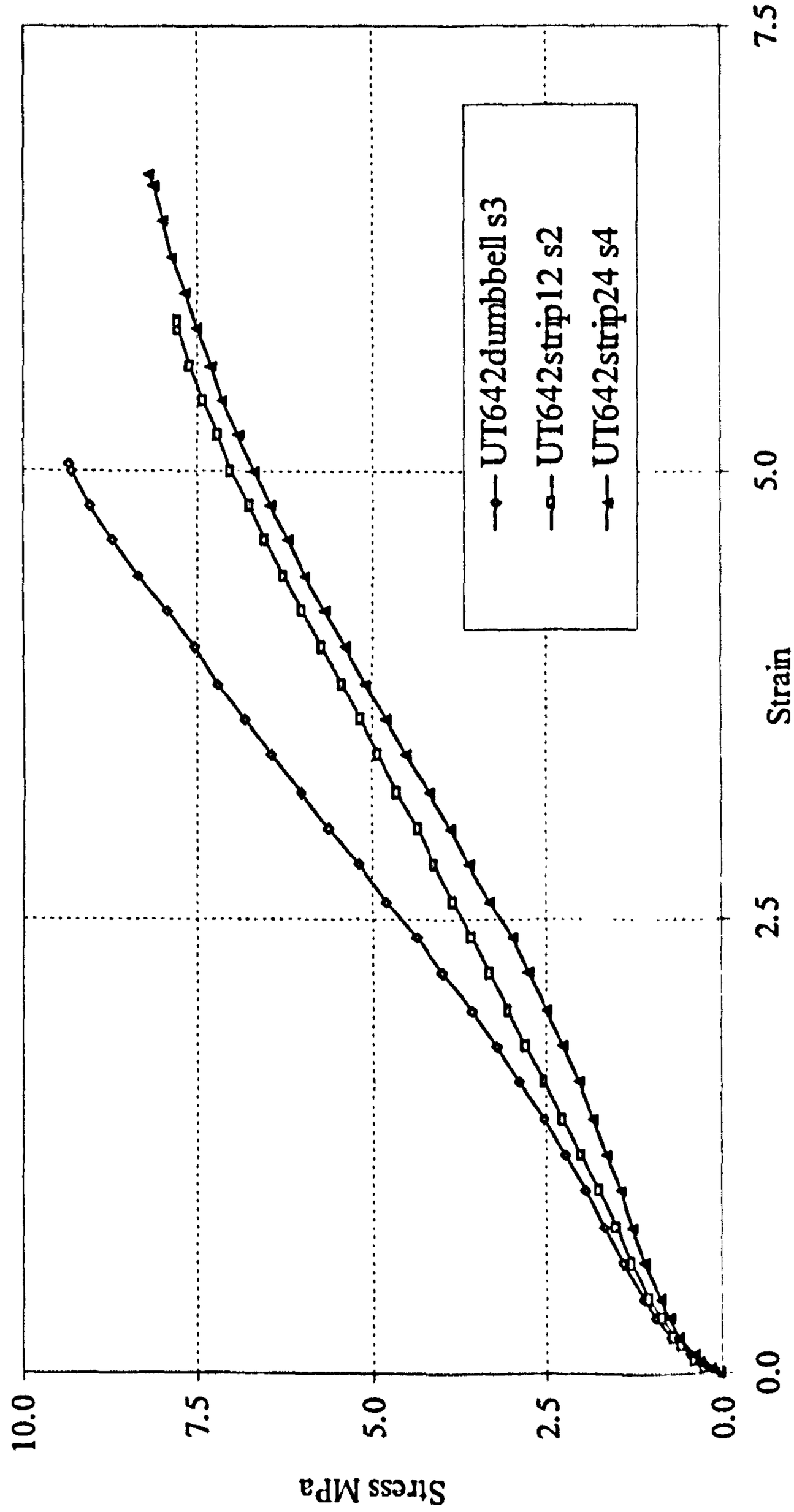

Fig. 4.53 Comparison of uniaxial tension of Nitrile642 with different specimen geometries and dimens

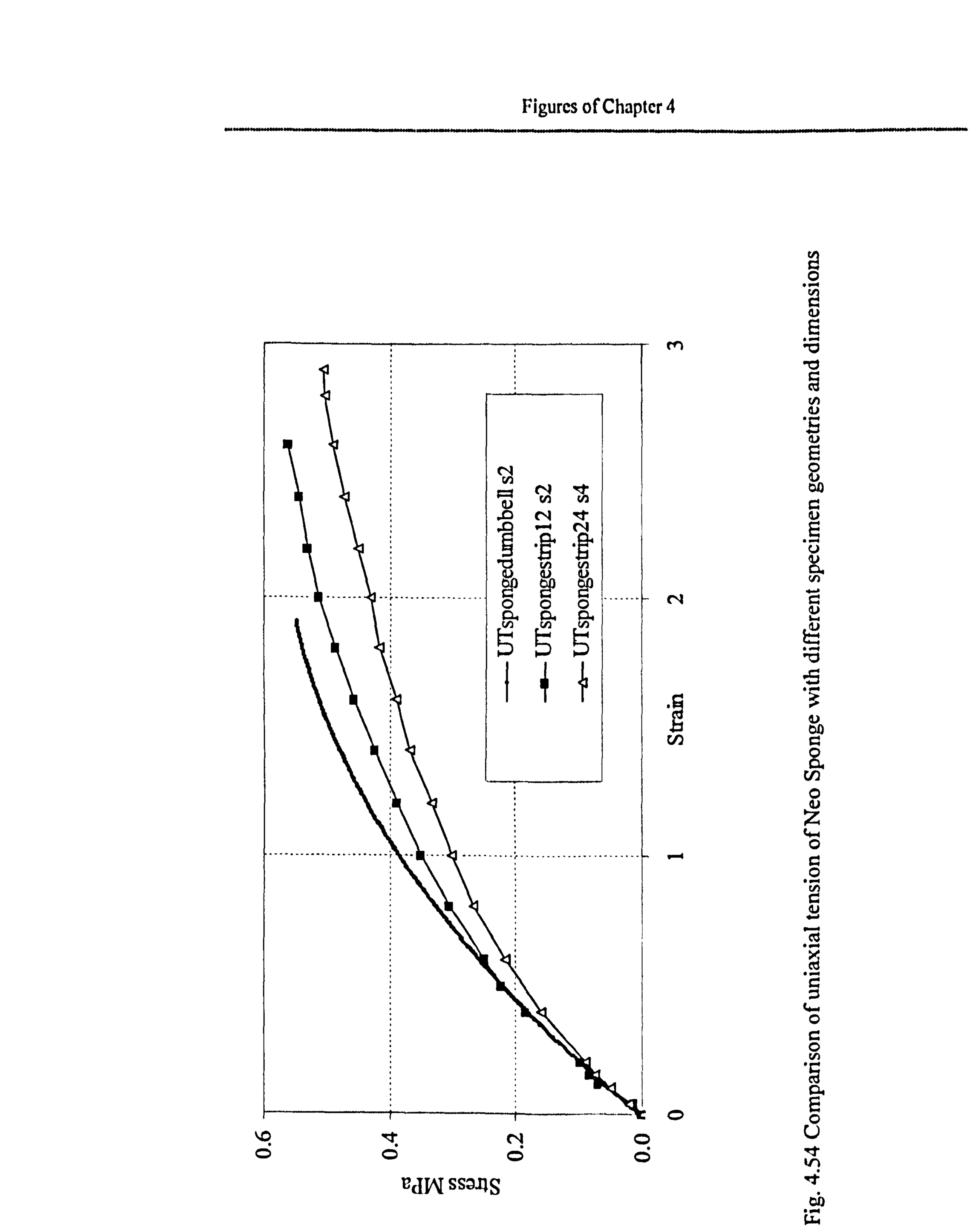

Fig. 4.54 Comparison of uniaxial tension of Neo Sponge with different specimen geometries and dimensions

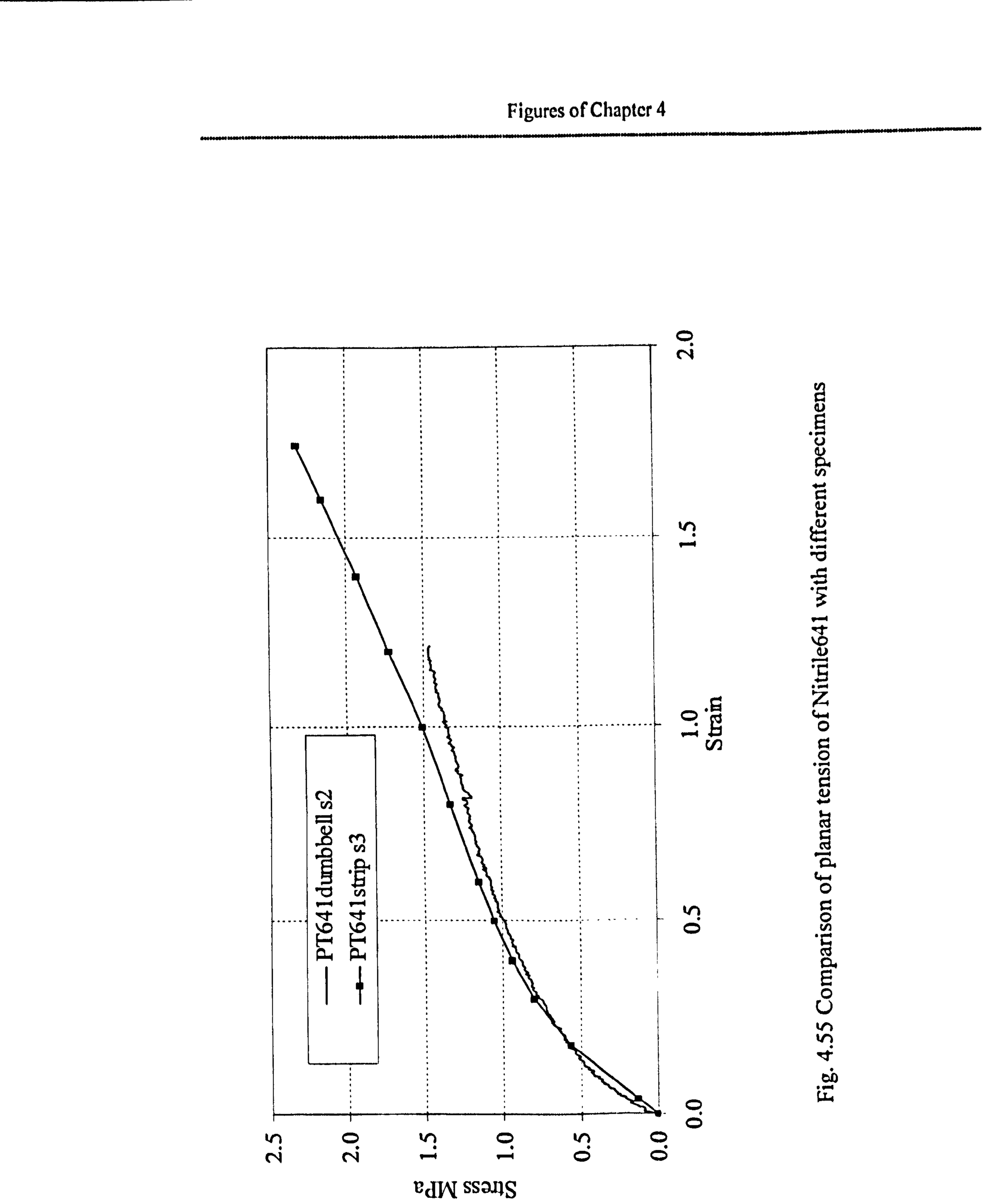

Fig. 4.55 Comparison of planar tension of Nitrile641 with different specimens

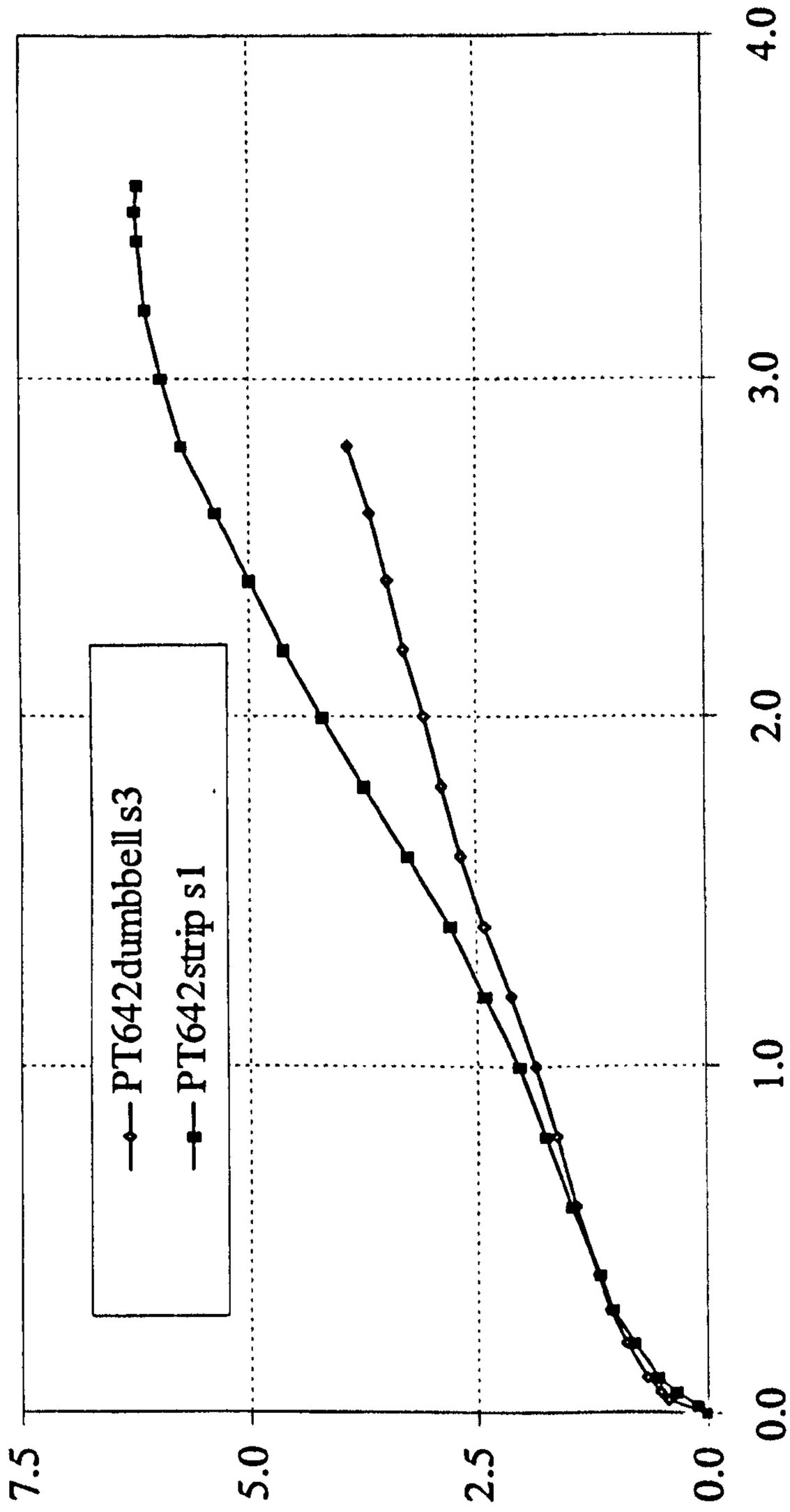

Fig. 4.56 Comparison of planar tension of Nitrile642 with different specimens

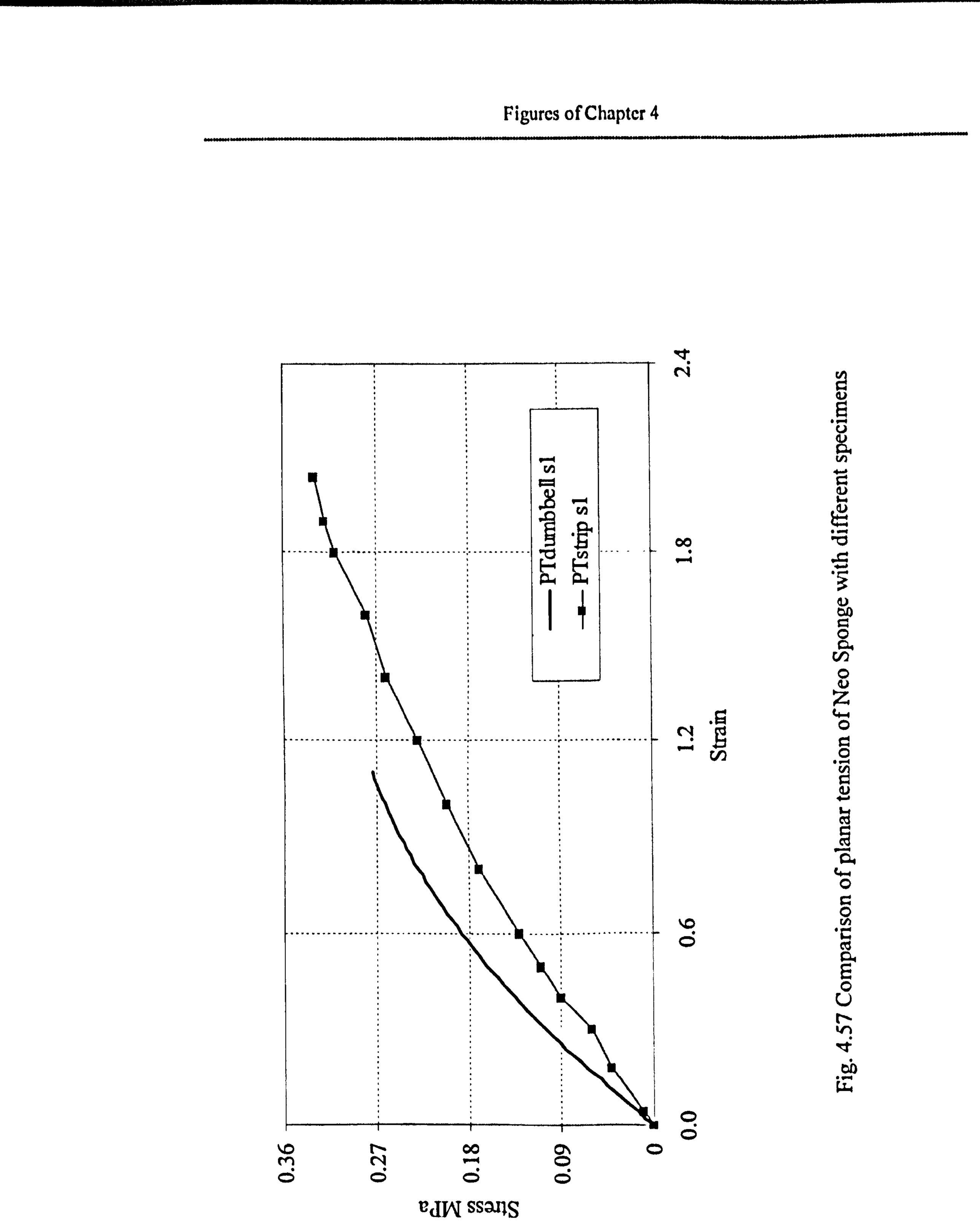

Fig. 4.57 Comparison of planar tension of Neo Sponge with different specimens

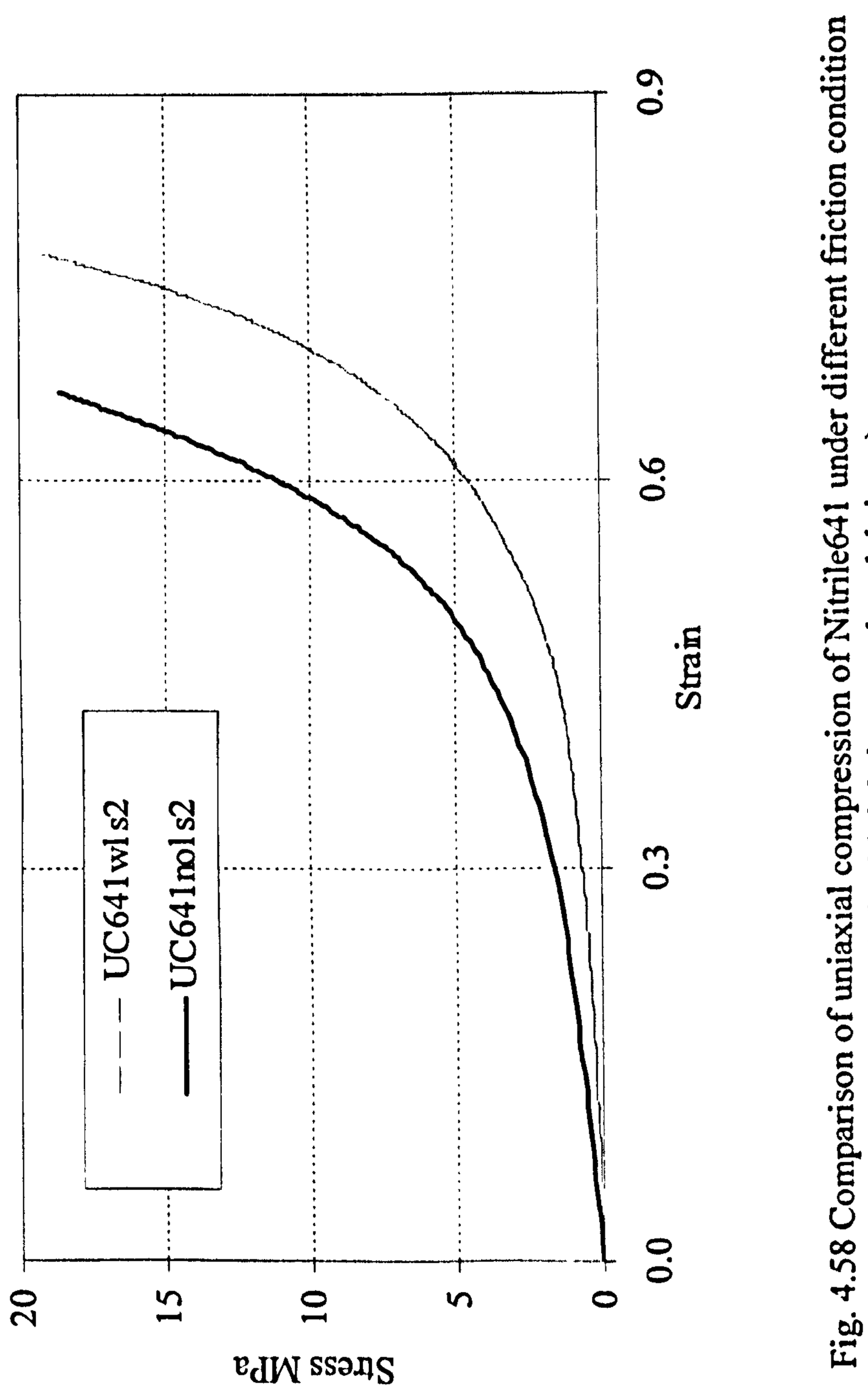

Fig. 4.58 Comparison of uniaxial compression of Nitrile641 under different friction conditions
(wl-with lubricant; nol-no lubricant)

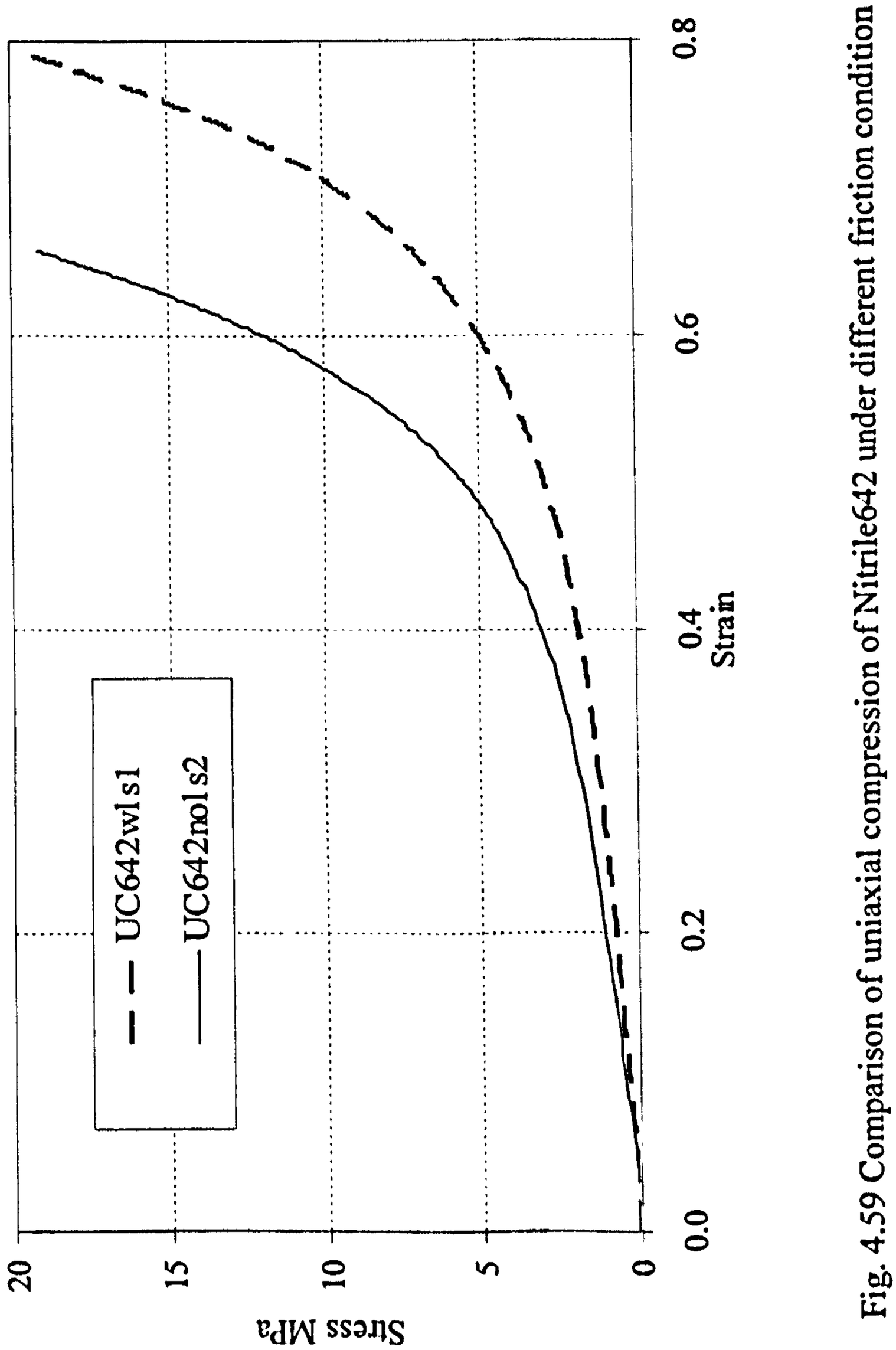

Fig. 4.59 Comparison of uniaxial compression of Nitrile642 under different friction condition

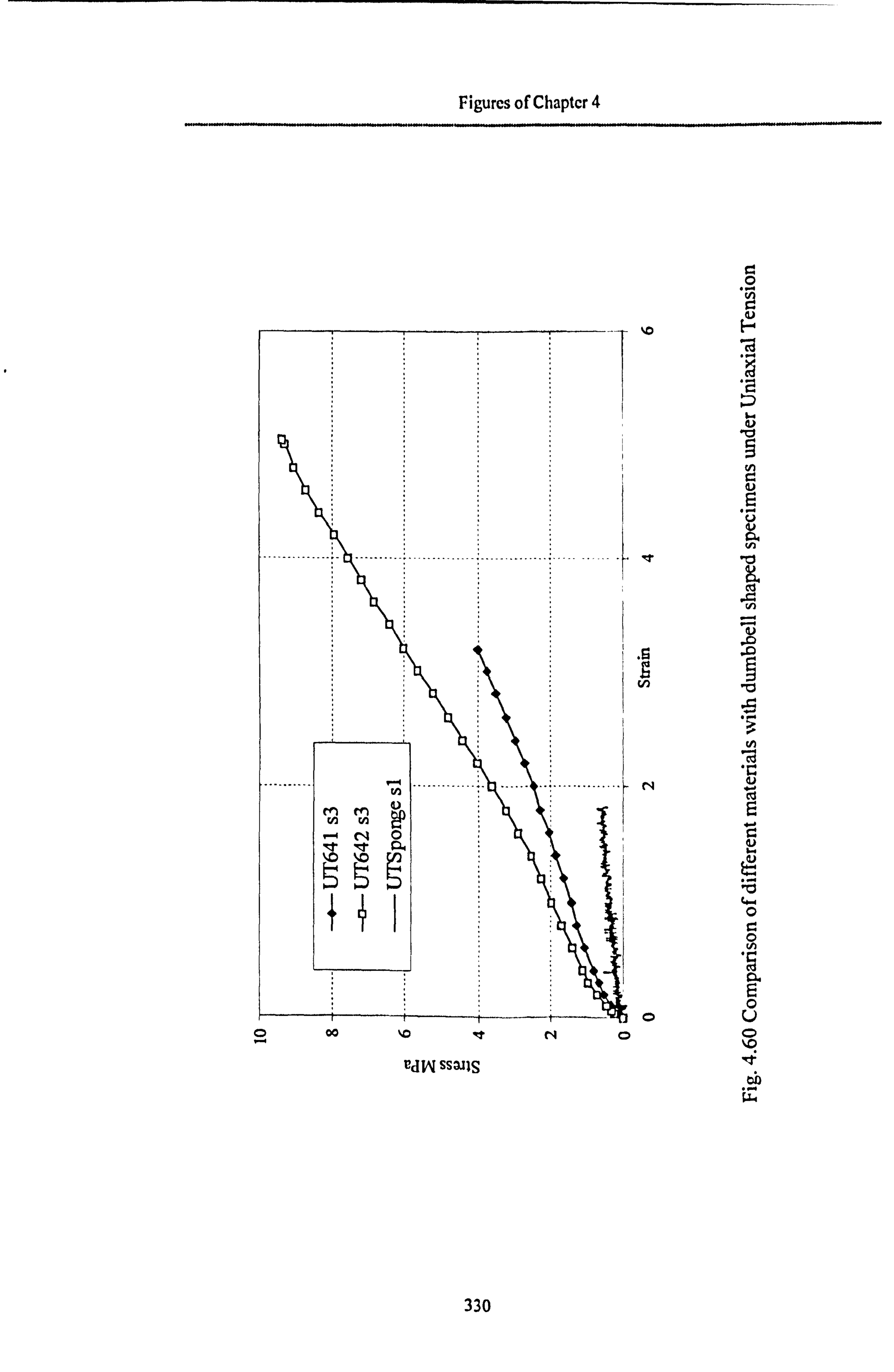

Fig. 4.60 Comparison of different materials with dumbbell shaped specimens under Uniaxial Tension

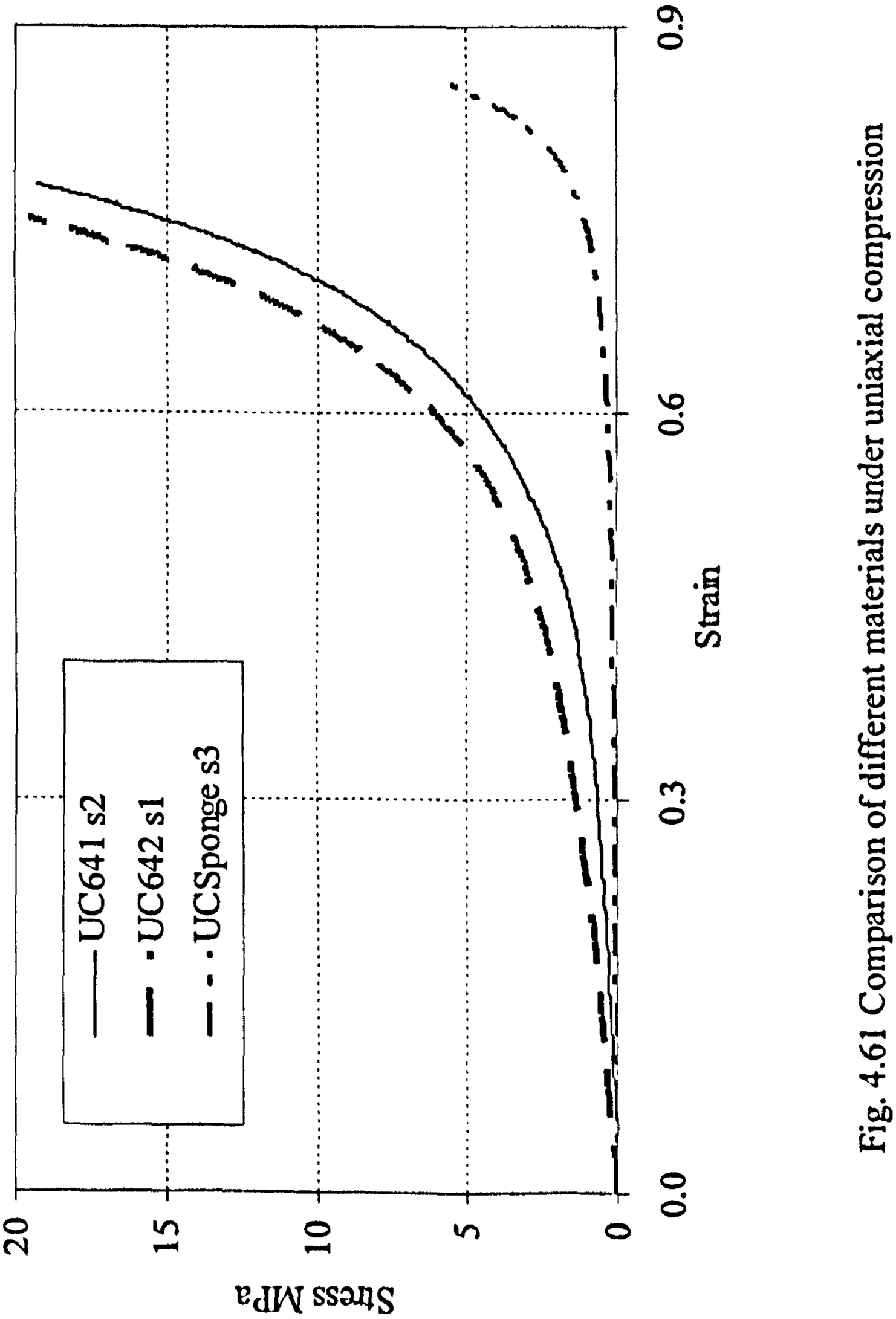

Fig. 4.61 Comparison of different materials under uniaxial compression

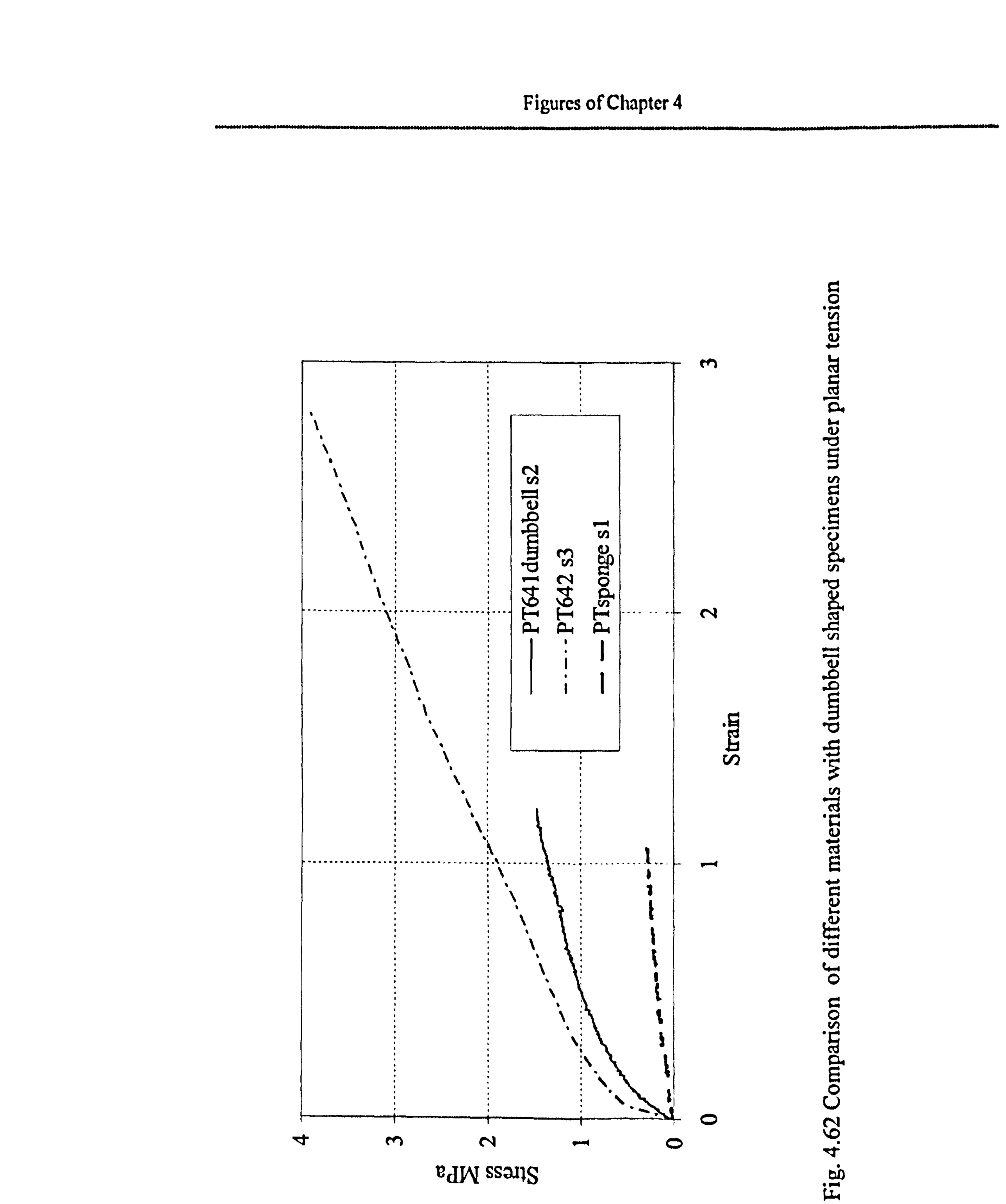

Fig. 4.62 Comparison of different materials with dumbbell shaped specimens under planar tension

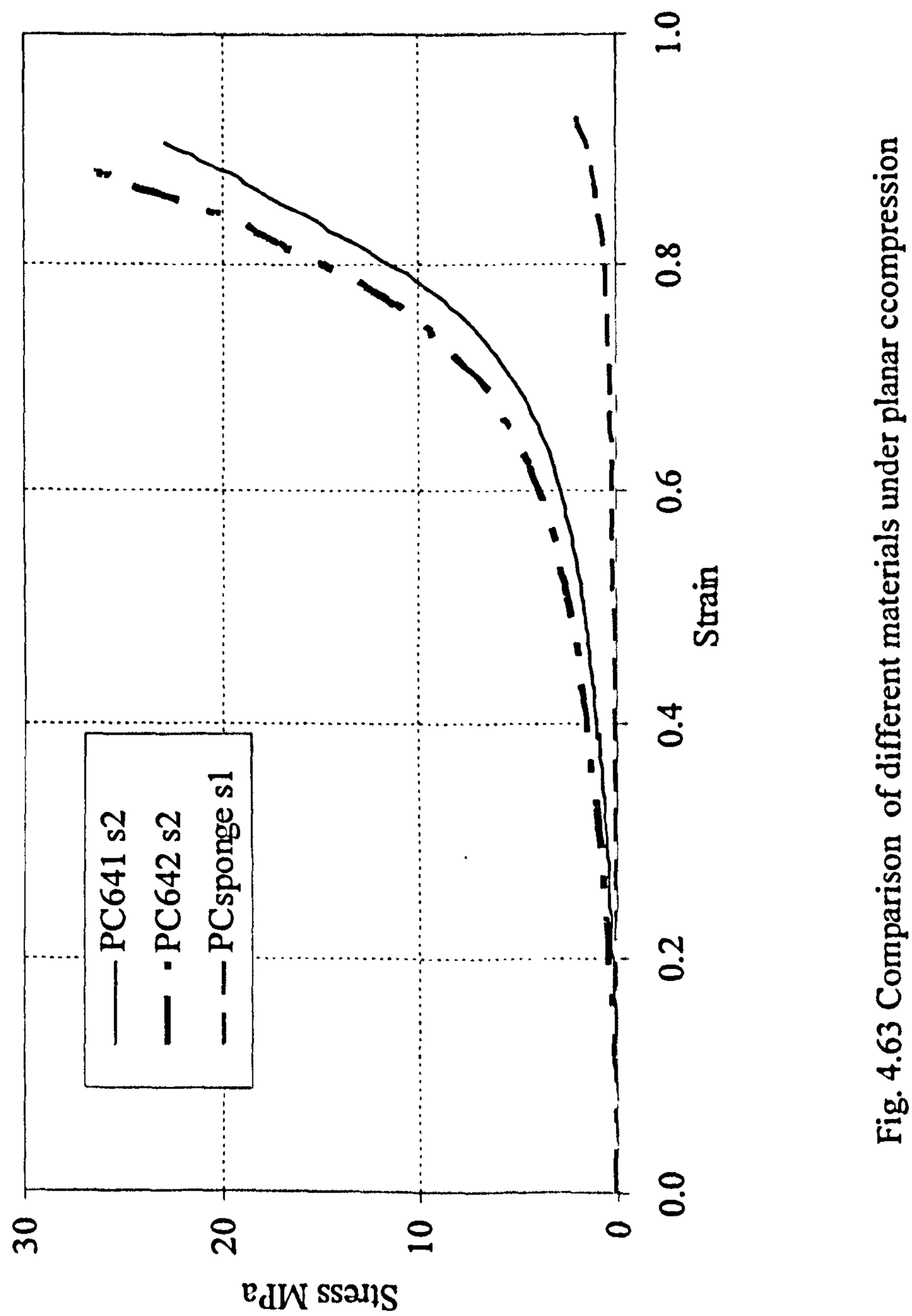

Fig. 4.63 Comparison of different materials under planar ccompression

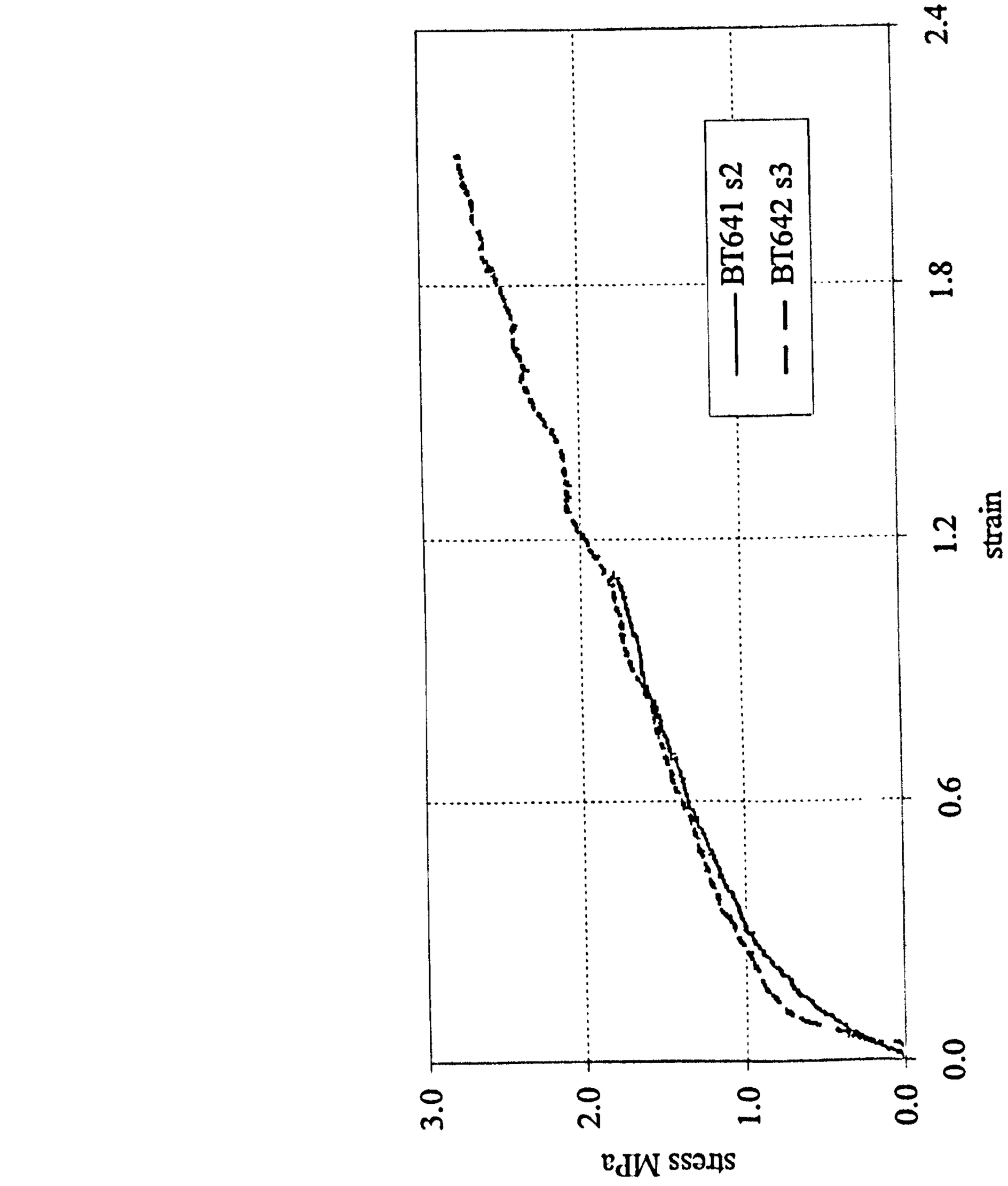

Fig. 4.64 Comparison of different materials under biaxial tension

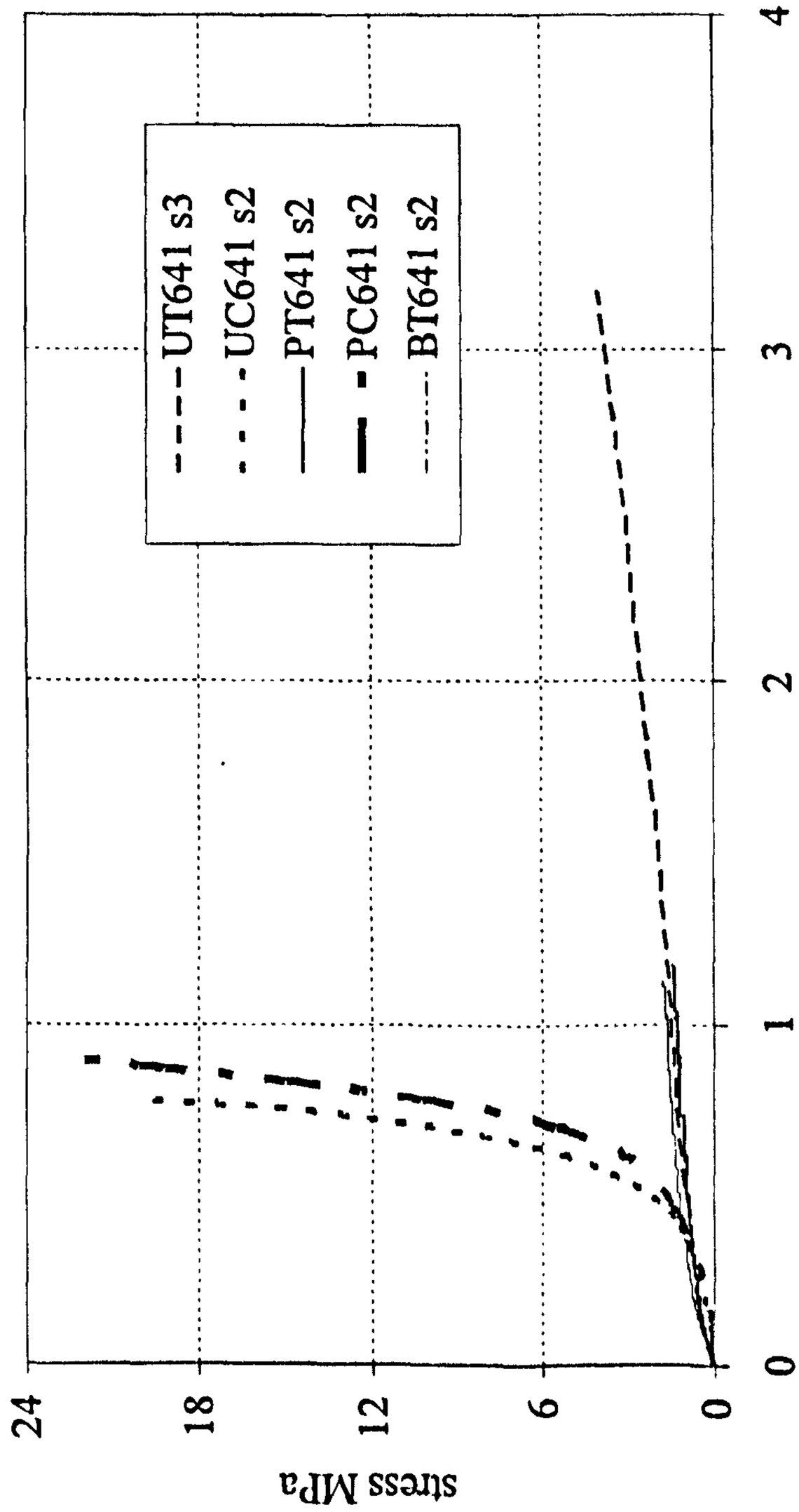

Fig. 4.65 Comparison of Nitrile641 under different loading conditions

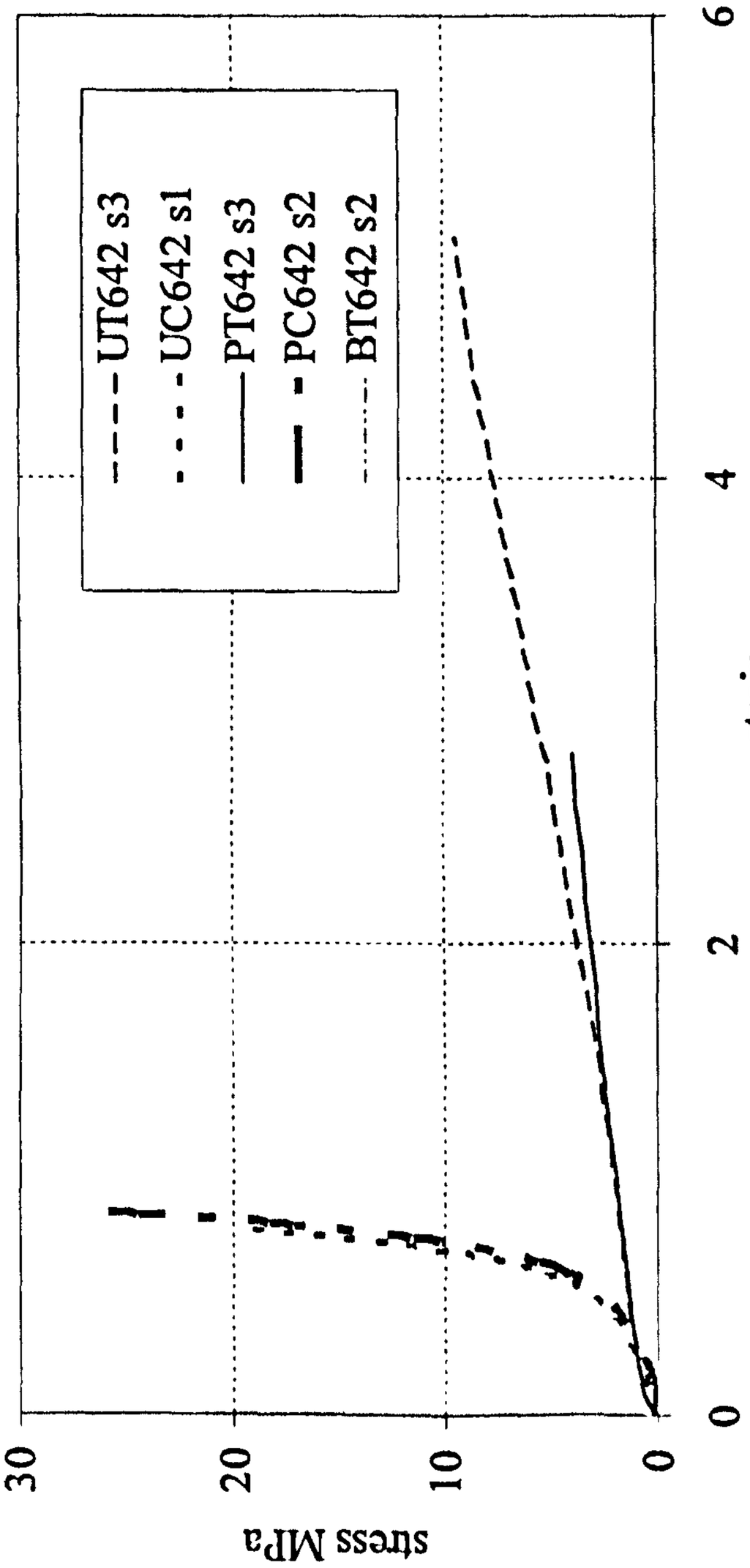

Fig. 4.66 Comparison of Nitrile642 under different loading conditions

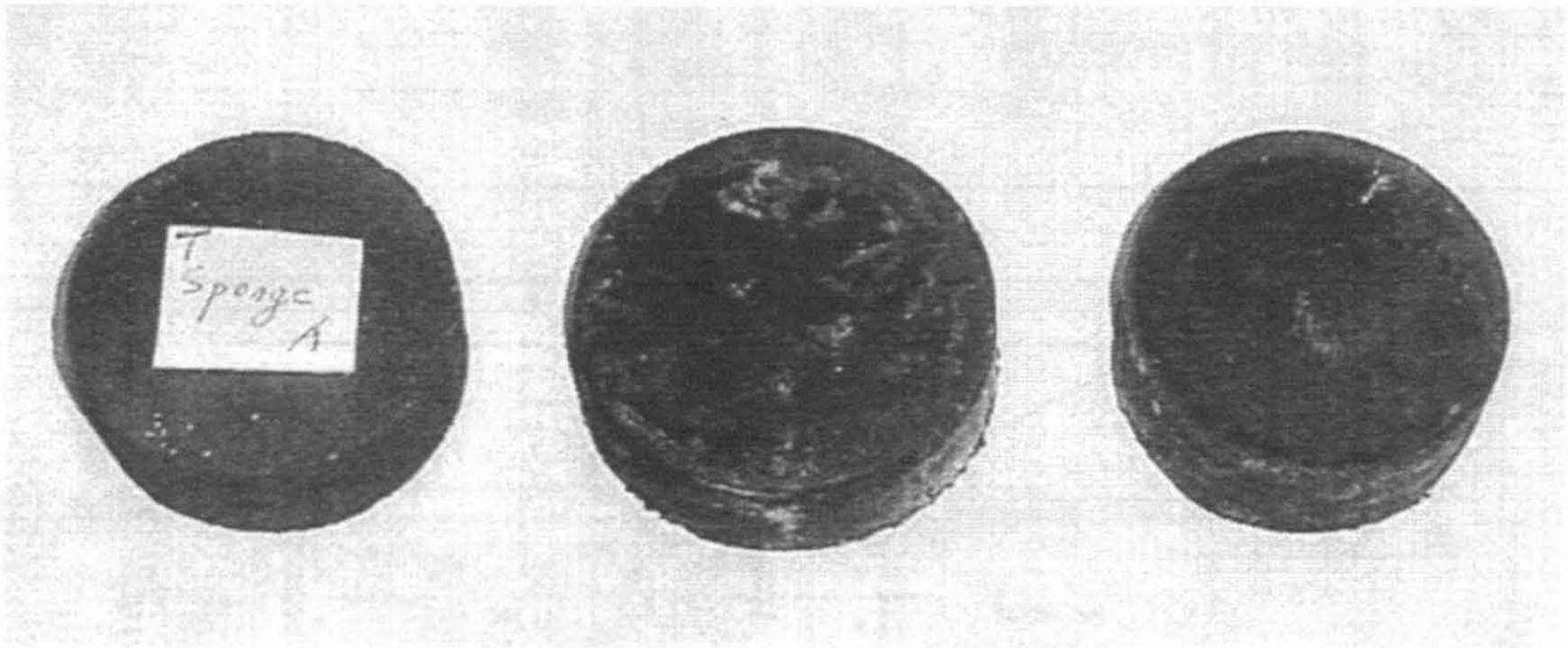

(a) Under uniaxial compression

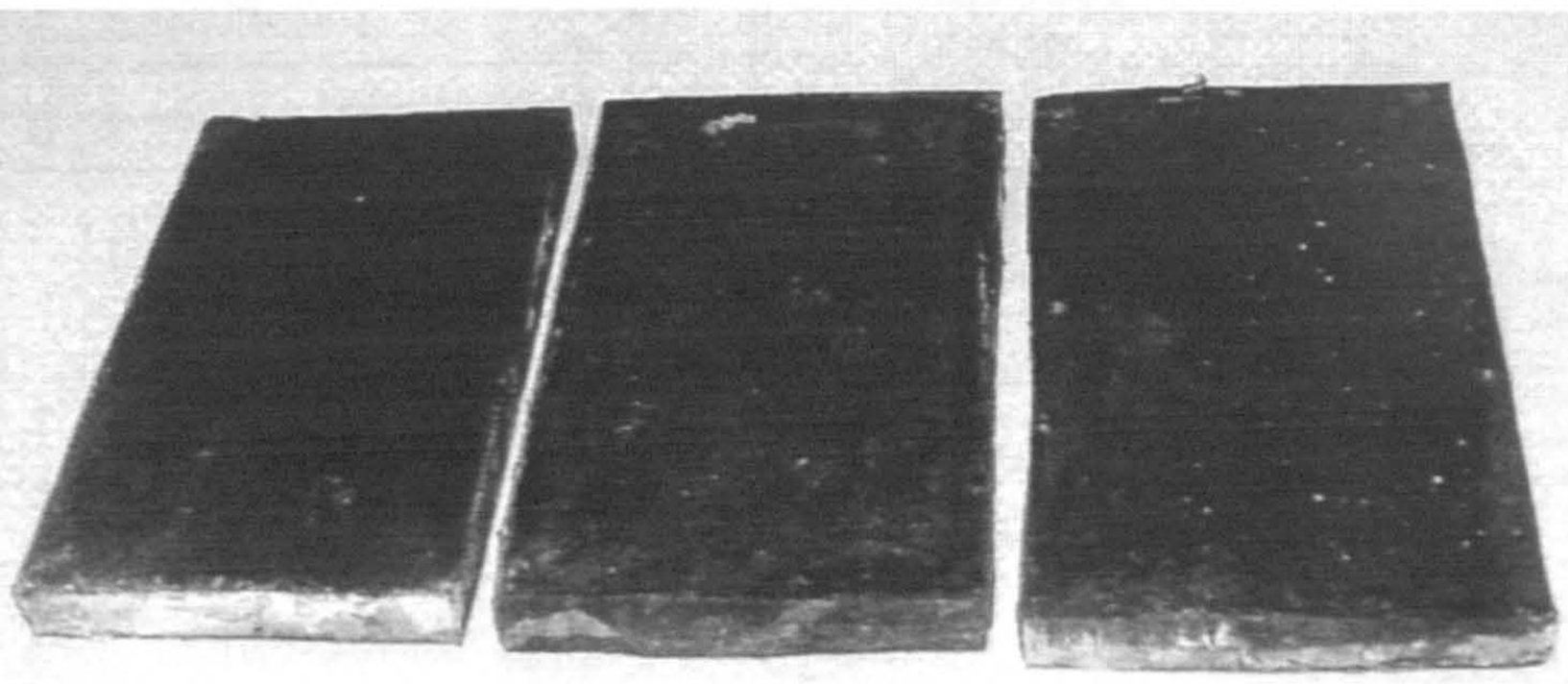

(b) Under planar compression

Fig. 4.67 Three types of materials after the testing under compression loading conditions

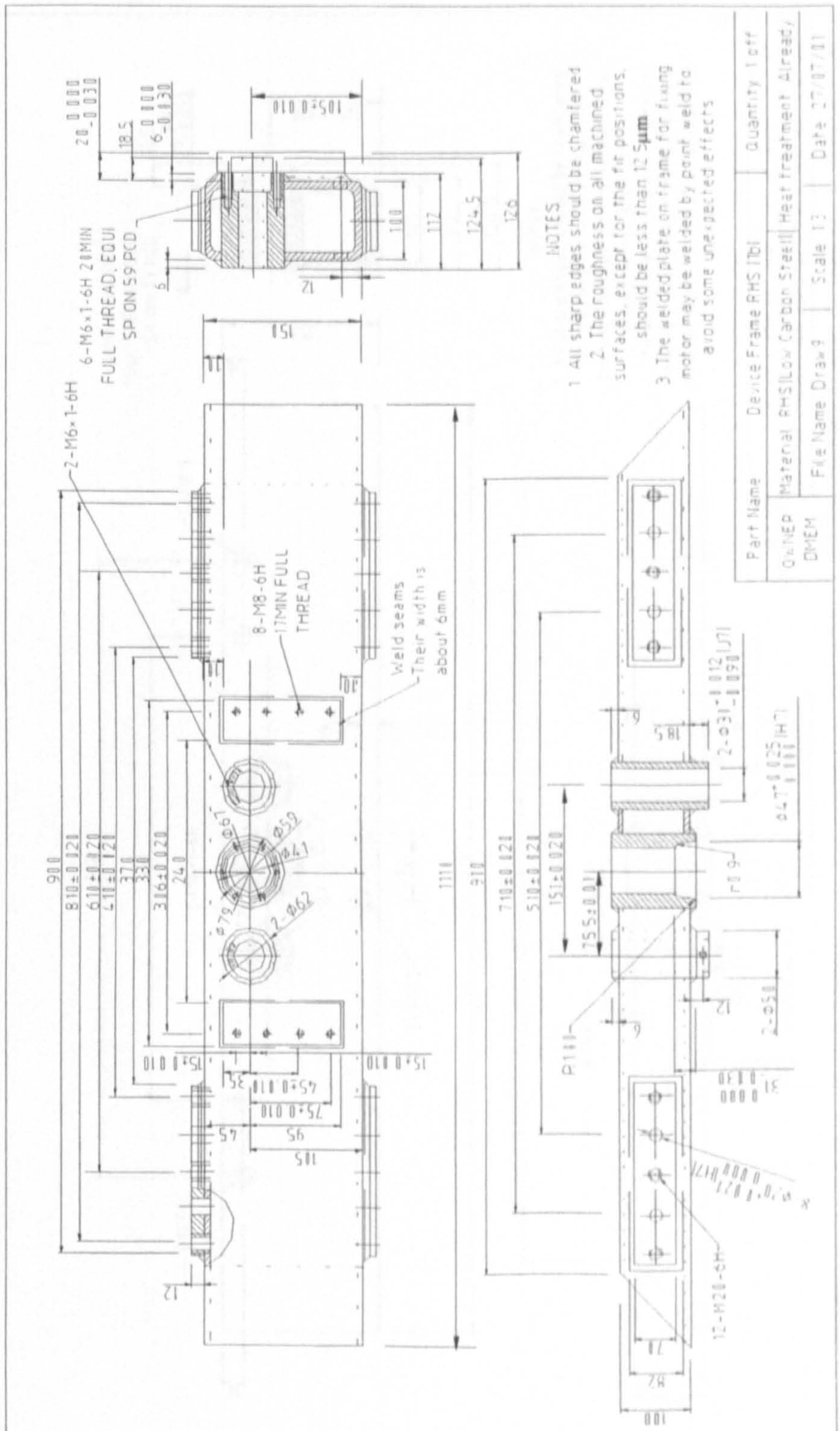

Fig. 4.1.1 The main frame design of the machine

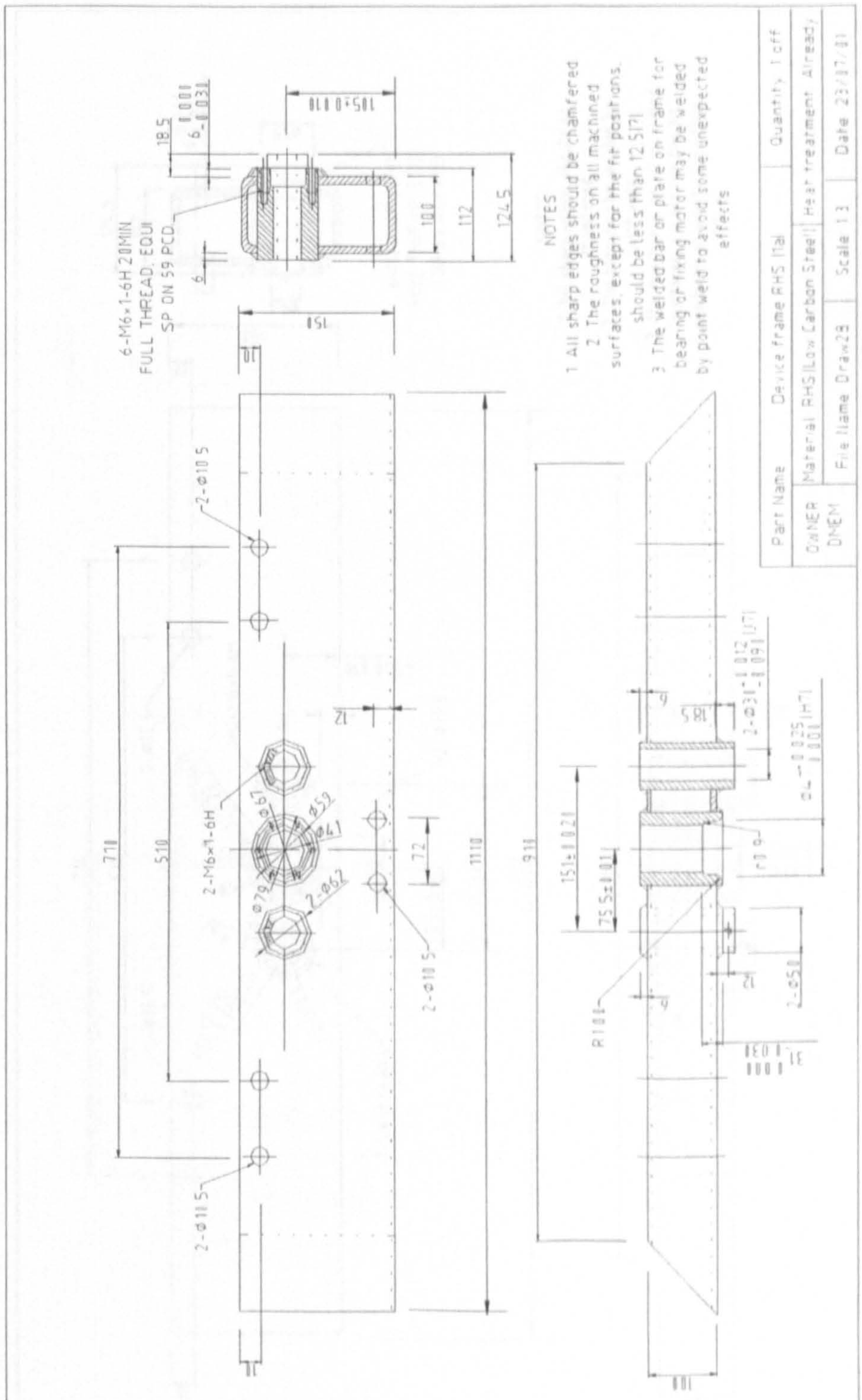

Fig. 4.1.2 The frame (opposite the main frame) design of the machine

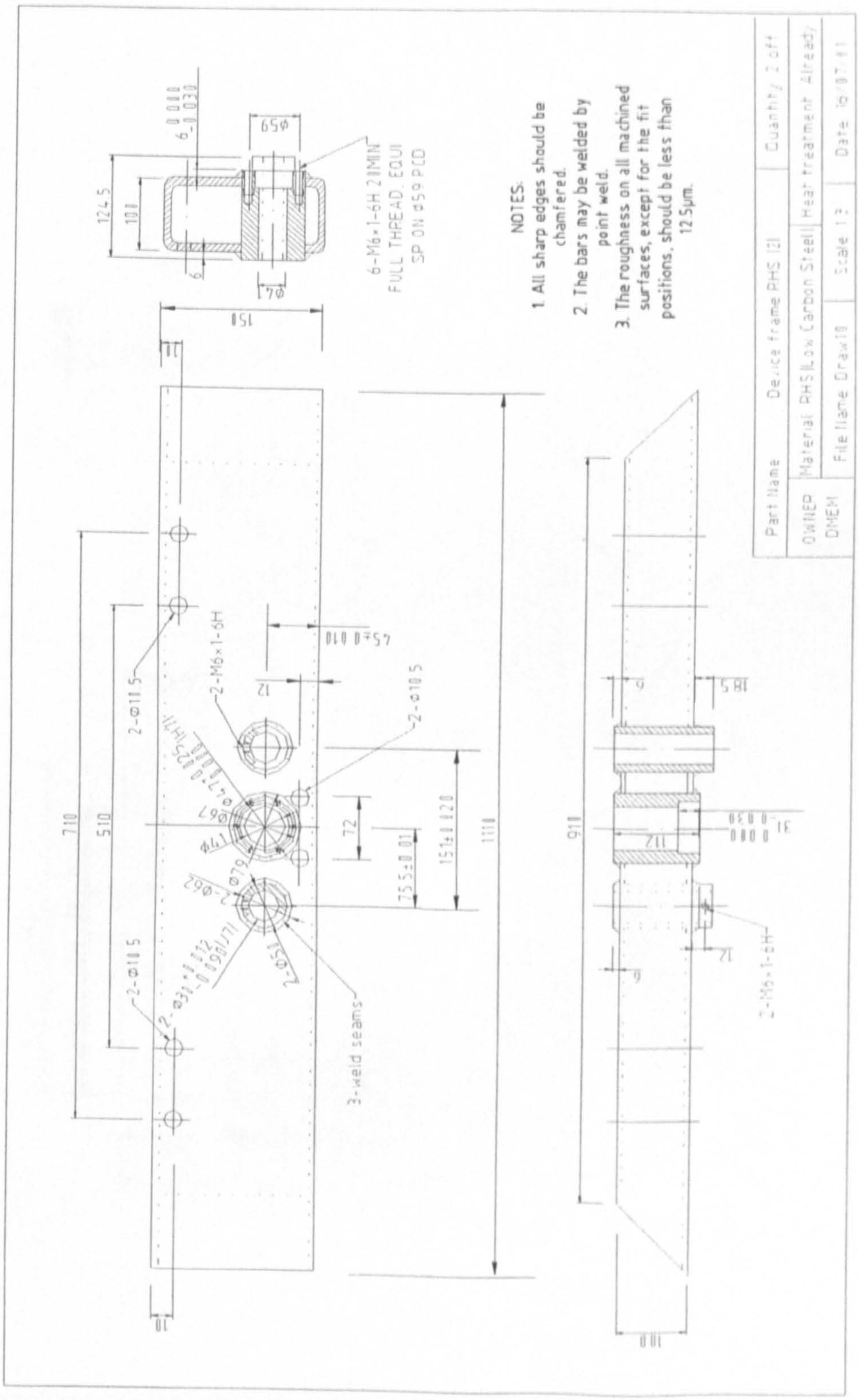

Fig. 4.1.3 The other two frame (perpendicular to the main frame) design

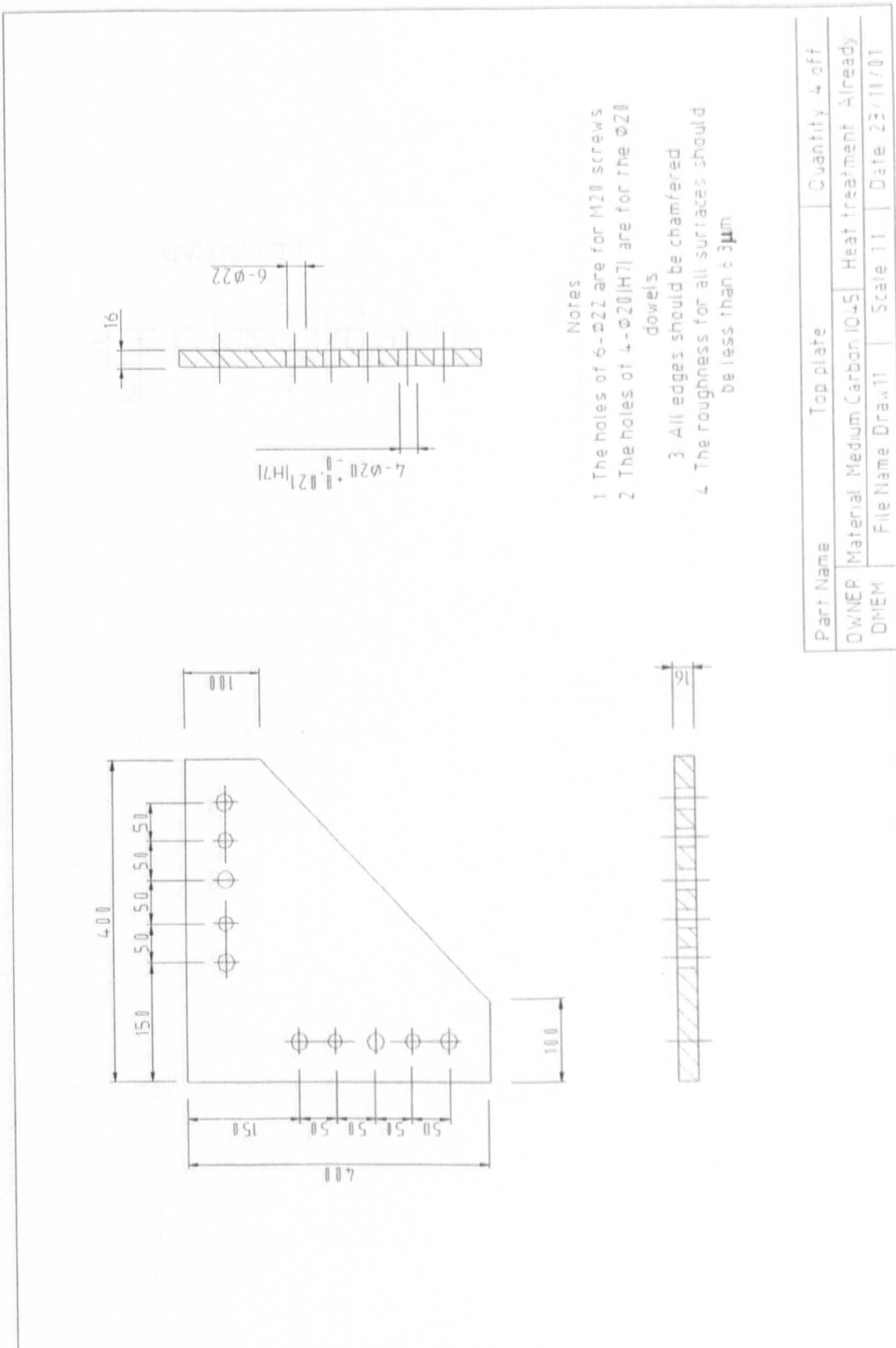

Fig. 4.1.4 The top corner plate design

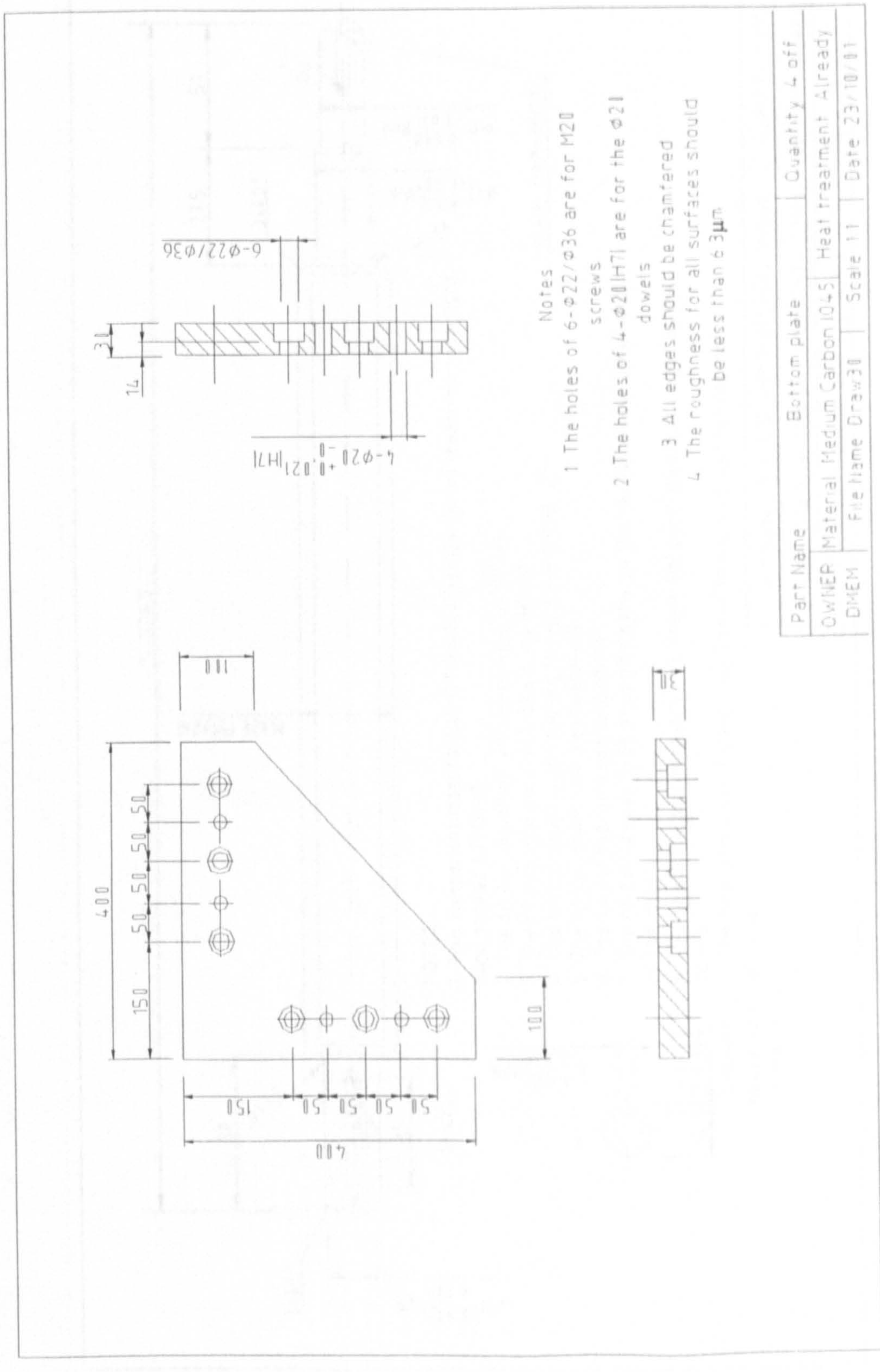

Fig. 4.1.5 The bottom corner plate design

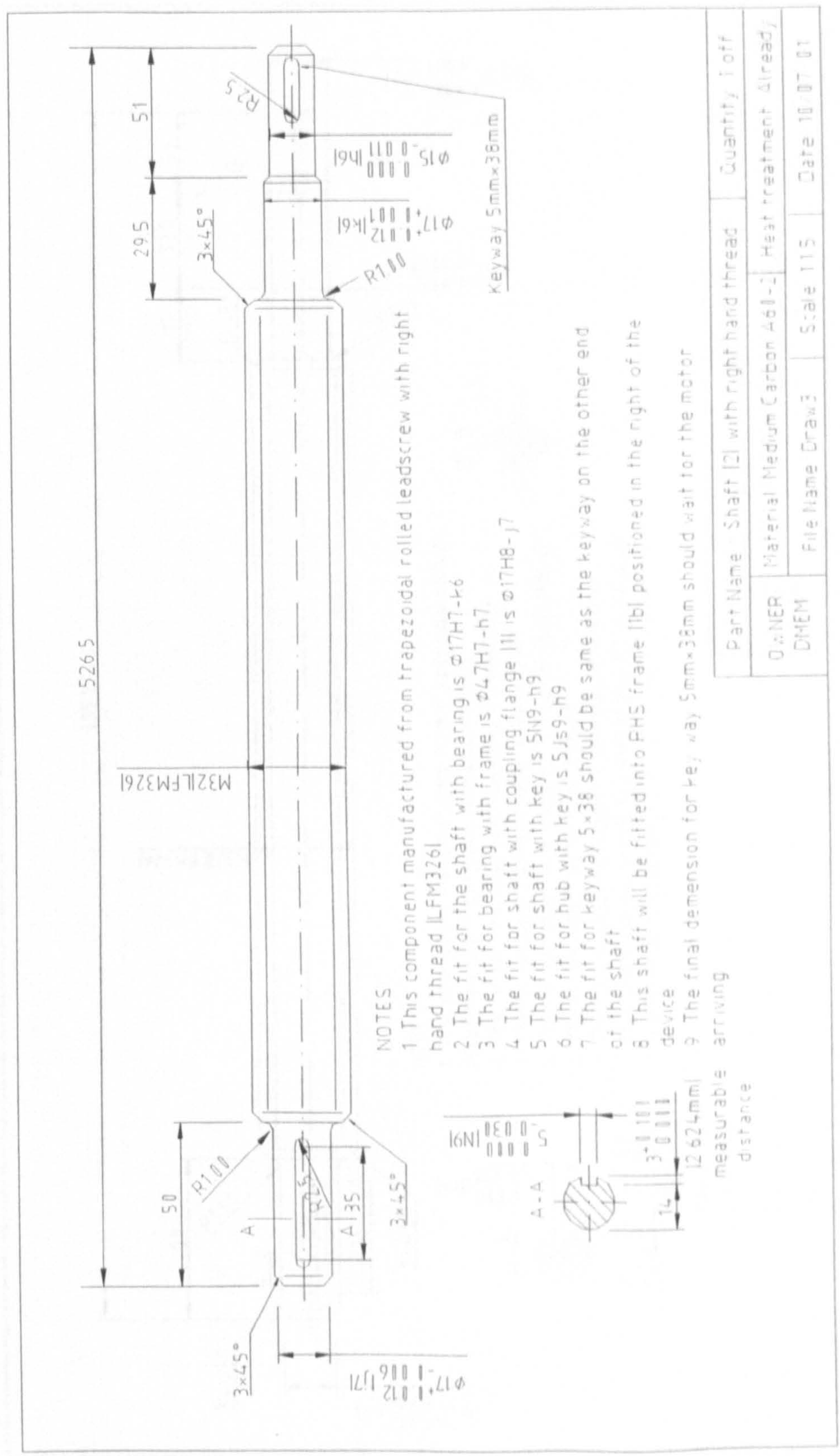

Fig. 4.1.6 The main shaft design

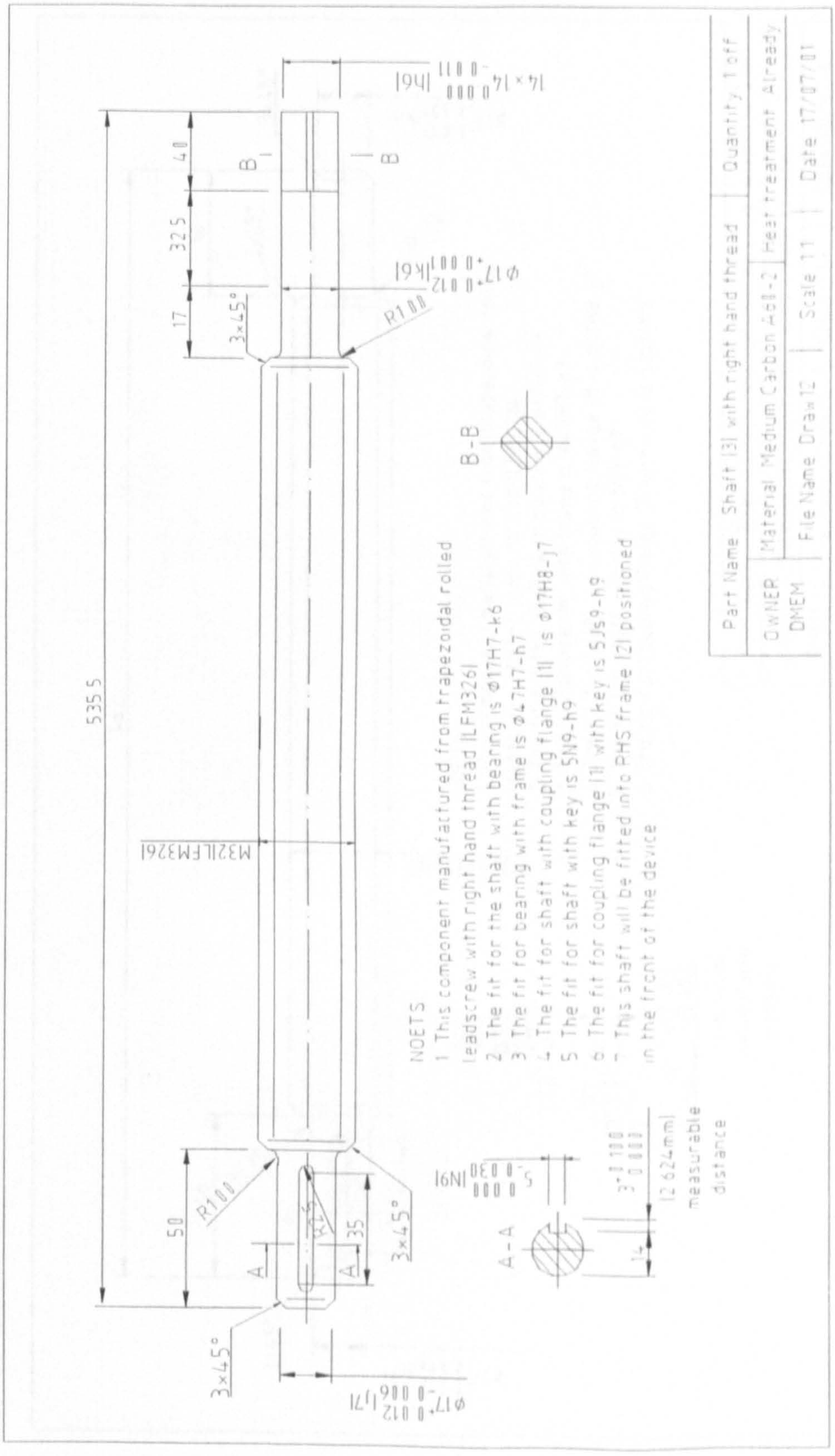

Fig. 4.1.7 The shaft (allowing manual operation) design

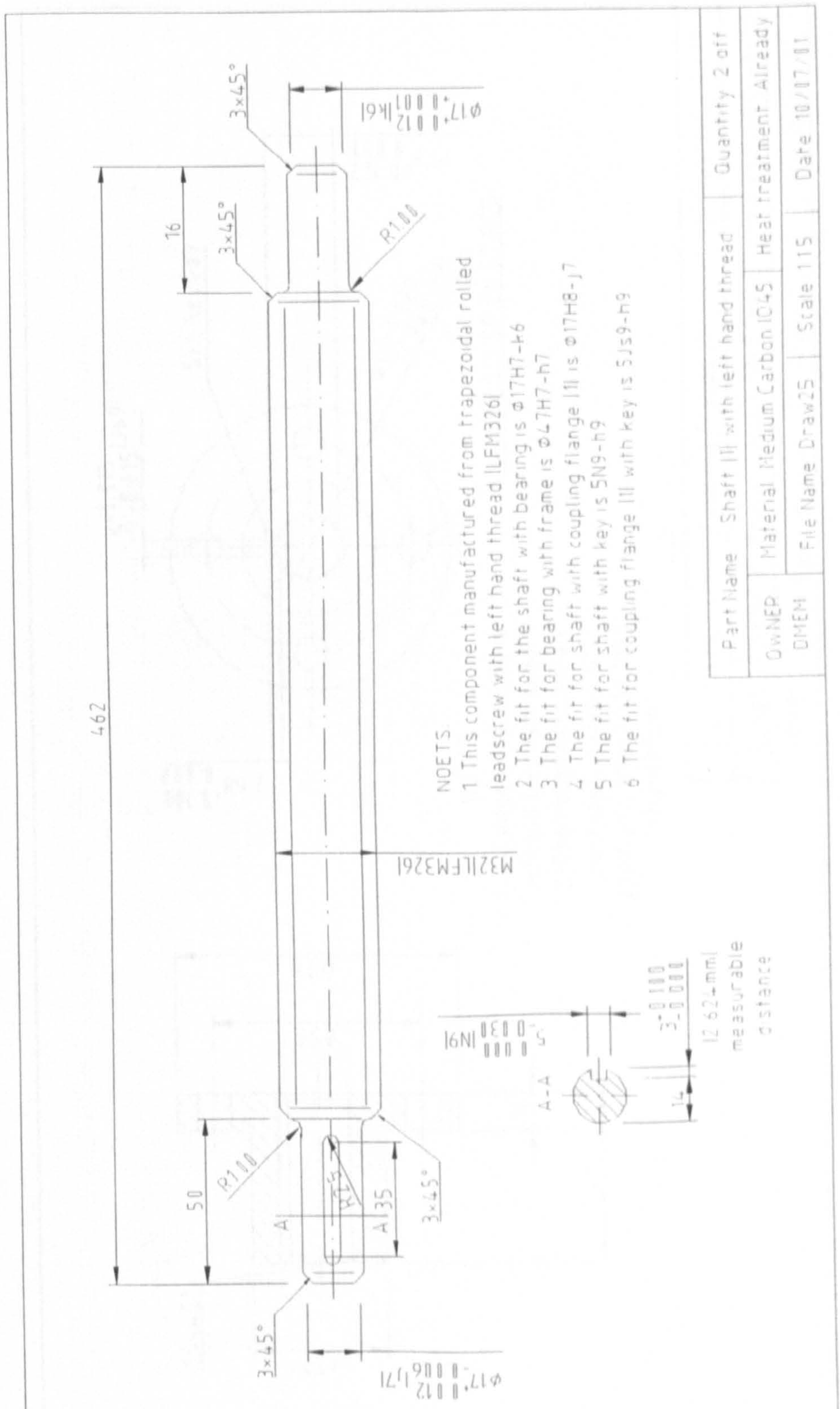

Fig. 4.1.8 The other two shaft design

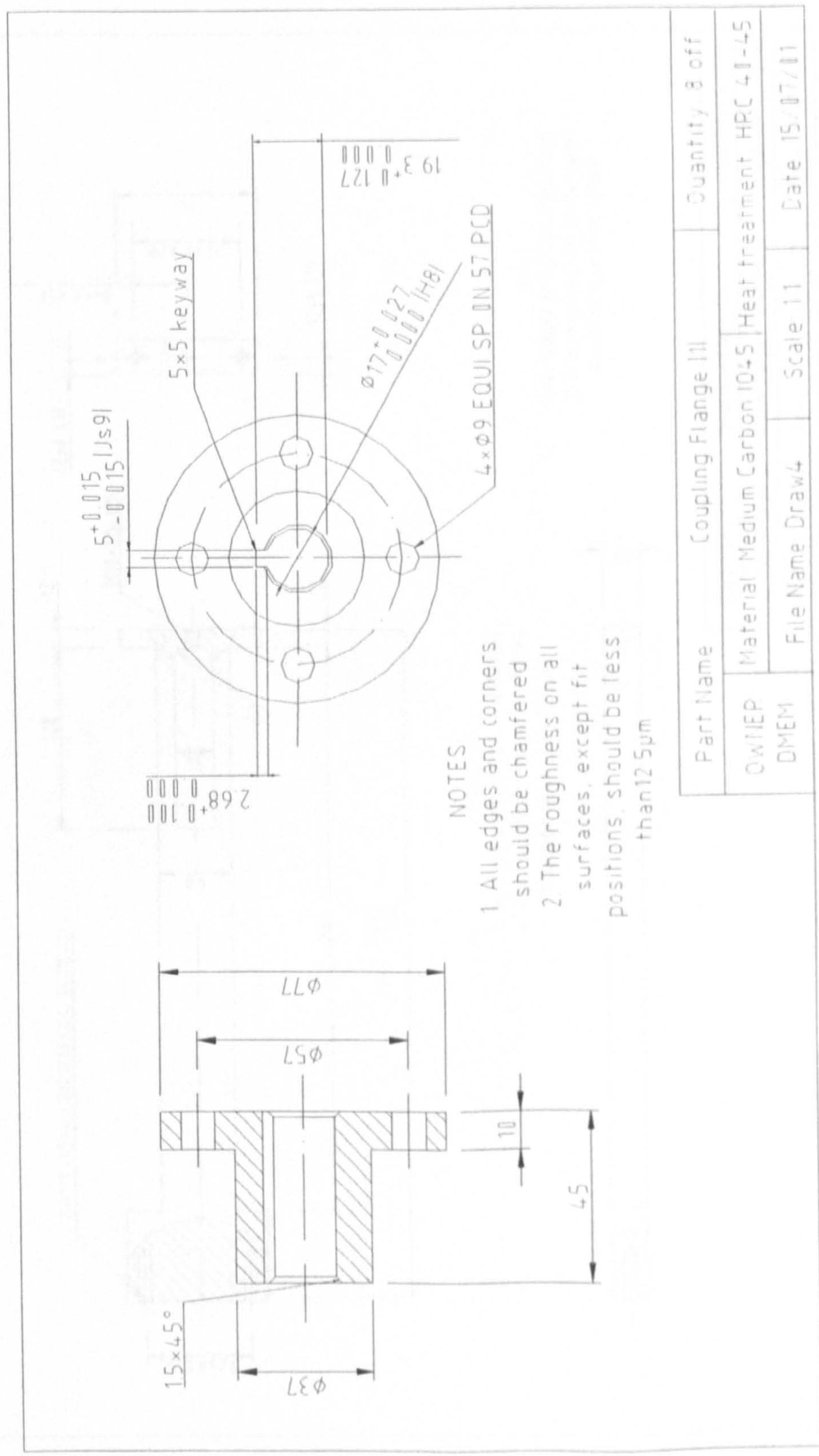

Fig. 4.1.9 The coupling flange (1) design

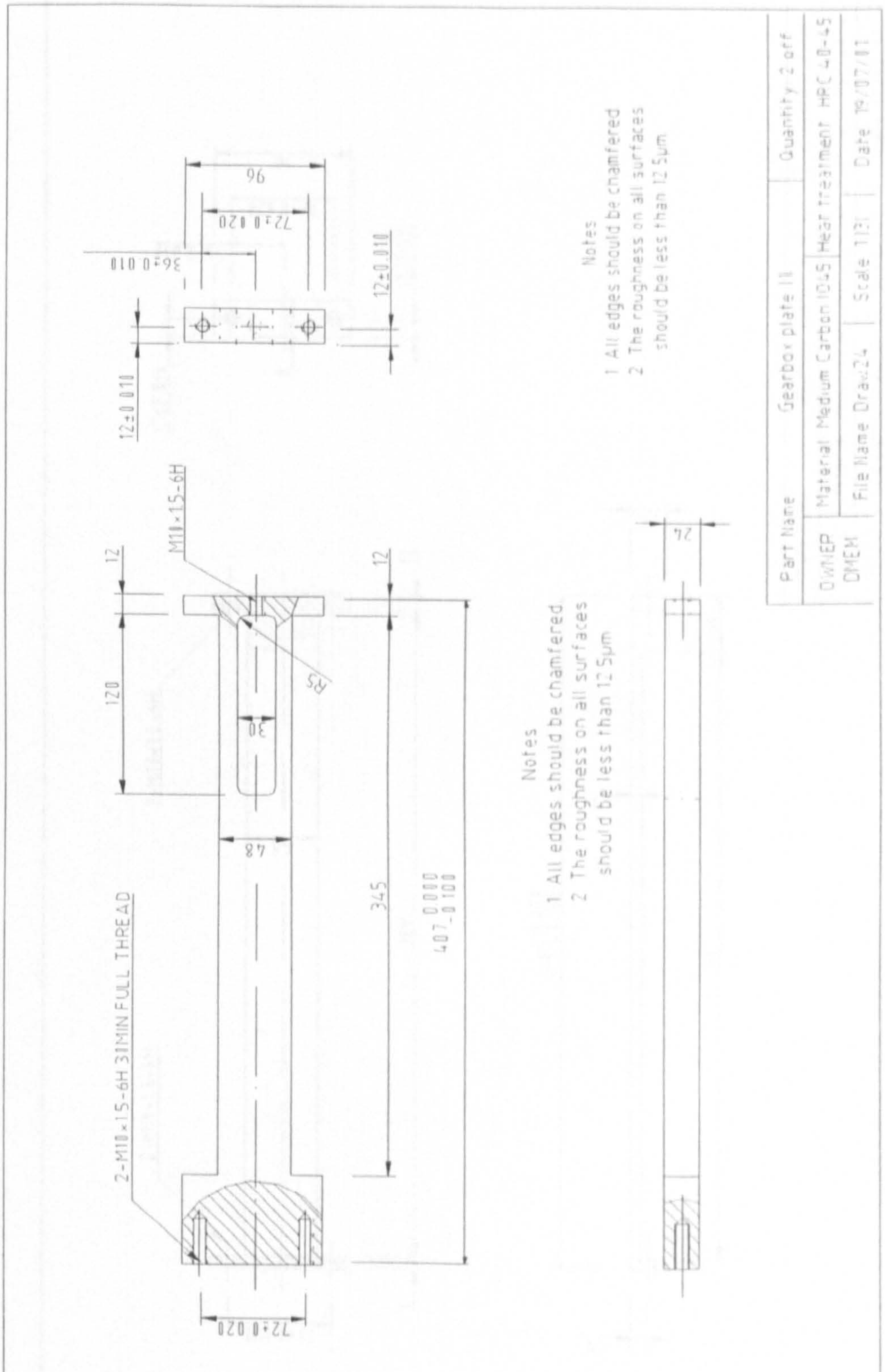

Fig. 4.1.10 The gearbox plate (1) design

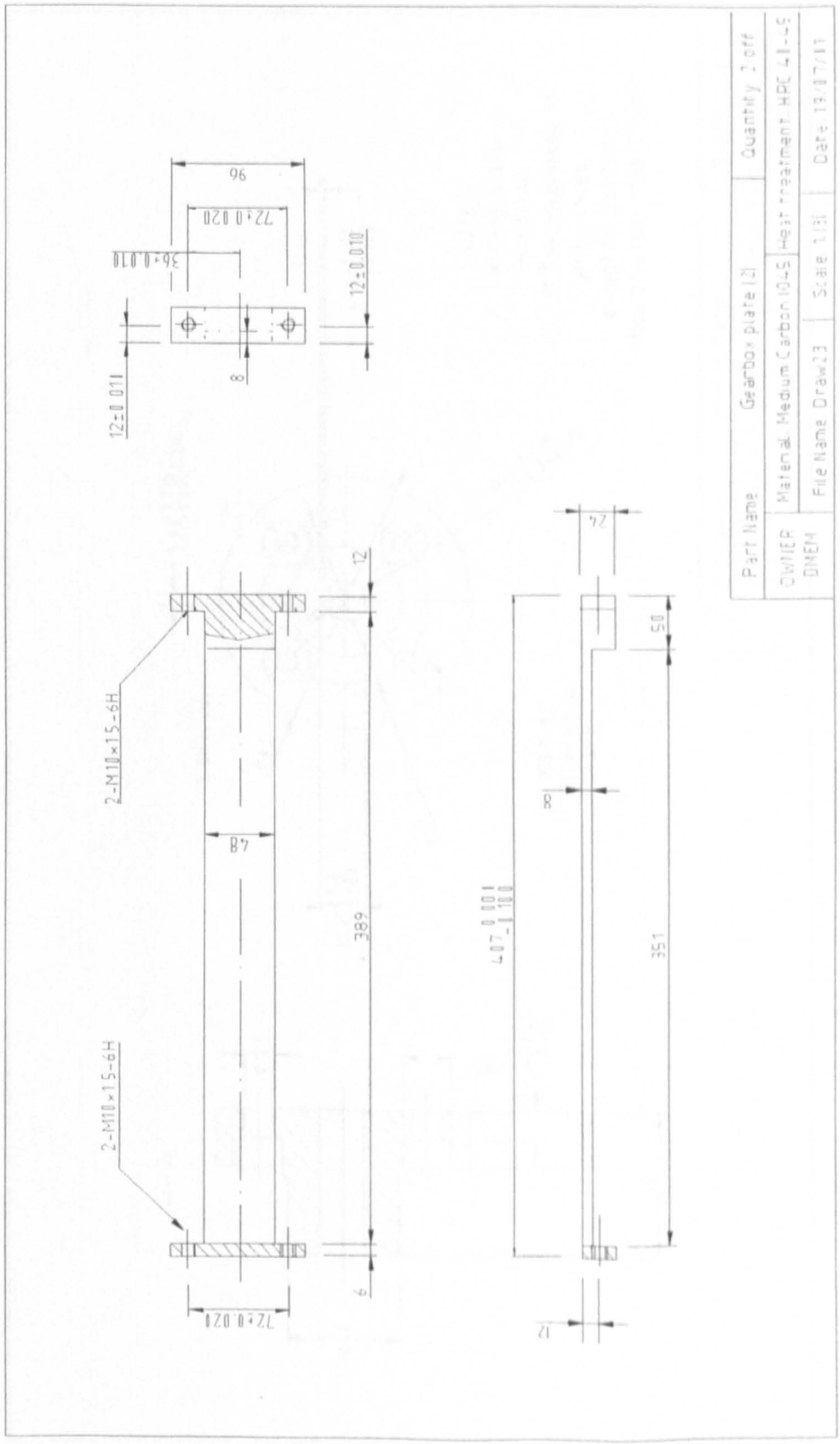

Fig. 4.1.11 The gearbox plate (2) design

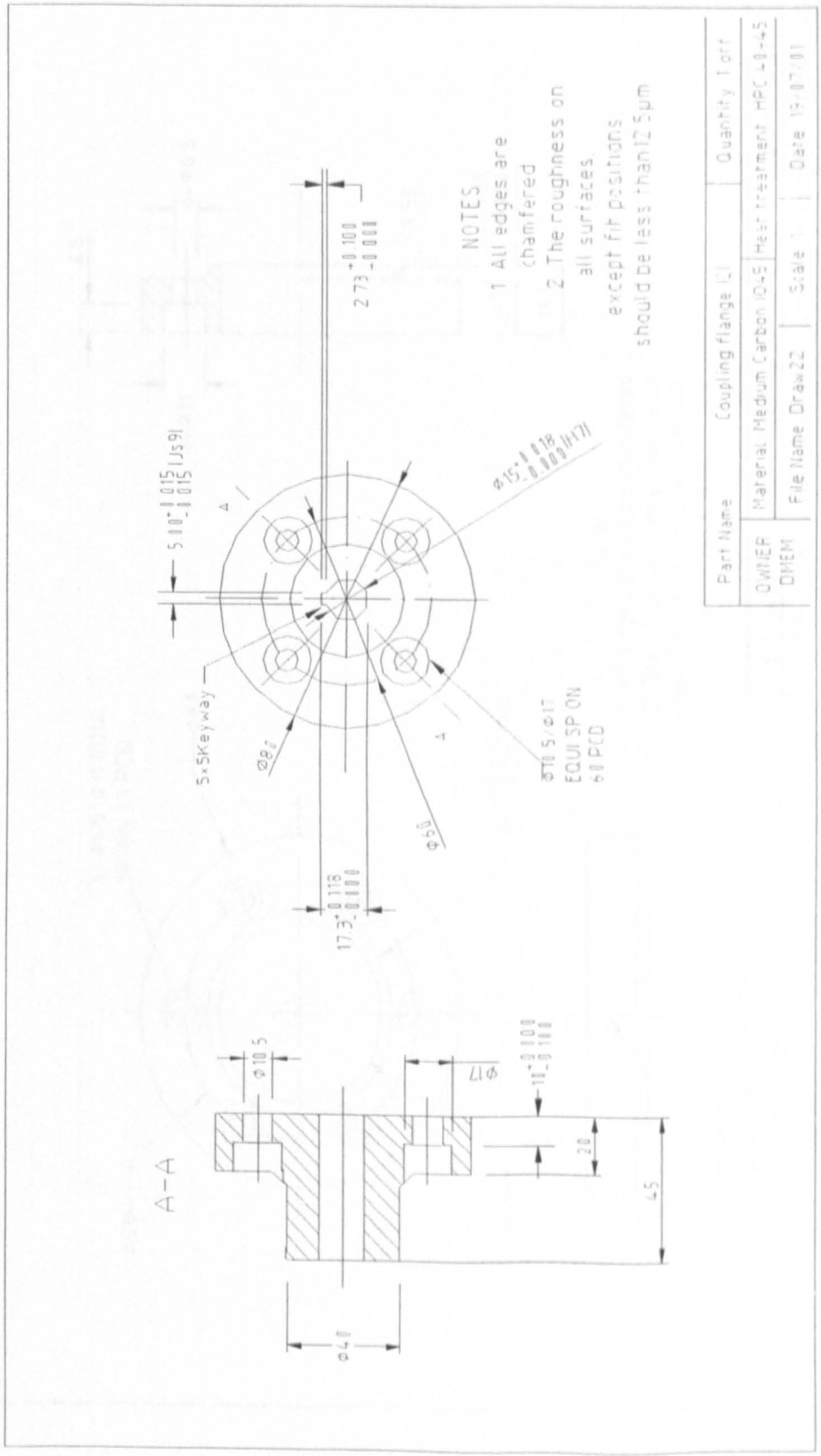

Fig. 4.1.12 The coupling flange (2) design

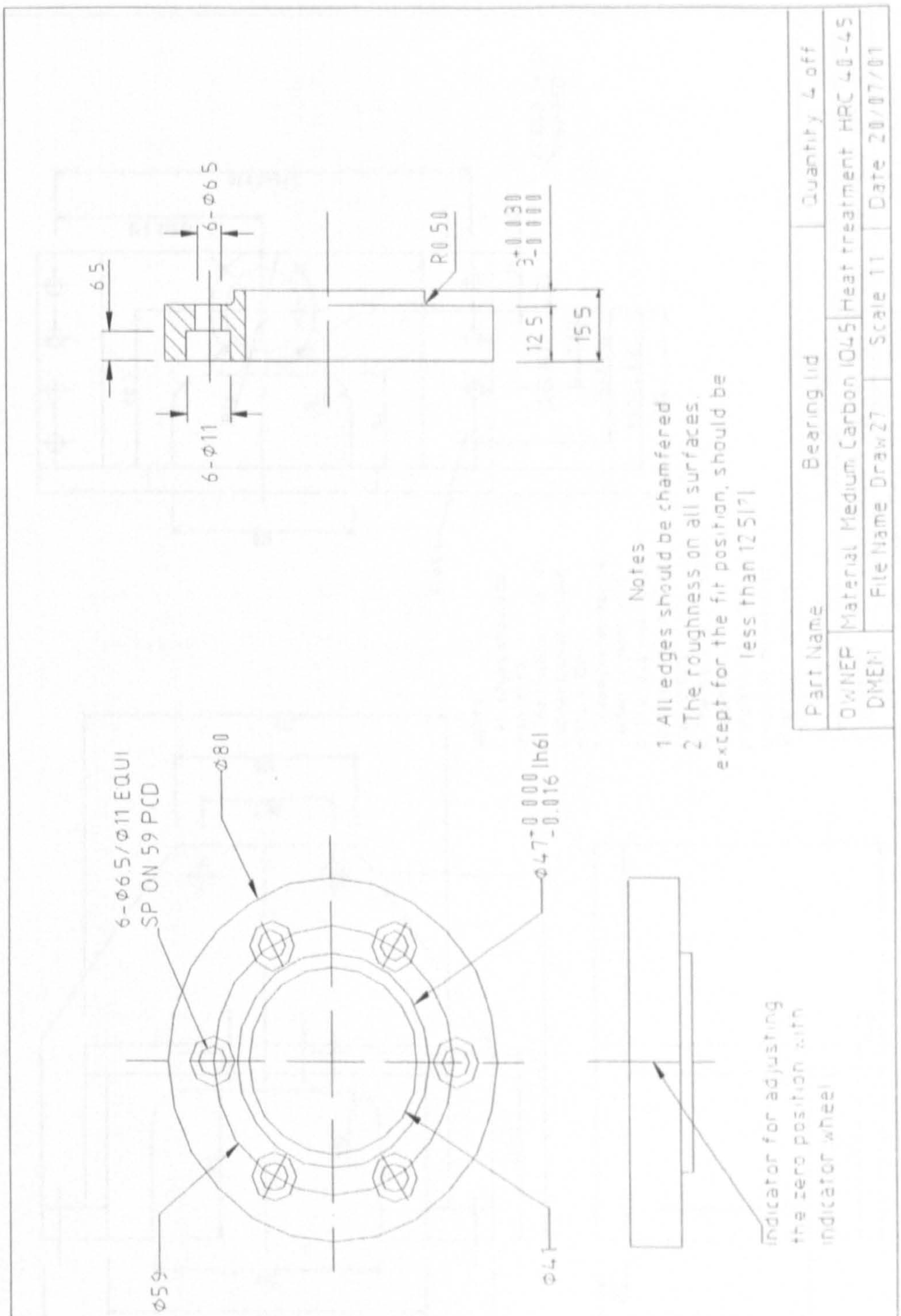

Fig. 4.1.13 The bearing lid design

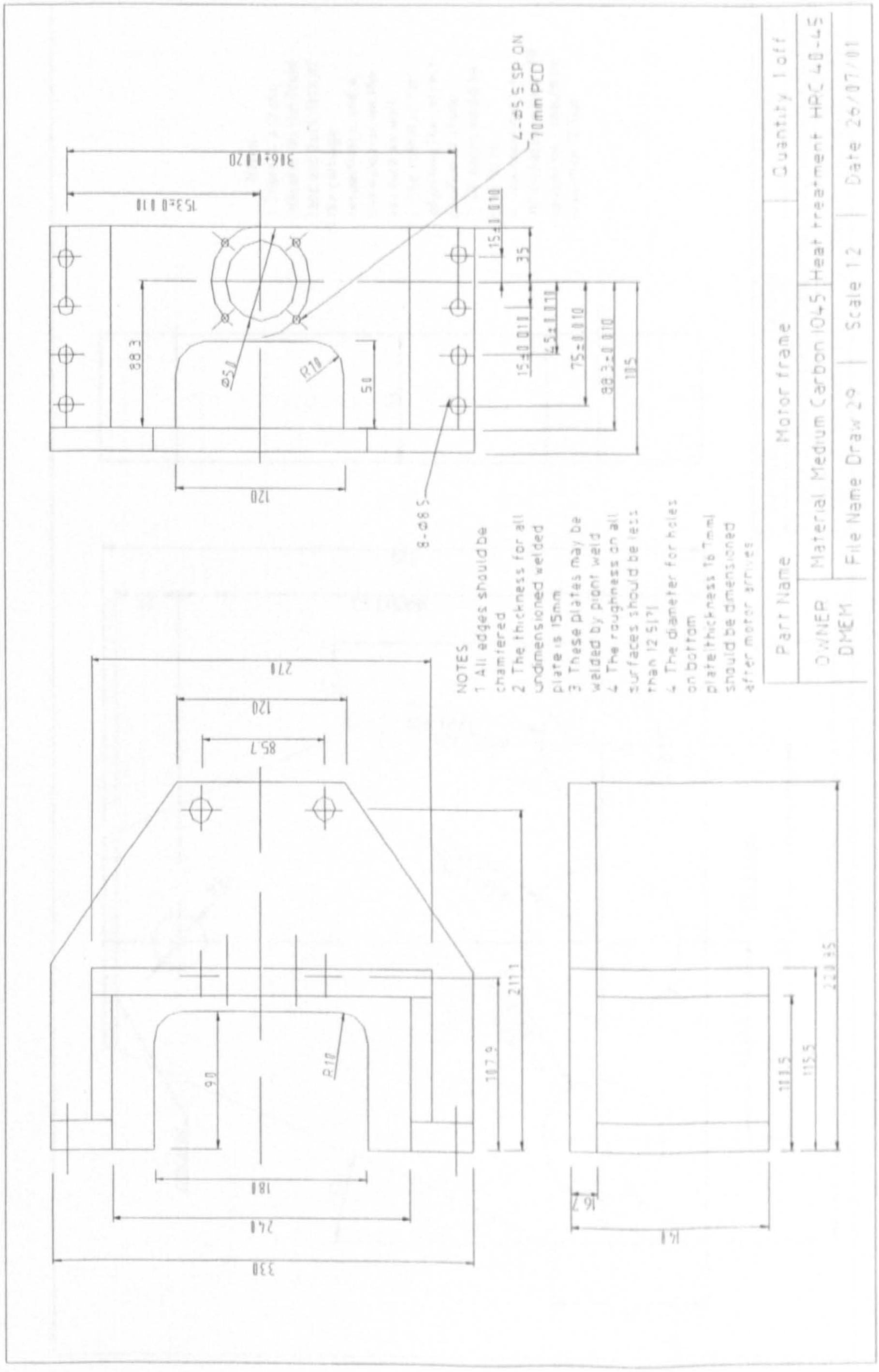

Fig. 4.1.14 The motor frame design

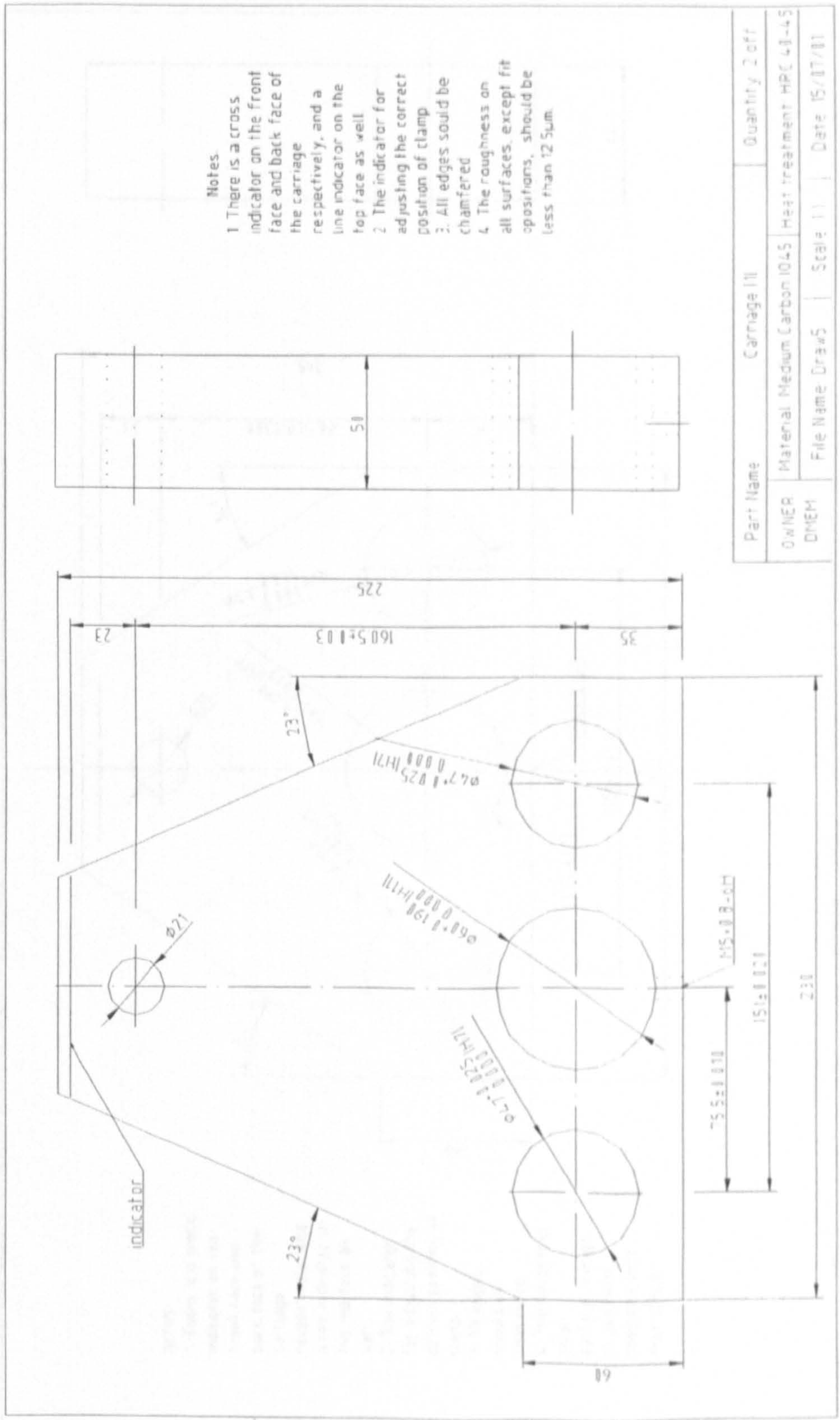

Fig. 4.1.15 The carriage (1) design

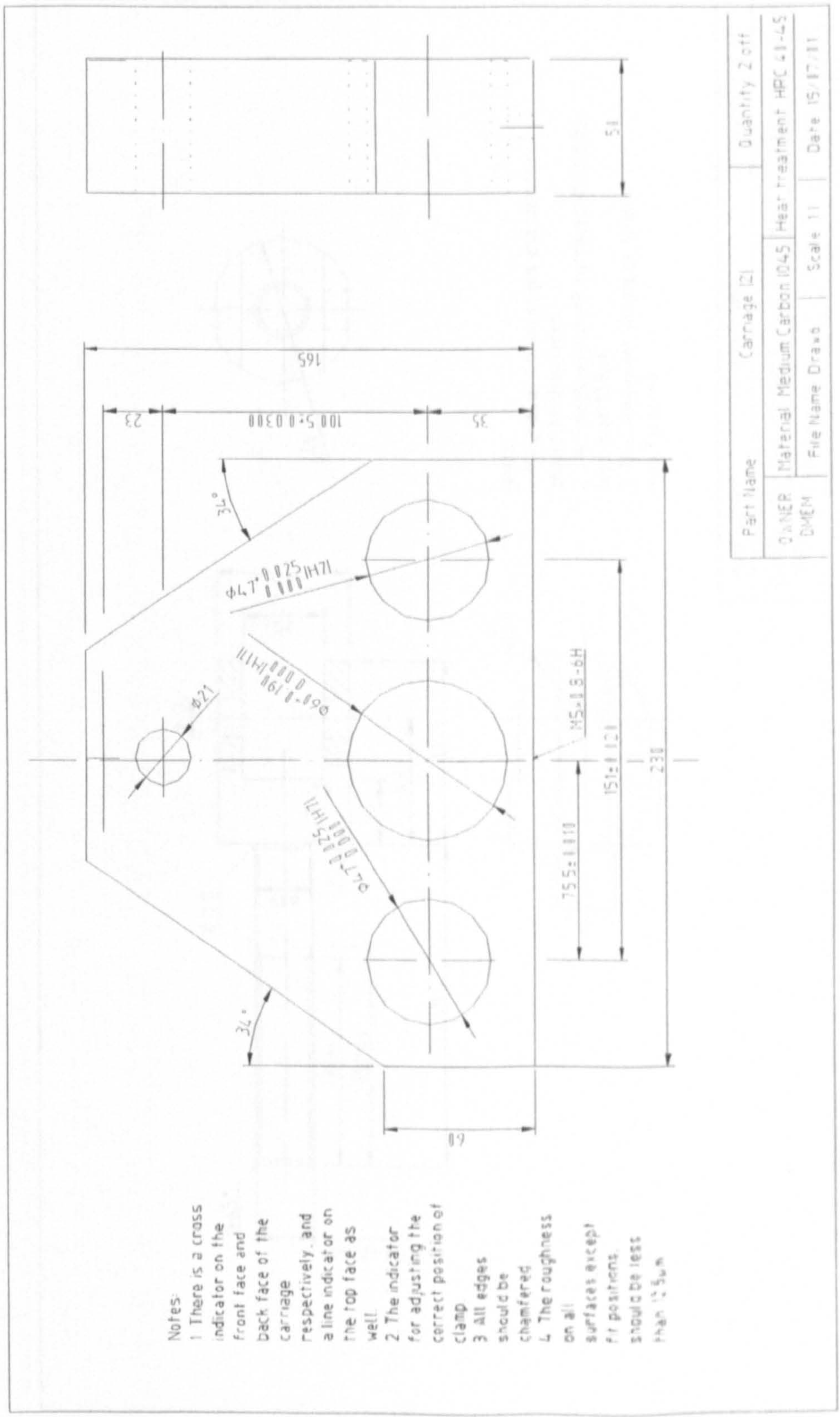

Fig. 4.1.16 The carriage (2) design

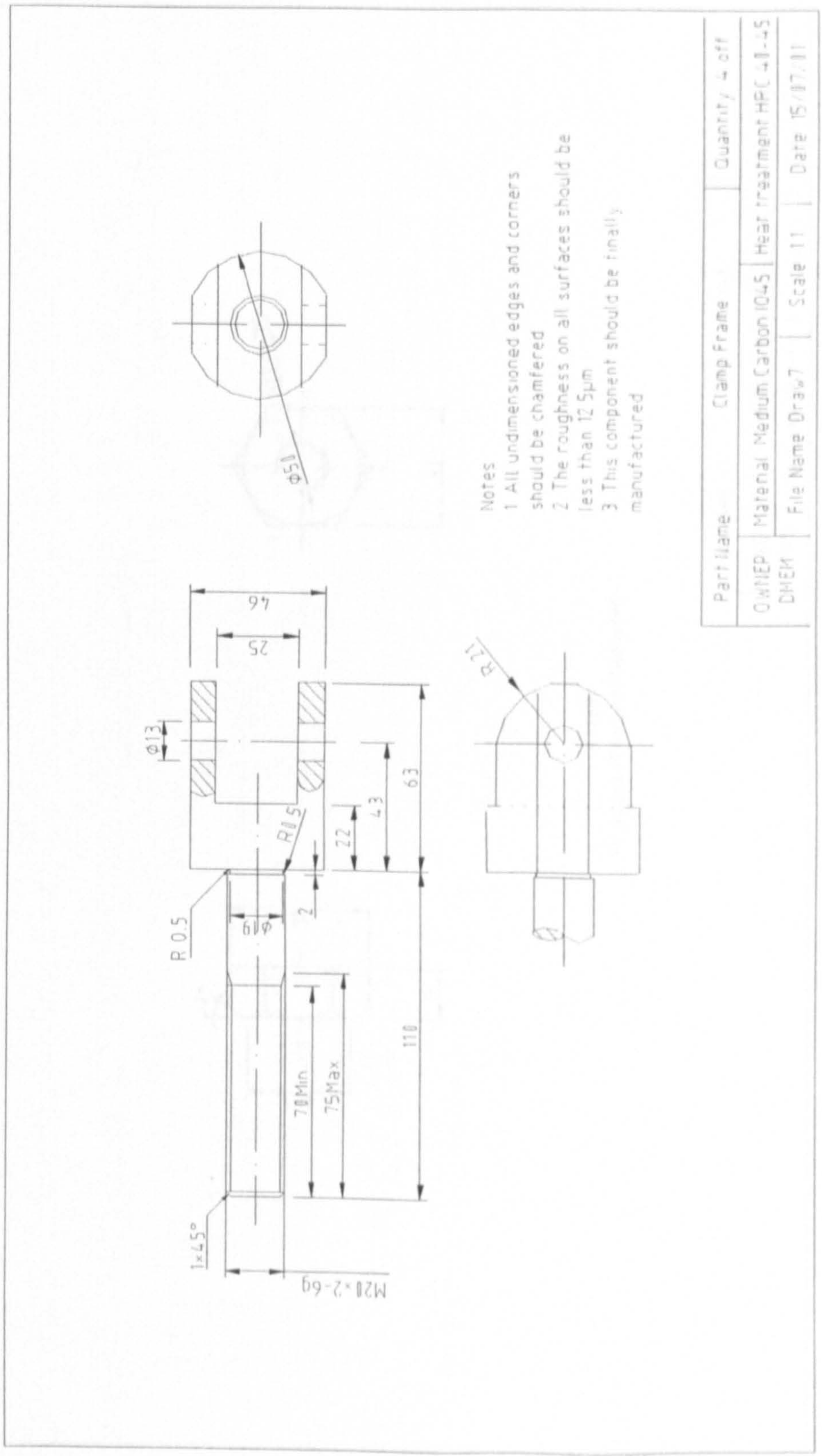

Fig. 4.1.17 The clamp frame design

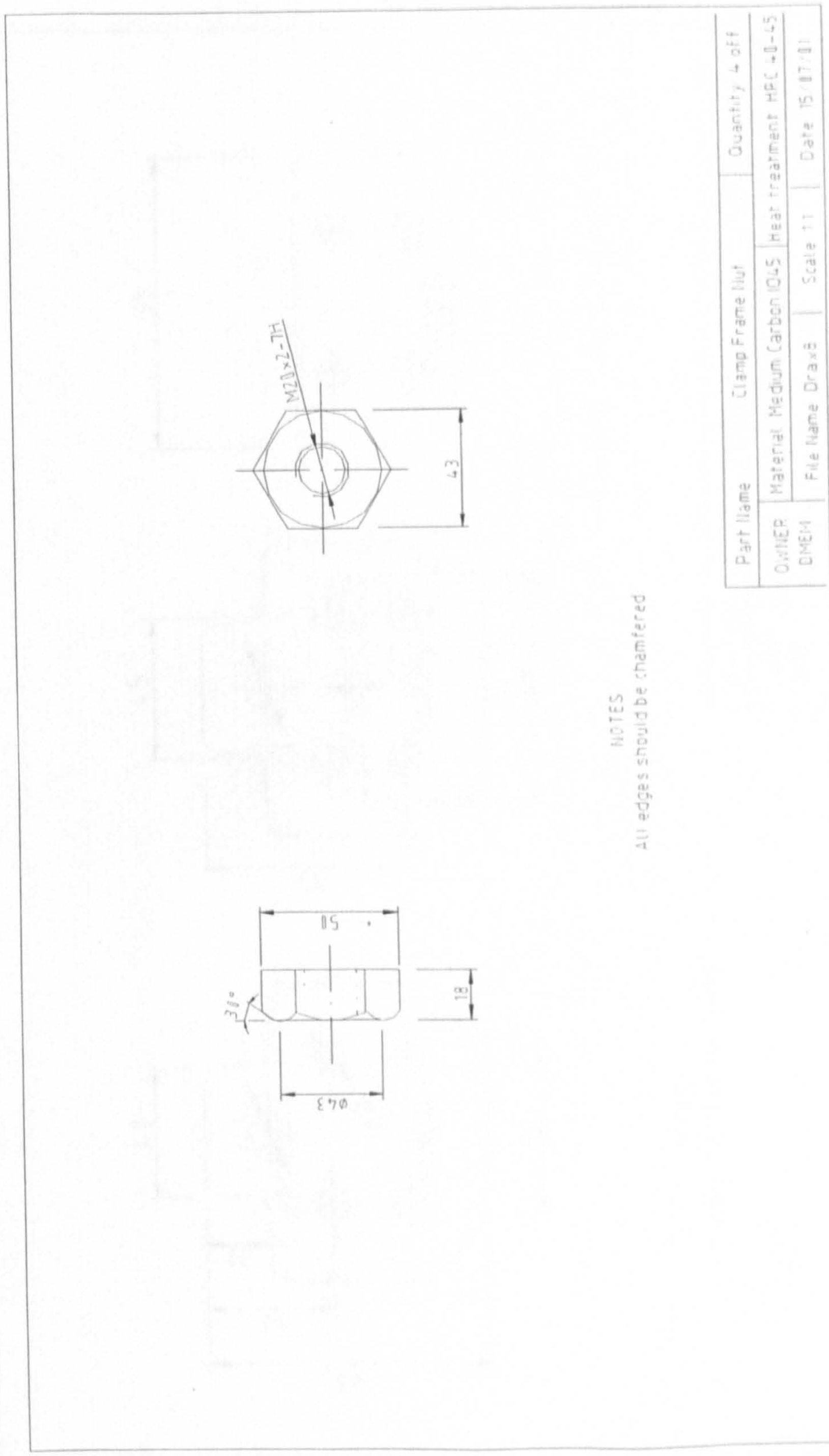

Fig. 4.1.18 The clamp frame nut design

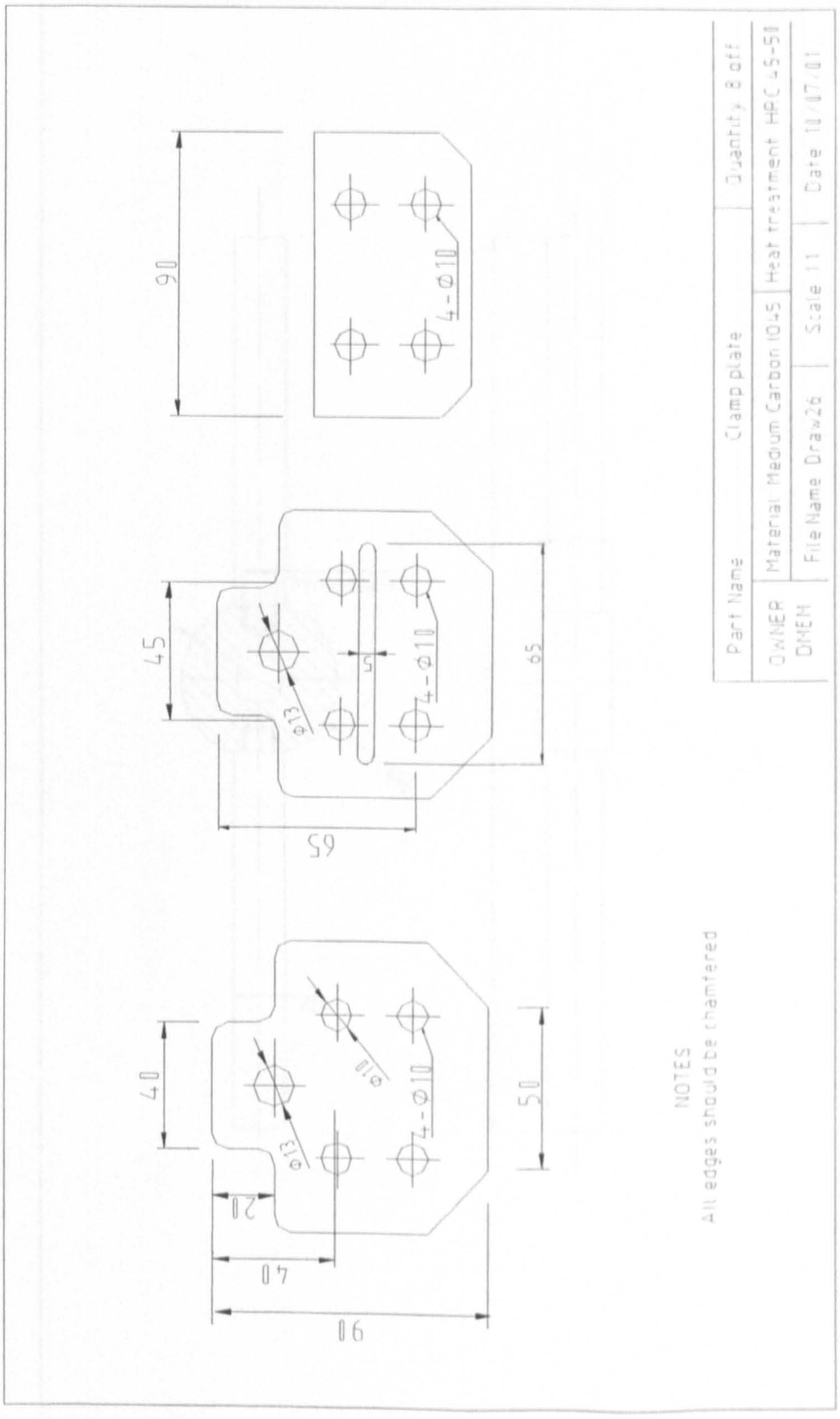

Fig. 4.1.19 The clamp plate design

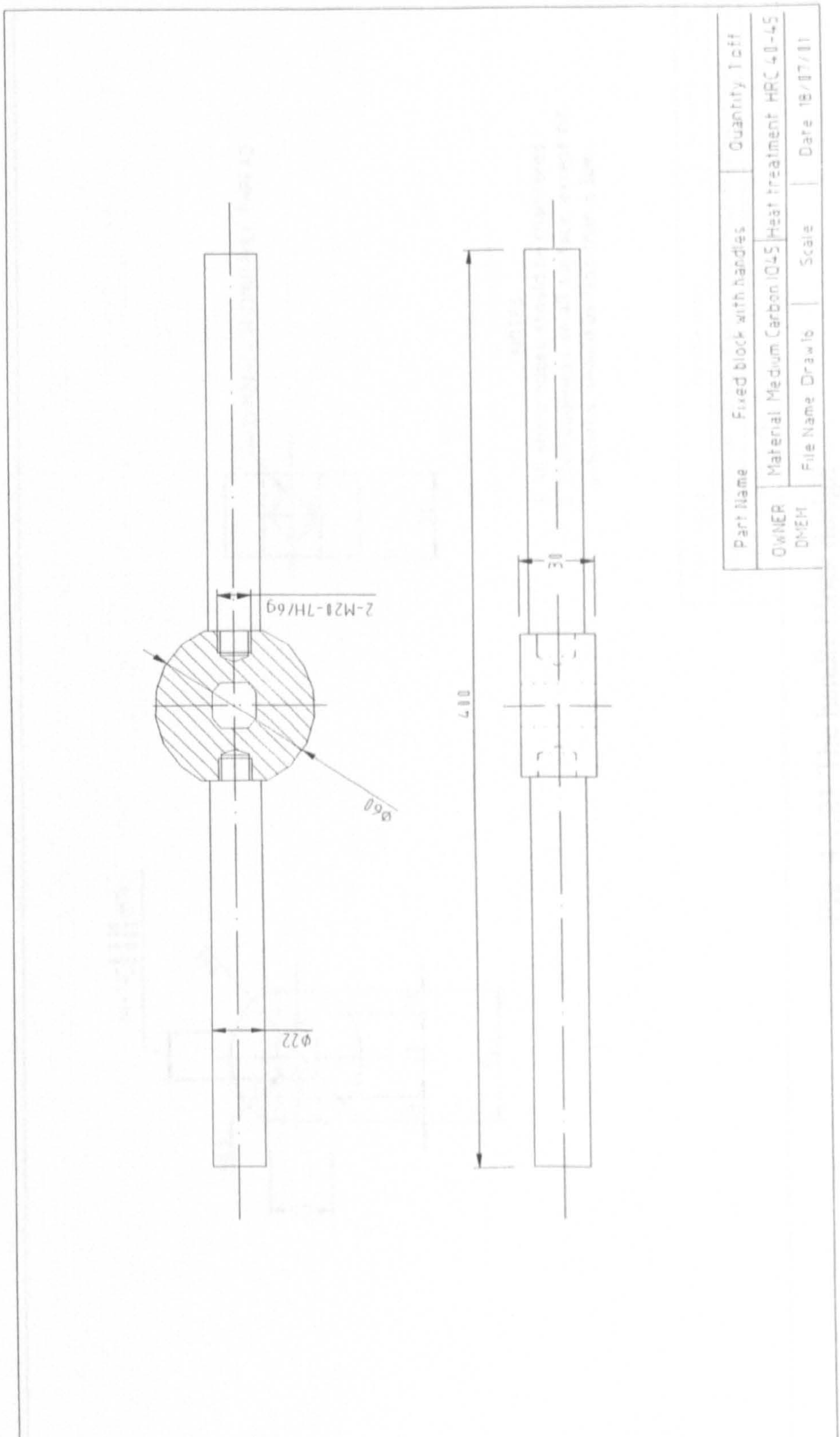

Fig. 4.1.20 The handles with fixed block

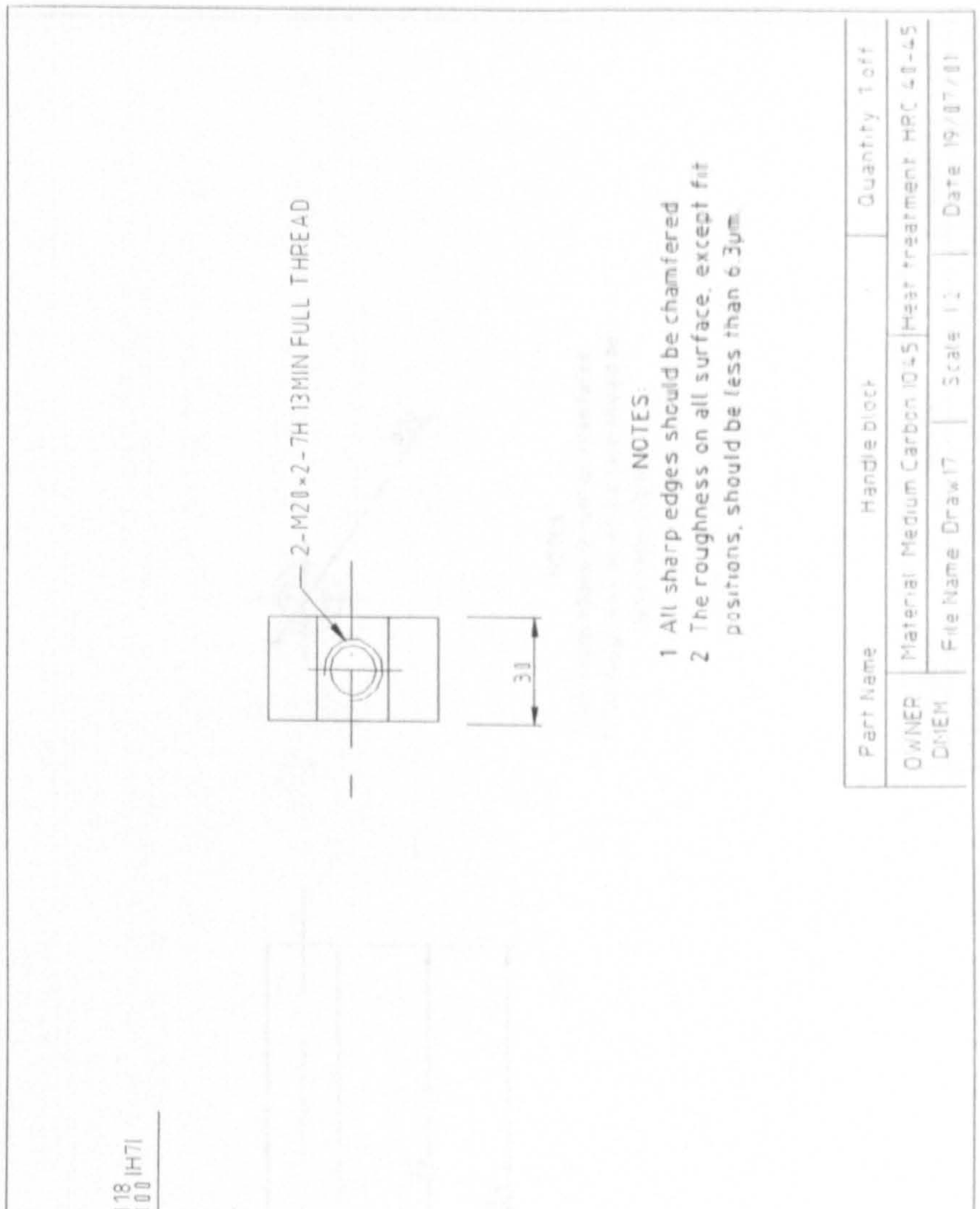

Fig. 4.1.21 The handle block design

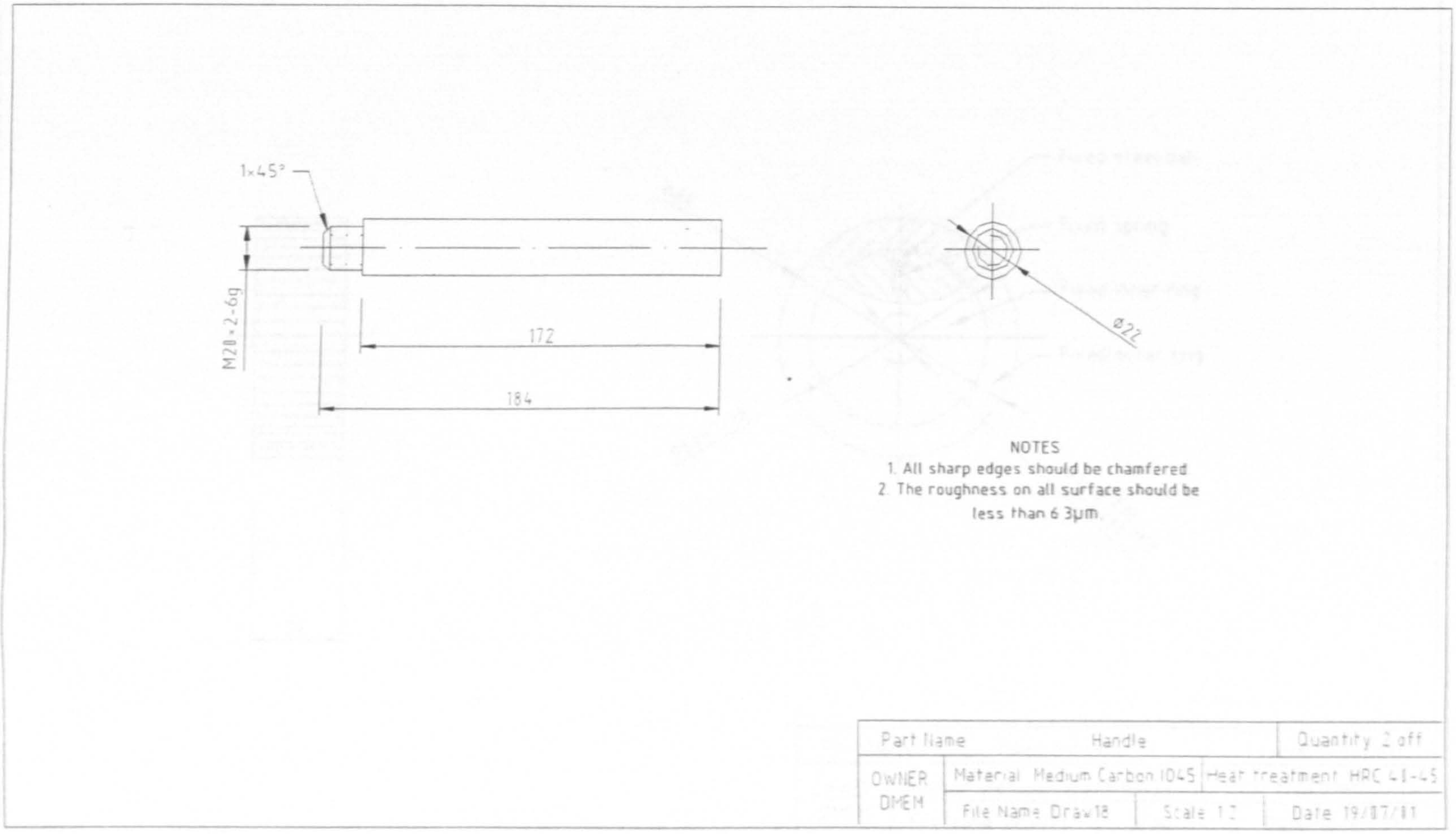

Fig. 4.1.22 The handle design

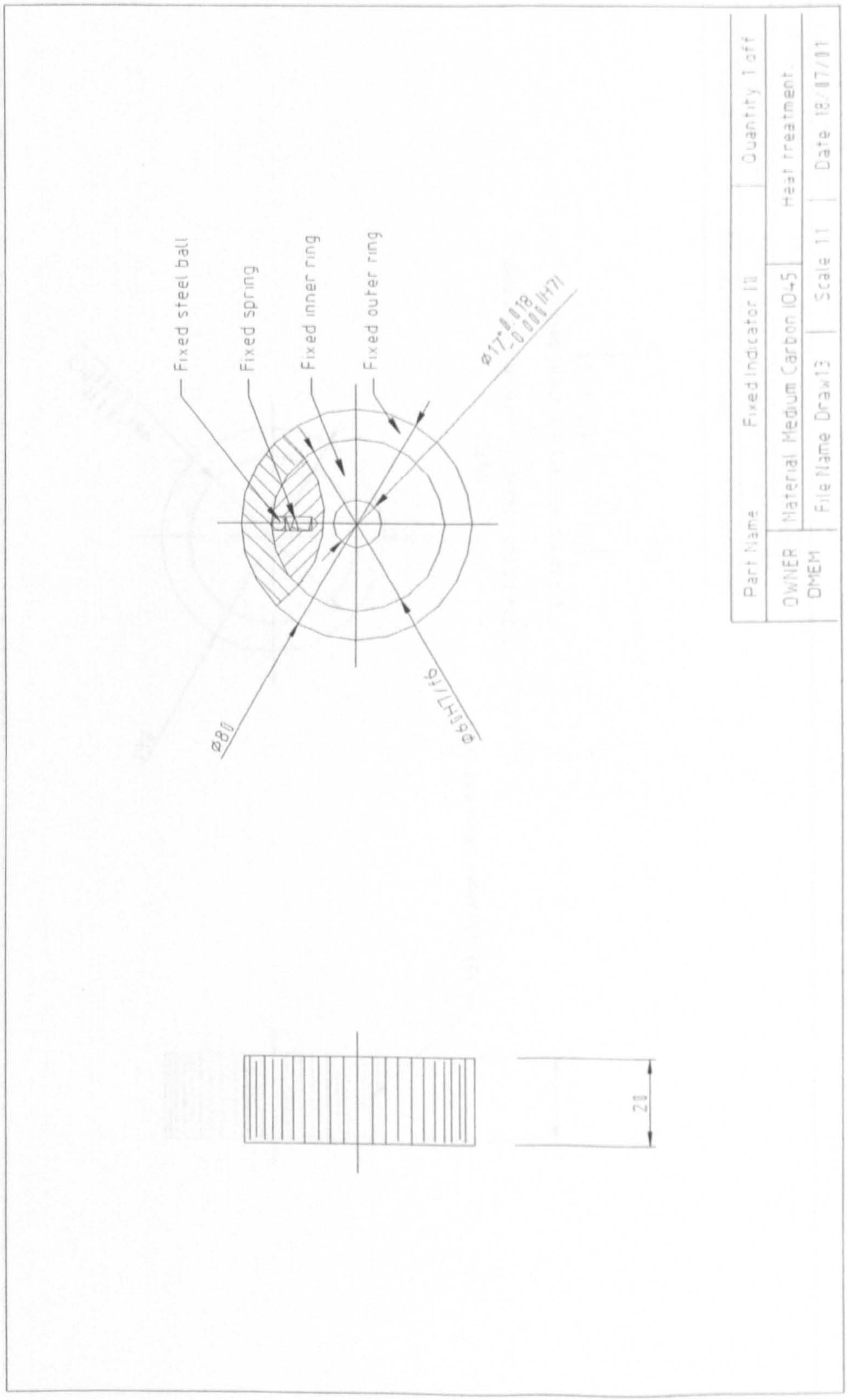

Fig. 4.1.23 The fixed indicator (1) design

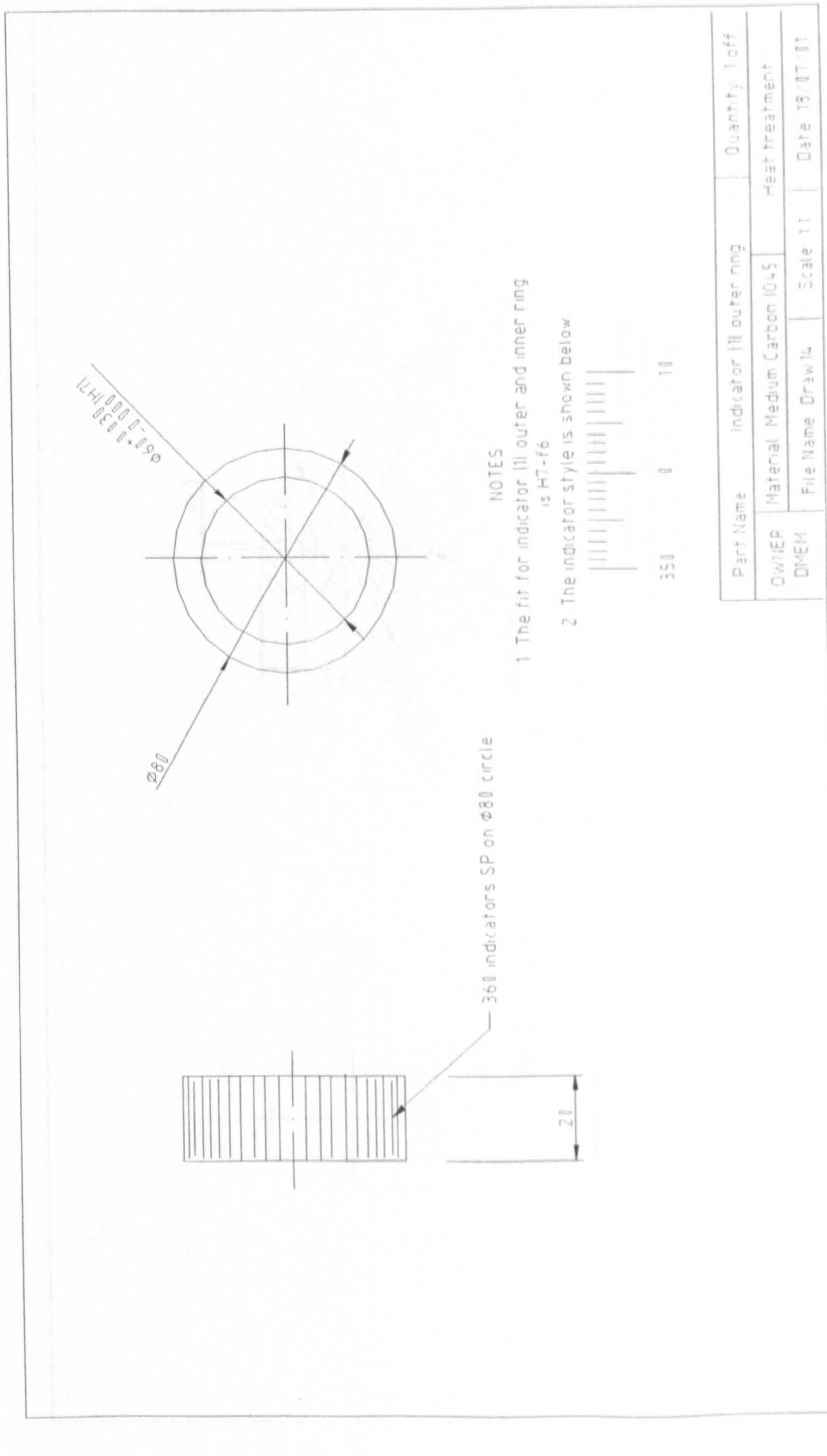

Fig. 4.1.24 The indicator (1) outer ring design

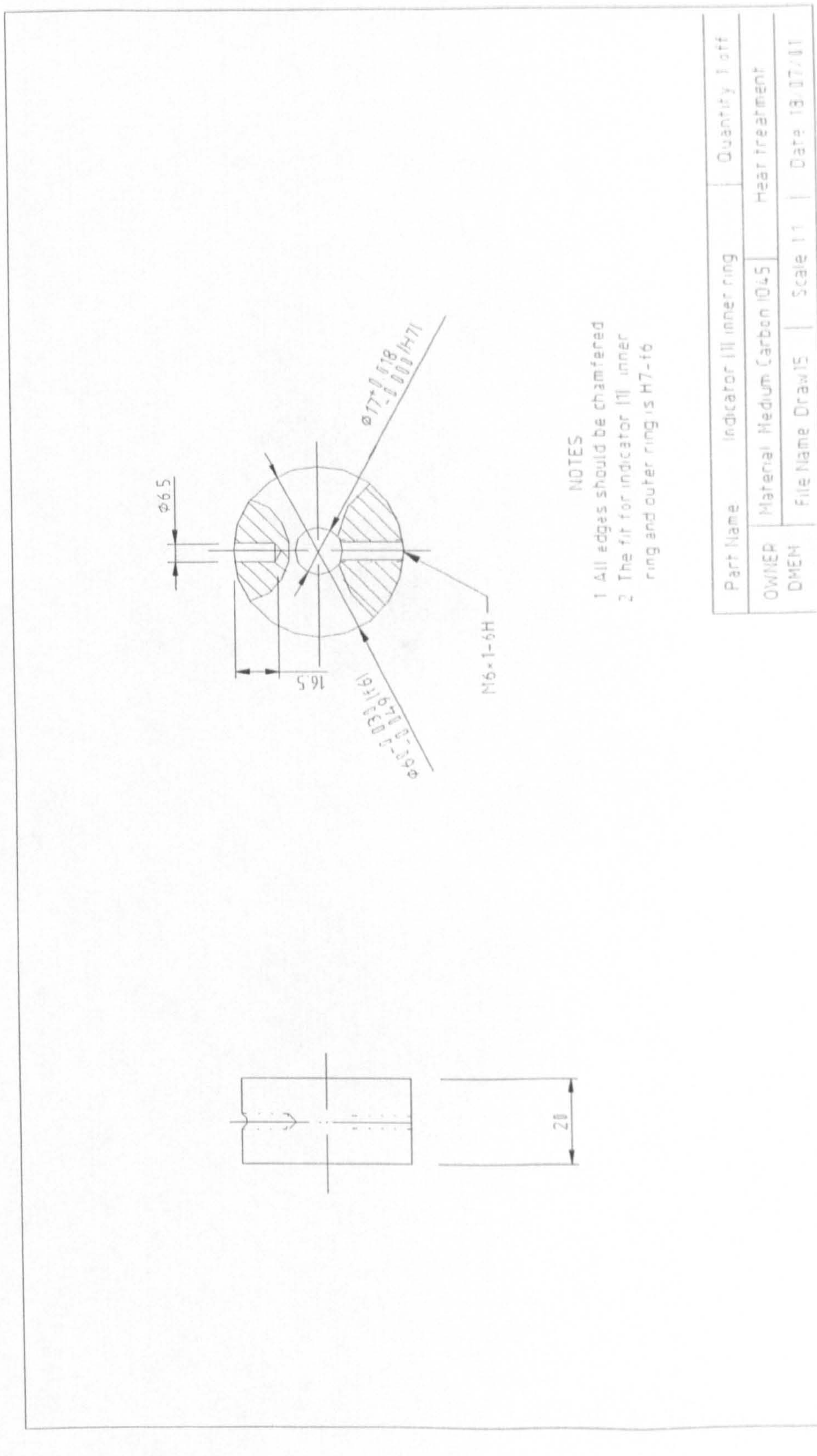

Fig. 4.1.25 The indicator (1) inner ring design

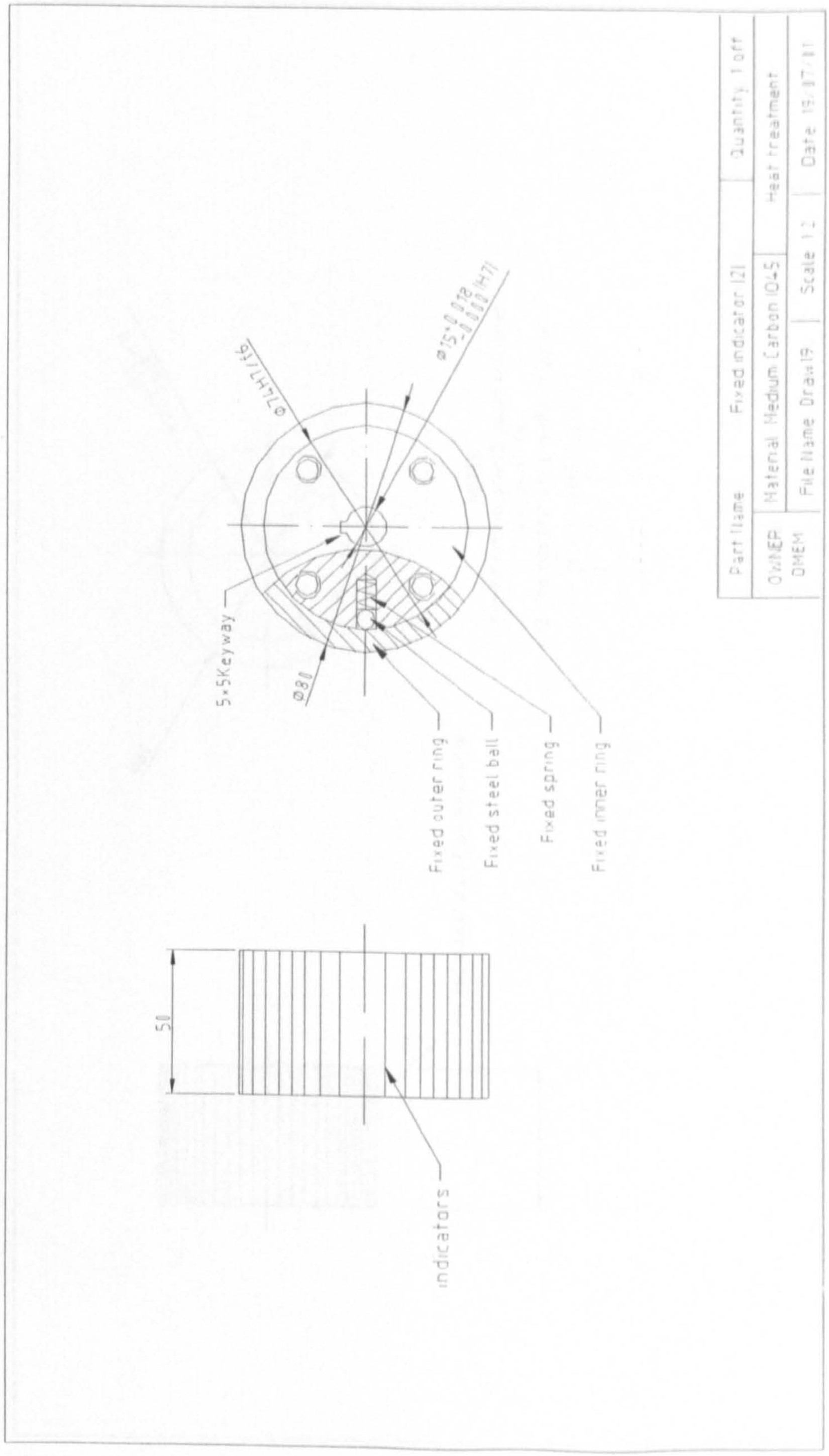

Fig. 4.1.26 The fixed indicator (2) design

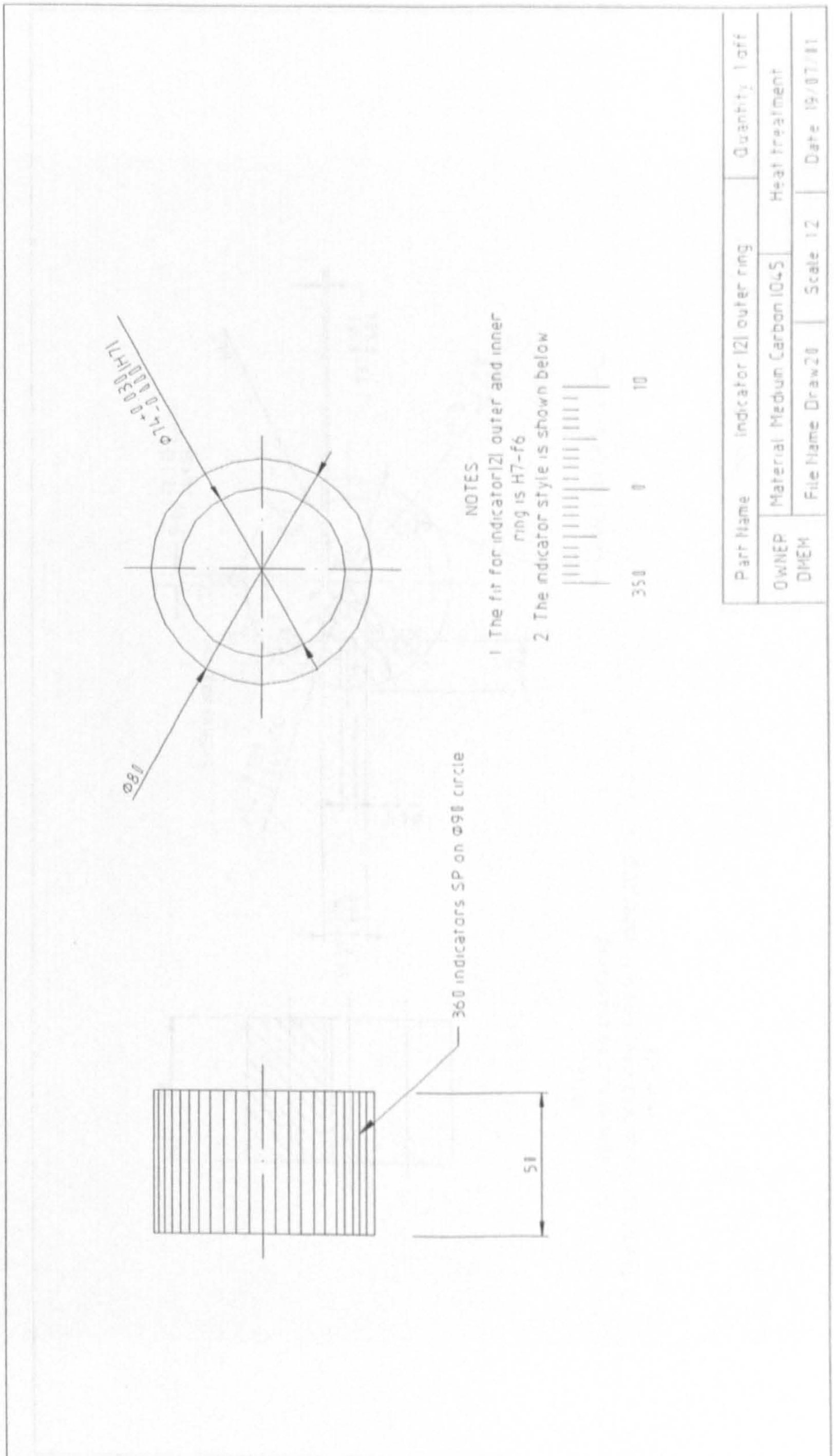

Fig. 4.1.27 The indicator (2) outer ring design

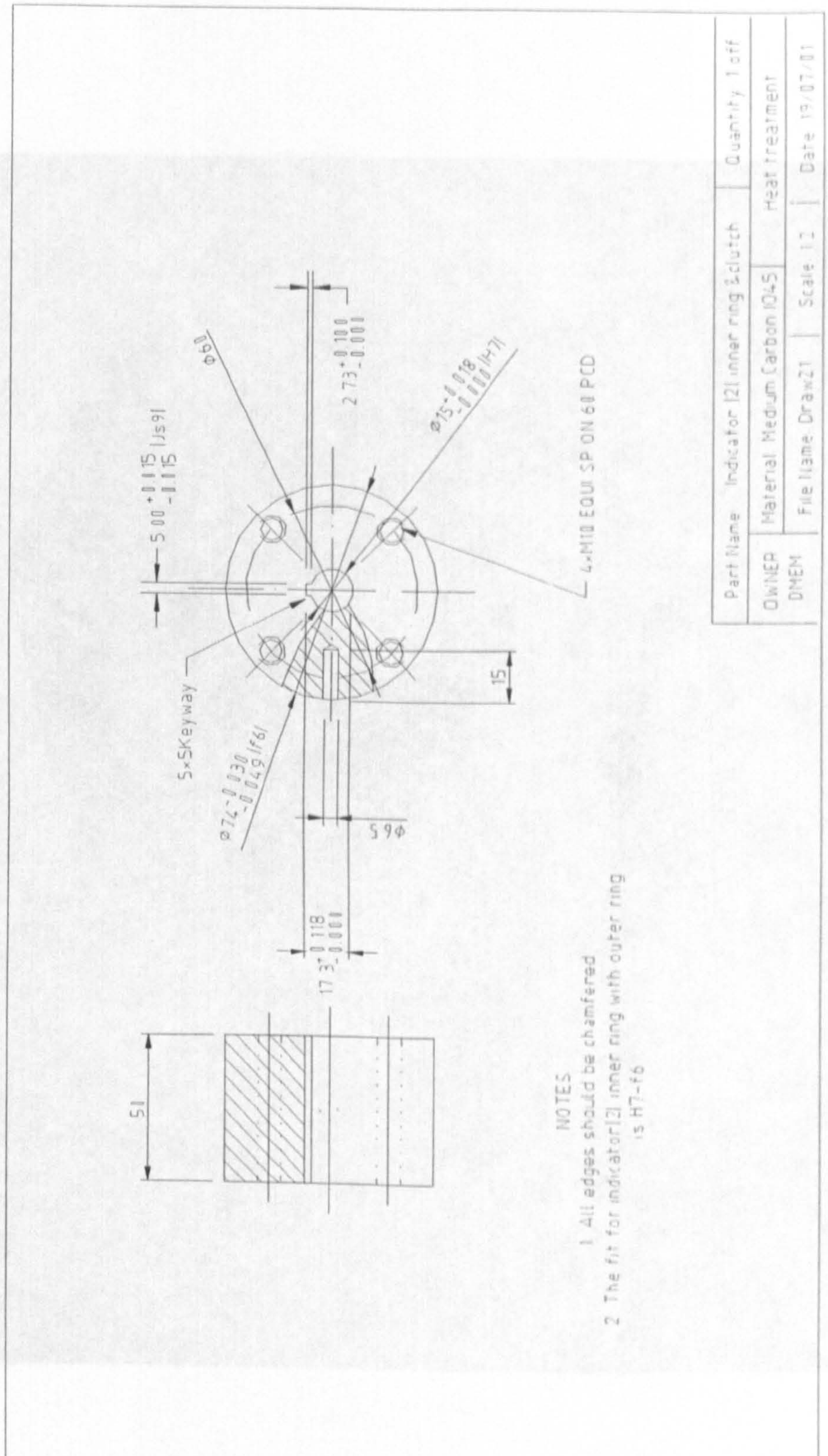

Fig. 4.1.28 The indicator (2) inner ring design

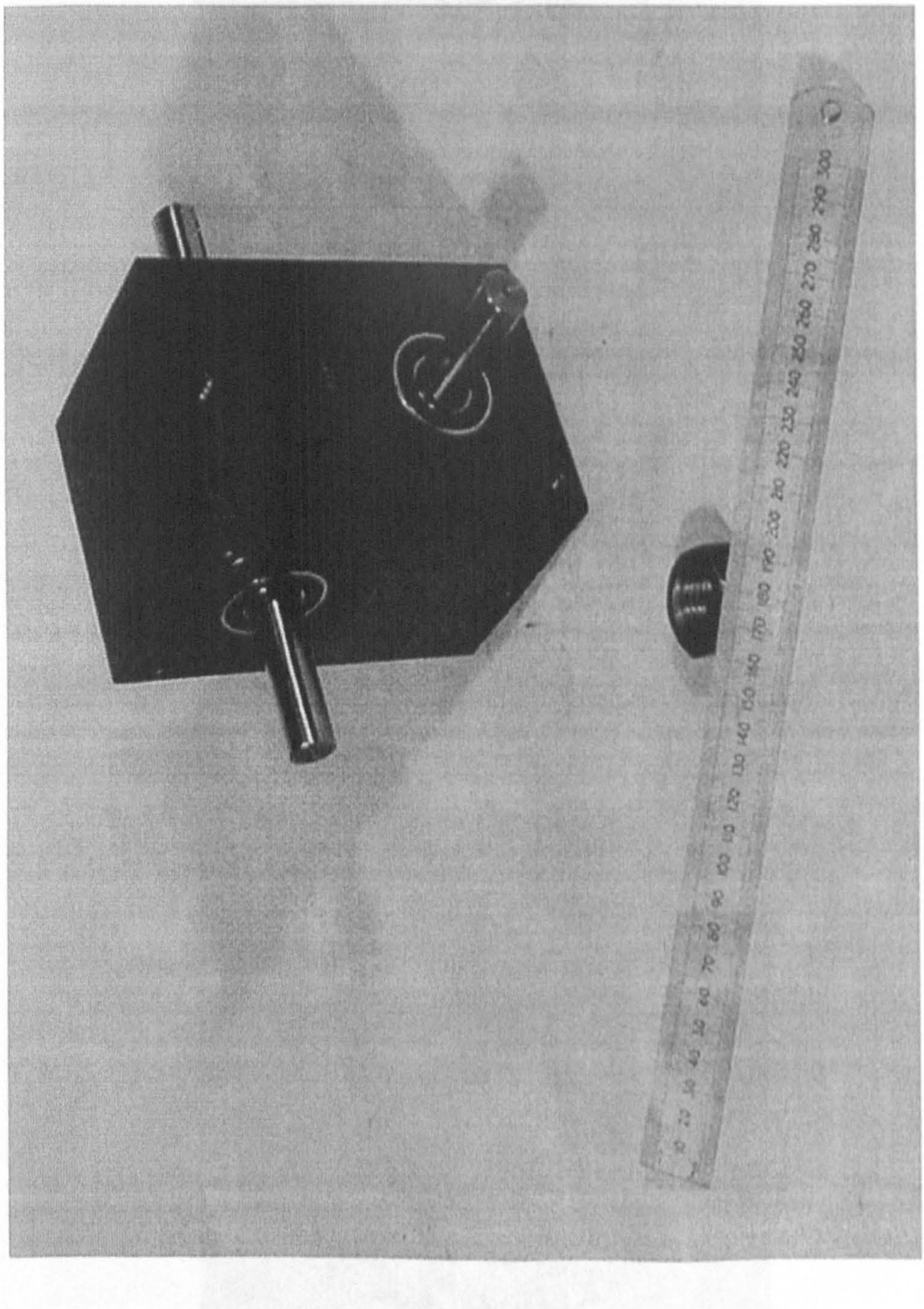

Fig 4.2.1 The gearbox

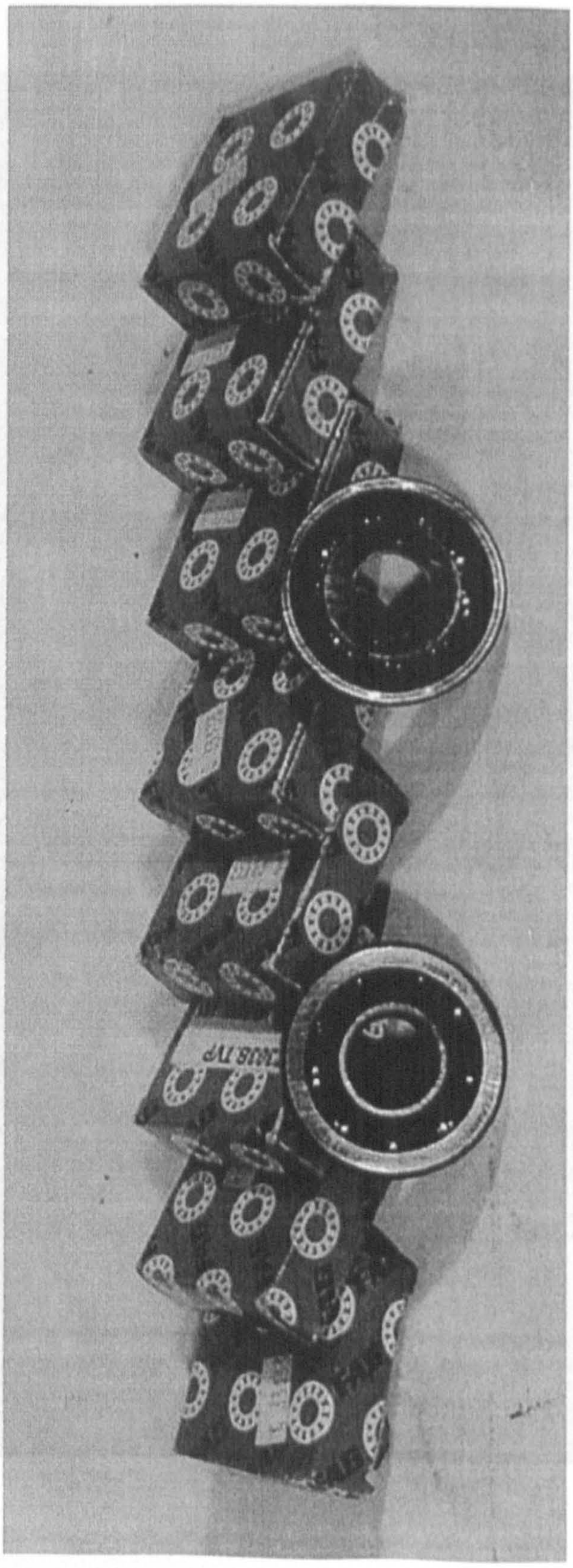

Fig 4.2.2 The bearings

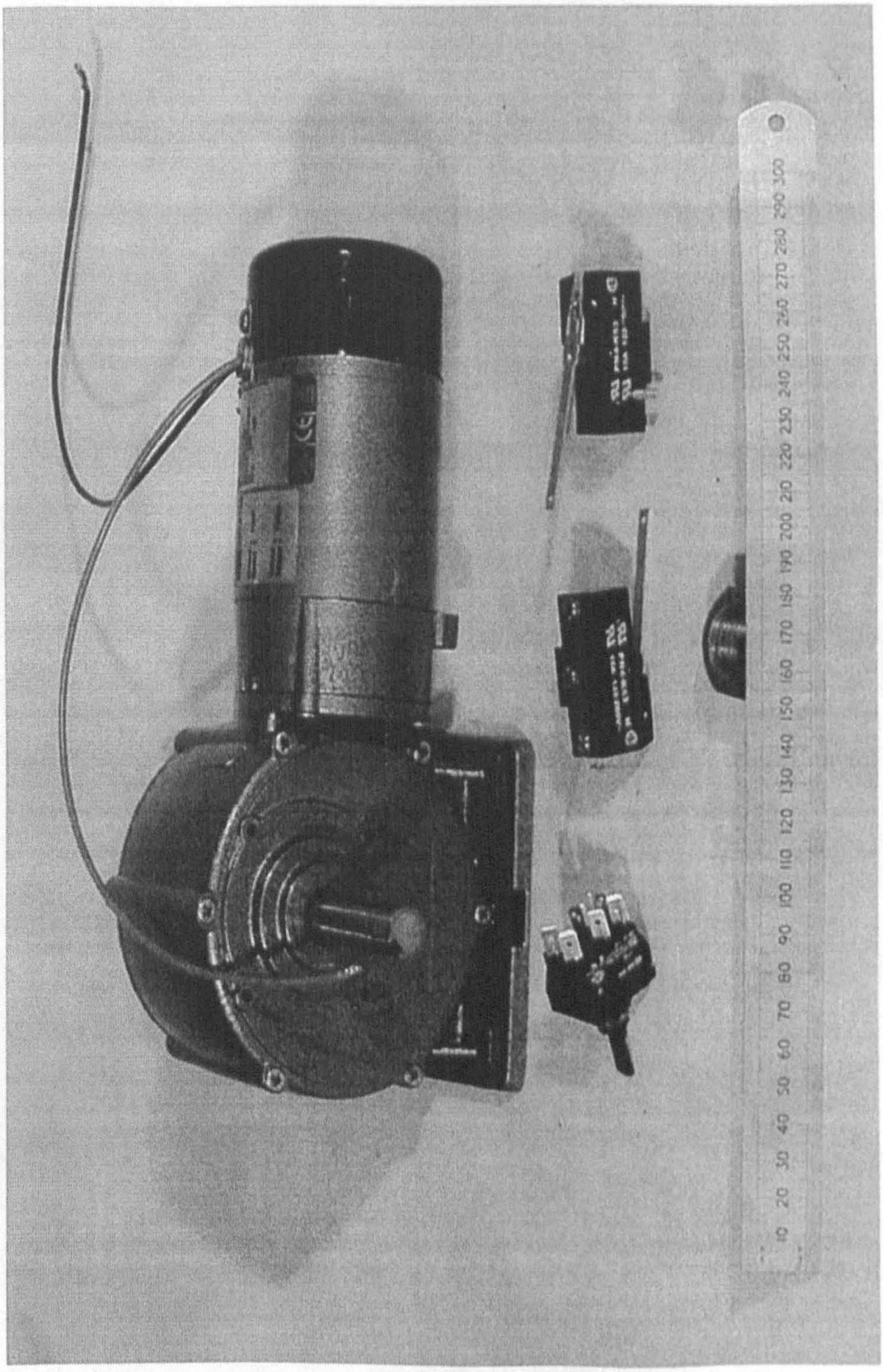

Fig 4.2.3 The motor and switches

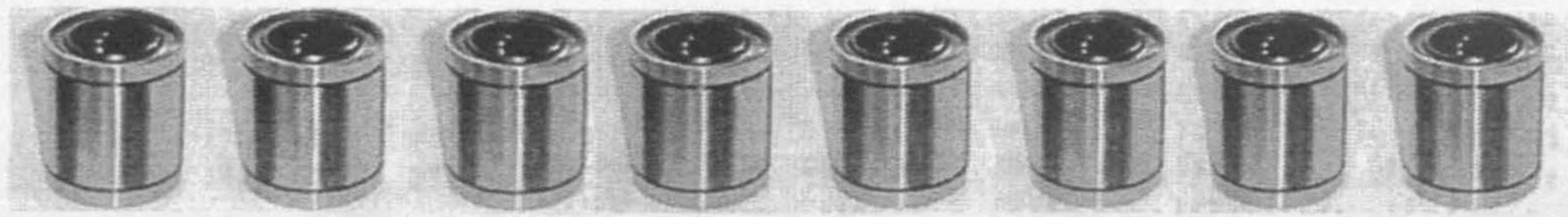

(a) The linear bearings

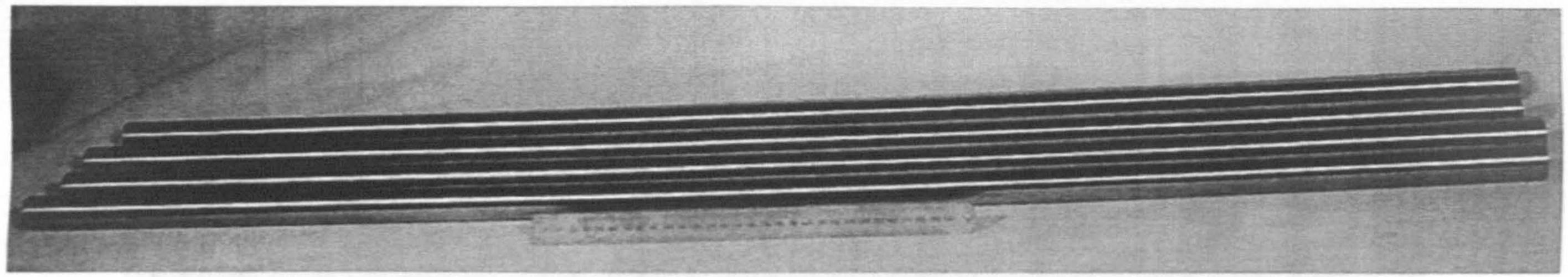

(b) The linear shafts

Fig 4.2.4 The linear shafts and linear bearings

(a) The inside view

(b) The outside view

Fig 4.2.5 The machine frame

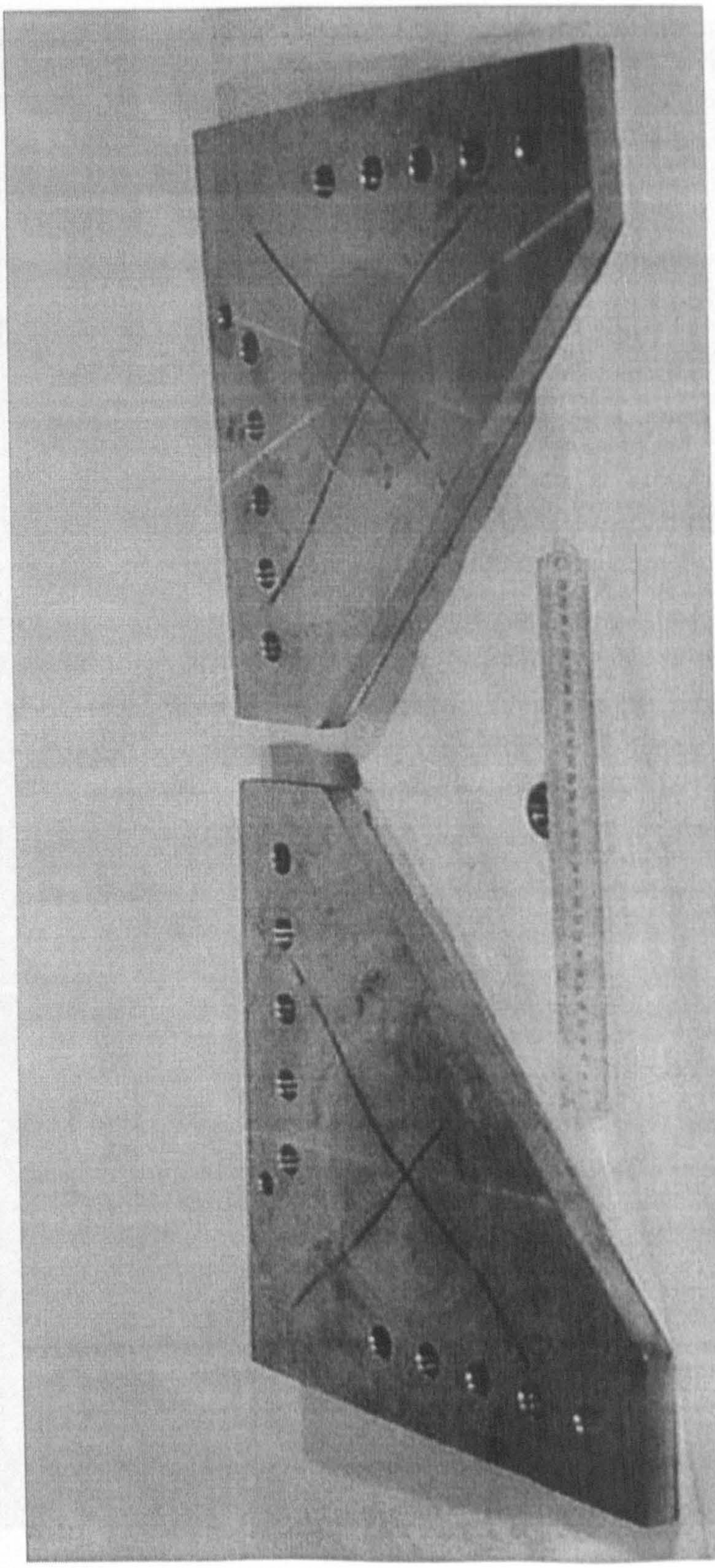

Fig 4.2.6 The corner plates

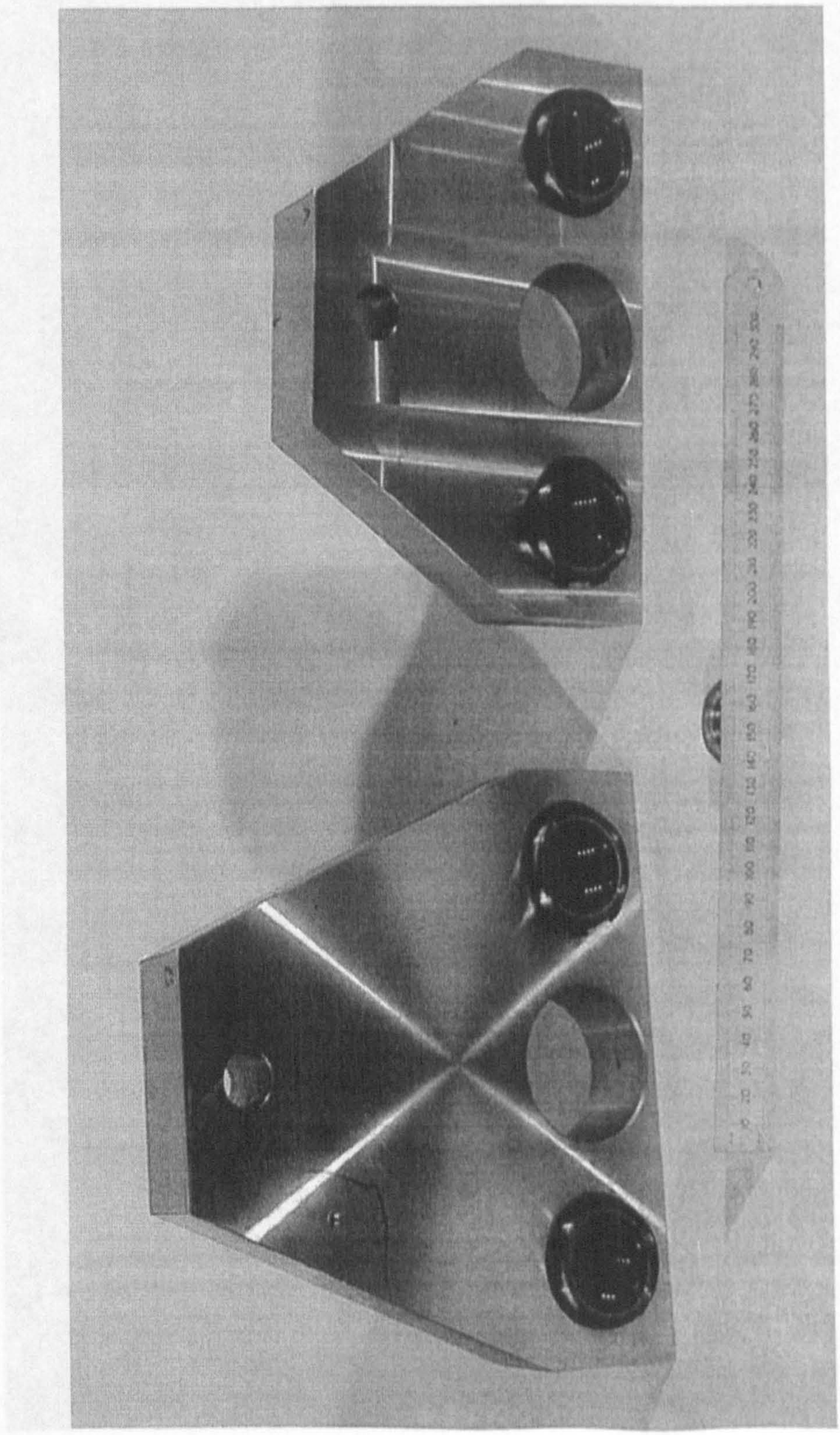

Fig 4.2.7 The carriages

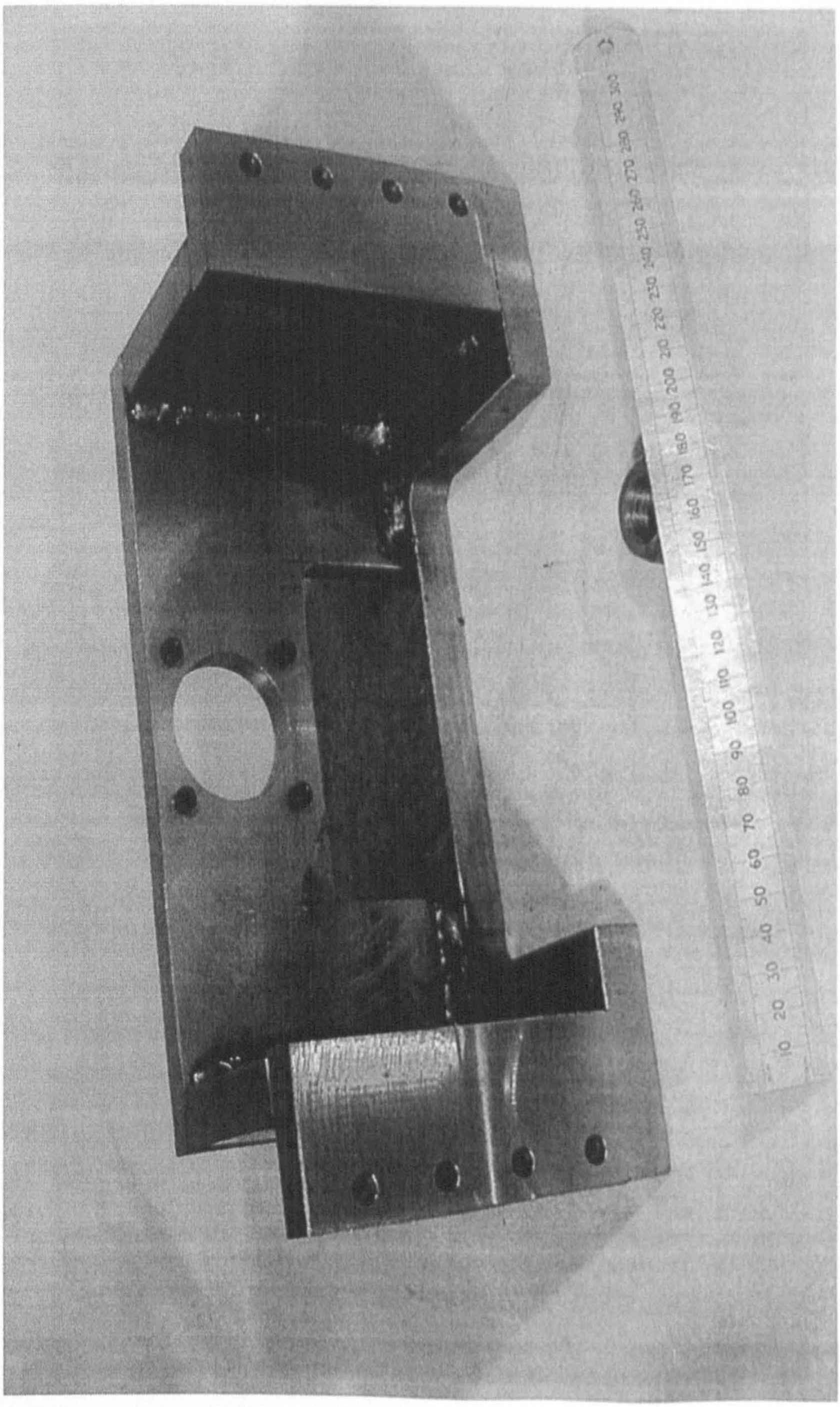

Fig 4.2.8 The motor frame

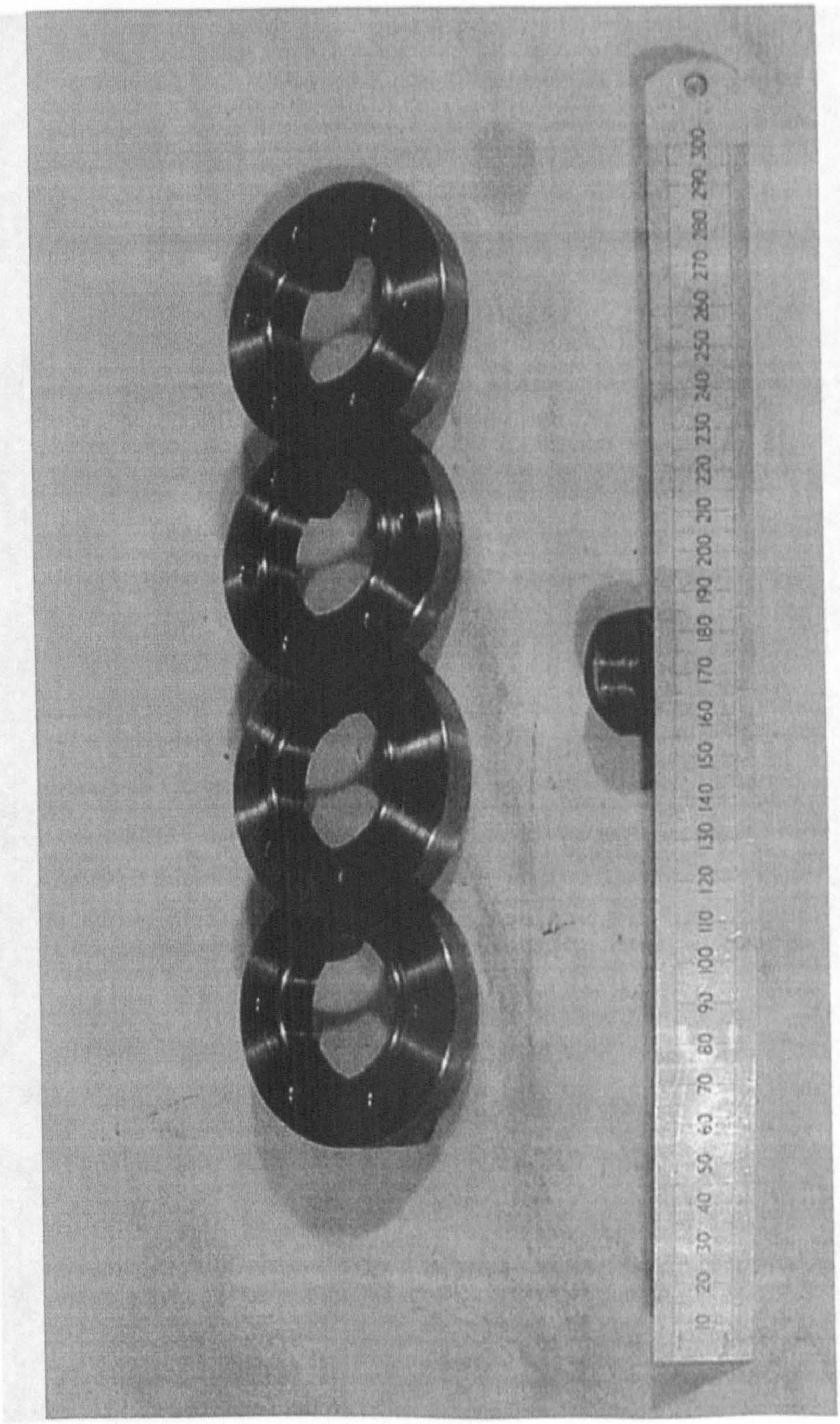

Fig 4.2.9 The bearing lids

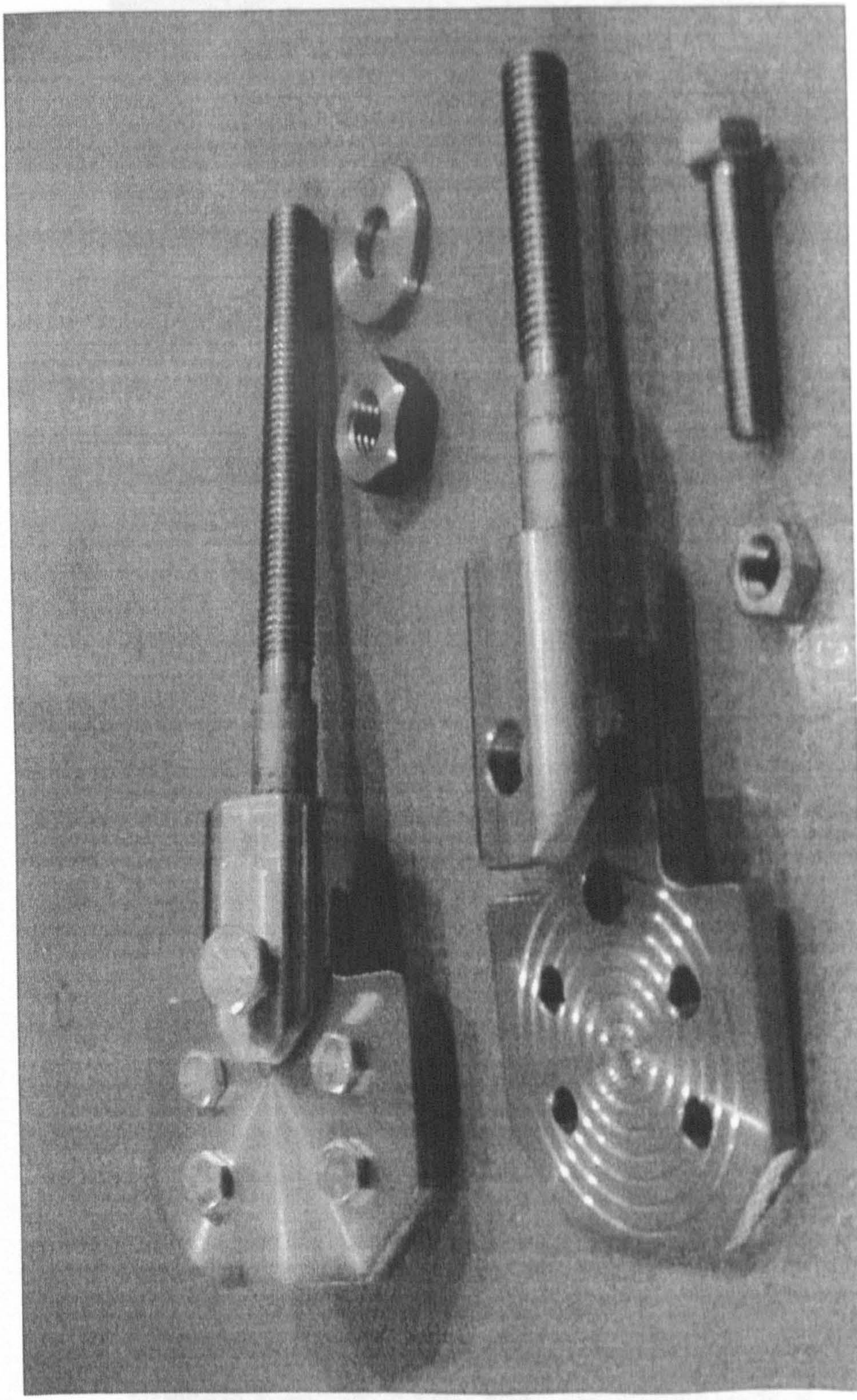

Fig 4.2.10 The clamp frames and plates

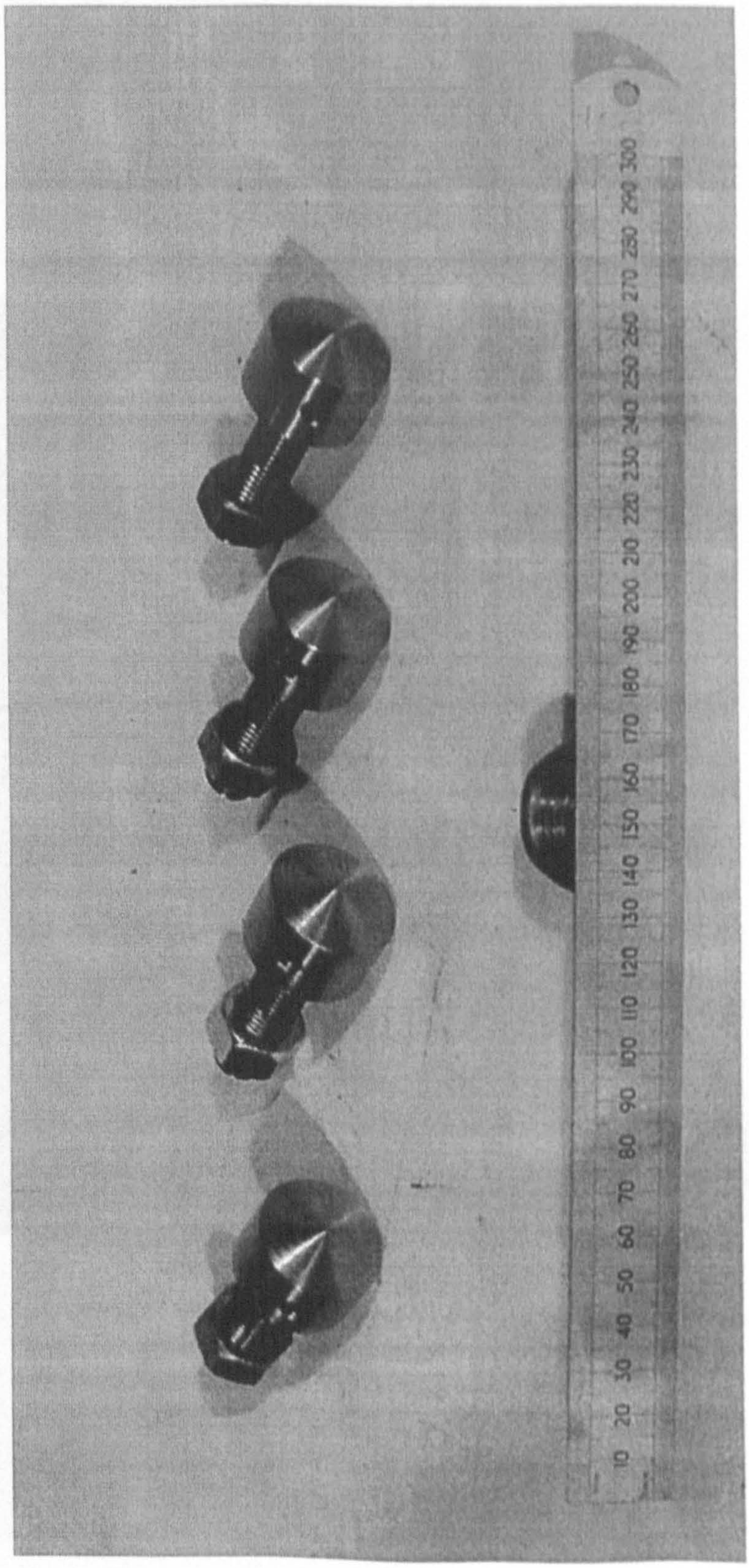

Fig 4.2.11 The screw feet

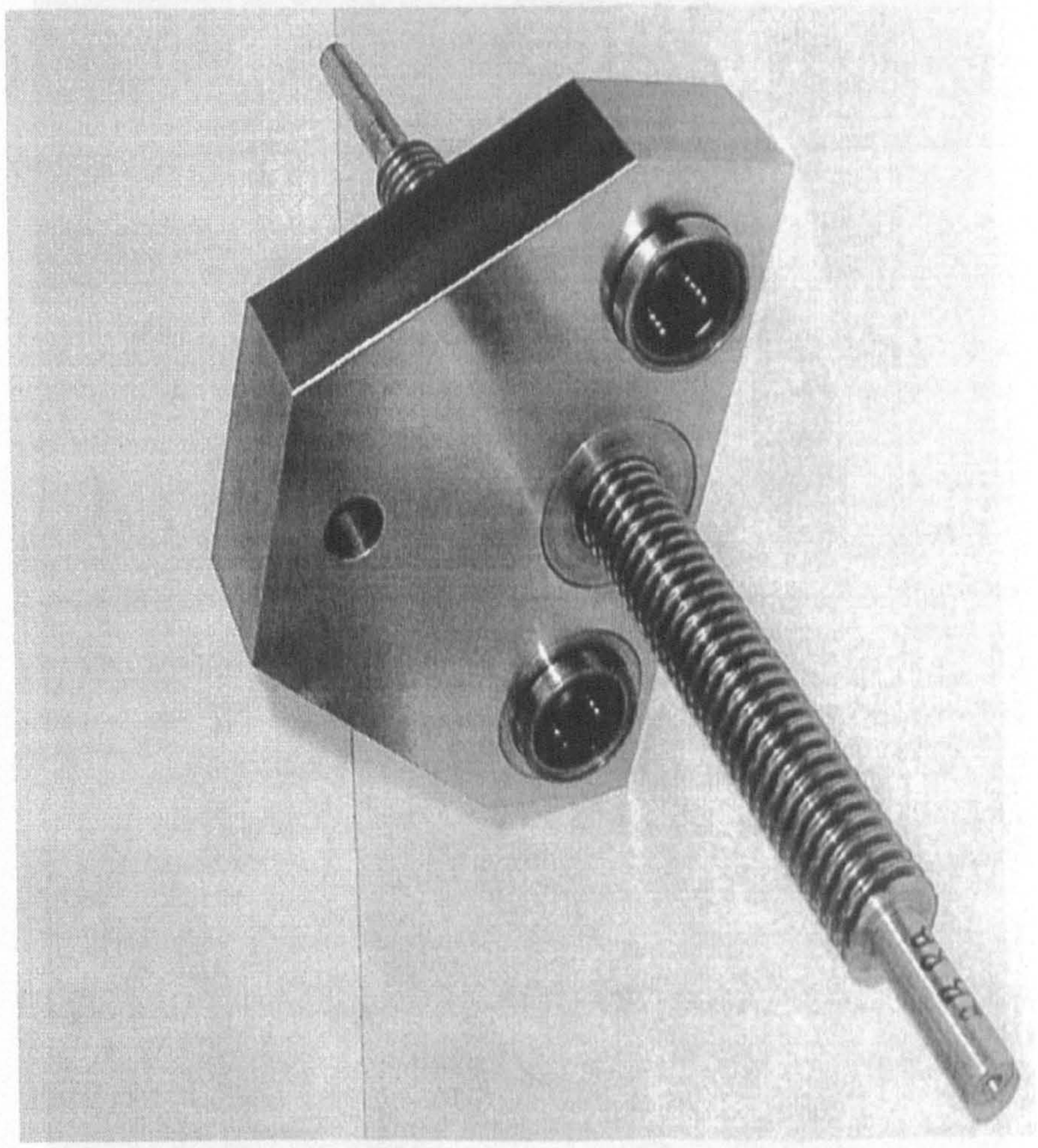

Fig 4.2.12 The assembled carriage

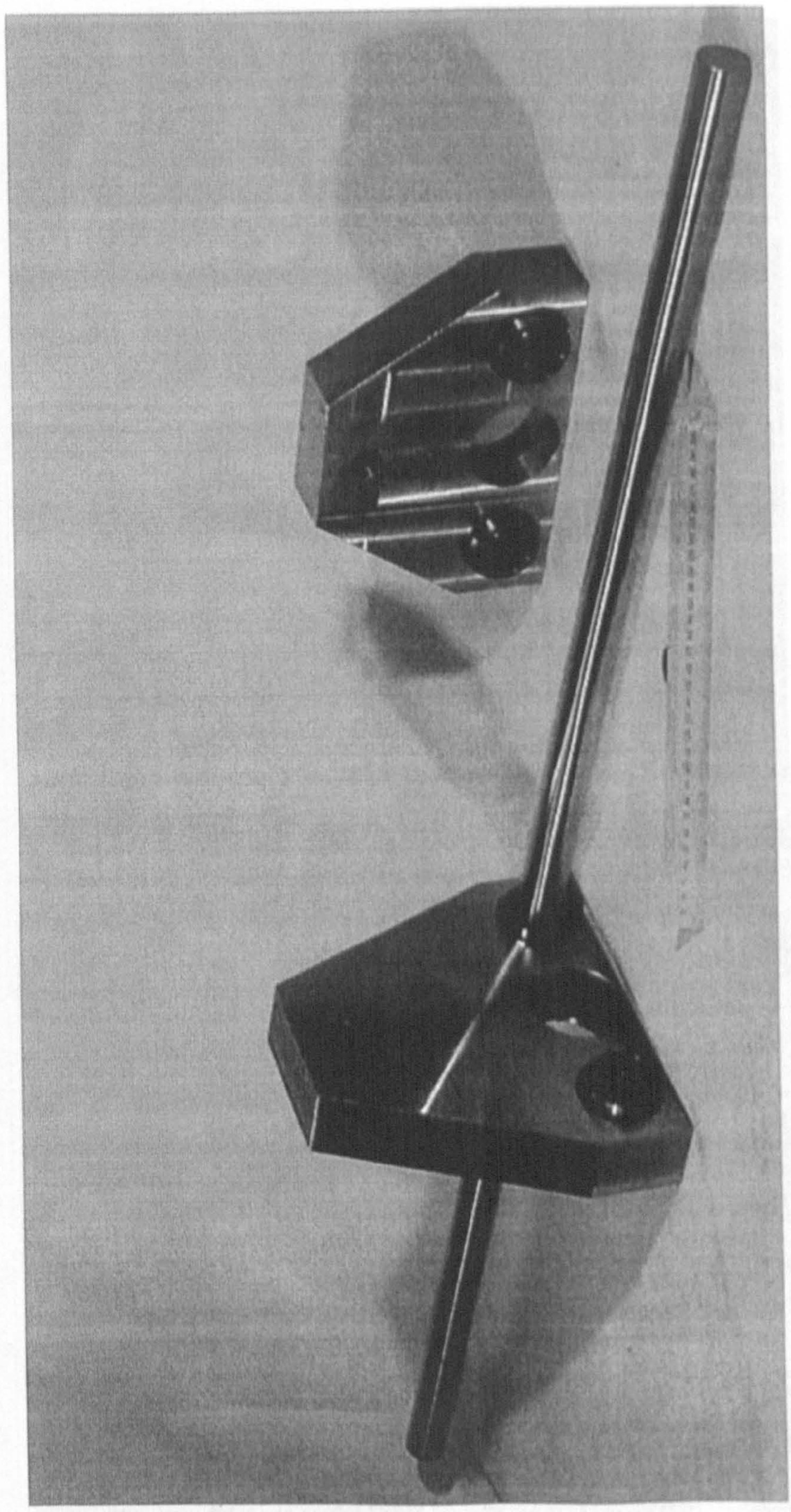

Fig 4.2.13 The carriage with linear shaft

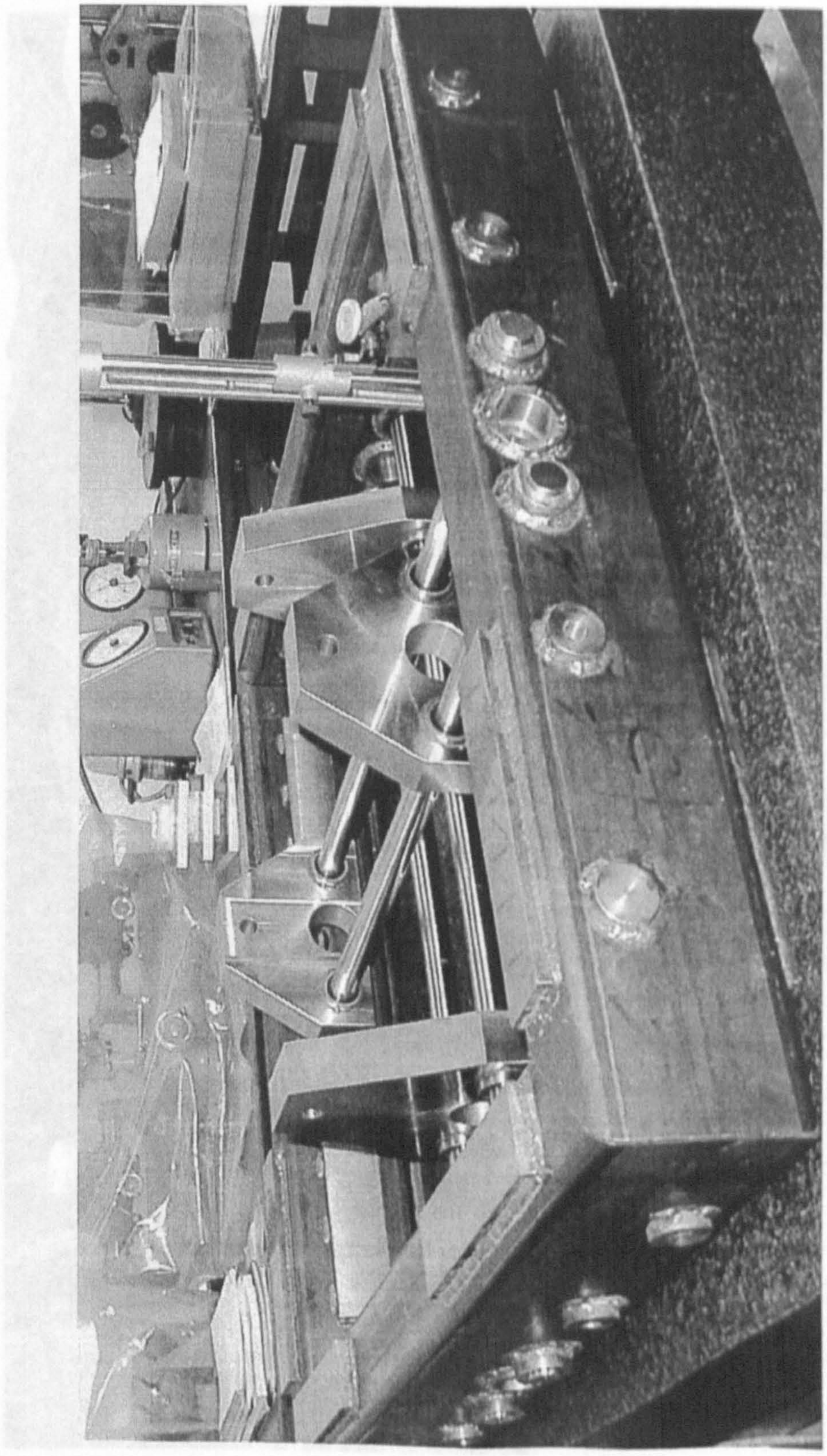

Fig 4.2.14 The four frames, carriages and linear shafts were in their initial assembly
(initial smoothness of carriage movement check)

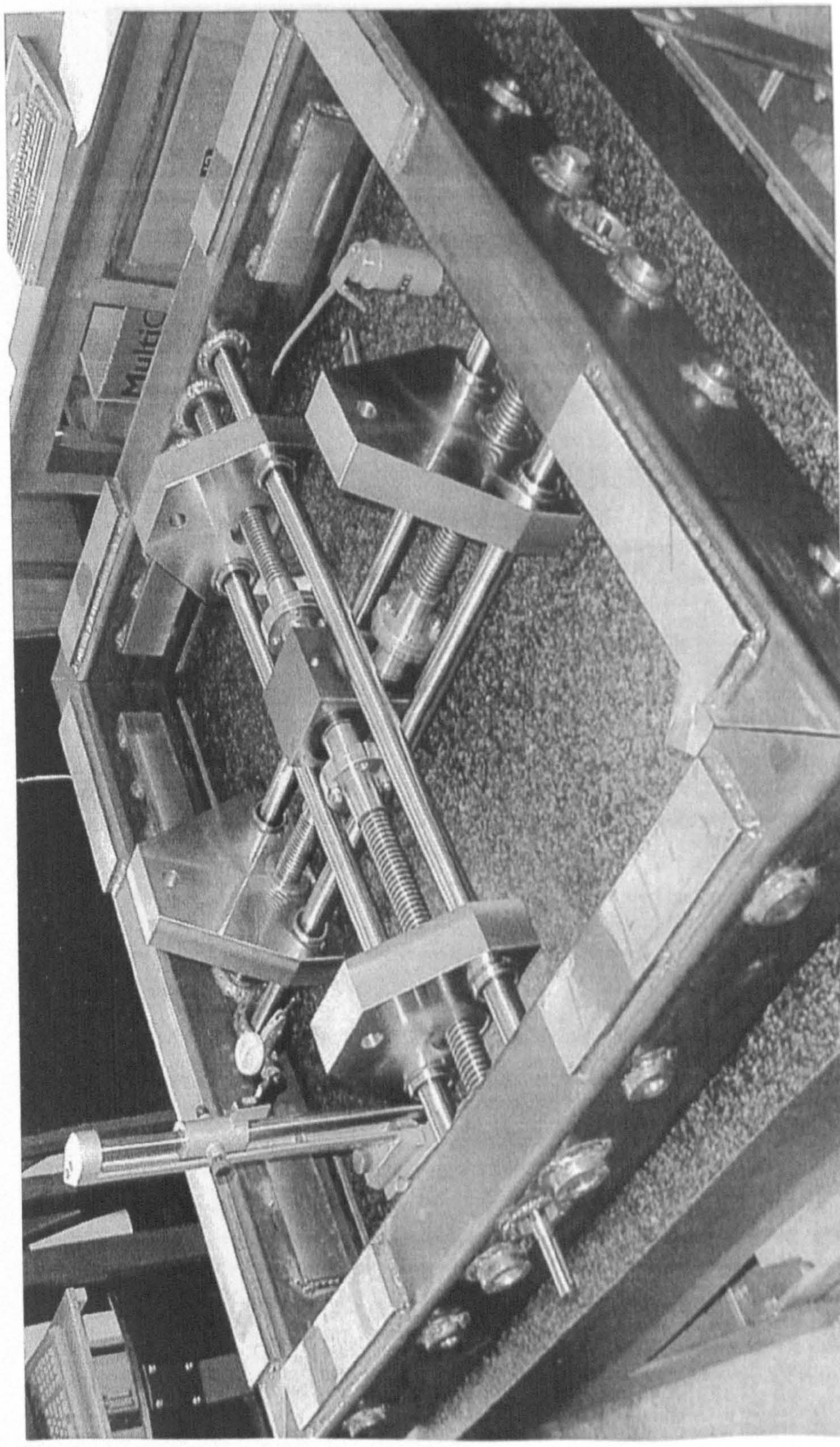

Fig 4.2.15 The full initial assembly

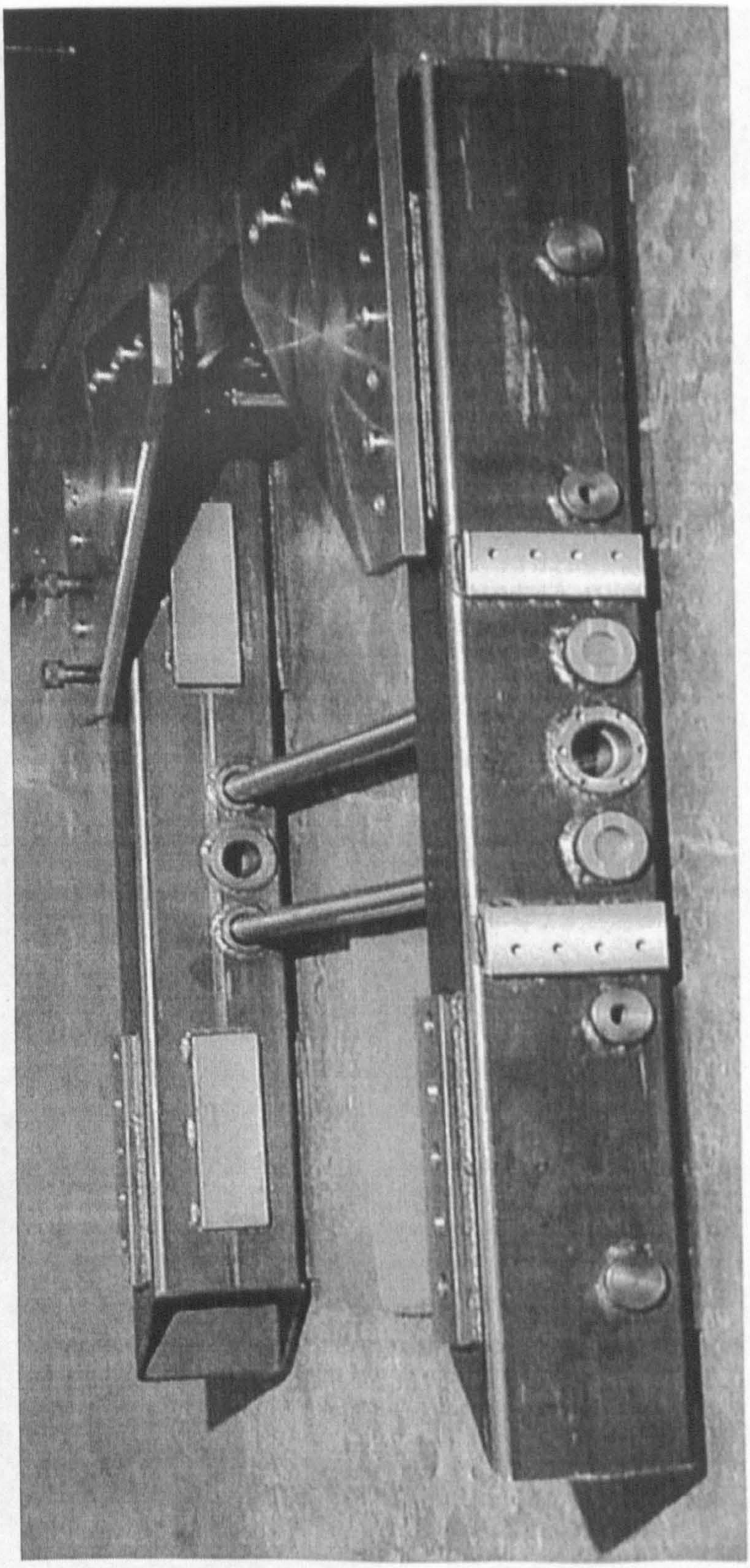

Fig 4.2.16 The frames and bottom corner plates in their working place Lab (M3) for the final assembling

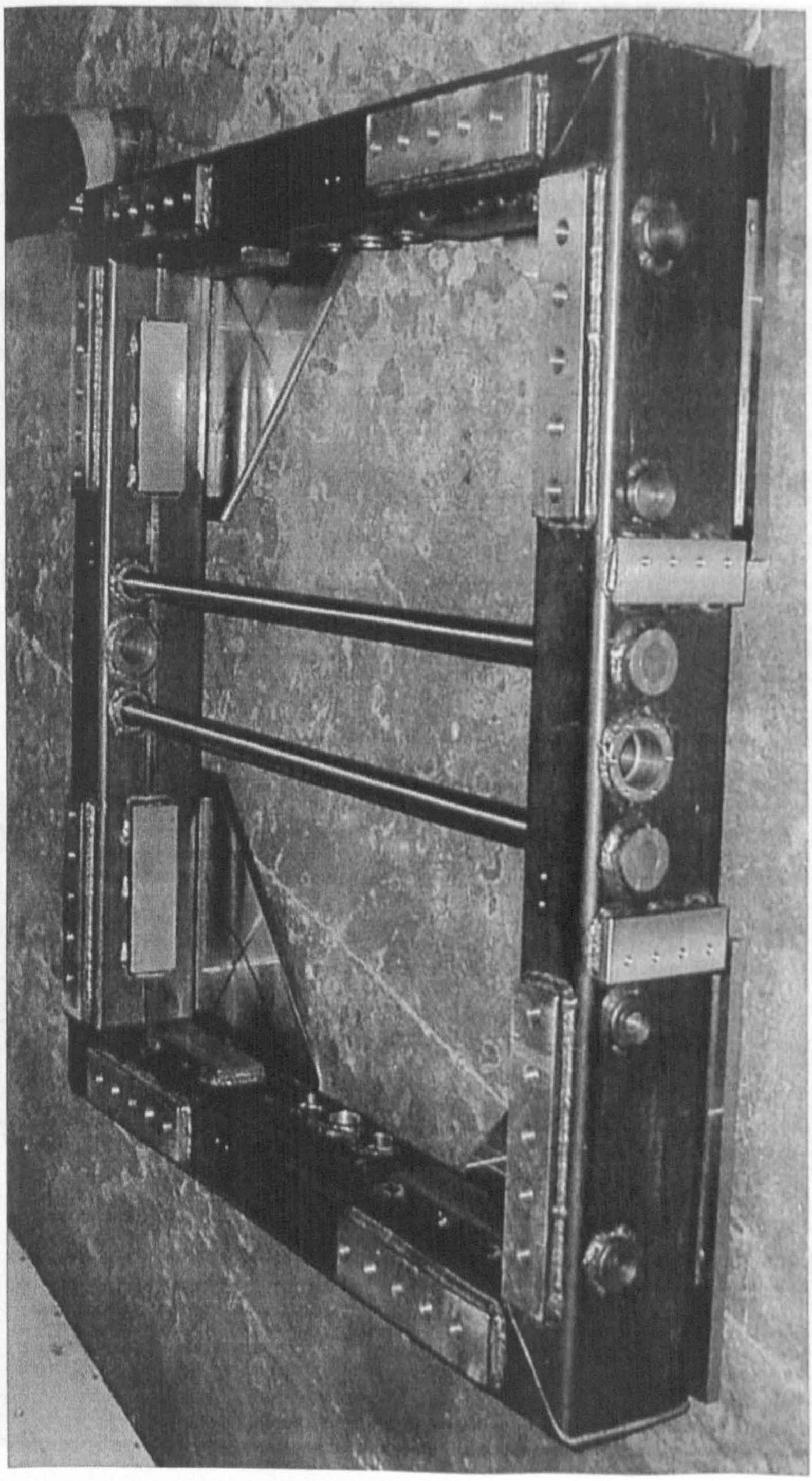

Fig 4.2.17 The frames and bottom corner plates were assembled

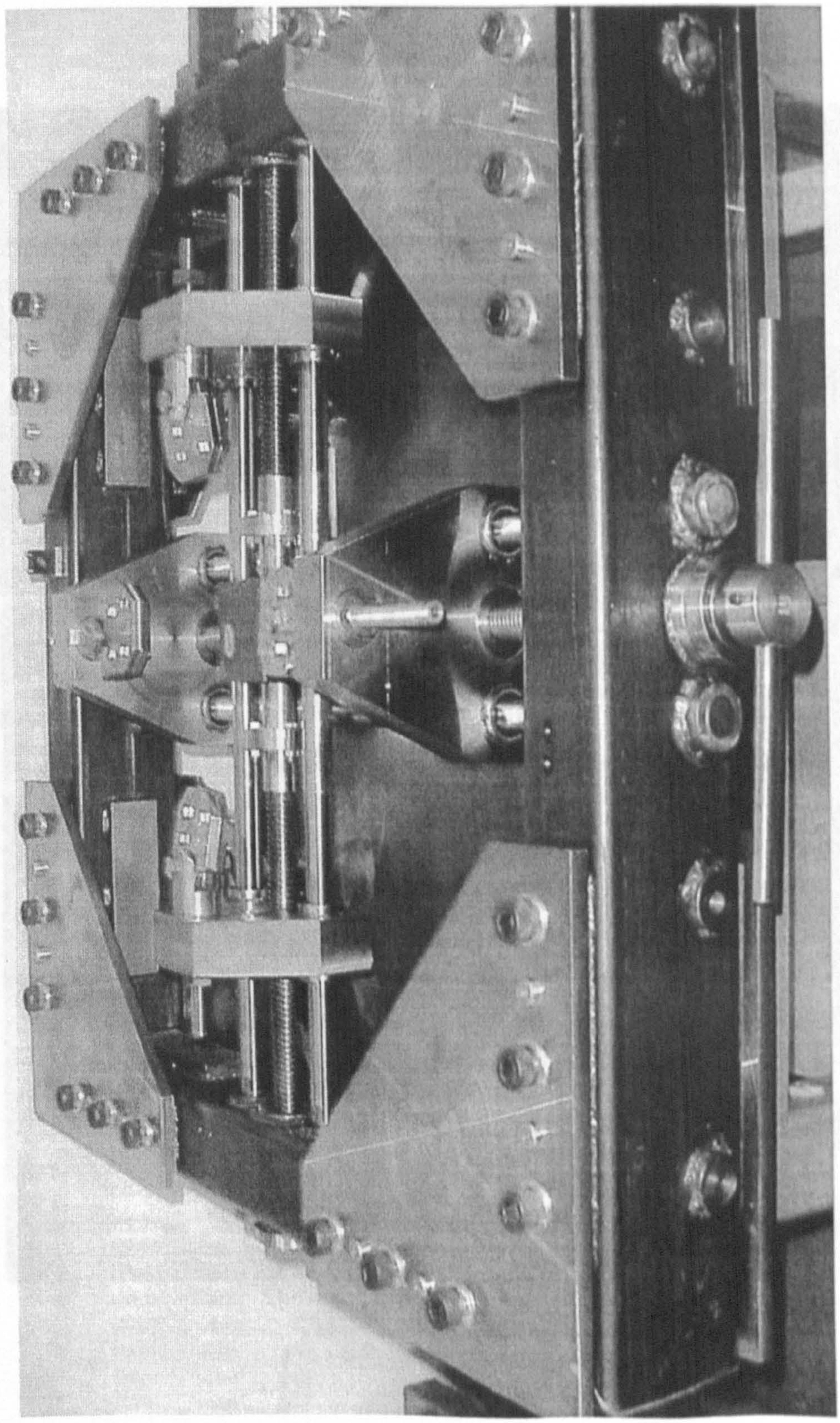

Fig 4.2.18 The most of the components were assembled in its (the machine's) working table

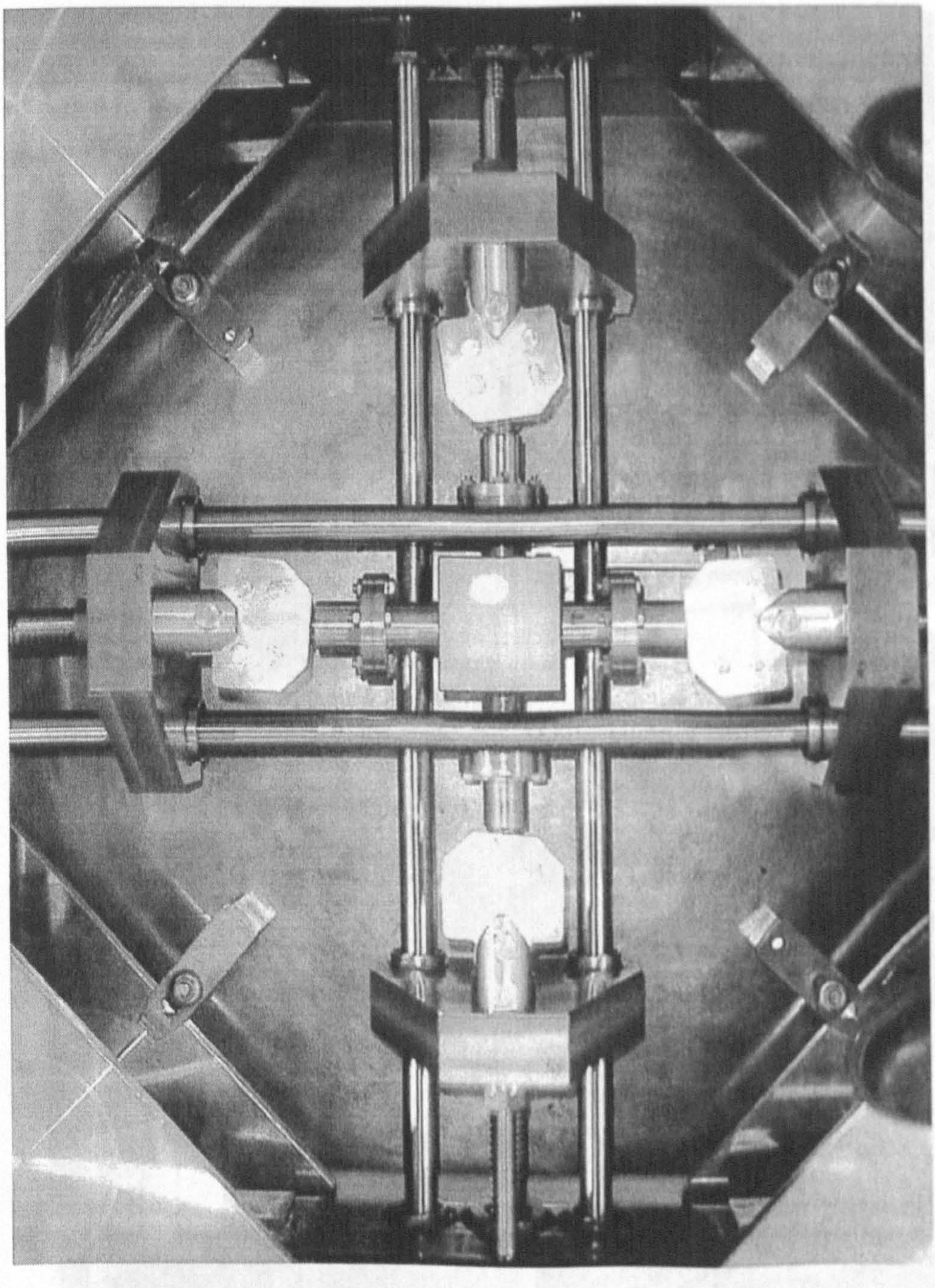

Fig 4.2.19 The four (bottom) corner plate clamps assembled

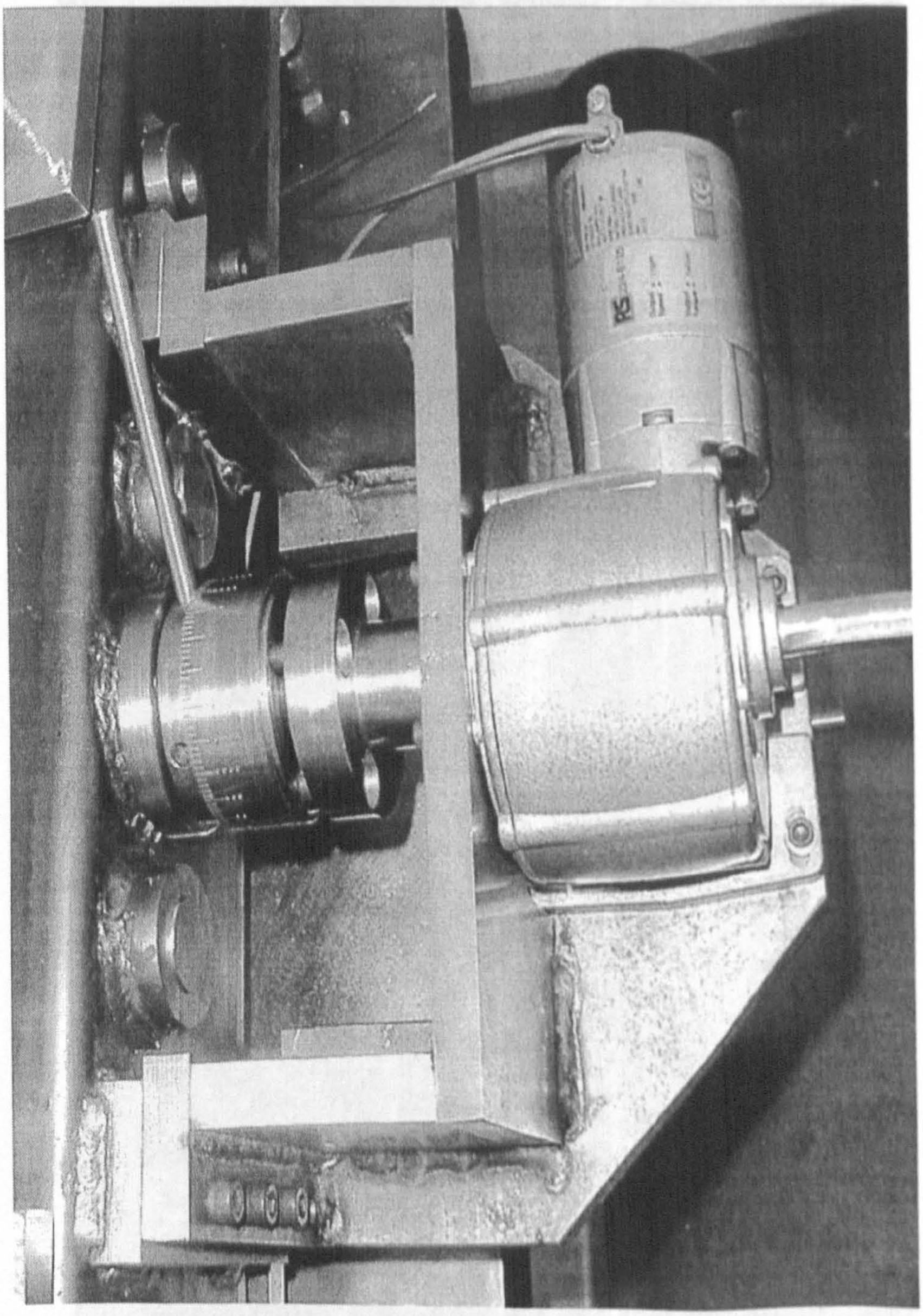

Fig 4.2.20 The motor and sliding clutch were assembled

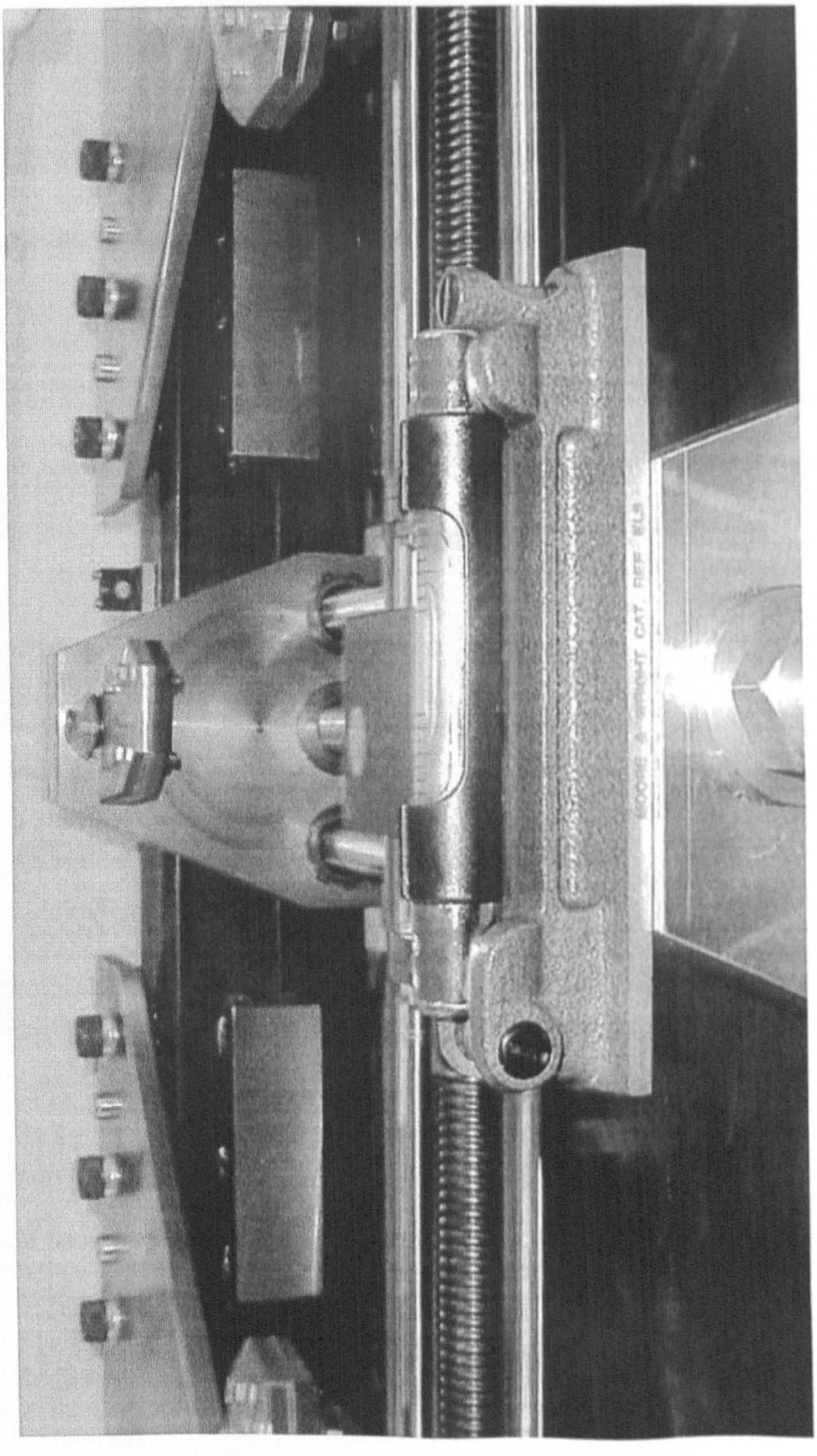

Fig 4.2.21 The final level check and adjustment

Figures of Chapter 5

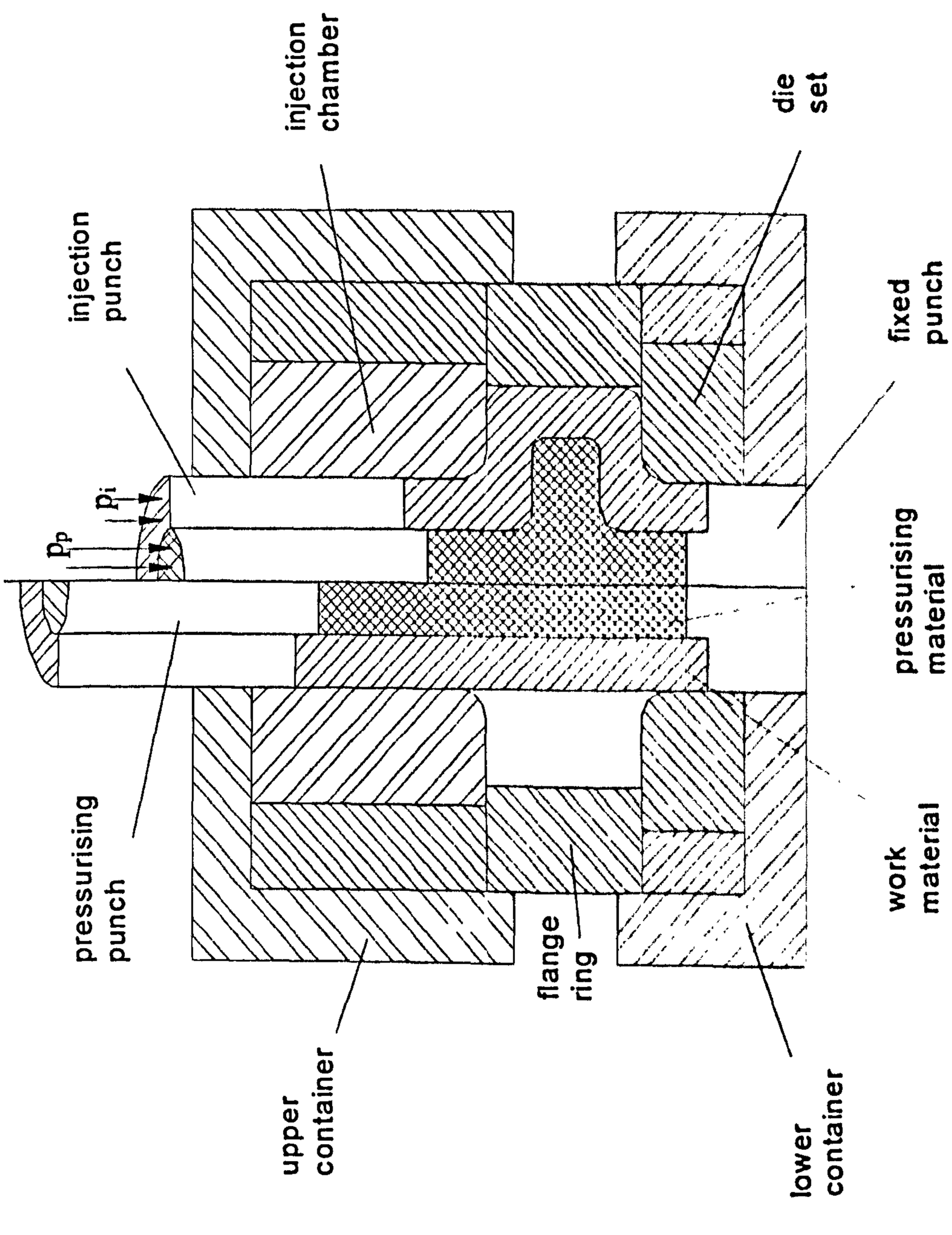

Fig. 5.1 The process configuration of PAIF

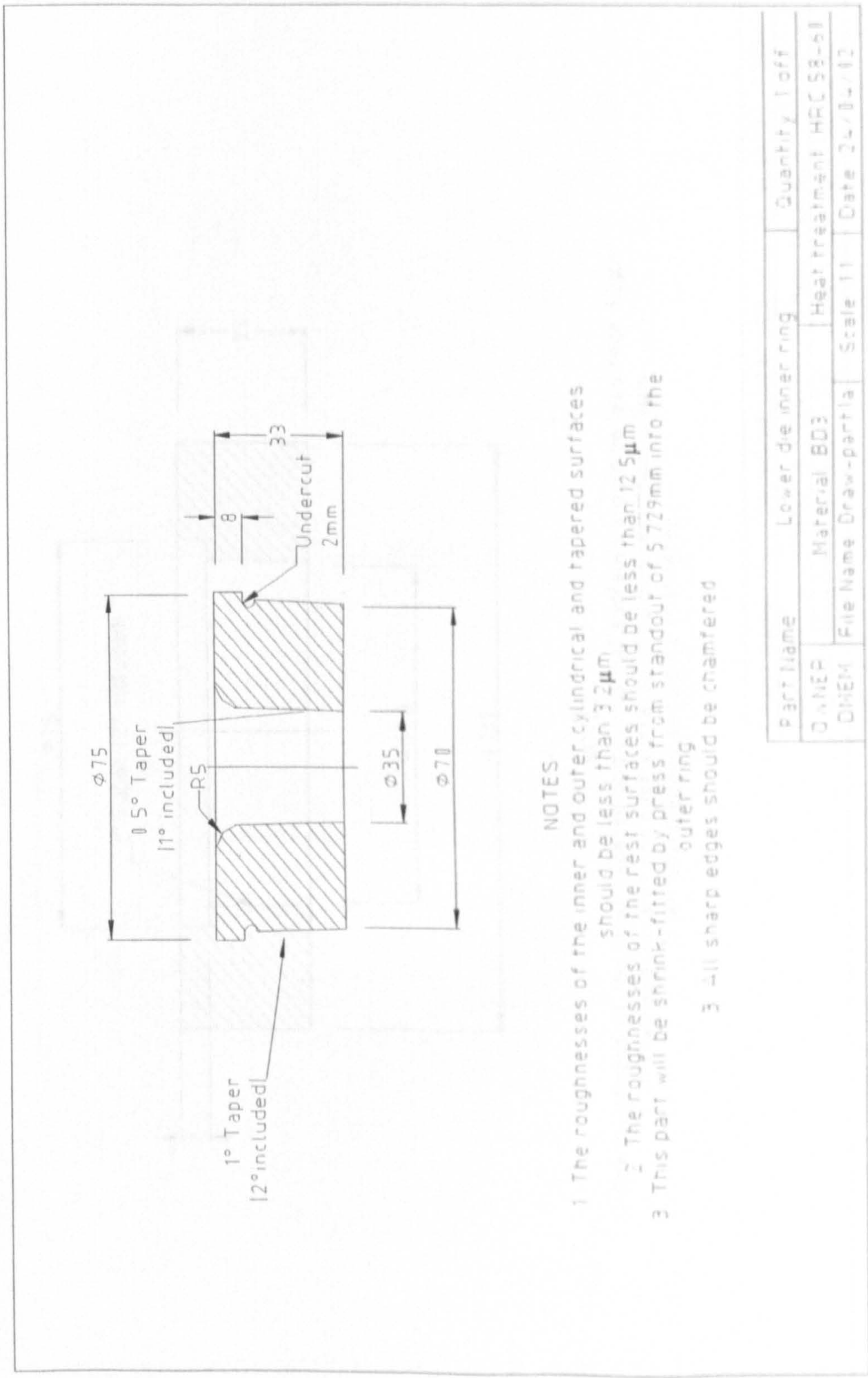

Fig. 5.2 The lower die inner ring

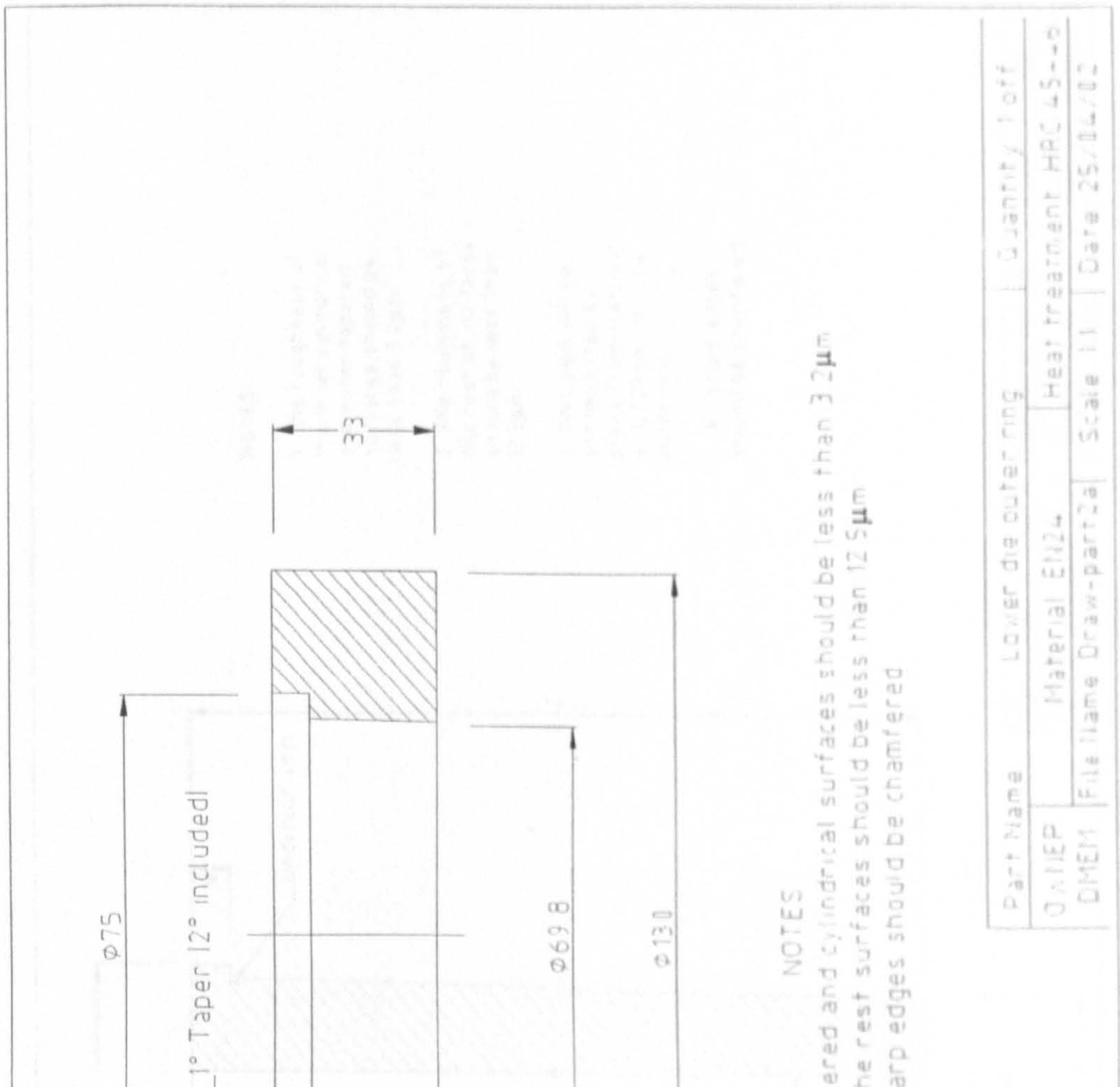

Fig. 5.3 The lower die for the outer ring

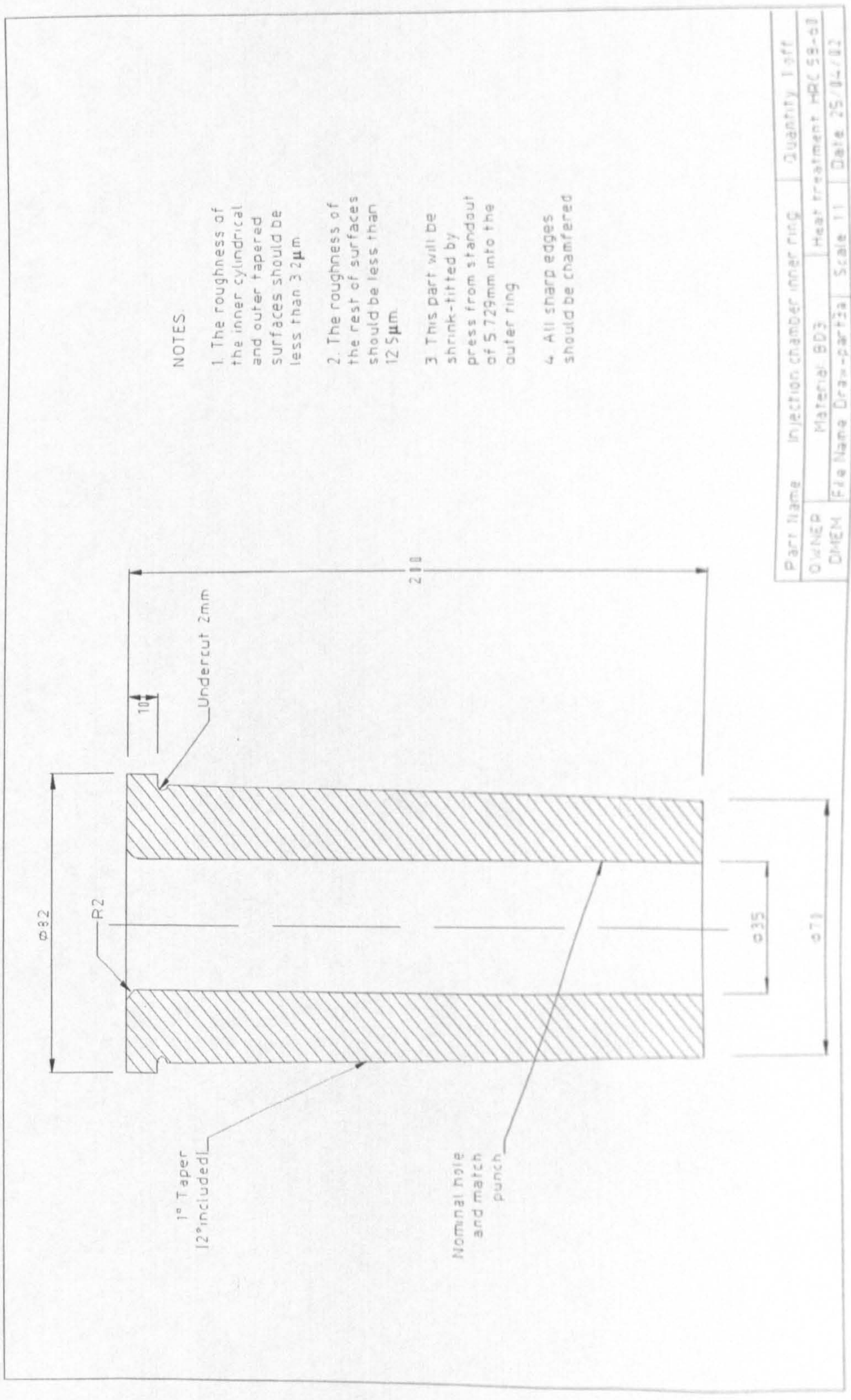

Fig. 5.4 The injection chamber inner ring

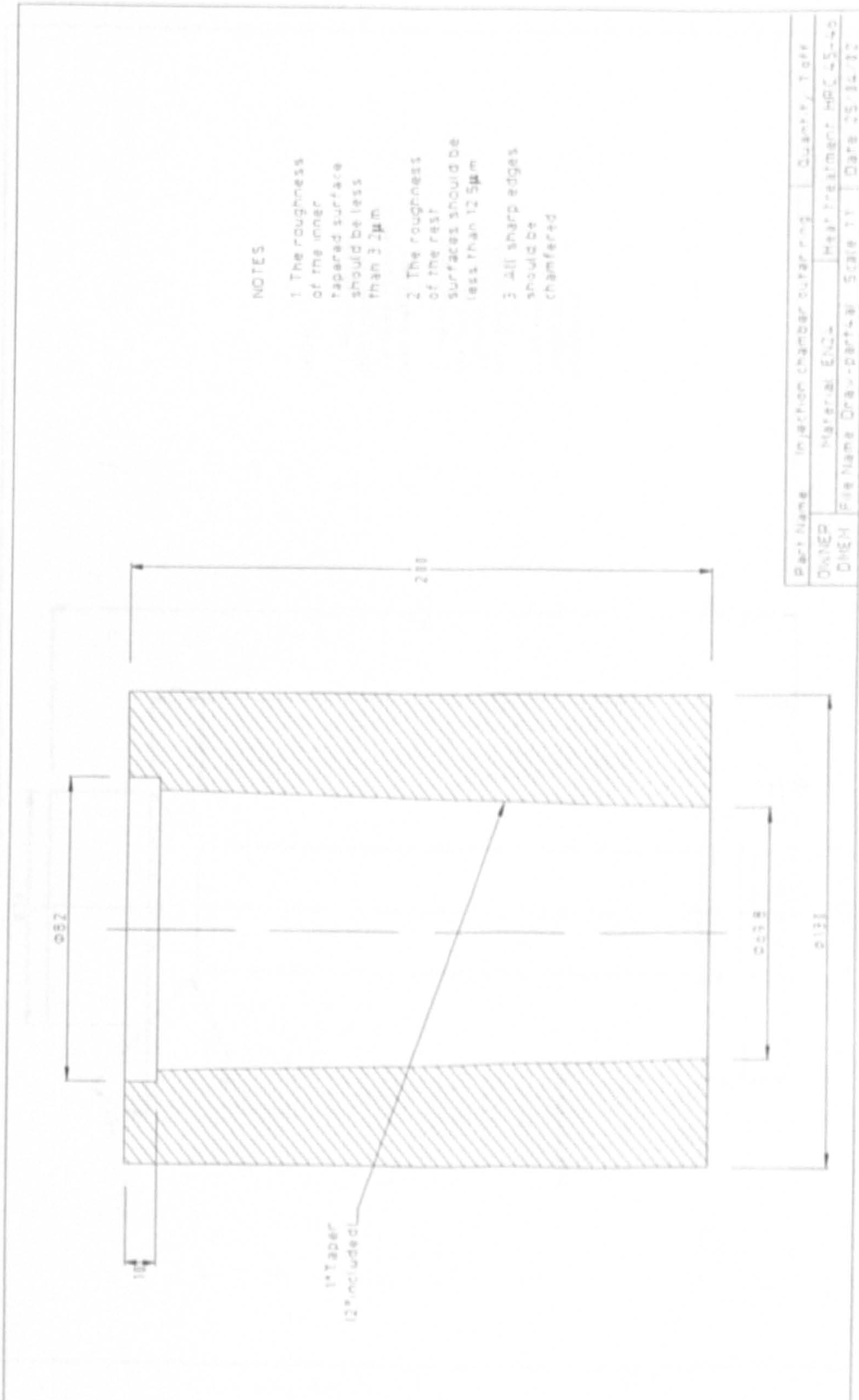

Fig. 5.5 The injection chamber outer ring

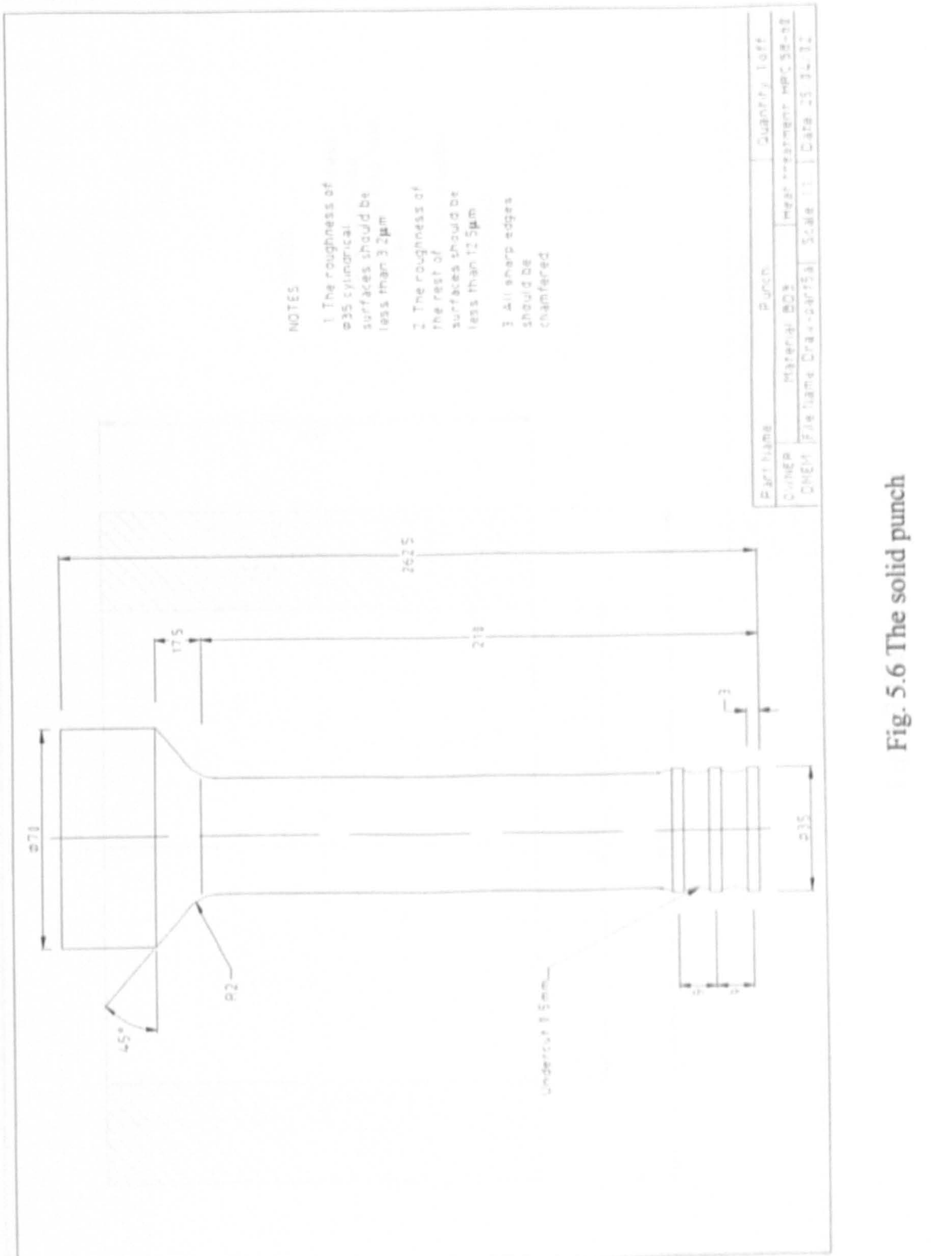

Fig. 5.6 The solid punch

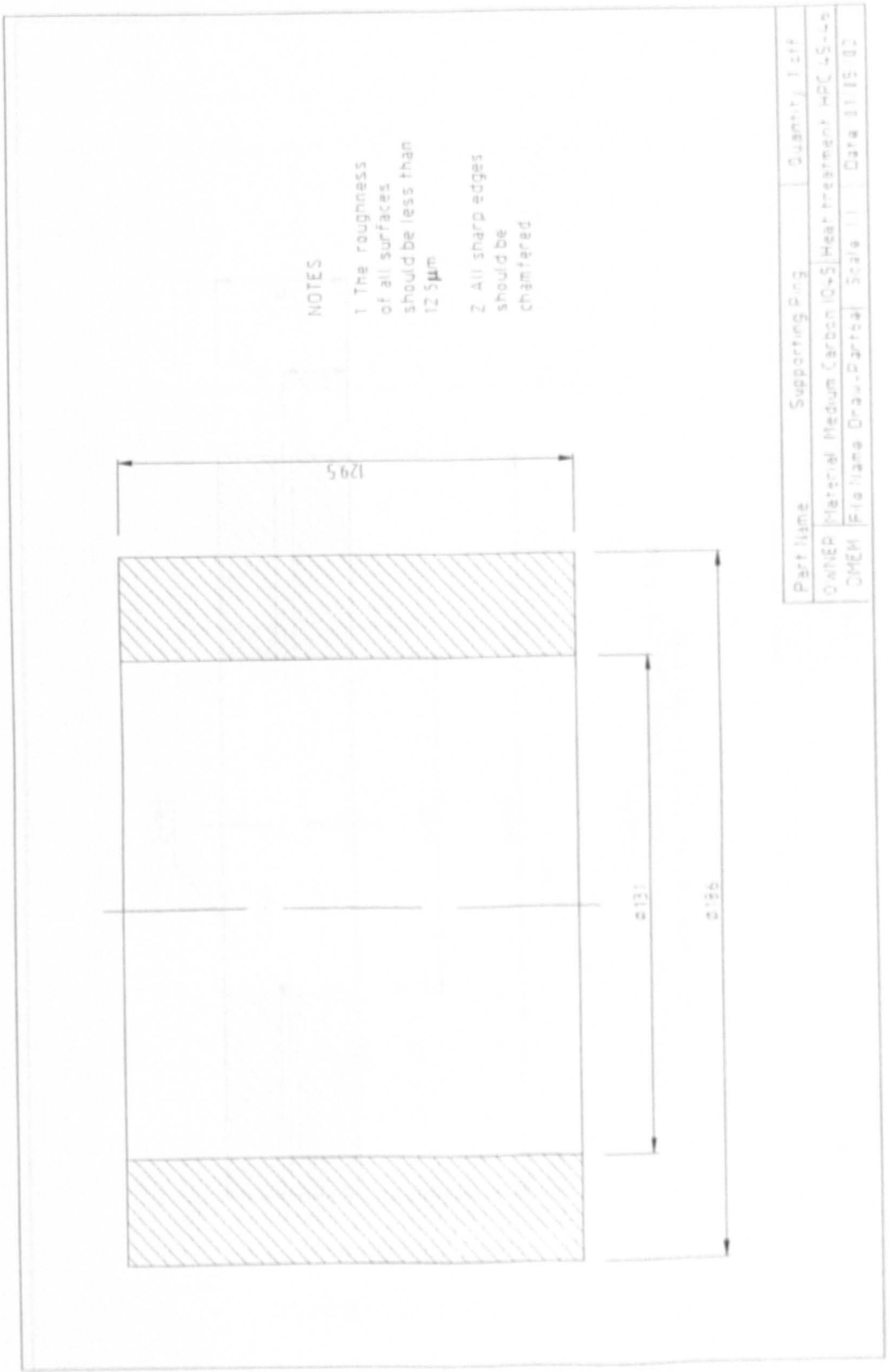

Fig. 5.7 The supporting ring

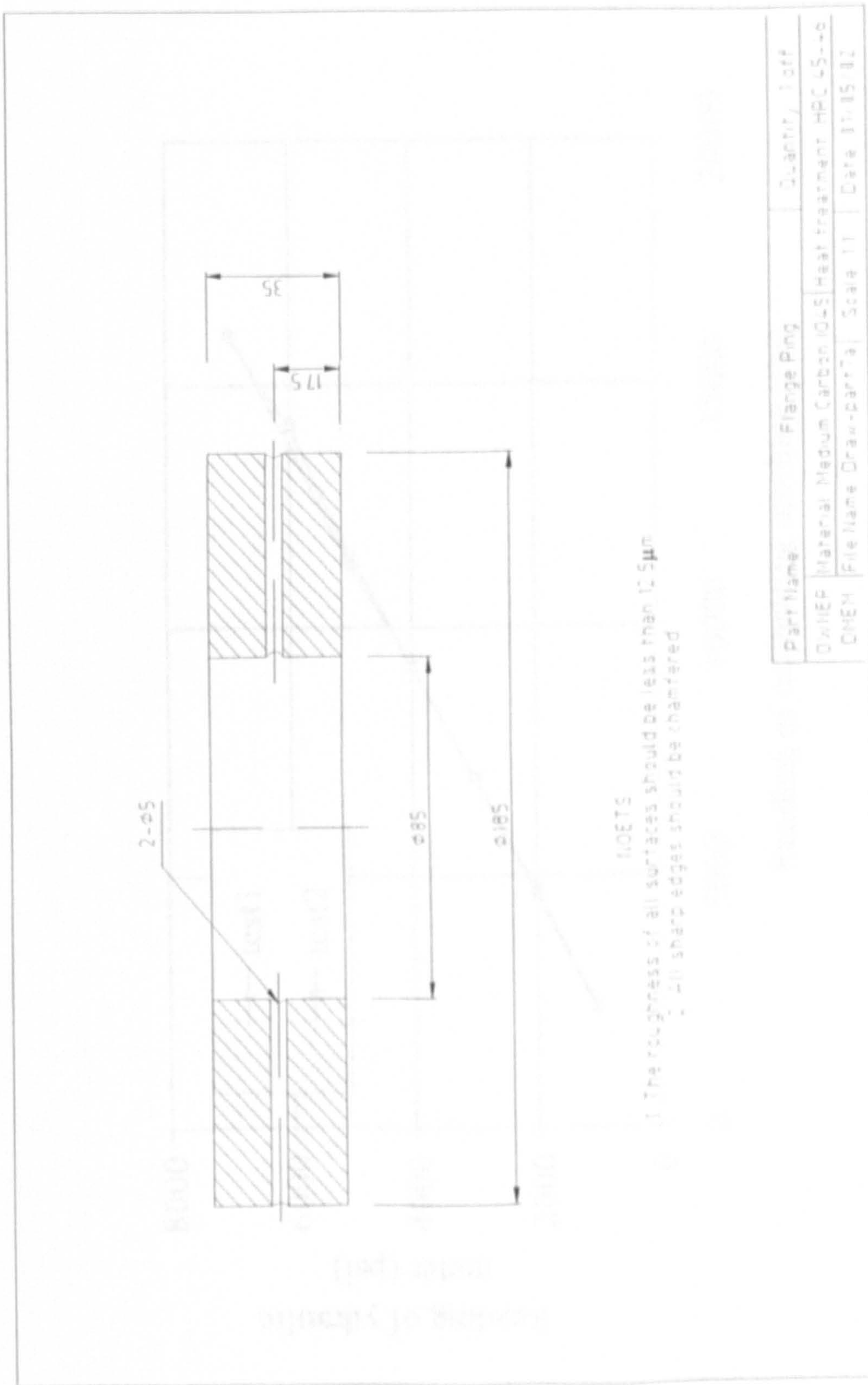

Fig. 5.8 The flange ring die

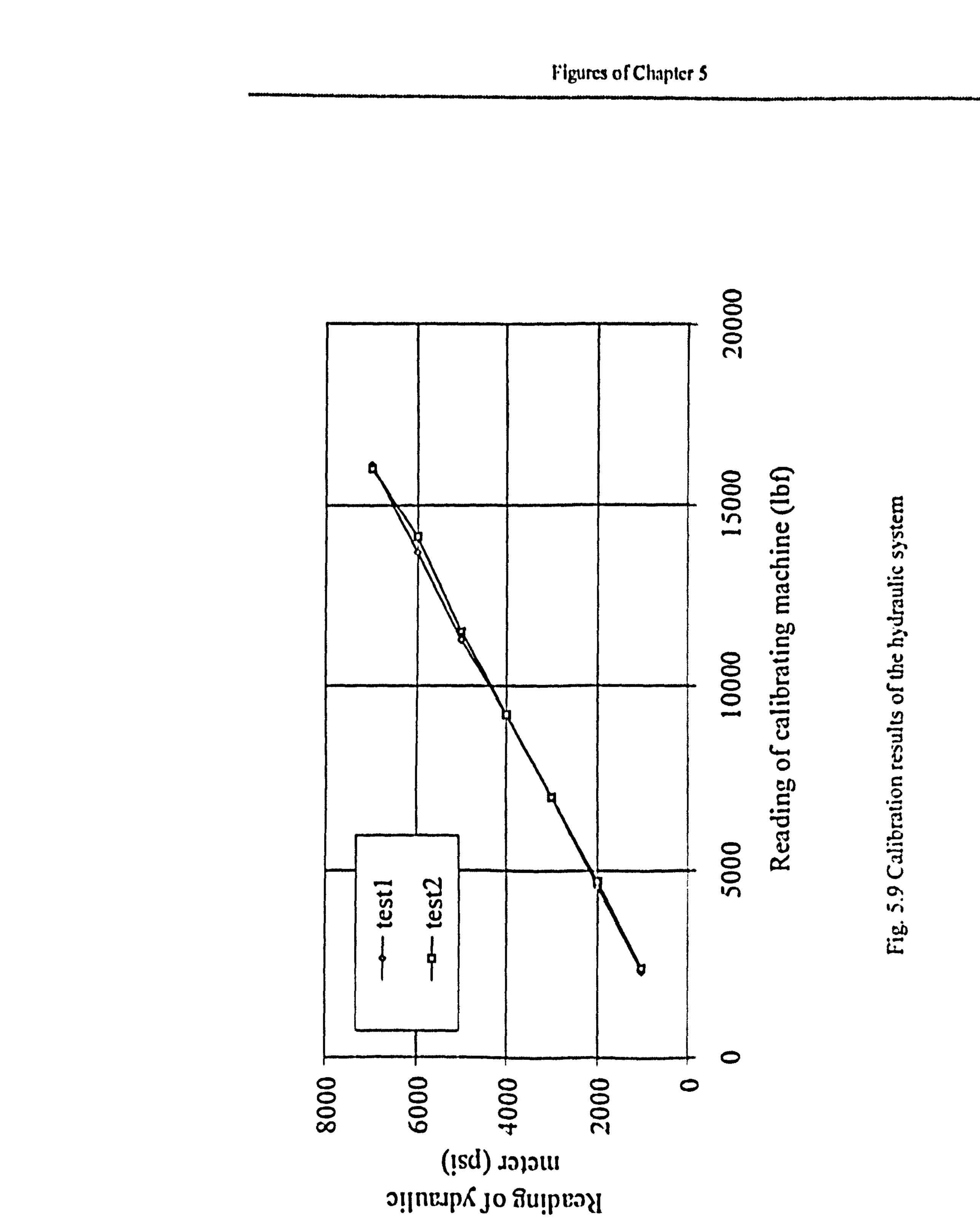

Fig. 5.9 Calibration results of the hydraulic system

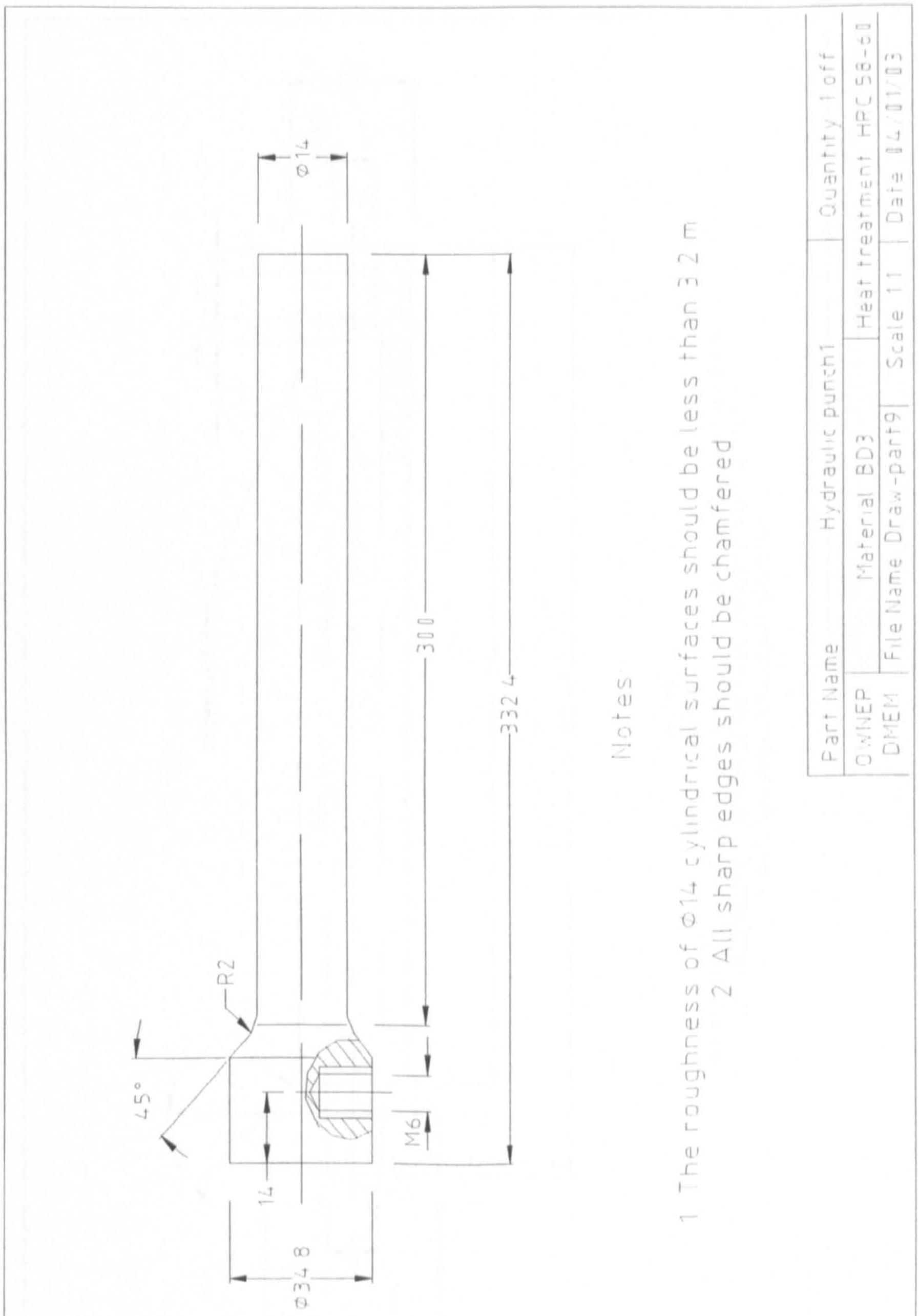

Fig. 5.10 The hydraulic inner punch

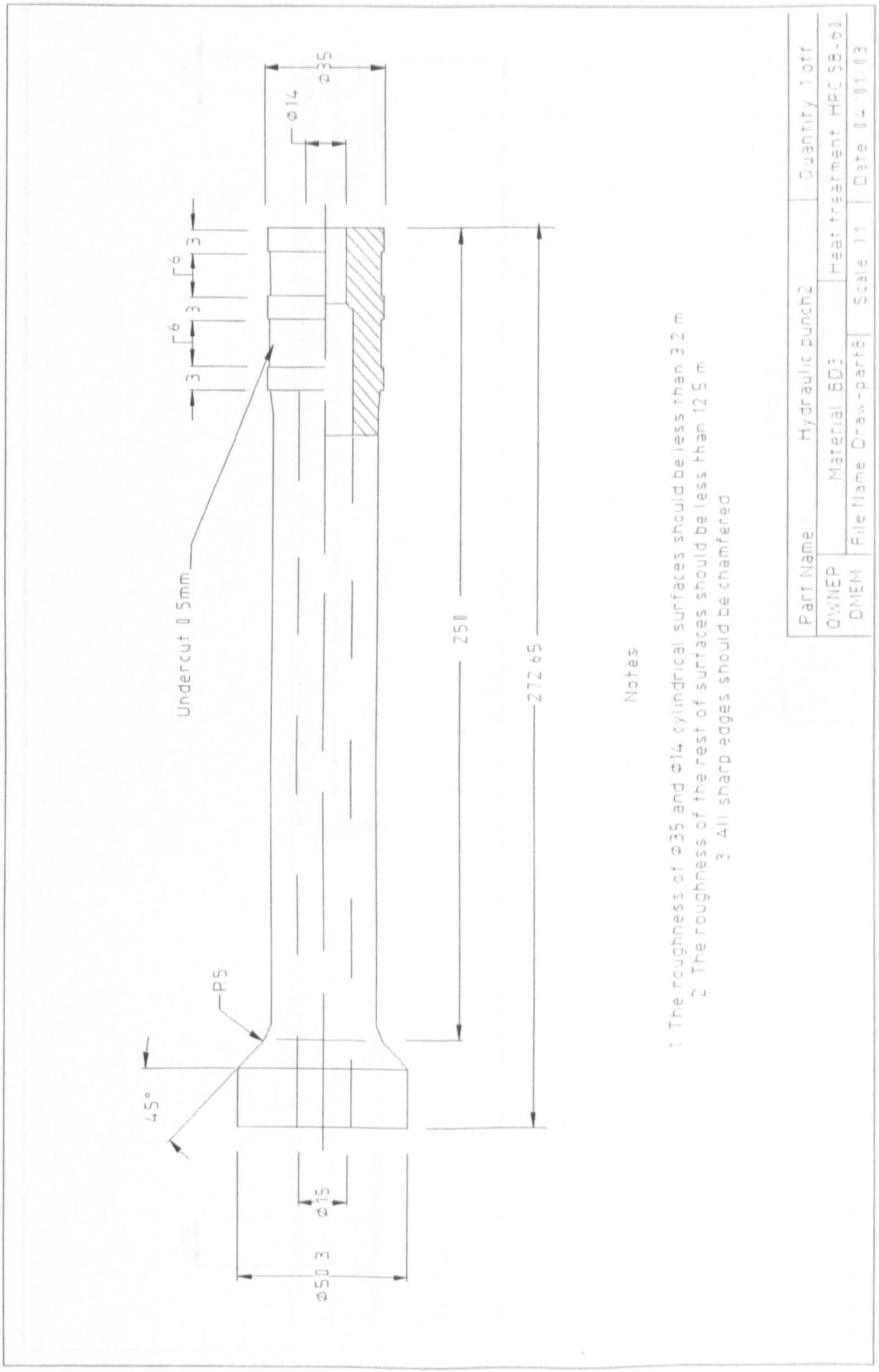

Fig. 5.11 The hydraulic outer punch

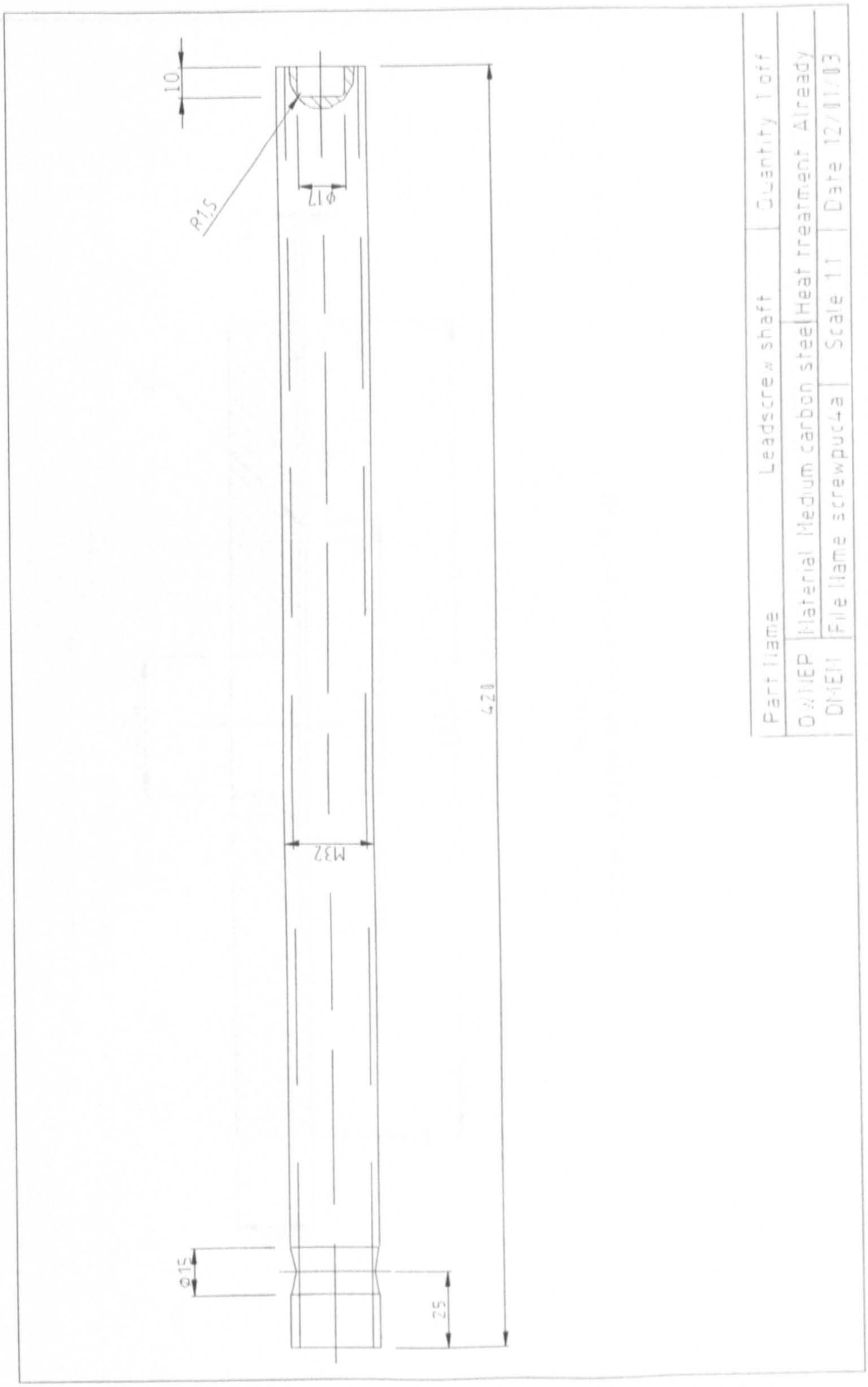

Fig. 5.12 The lead-screw shaft

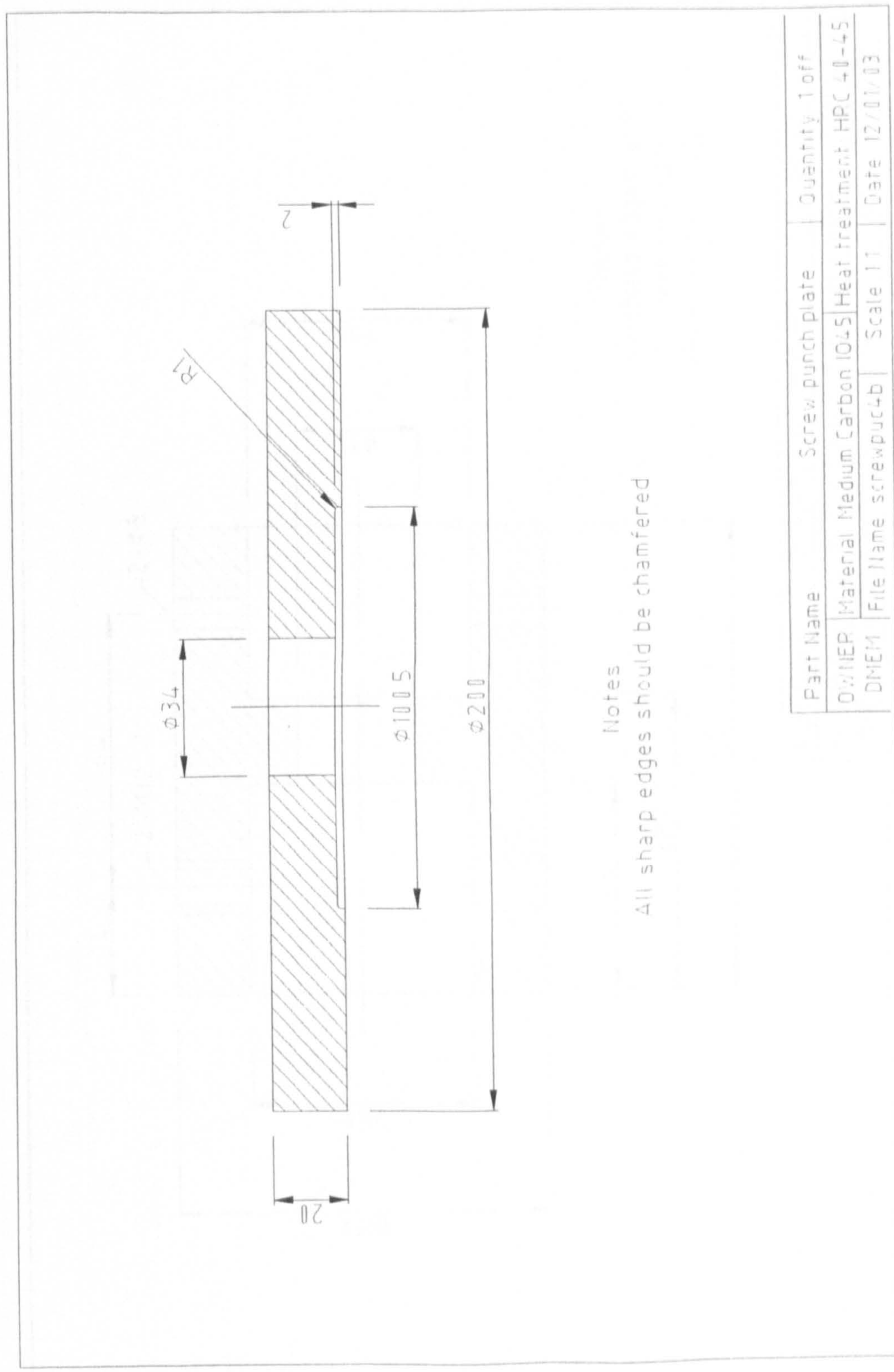

Fig. 5.13 The screw punch plate

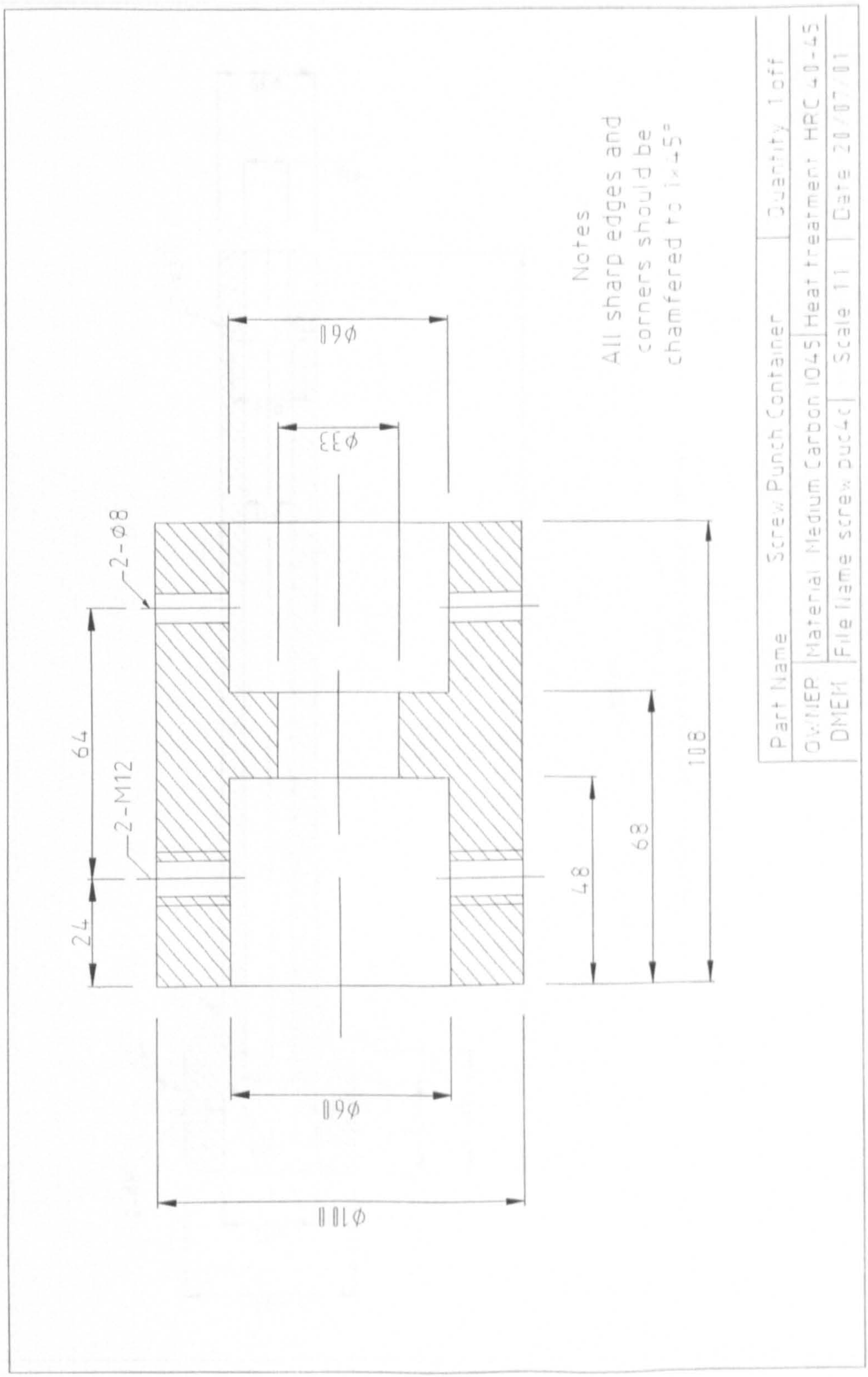

Fig. 5.14 The screw punch container

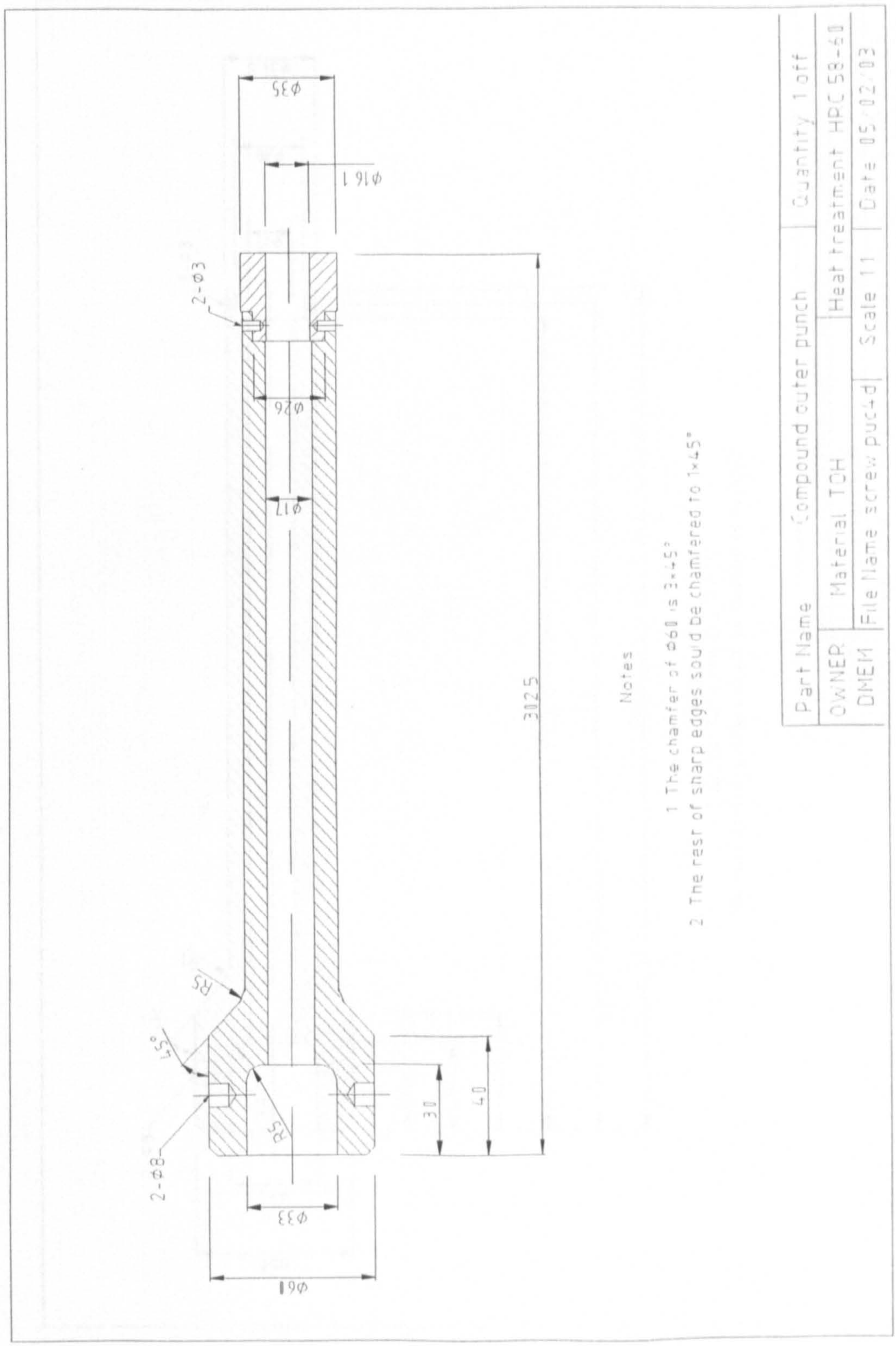

Fig. 5.15 The compound outer punch

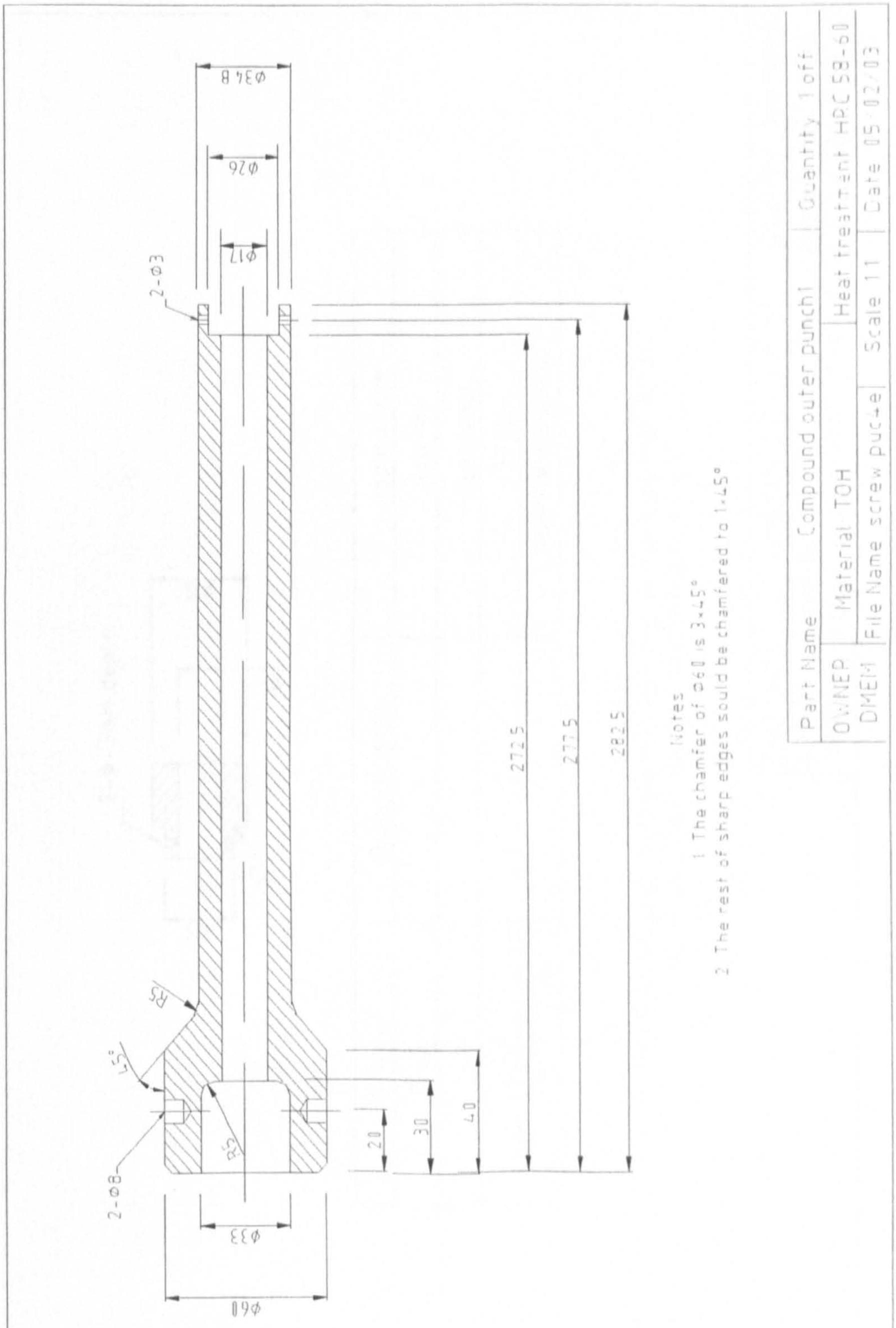

Fig. 5.16 The compound outer punch part 1

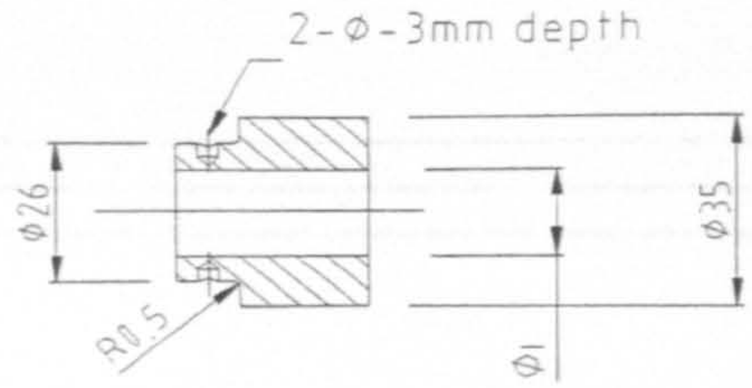

ø1 (mm)	Quantity offs	Applications
15.65	1	Nylon66
13.8	1	Red Qsash
14.72	1	PTFE
16.1	1	HDPE & Nitrile642

Notes
1. The roughness of surface ø35 and ø1 should be less than 3.2 m
2. All sharp edges sould be chamfered to 0.5×45°

Part Name	Compound outer punch2		Quantity See table
OWNER DMEM	Material TOH		Heat treatment HPC 58-60
	File Name screw puc4f	Scale 1:1	Date 05/02/03

Fig. 5.17 The compound outer punch part 2

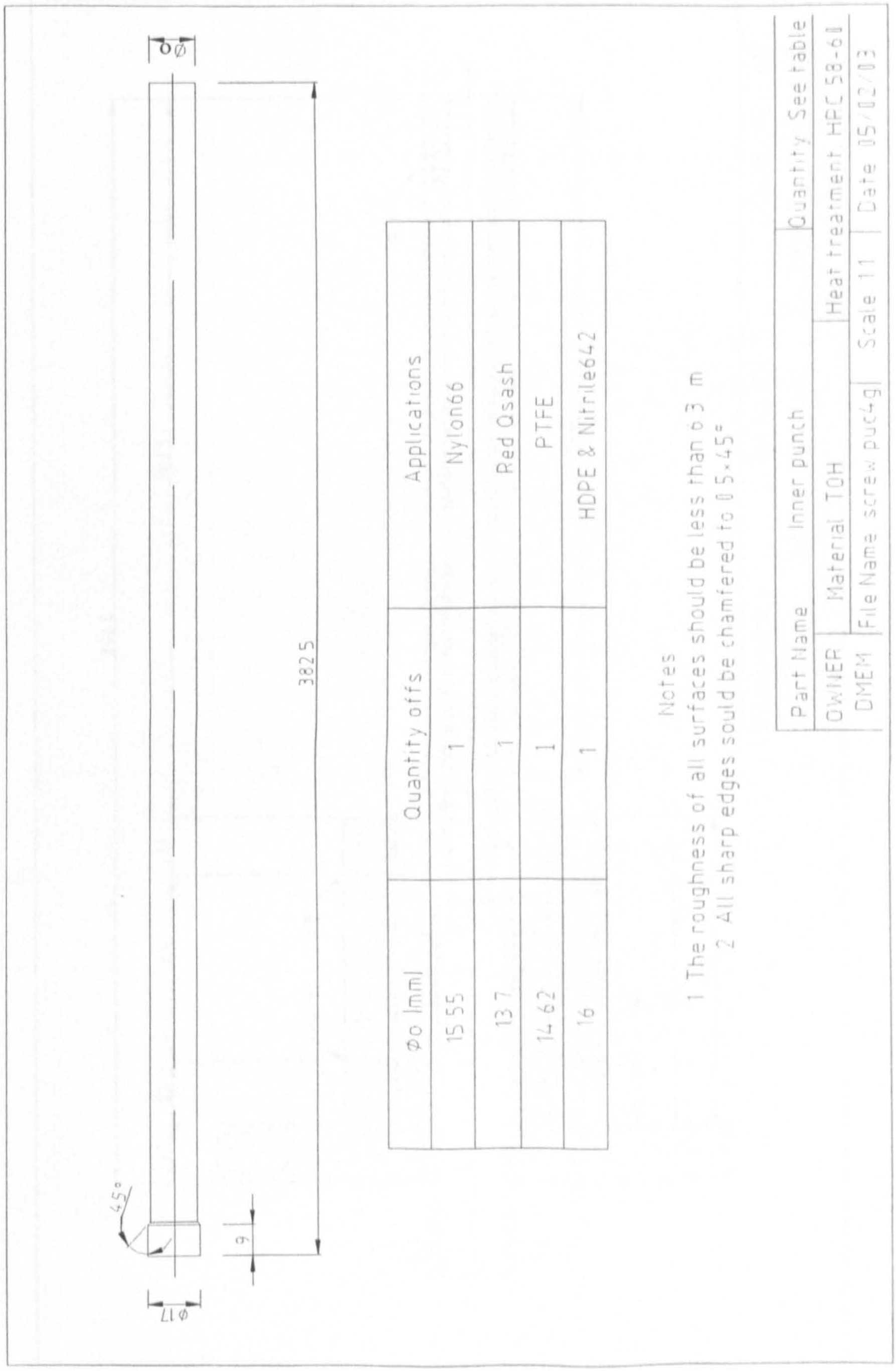

Fig. 5.18 The inner punch

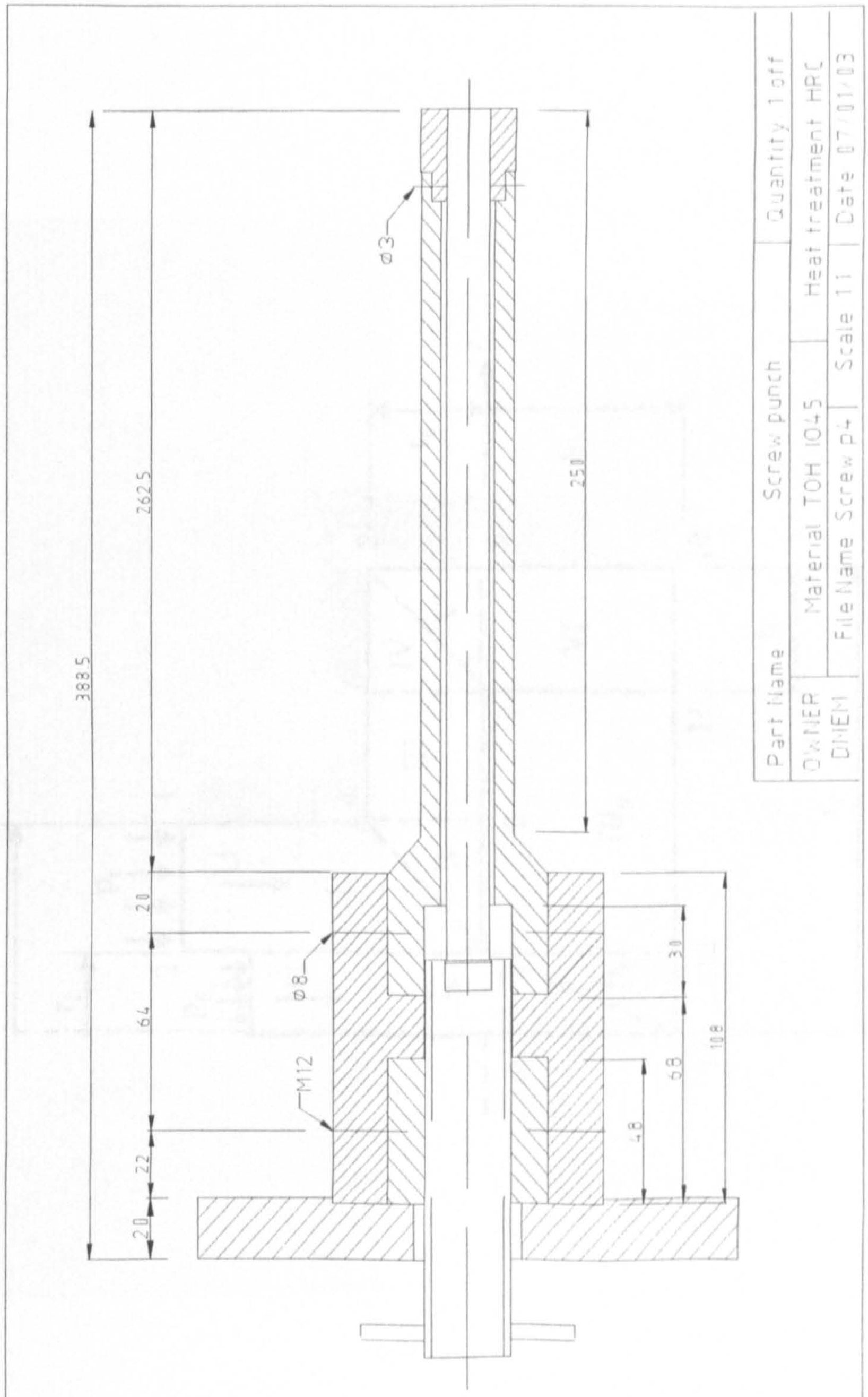

Fig. 5.19 The assembled screw punch

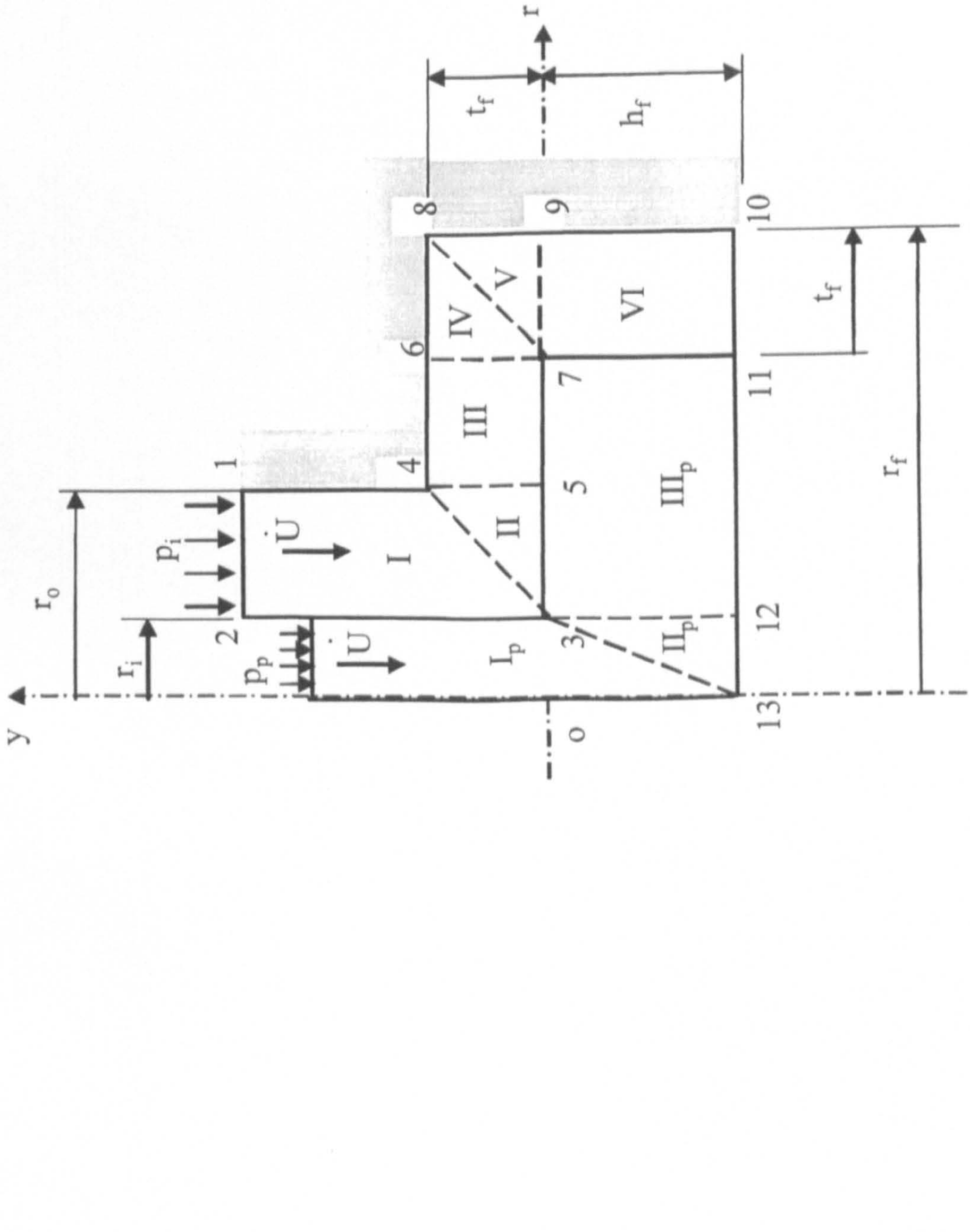

Fig. 5.20 Definition of the deformation zones

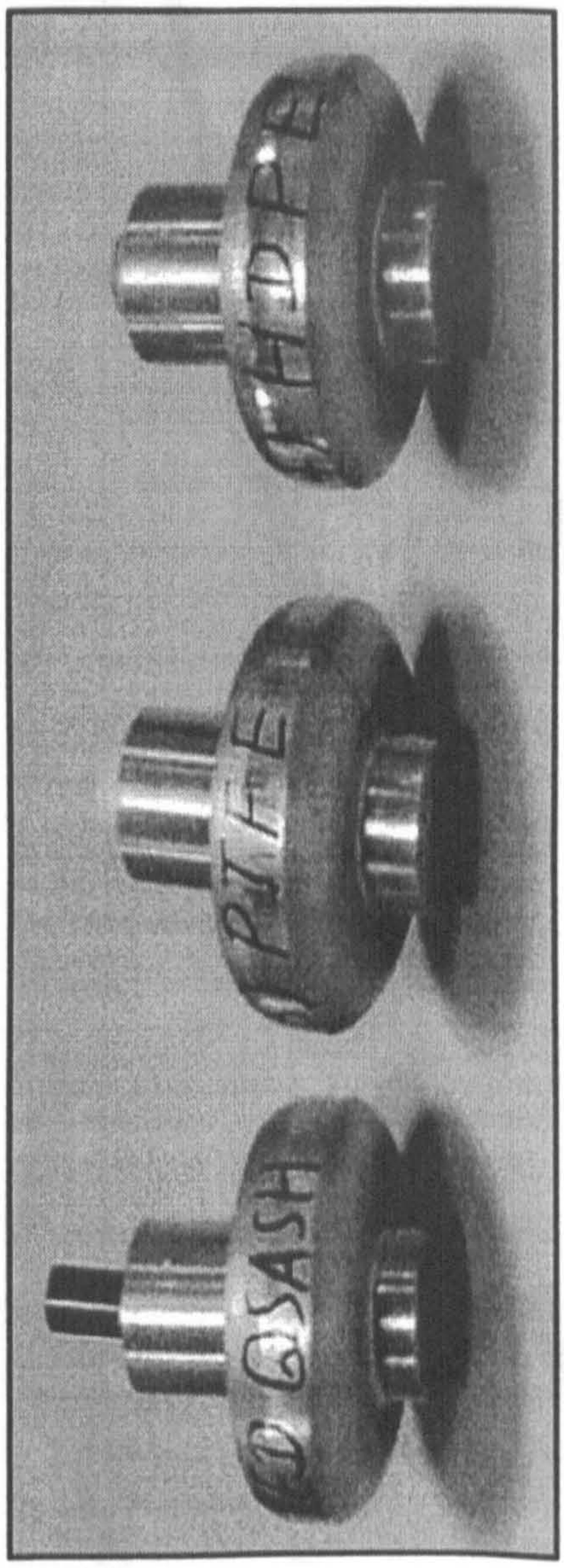

Specimens with flange-diameter 85 mm

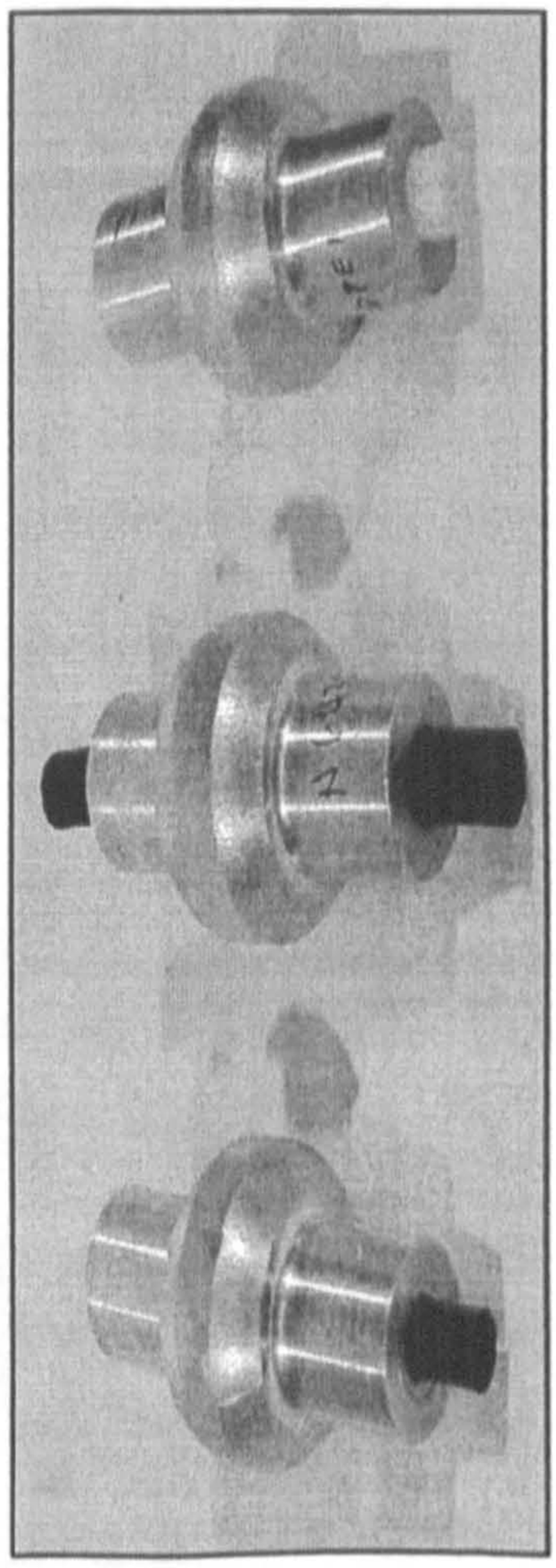

Specimens with flange-diameter 60 mm

Fig. 5.21 Specimens produced by the tube forming experiment

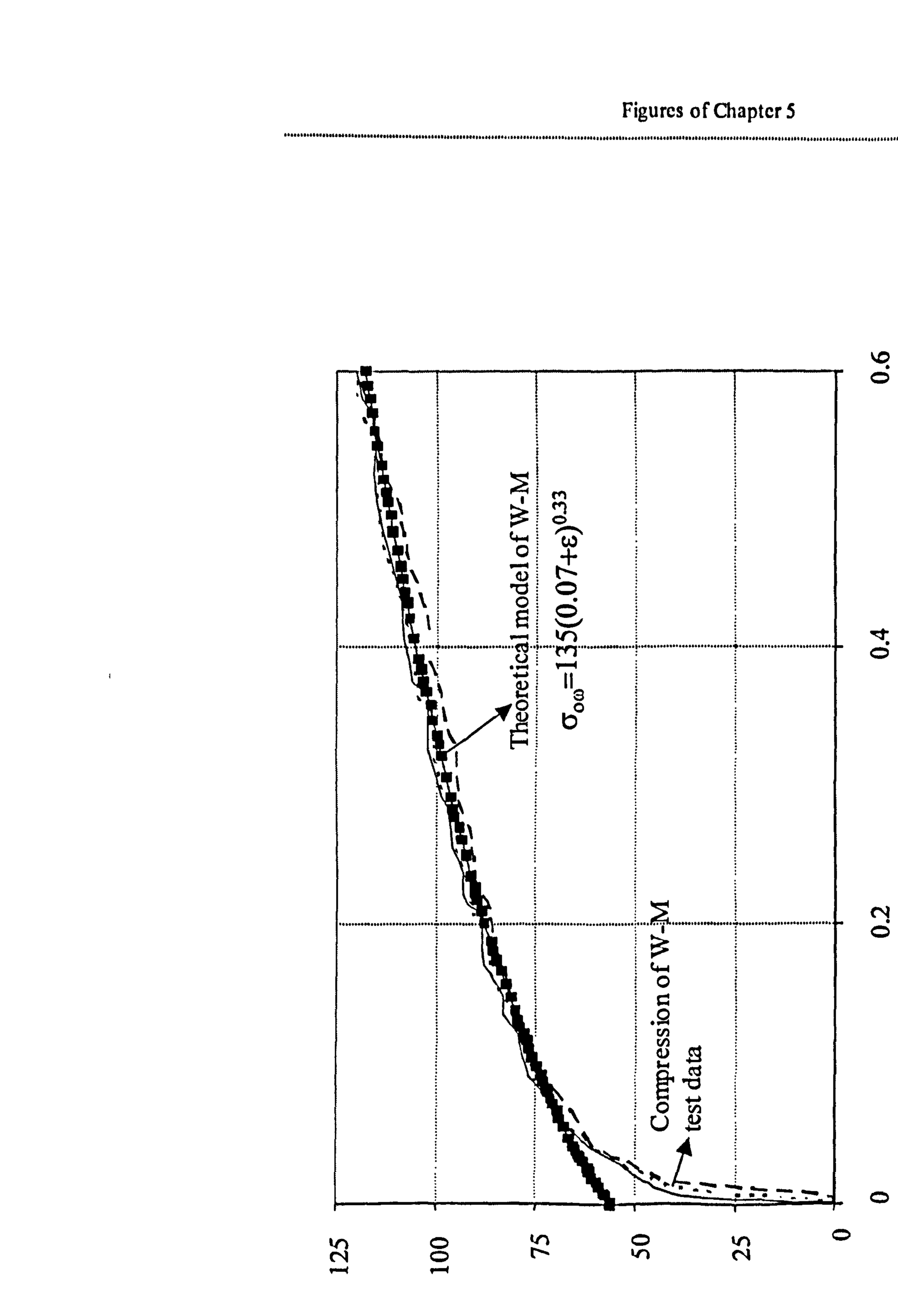

Fig. 5.22 Work material properties and its theoretical model

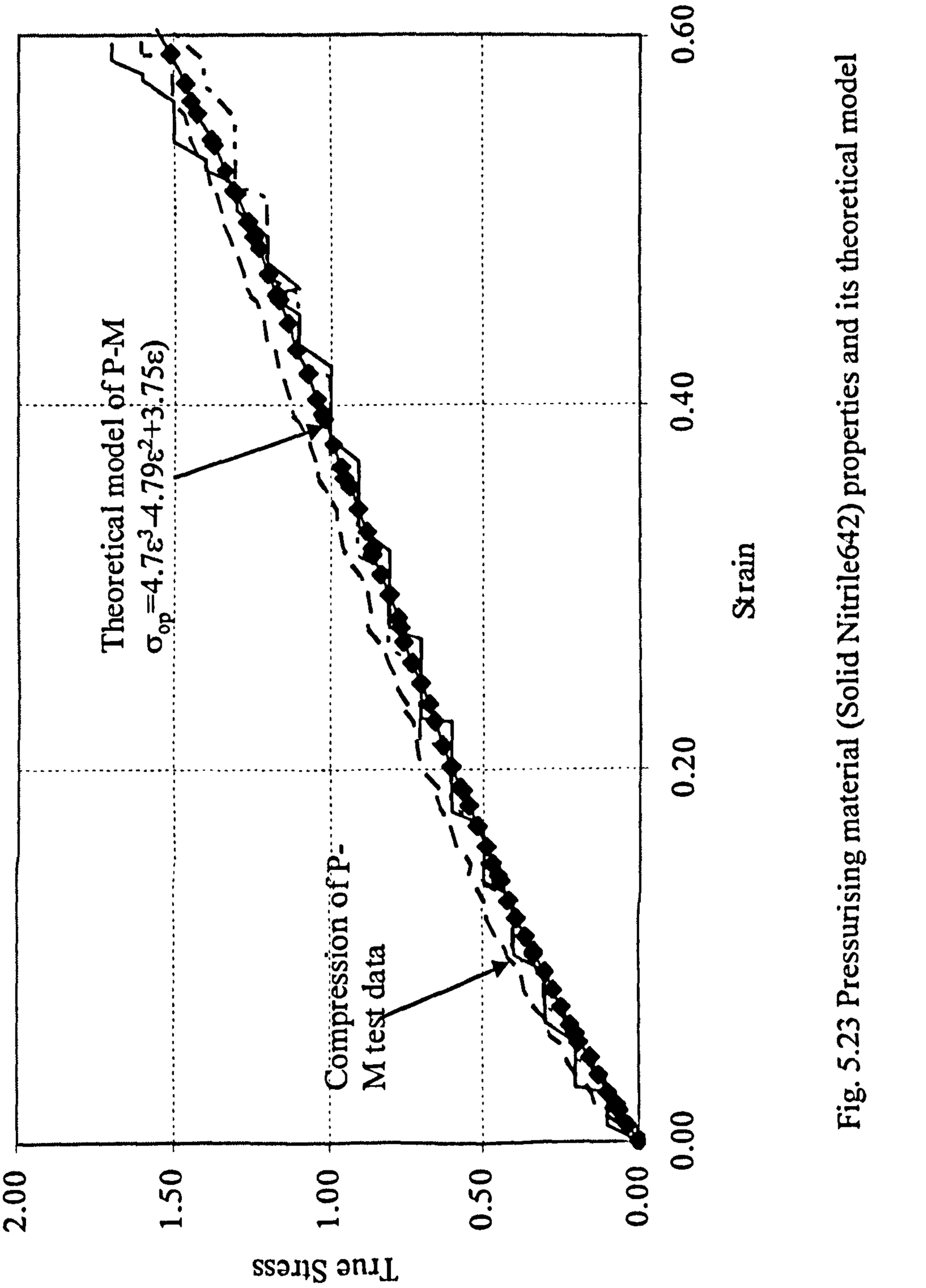

Fig. 5.23 Pressurising material (Solid Nitrile642) properties and its theoretical model

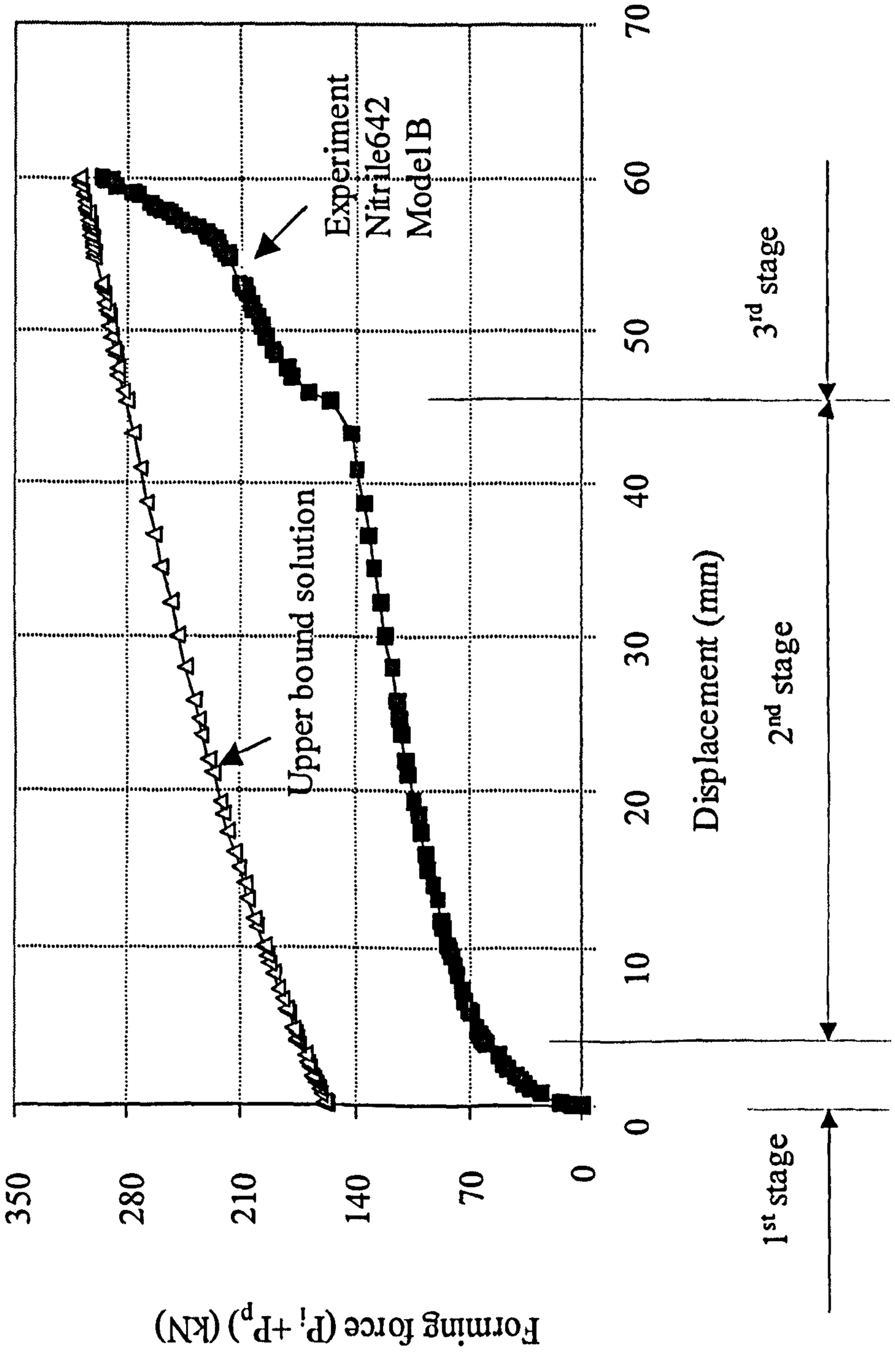

Fig. 5.24 Comparison of the upper bound solution and the experimental results

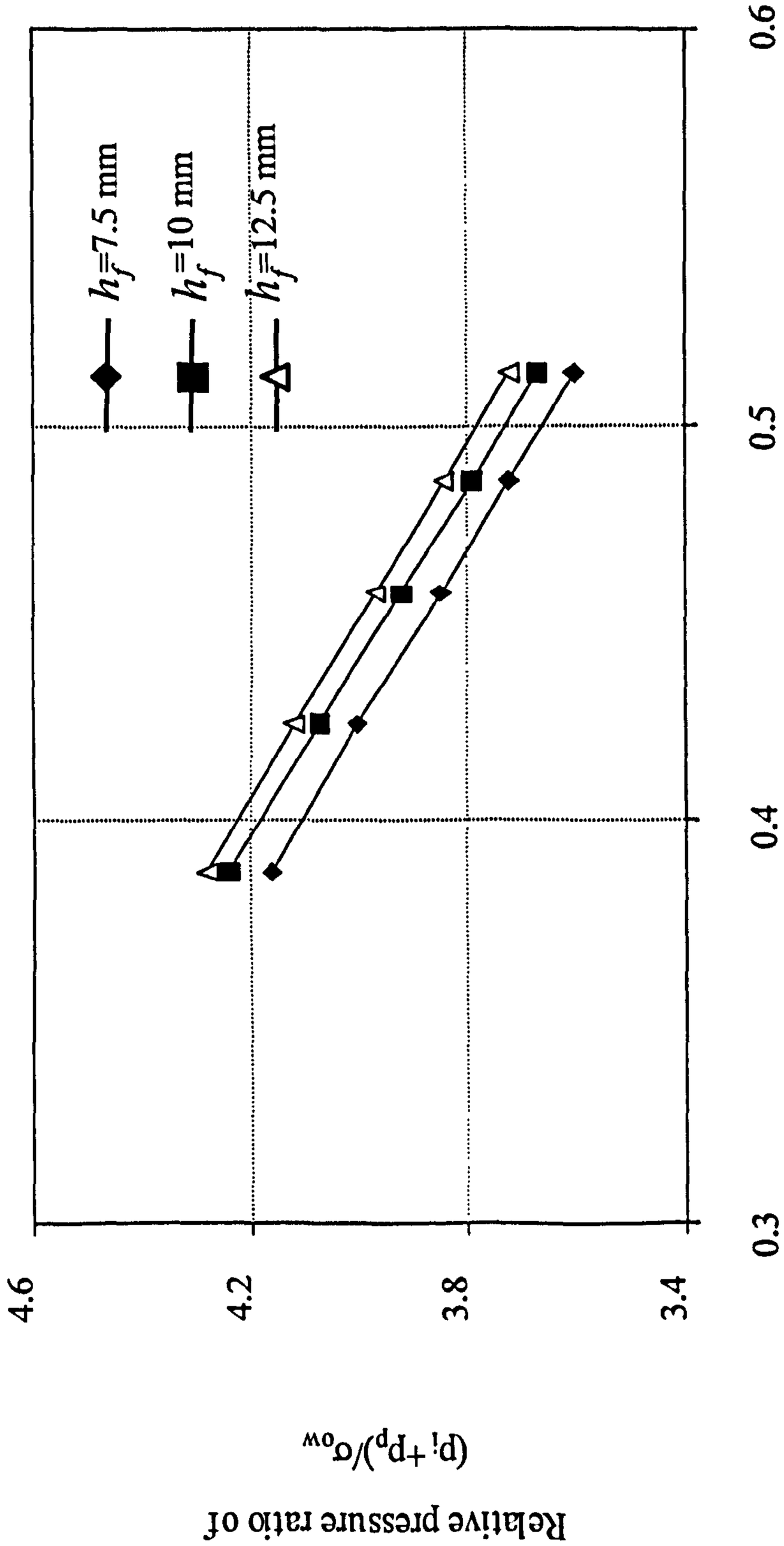

Fig. 5.25 Effect of the flange height and mean radius of the billet on the relative pressure

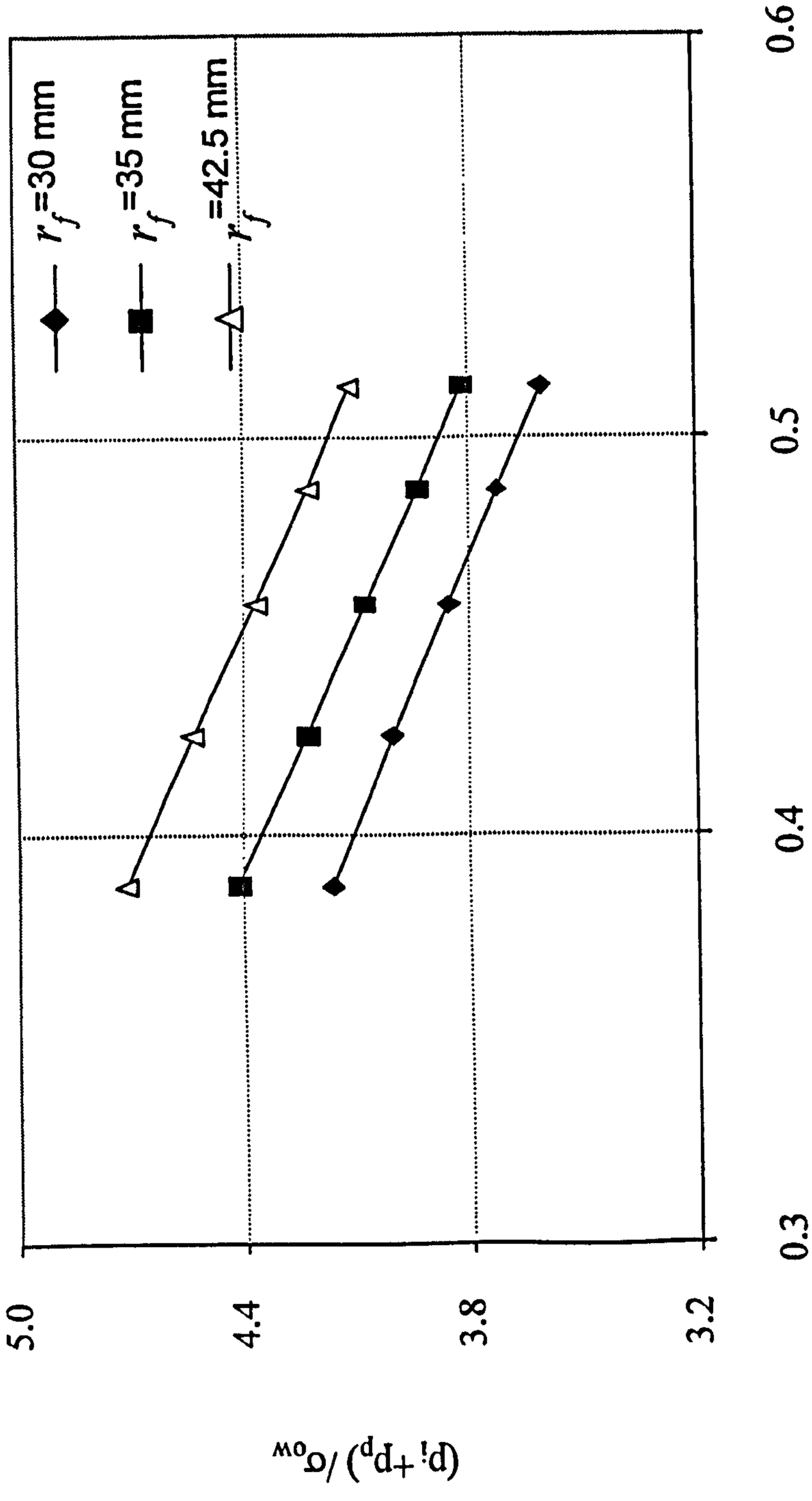

Fig. 5.26 Effect of the flange radius and mean radius of the billet on the relative pressure

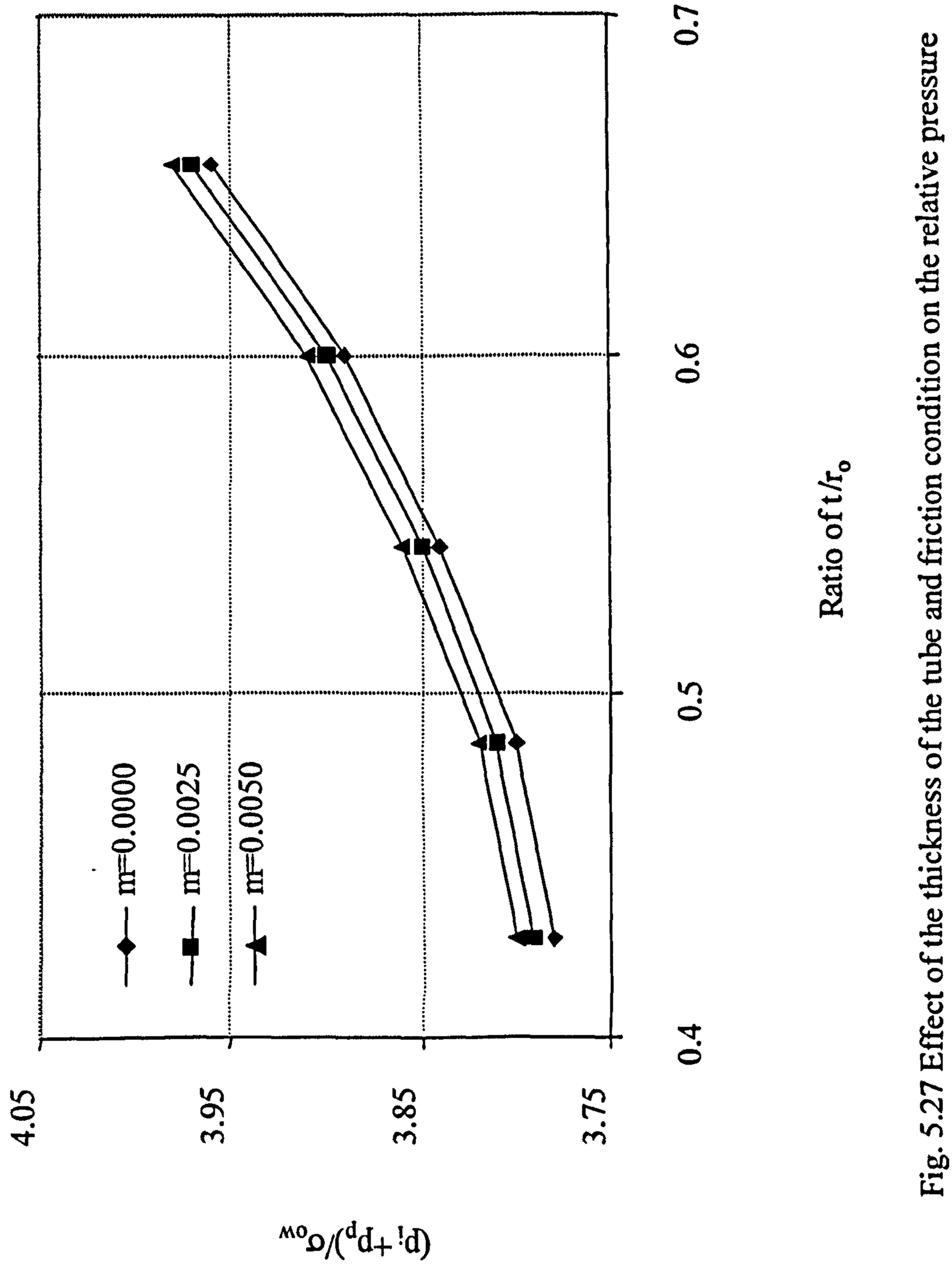

Fig. 5.27 Effect of the thickness of the tube and friction condition on the relative pressure

Figures of Chapter 6

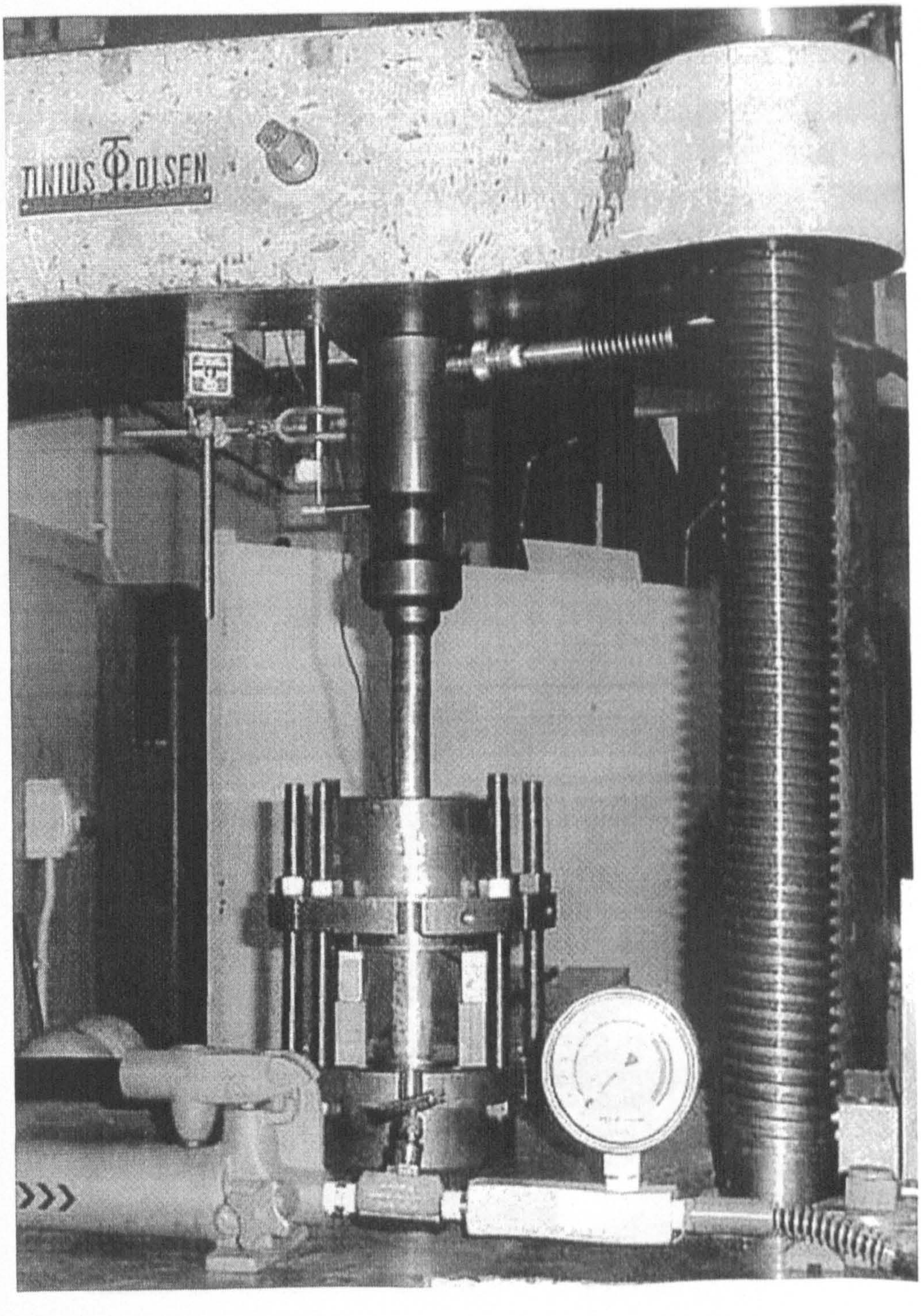

Fig. 6.1 The experimental set-up

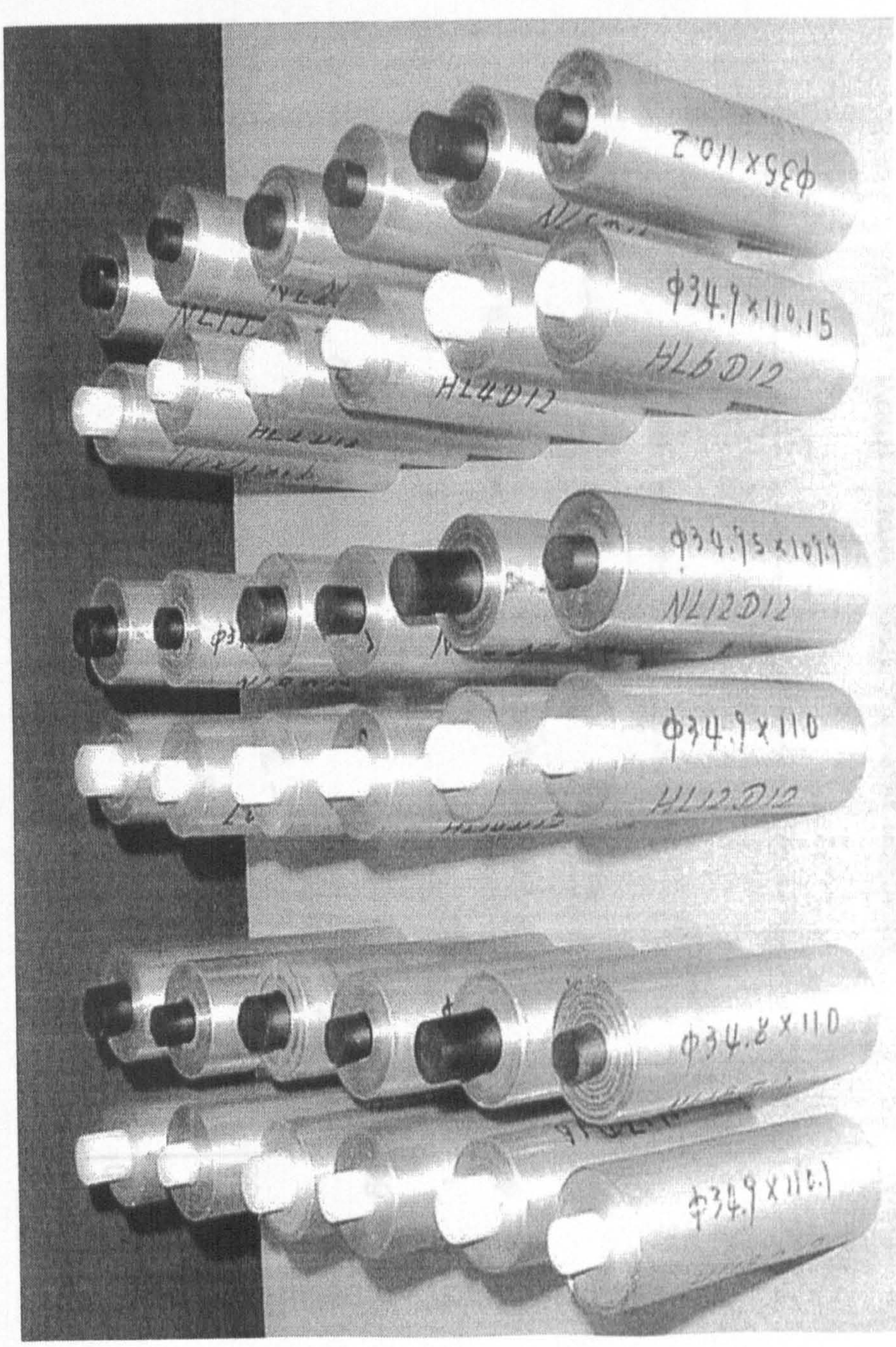

Fig. 6.2 The specimens

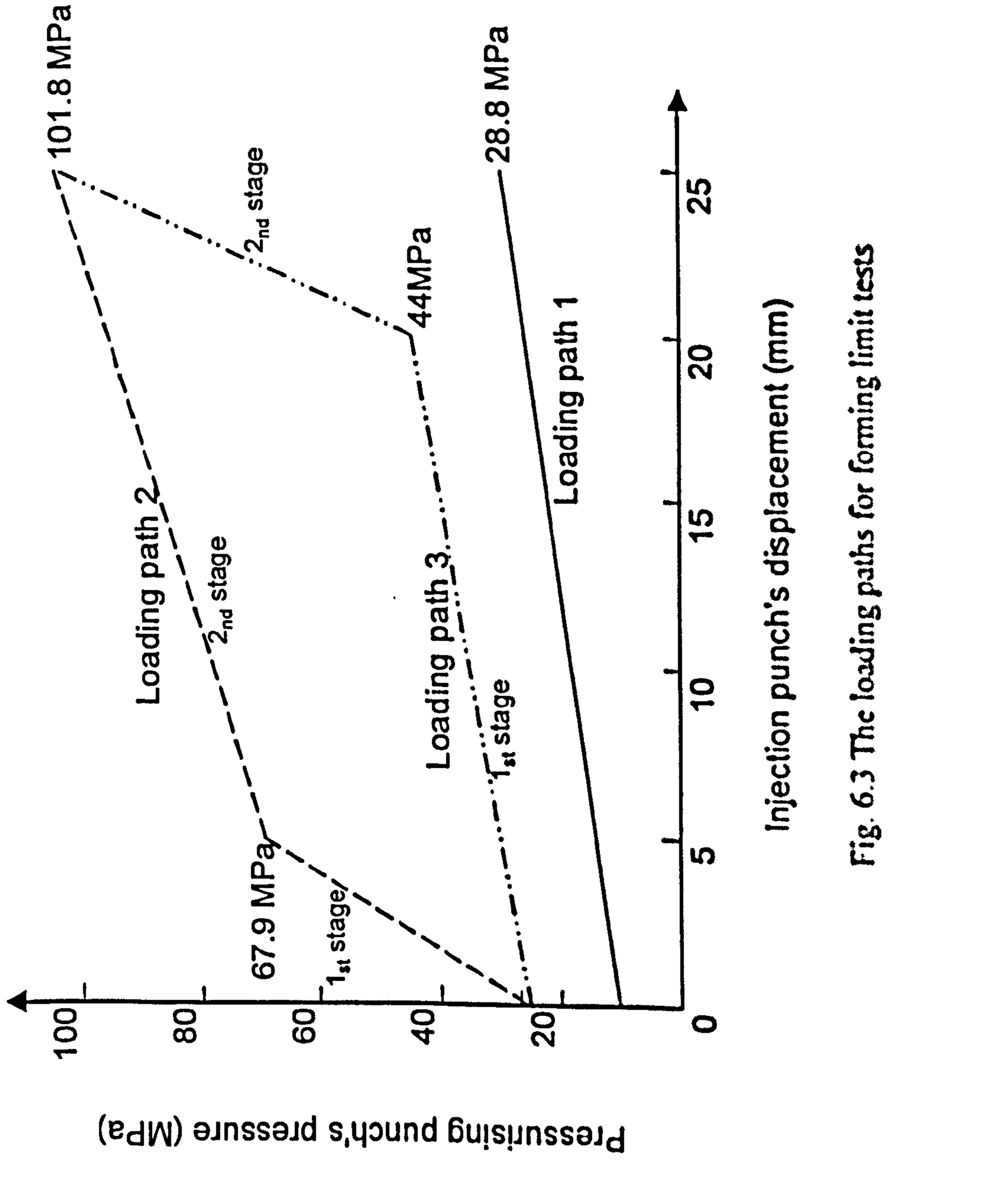

Fig. 6.3 The loading paths for forming limit tests

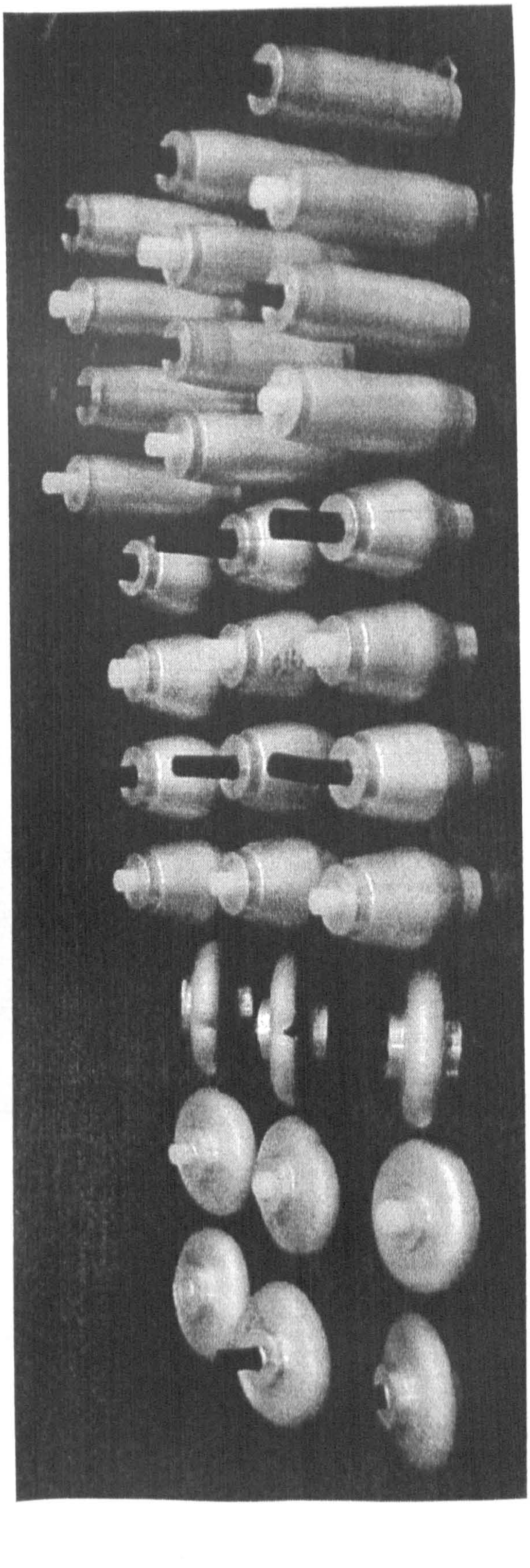

Fig. 6.4 The failure modes produced experimentally

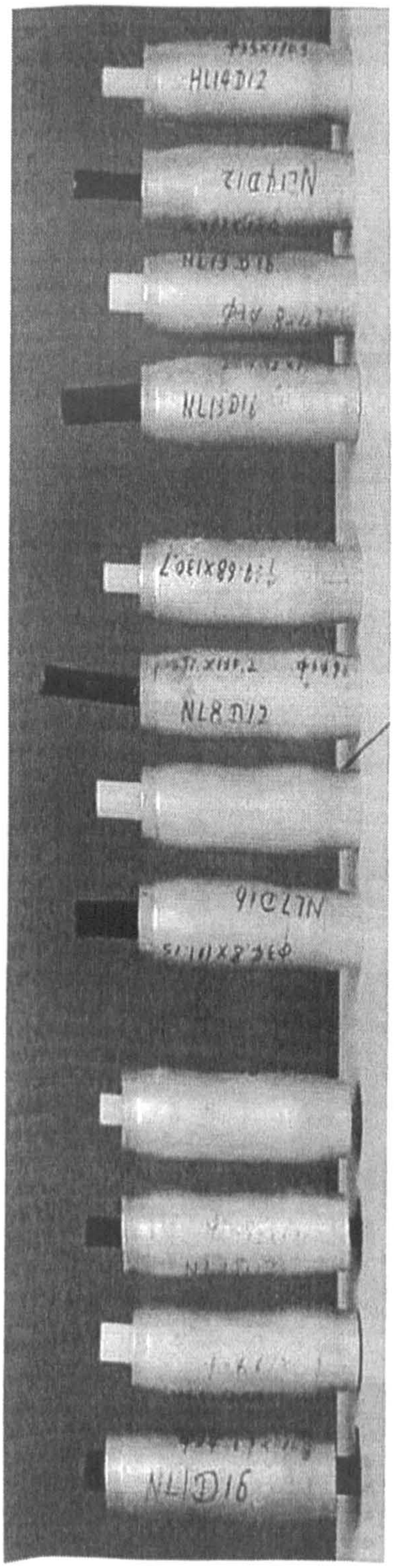

Loading path 3 Loading path 2 Loading path 1

(a) T=2.52

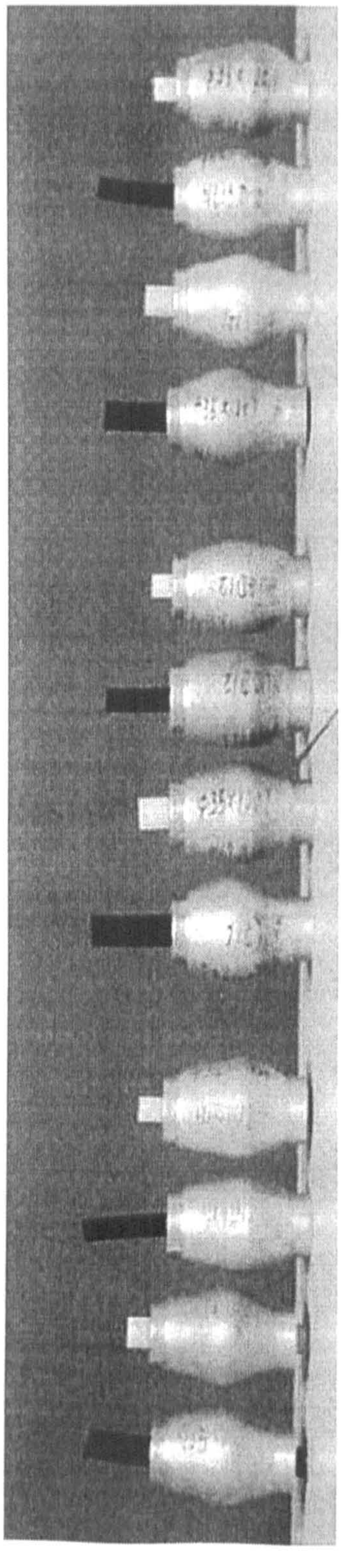

Loading path 3 Loading path 2 Loading path 1

(b) T=1.52

Fig. 6.5 The failure modes for higher aspect ratios

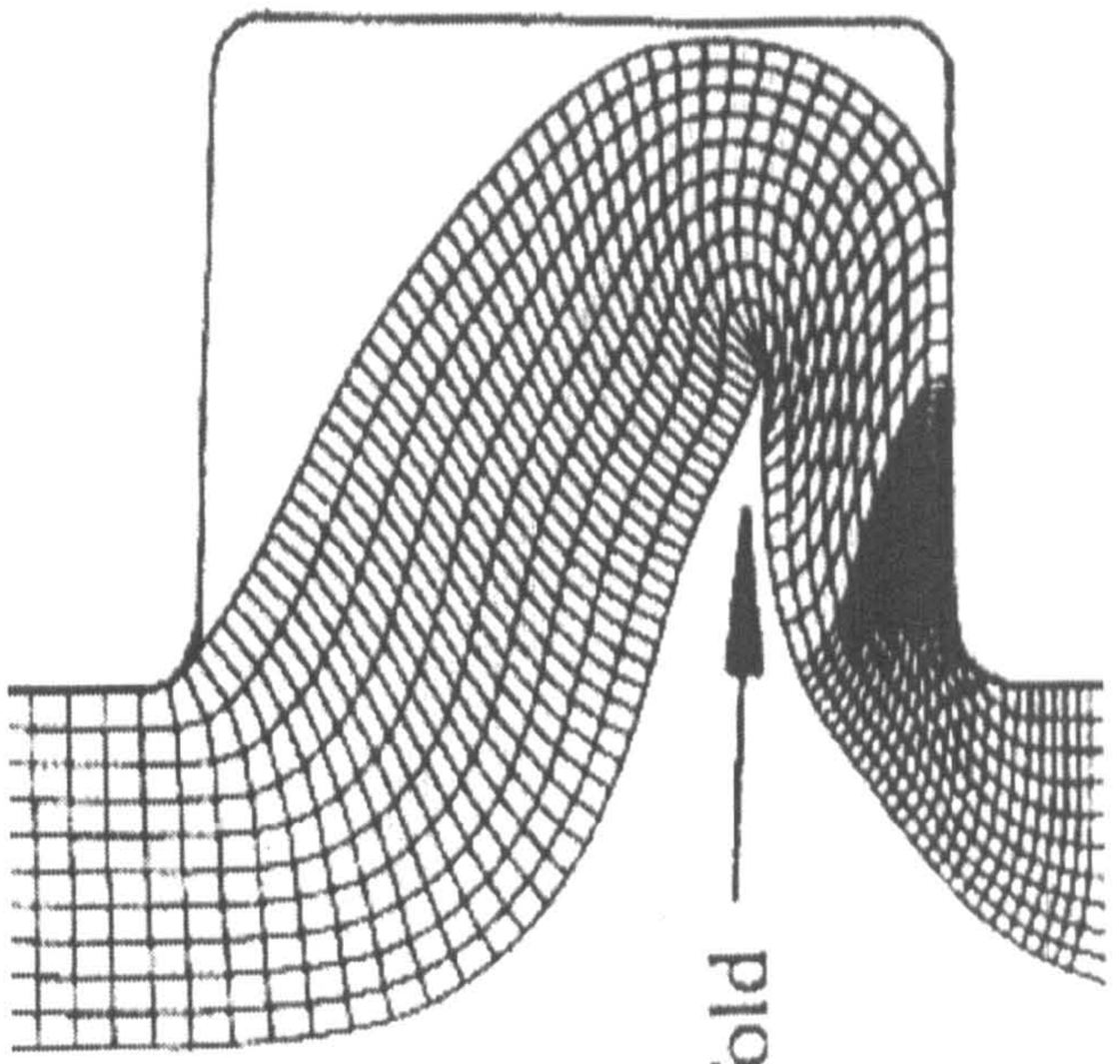

(b) FE simulation

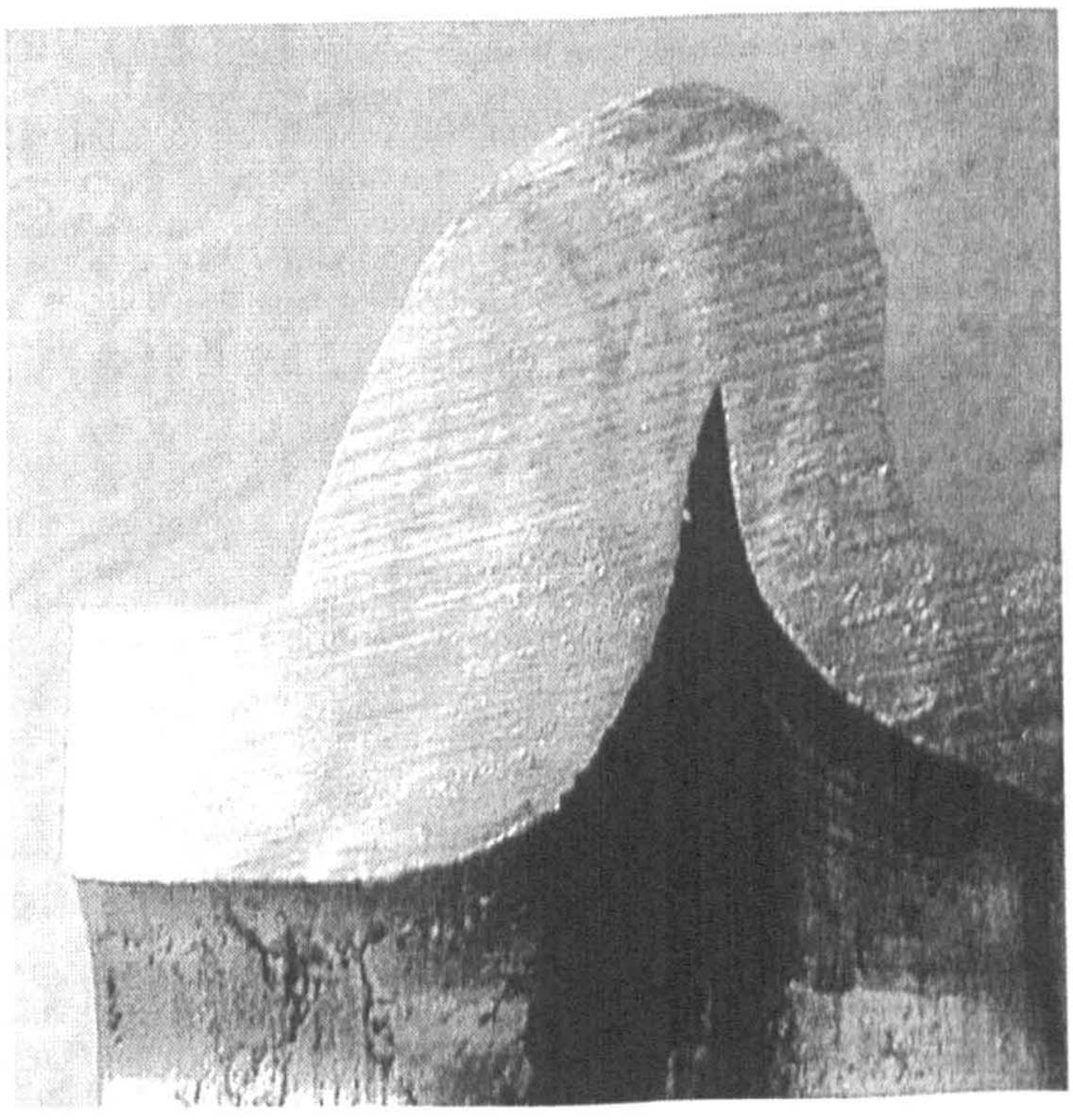

(a) experimental

Fig. 6.6 Comparison of an experimental and FE simulation result

Failure mode features of PAIF	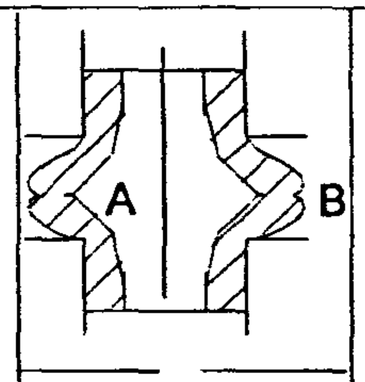 A. folding due to insufficient perssurisation B. fracture due to smaller aspect ratio	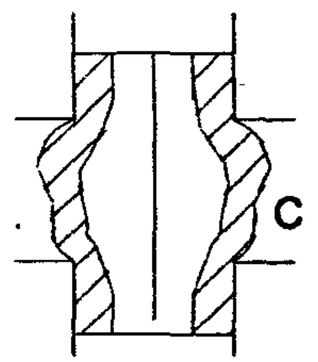 C. material folding due to insufficient perssurisation	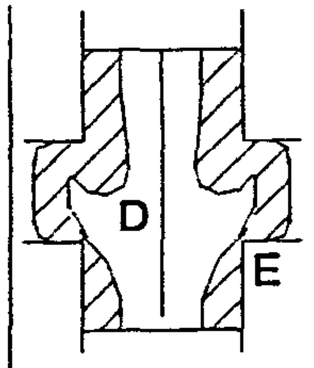 D. material accumulated E. weakend section due to larger injection at a final stage	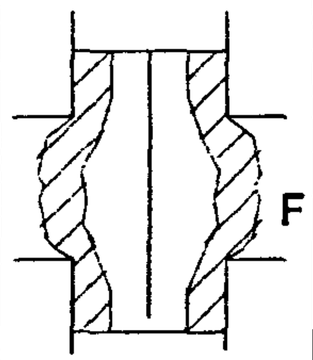 F. material buckling dut to larger aspect ratio	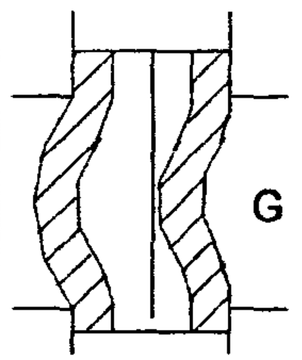 G. material bending due to larger aspect ratio and asymmetrical load	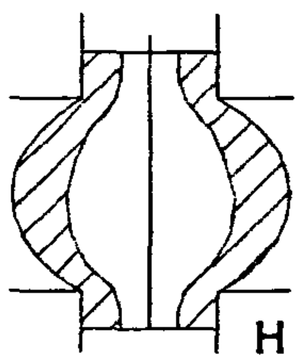 H. weakend sections due to high pressurisation & less injected tube
Aspect ratio of t/Ø	<0.7	0.7-1.5	0.7-1.5	1.5-2.0	2.0-3.0	2.0-3.0
1 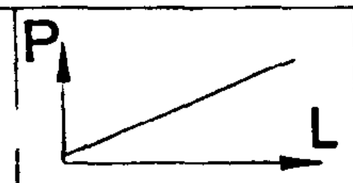	A+B	C	D+E	F	G	
2 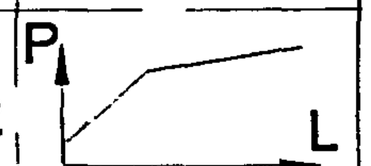	B		D+E	F	G	H
3 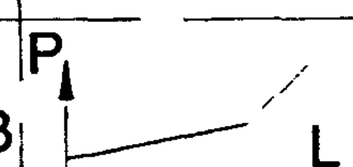	B		D+E	F	G	H
Loading path	Note 1. In section-aspect ratio, t is for flange height & Ø is for the outer diameter of billet. 2. In section-loading path, P is inner punch's load & L is outer punch's displacement.					

Fig. 6.7 Failure modes and aspect ratios

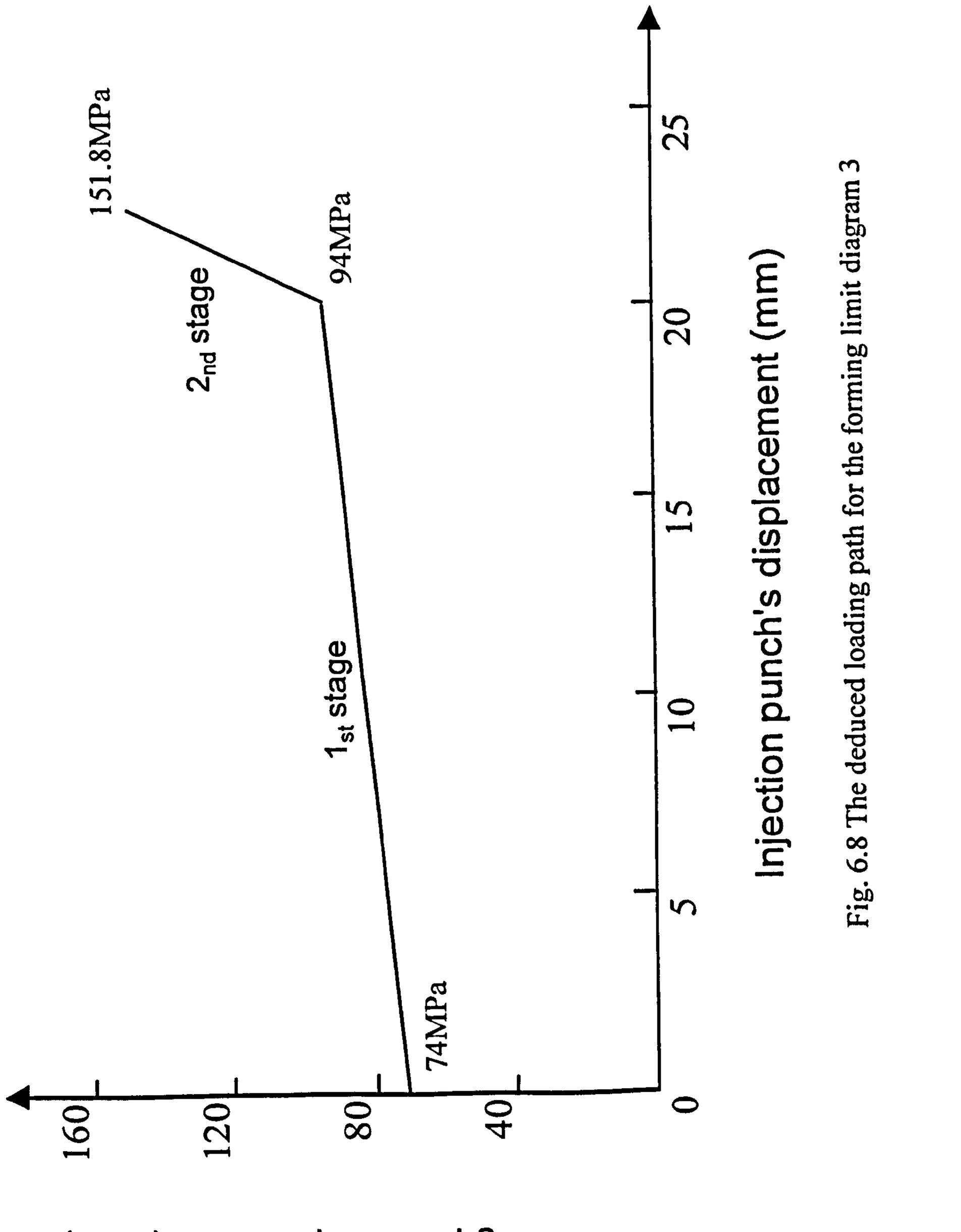

Fig. 6.8 The deduced loading path for the forming limit diagram 3

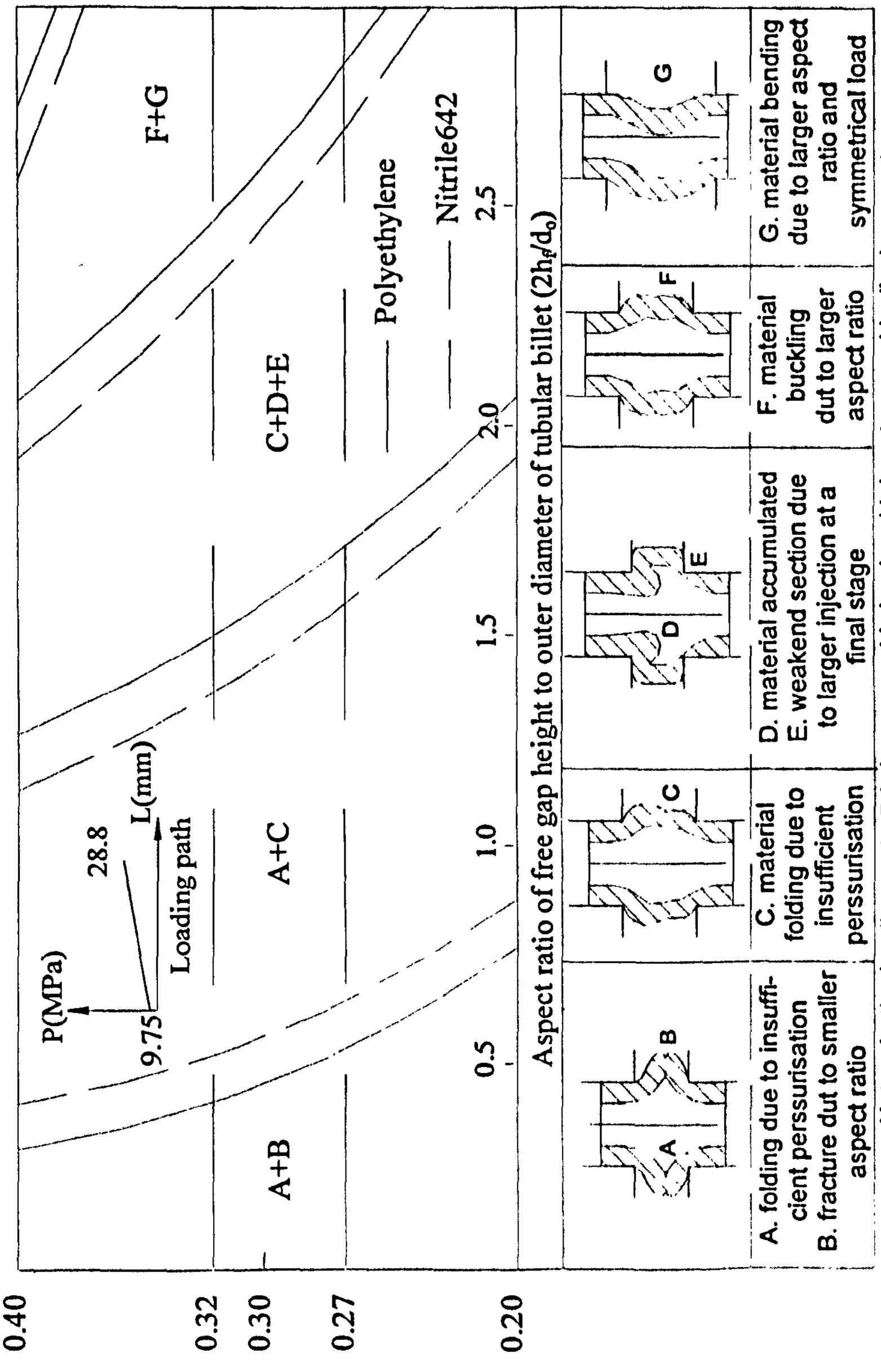

Fig. 6.9 Forming limit diagram 1 (for loading path 1 in Fig. 6.3)

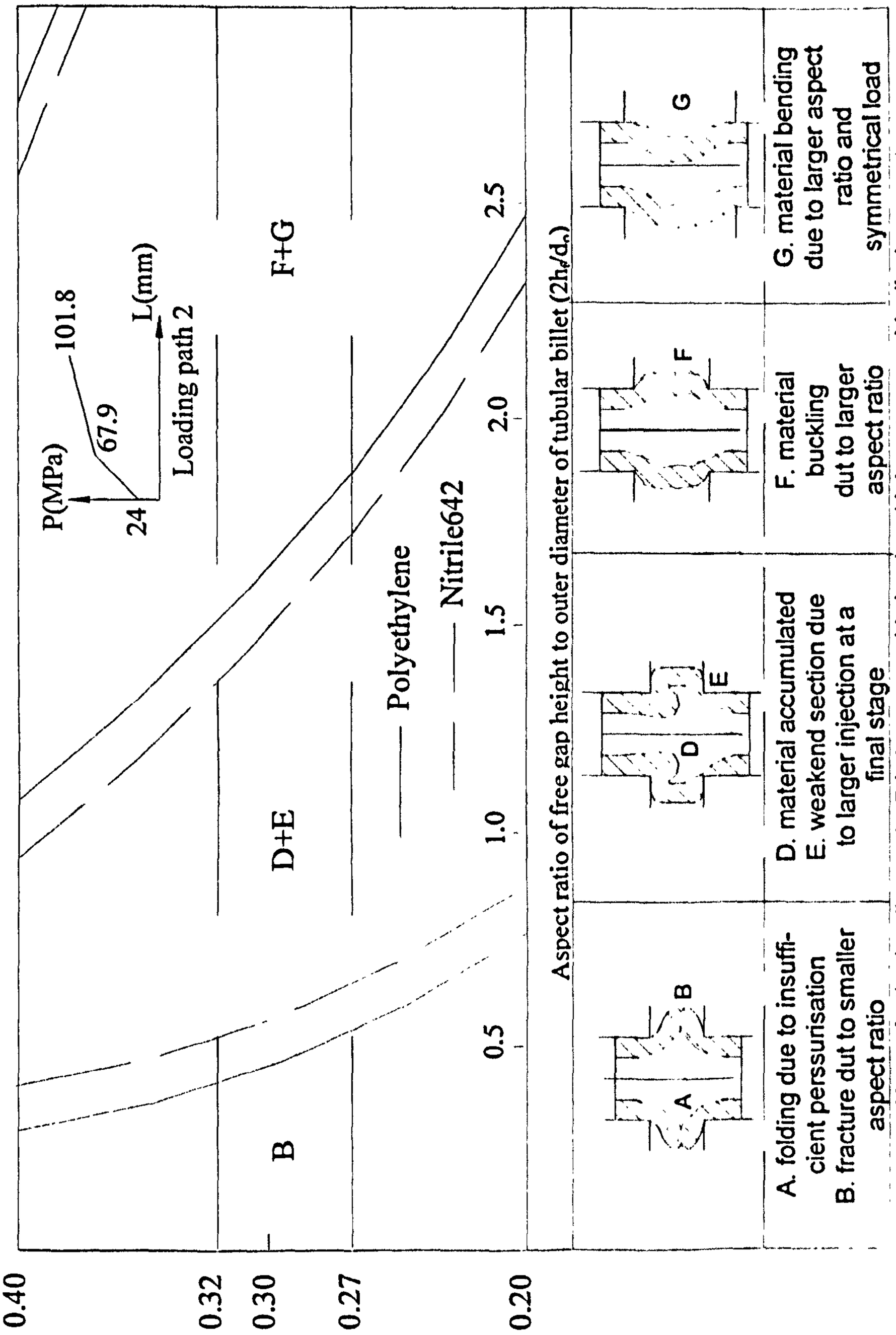

Fig. 6.10 Forming limit diagram 2 (for loading path 2 in Fig. 6.3)

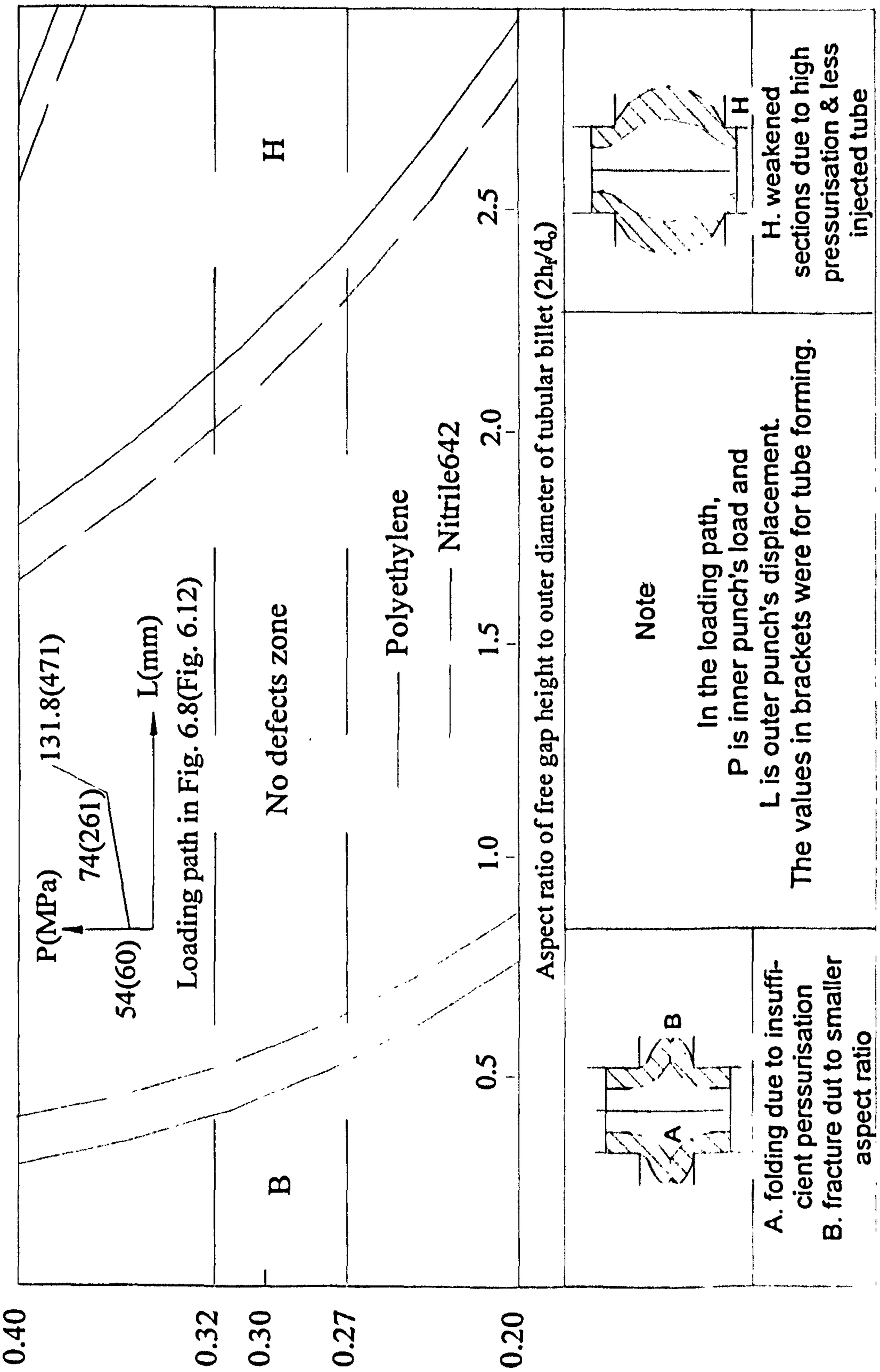

Fig. 6.11 Forming limit diagram 3 (for loading paths in Figs. 6.8 and 6.12)

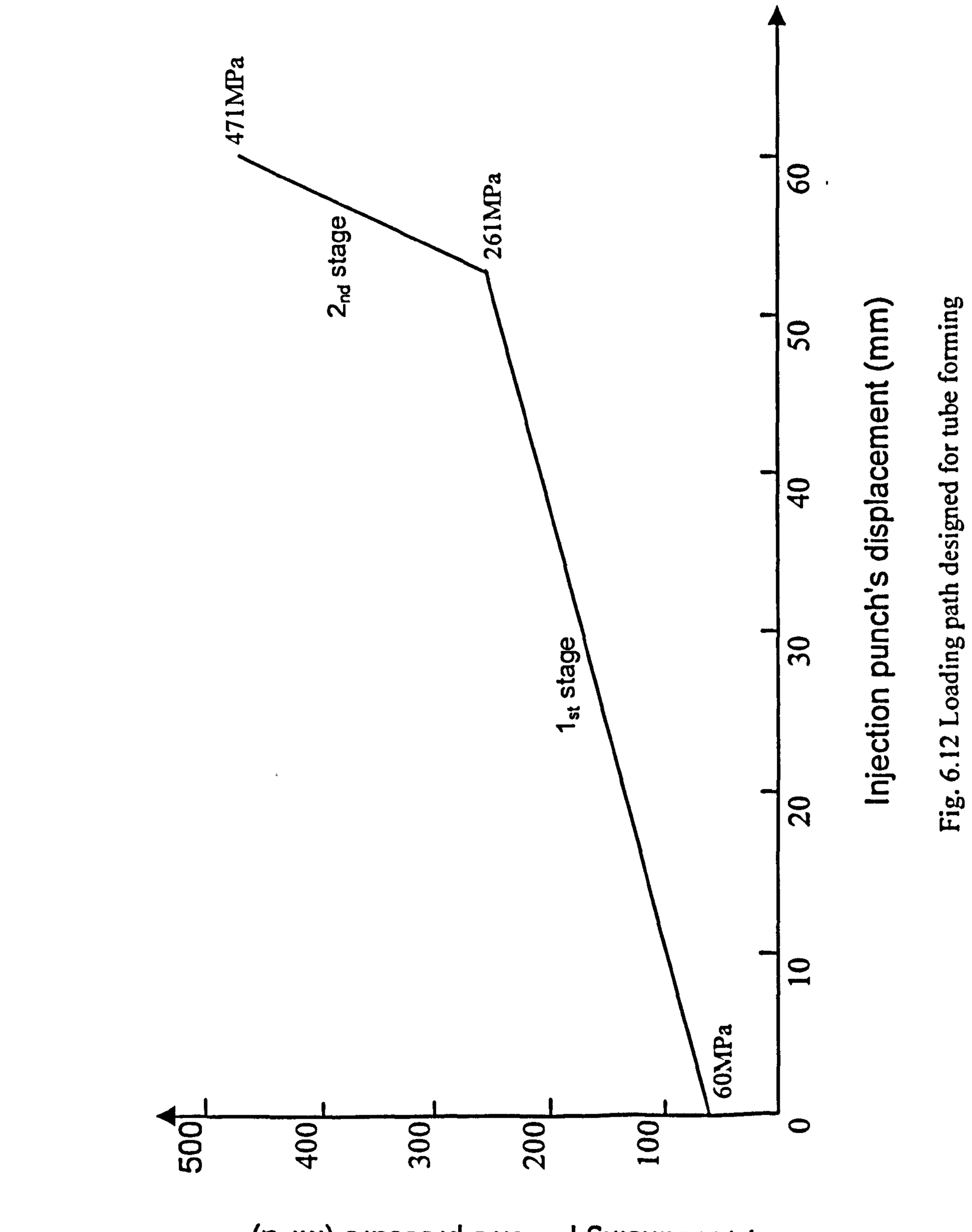

Fig. 6.12 Loading path designed for tube forming

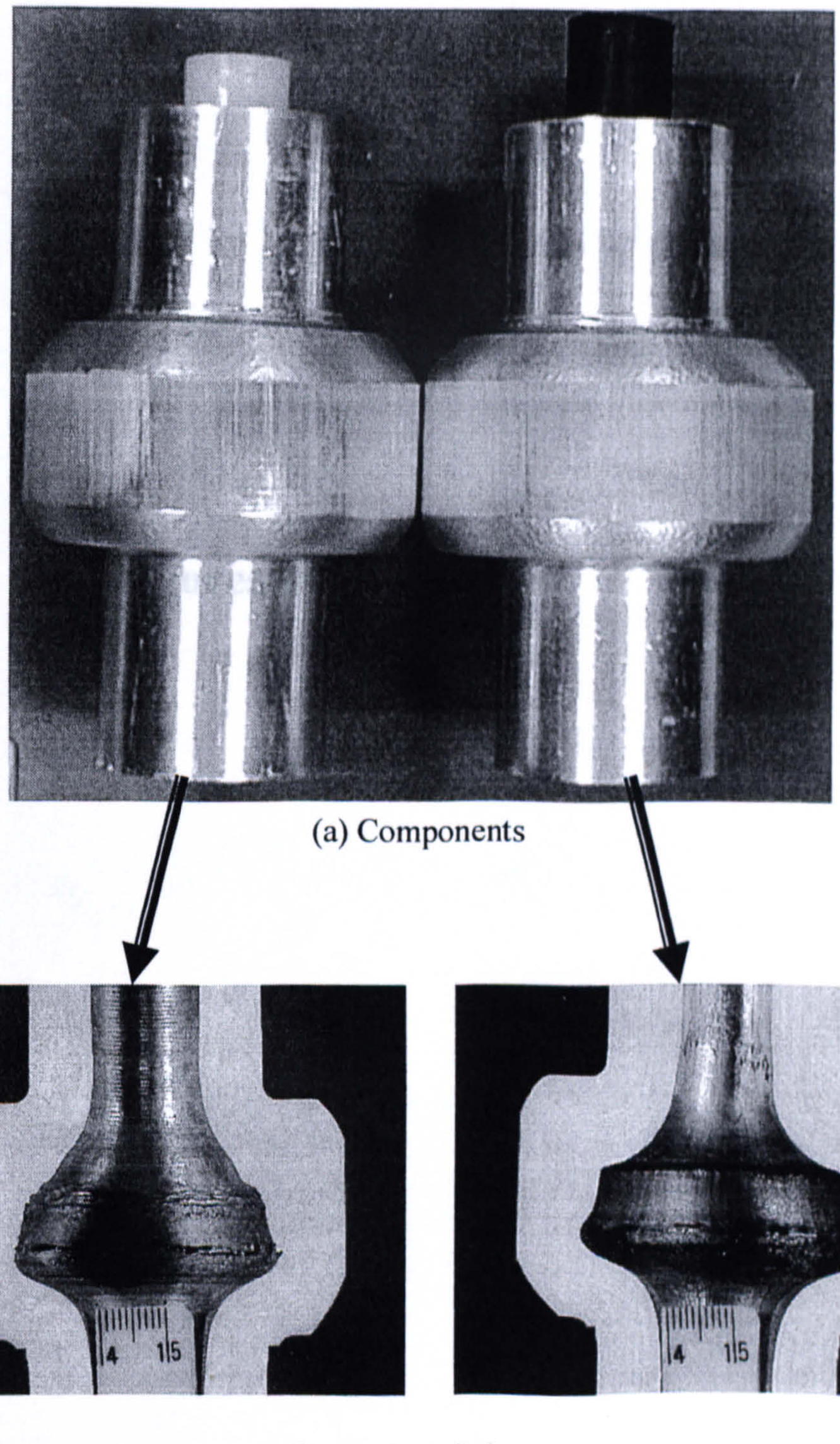

(a) Components

(b) Sectioned views

Fig. 6.13 The formed tubular components and their sectioned views

Figures of Chapter 7

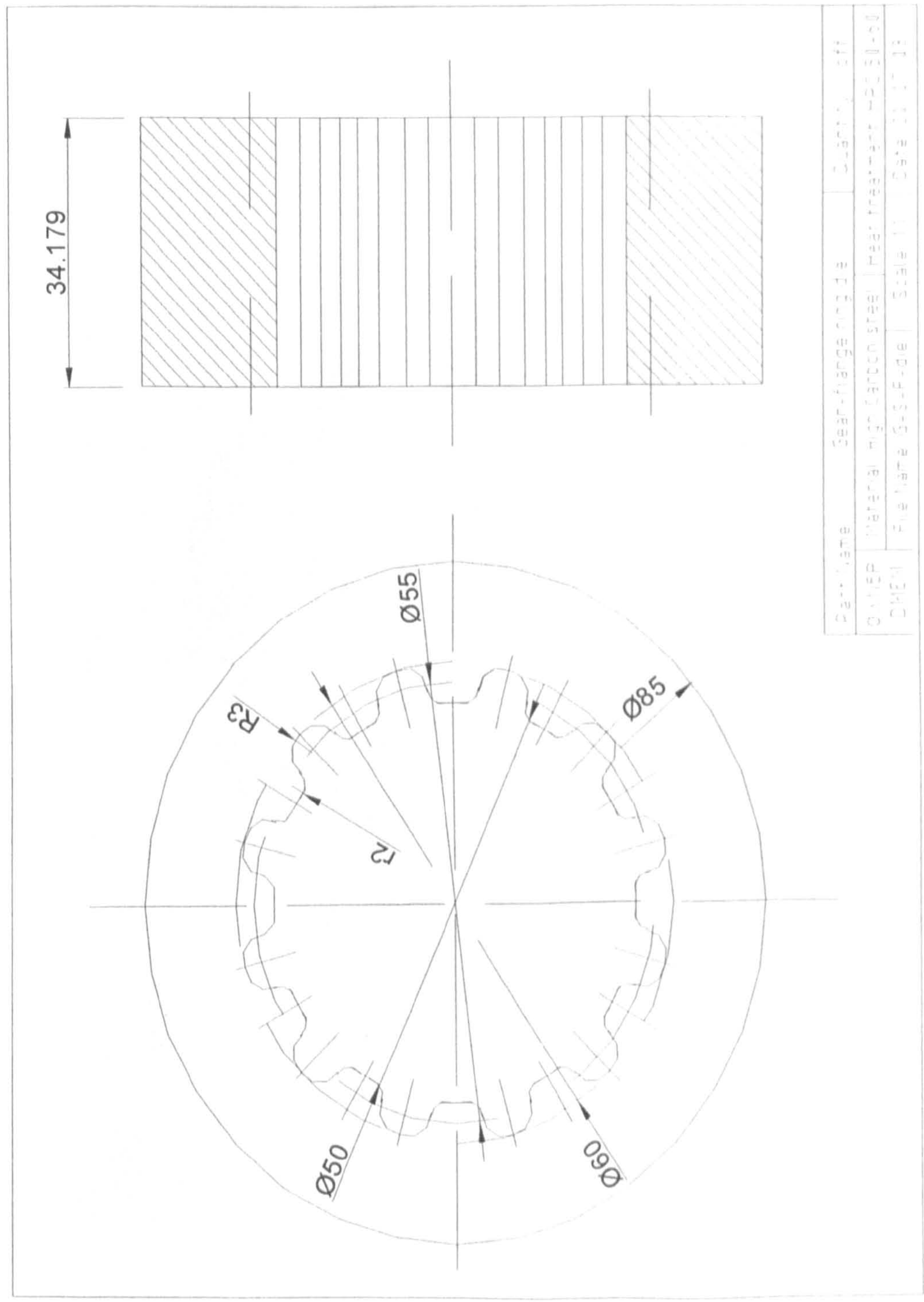

Fig. 7.1 The forming die designed for the forming of the gear-shaft

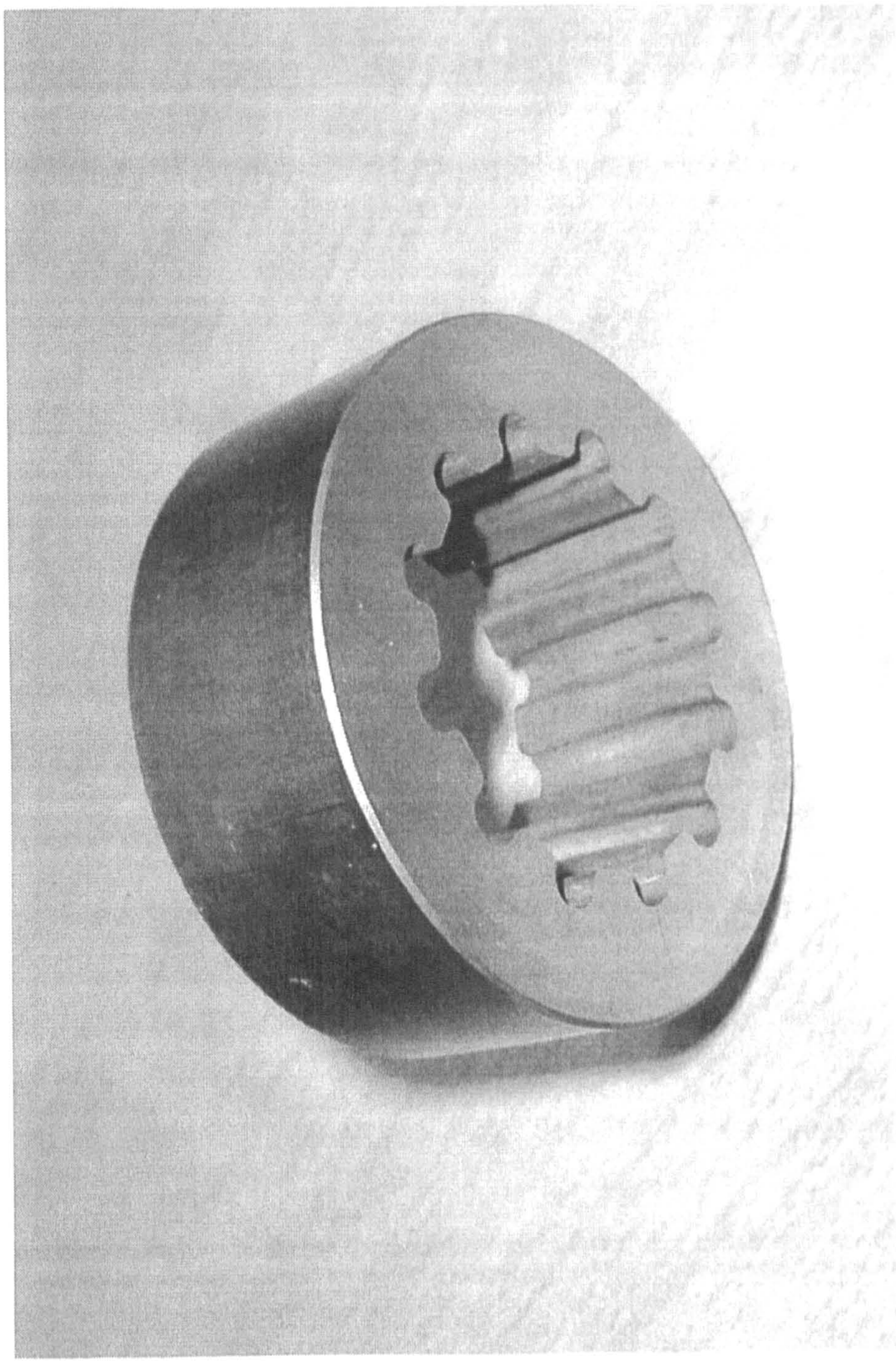

Fig. 7.2 The forming die fabricated

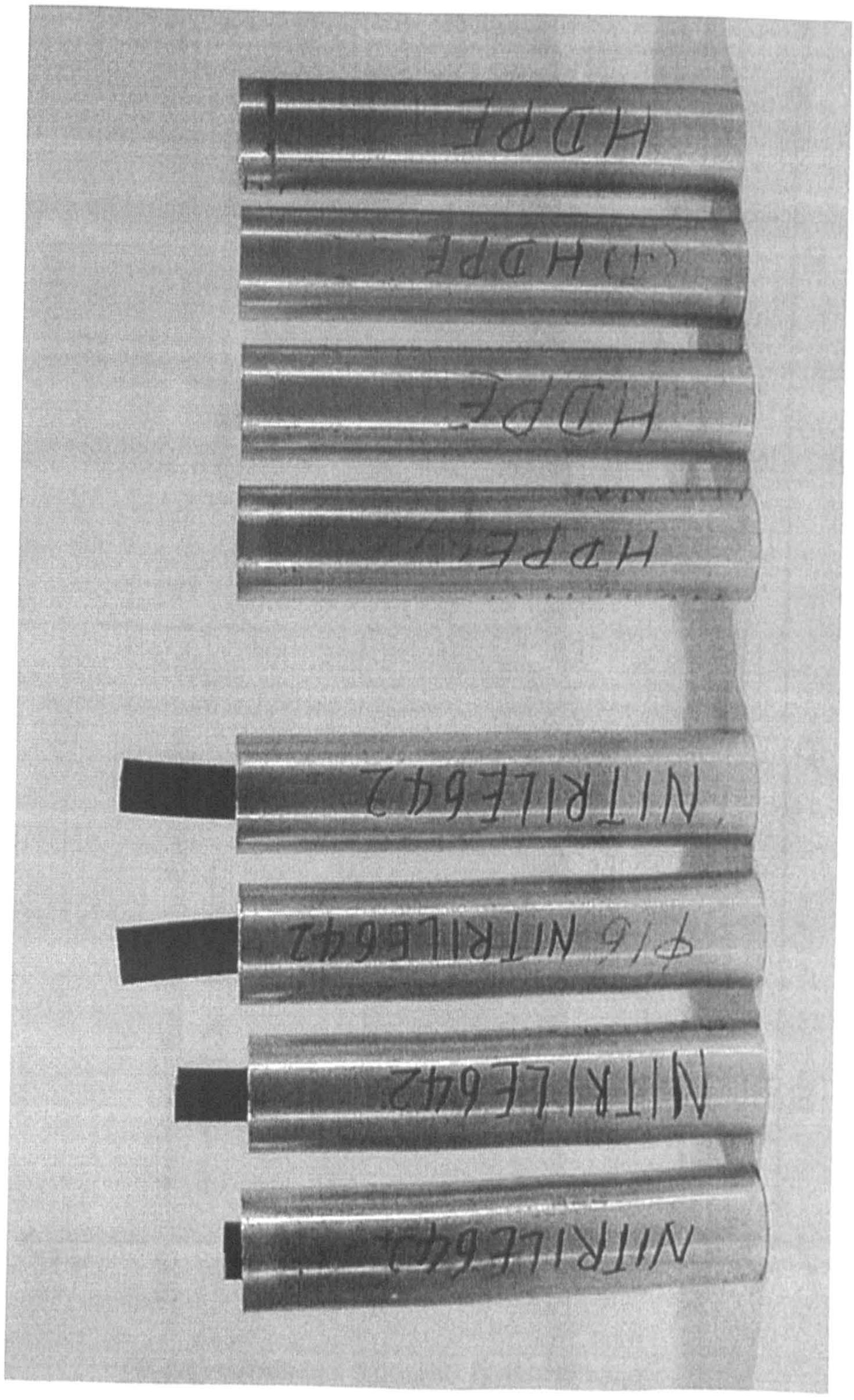

Fig. 7.3 The specimens for the forming of the gear-shafts

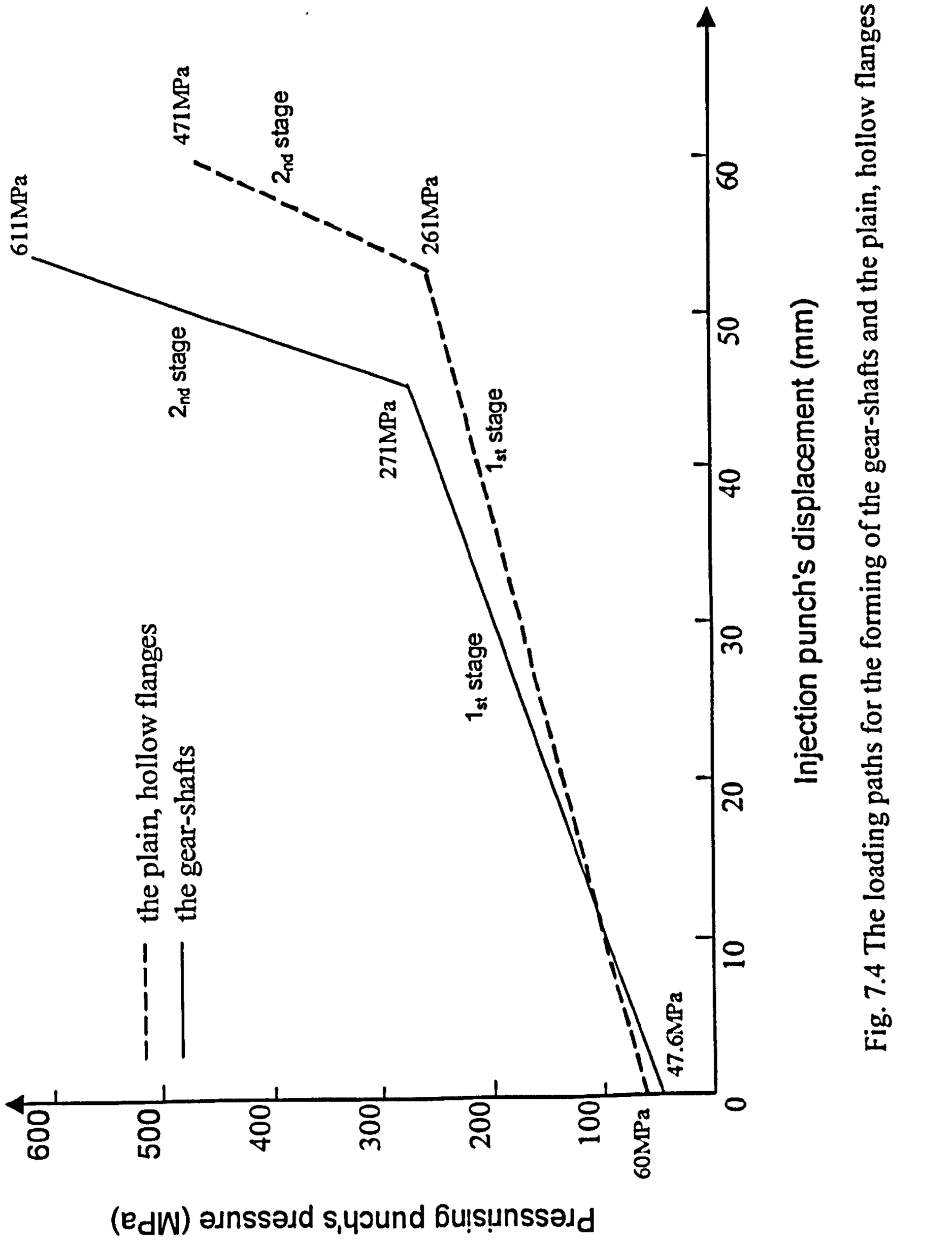

Fig. 7.4 The loading paths for the forming of the gear-shafts and the plain, hollow flanges

Fig. 7.5 The gear-shaft formed from a tubular billet

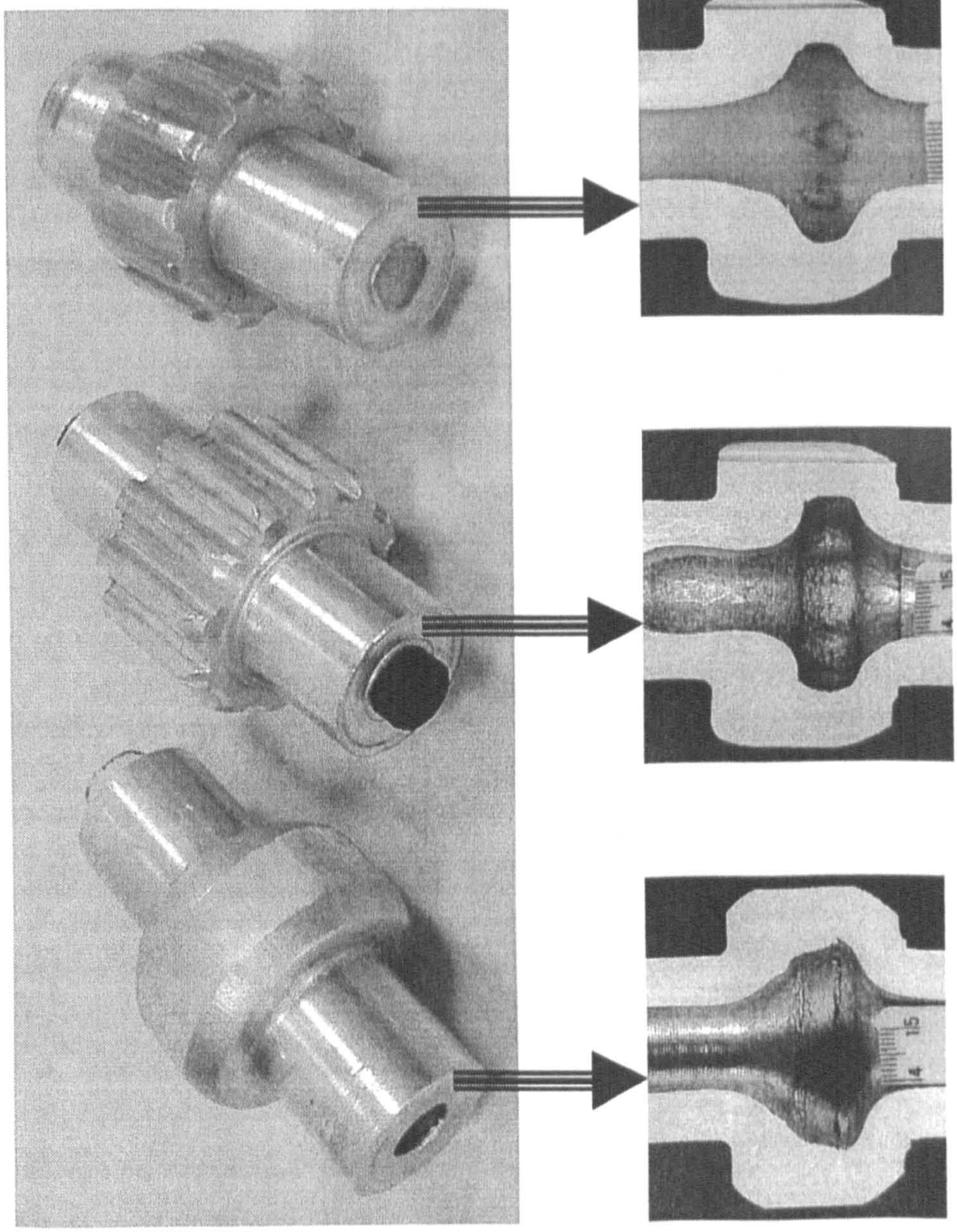

Fig. 7.6 The specimens produced with PAIF

(a) The components produced

(b) The axial sectioned views

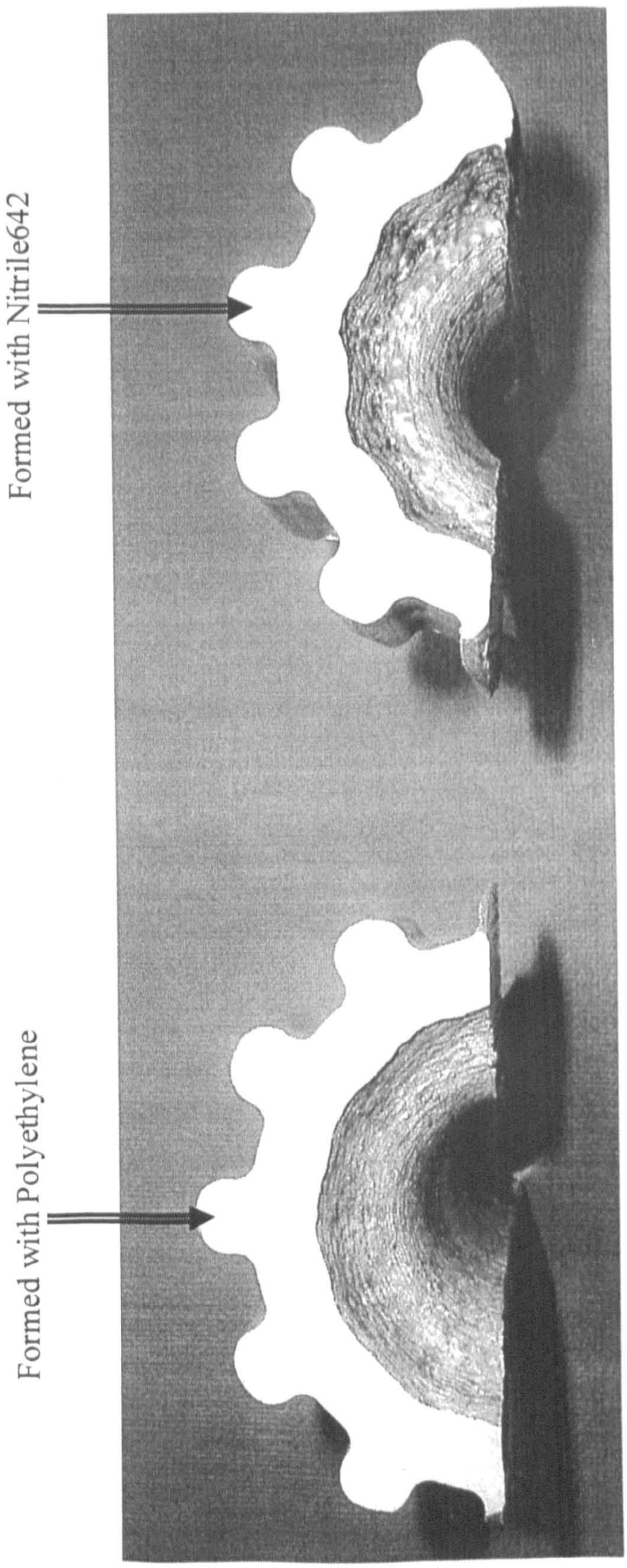

Fig.7.7 The radial sectioned views of the gear-shafts formed

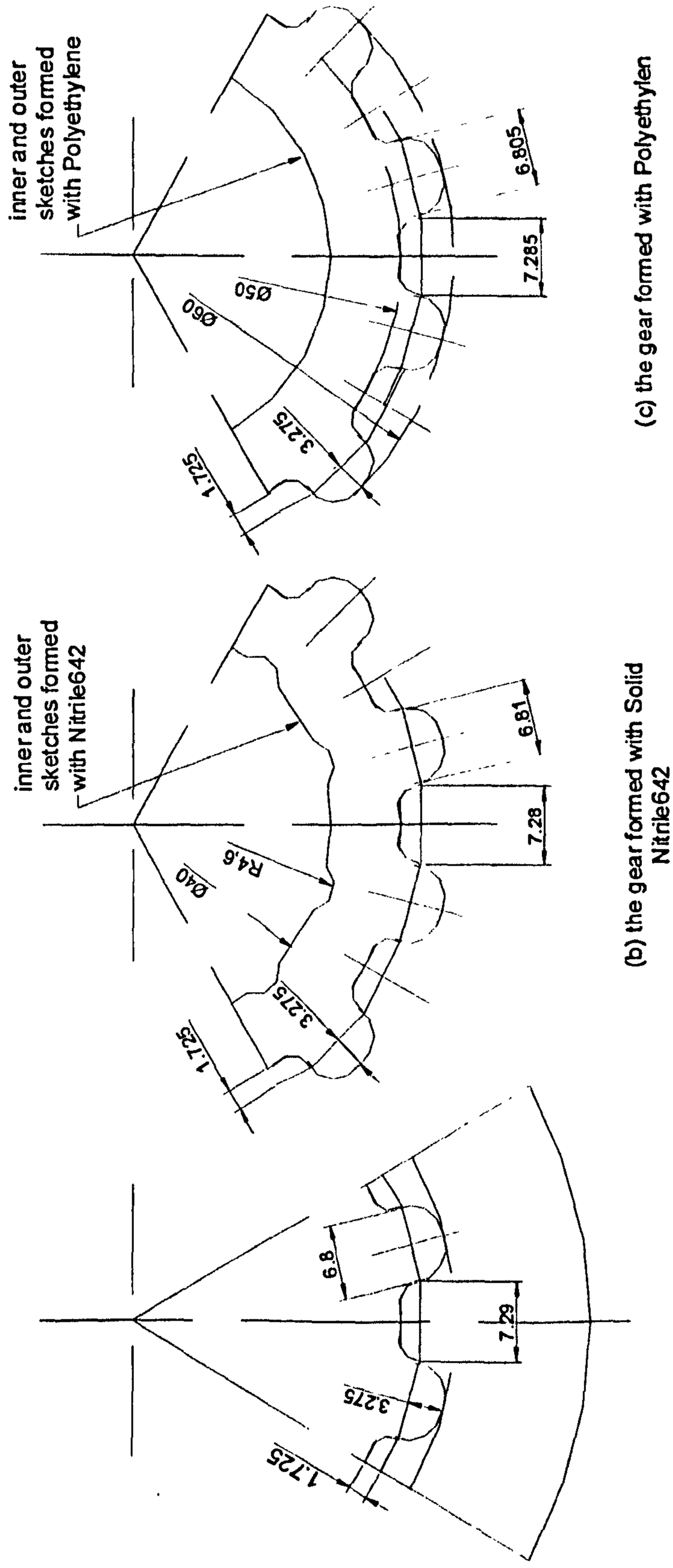

Fig.7.8 The profile of the forming die and the gear-shafts formed